NASA CONTRACTOR REPORT

NASA CR-2384

NASA CR-2384

INTEGRATED POWER/ATTITUDE CONTROL SYSTEM (IPACS) STUDY

Volume II - Conceptual Designs

by J. E. Notti, A. Cormack III, W. C. Schmill, and W. J. Klein

Prepared by
ROCKWELL INTERNATIONAL
SPACE DIVISION
Downey, Calif, 90241
for Langley Research Center

NATIONAL AERONAUTICS AND SPACE ADMINISTRATION • WASHINGTON, D. C. • APRIL 1974

1. Report No.	2. Government Accession No.	3. Recipient's Catalog No.
NASA CR-2384		

4. Title and Subtitle	5. Report Date
INTEGRATED POWER/ATTITUDE CONTROL SYSTEM (IPACS) STUDY- VOLUME II CONCEPTUAL DESIGNS	April 1974
	6. Performing Organization Code
7. Author(s)	8. Performing Organization Report No.
J. E. Notti, A. Cormack III, W. C. Schmill, and W. J. Klein	SD 73-SA-0101-2
	10. Work Unit No.
9. Performing Organization Name and Address	909-74-35-01
Rockwell International Space Division Downey, CA.	11. Contract or Grant No. NAS1-11732
	13. Type of Report and Period Covered
12. Sponsoring Agency Name and Address	Contactor Report
National Aeronautics and Space Administration Washington, D.C. 20546	14. Sponsoring Agency Code

15. Supplementary Notes

This is a final report.

16. Abstract

An Integrated Power/Attitude Control System (IPACS) concept consisting of an array of spinning flywheels, with or without gimbals, capable of performing the dual function of power storage and generation, as well as attitude control has been investigated. This system provides attitude control through momentum storage, and replaces the storage batteries onboard the spacecraft. The results of the investigation are presented in two volumes. Volume I contains the trade-off studies performed to establish the feasibility, cost effectiveness, required level of development, and boundaries of application of IPACS to a wide variety of spacecraft. Volume II presents the conceptual designs for a free-flying research application module (RAM), and for a tracking and data relay satellite (TDRS). Volume II also contains results from dynamic analyses and simulations of the IPACS conceptual designs.

17. Key Words (Suggested by Author(s))	18. Distribution Statement
Integrated Power/Attitude Control System Attitude control Power storage and generation Battery replacement Weight, volume, and cost savings	UNCLASSIFIED- UNLIMITED

19. Security Classif. (of this report)	20. Security Classif. (of this page)	21. No. of Pages	22. Price*
UNCLASSIFIED	UNCLASSIFIED	212	$5.50

*For sale by the National Technical Information Service, Springfield, Virginia 22151

FOREWORD

This report was prepared by the Space Division of Rockwell International for the National Aeronautics and Space Administration's Langley Research Center in accordance with the requirements of Exhibit A of Contract NAS1-11732. The contract directed a 13-month study of spacecraft integrated electrical power and attitude control subsystems which utilize flywheels to perform the dual functions of energy storage and attitude control.

The results of this study are presented in two volumes. Volume I, Feasibility Studies (SD 73-SA-0101-1), presents feasibility and cost-effectiveness comparison studies defining the use of integrated power and attitude control subsystems for seven spacecraft missions. Volume II, Conceptual Design (SD 73-SA-0101-2), presents specific designs for a satellite and a Shuttle research and application module mission.

The authors wish to acknowledge the individuals who participated in the conduct of the study. In particular Dr. E.W. Manteuffel of the Sheltered Workshop, Binghamton, New York, designed the permanent magnet motor-generators. Additional contributors include:

B.J. Call	Rotor Design
E.J. Mulcahy	Rotor Design
V. Van Camp	Electrical Power
P.W. Welch	Dynamic Analysis

CONTENTS

ILLUSTRATIONS

Figure

Page

TABLES

INTEGRATED POWER/ATTITUDE CONTROL SYSTEM (IPACS) STUDY
VOLUME II - CONCEPTUAL DESIGNS

by

J.E. Notti, A. Cormack III, W.C. Schmill, W.J. Klein
Space Division, Rockwell International

S.B. Hamilton, R.C. Wells
Aircraft Equipment Division, General Electric

SUMMARY

A study has been conducted to evaluate the concept of an integrated power and attitude control system (IPACS) for spacecraft application. The IPACS is defined as a system capable of performing the functions of power generation, energy storage, power conditioning and distribution, and momentum exchange attitude control. The primary feature of the IPACS concept is the use of spinning flywheels to perform the dual functions of storing electrical energy and providing momentum exchange for attitude control.

The major objectives of the study were: (1) determine the feasibility and cost effectivness of the concept, (2) establish boundaries of application for manned and unmanned spacecraft, (3) identify hardware developments required for the conceptual designs, and (4) prepare conceptual designs for two missions.

Feasibility was evaluated by comparing the physical and performance characteristics of candidate IPACS designs with comparable characteristics of the baseline electrical power and attitude control subsystems as defined in previous studies. Seven spacecraft/missions were studied: (1) a low orbit satellite (Earth Observations Satellite - EOS); (2) a geosynchronous vehicle (Tracking and Data Relay Satellite - TDRS); (3) a planetary spacecraft (Mariner Jupiter/Saturn - MJS); (4) an extended duration (30-day) shuttle sortie mission; (5) a free-flying shuttle research and applications module (RAM); (6) a Modular Space Station (MSS); and (7) a seven-day shuttle sortie mission with the Advanced Technology Laboratory (ATL) payload.

Simultaneous electrical energy storage and attitude control by means of flywheel arrays appeared technically feasible for all missions studied. Both electrical power and attitude control performance requirements can be satisfied by high-speed flywheel energy-momentum units utilized in conventional gimbaled or non-gimbaled arrays.

The IPACS systems are predicted to weigh less than conventional electrical power and attitude control systems utilizing batteries or fuel cells for all missions except the planetary. As electrical energy storage elements, high speed energy-momentum units are predicted to produce about twice the energy density of spacecraft battery systems at comparable development levels. The weight advantage of flywheel units increases as mission life and the number of charge-discharge cycles increases.

Systems of two development levels are postulated. In the current technology systems the use of high speed ball bearings and permanent magnet motors is defined. The applications require development testing for design verification. The advanced technology flywheel systems require the continued development of composite rotors and an extension of the current magnetic suspension bearing design technology to the high speed operating regime.

The studies did not show any inherent power, energy, or control boundaries which limit IPACS in spacecraft applications. Power levels to 80 KW and energy storage to 70 KW-hr are obtainable for designs sized to spacecraft dimensional constraints. Attitude control dynamic range and pointing accuracy are expected to be approximately that of current control moment gyros.

Cost effectiveness was evaluated by comparing estimated costs of IPACS designs with the original cost estimates of the designs for the conventional power and control subsystems. IPACS appeared cost competitive for all missions except the planetary MJS mission and the particular 30-day shuttle sortie mission studied. This shuttle mission was characterized by a short term 60 KW power requirement for a few cycles. The planetary mission was characterized by a low energy storage requirement for three discharge cycles at planet encounter. In both cases, IPACS development costs exceeded costs of a short life, high energy density battery system. IPACS was shown to promise significant cost advantages for spacecraft with extended life missions or a recurring mission usage such as the RAM and ATL shuttle missions. In extended life missions IPACS development costs were similar to those required for conventional systems and operational cost significantly better by reason of the predicted life and refurbishment advantages of the flywheel systems.

Dynamic analyses and digital computer simulations were performed for both the RAM and TDRS conceptual designs. This work confirmed analytical predictions and demonstrated the feasibility of revising generic control laws to operate the flywheels for simultaneous energy transfer and attitude control. Control response in the presence of energy charge-discharge cycles was shown equivalent to conventional response for both gimbaled and non-gimbaled systems. Digital computer simulations of the solar array, power bus and motor generator system were performed. Motor-generator loop stability and power response in the presence of solar array output changes and load variations were shown to be satisfactory.

INTRODUCTION

Background

During the last several years a number of different approaches to electrical power subsystems have been identified and studied for the postulated spacecraft of NASA mission models. In practically all designs the energy storage function is performed by use of rechargeable battery systems. Designs have emphasized the performance aspects of energy storage capability and charge - discharge cycles because of their direct relationship to the more important factors of battery subsystem weight and life. Cycle life factors are of particular importance to batteries which have an inherent characteristic of decreasing life with an increasing number of charge - discharge cycles.

The requirement for spacecraft lifetimes in excess of five years or the requirement for long quiescent periods, both characteristic of Shuttle era designs, results in relatively high battery subsystem weight. Achievable energy storage densities vary appreciably among spacecraft designs. In general, battery subsystems commonly constitute 30 percent of an electrical power system weight and have, in specific designs, approached 50 percent.

Developments of recent years have shown that spinning flywheel designs can be made to provide higher energy densities than can be expected from several conventional electrochemical devices. The spinning flywheel is studied herein as a potential competitor for spacecraft electrical energy storage as well as attitude control. In spacecraft applications, the flywheel concept is enhanced in that even a parity in energy density between the flywheel and battery subsystems may result in significant advantage for the flywheel subsystem. This is because many spacecraft designs currently employ spinning flywheels in reaction and momentum exchange attitude control systems. If a flywheel subsystem can be designed to perform efficiently the dual functions of electrical energy storage and momentum storage for attitude control, advantage can accrue through deletion of batteries and associated electronics.

The purpose of this study was to determine the mission applications of an integrated power and attitude control system (IPACS) which utilizes spinning flywheels for both electrical energy storage and attitude control. Applicability was to be determined by studying feasibility, cost-effectiveness, and specific designs for selected mission/vehicles from the spacecraft mission classes of unmanned satellites, extended Space Shuttle sortie missions, Shuttle research and applications modules, and space stations. The study was to determine the extent to which the IPACS concept is practical considering both current and anticipated technology developments.

IPACS Concept

The IPACS concept consists of solar cell arrays, energy-momentum (E-M) wheel subassemblies, gimbals, gimbal actuators and sensors, power conditioning and distribution components, and all computer electronics associated with power and attitude control functions. Figure I-1 illustrates the system concept. Electrical power is supplied directly from the solar array to the loads through a regulated spacecraft bus. Electrical energy is stored in the rotating wheel and discharged to the loads when required. Spacecraft attitude control is accomplished simultaneously by changing the angular momentum state of the flywheel. Momentum changes for attitude control torque generation can be accomplished by conventional means. The energy-momentum wheel is either used in the reaction mode (in which applied motor torques change the spin speed of the wheel and react upon the vehicle) or the gimbaled mode (in which the wheel angular momentum vector is precessed to generate vehicle torques).

The central power and control electronics element controls both electrical power and attitude control functions. A single dc permanent magnet unit acts as both a motor to store energy and a generator to provide energy to the loads. Electrical power is regulated by detecting the difference between main bus voltage and the reference voltage and using the difference signal to switch motor-generator modes.

The system utilizes no batteries and performs all the functions of conventional spacecraft power and control subsystems.

Study Objectives

The objectives of the IPACS study as structured under the direction of NASA/LRC were: (1) to determine the feasibility and cost-effectiveness of a solar array energy wheel system capable of dual functions of spacecraft electrical energy storage and attitude control; (2) to establish the boundaries of application of this system for both manned and unmanned spacecraft; (3) to identify hardware components considered critical to the viability of the concept and to define the level of development required; and (4) to generate conceptual designs for two specific systems to be selected at the conclusion of the feasibility analysis. A contract change authorization issued after mid-term review provided an additional objective of studying the feasibility and cost-effectiveness of the IPACS concept as applied to the Langley Research Center Application and Technology Laboratory (ATL) seven-day Shuttle sortie mission.

Study Scope and Qualifications

The study began with a definition of missions for the four mission classes of the statement of work. Spacecraft and subsystem requirements for electrical power and attitude control were then compiled and analyzed. Specific candidate

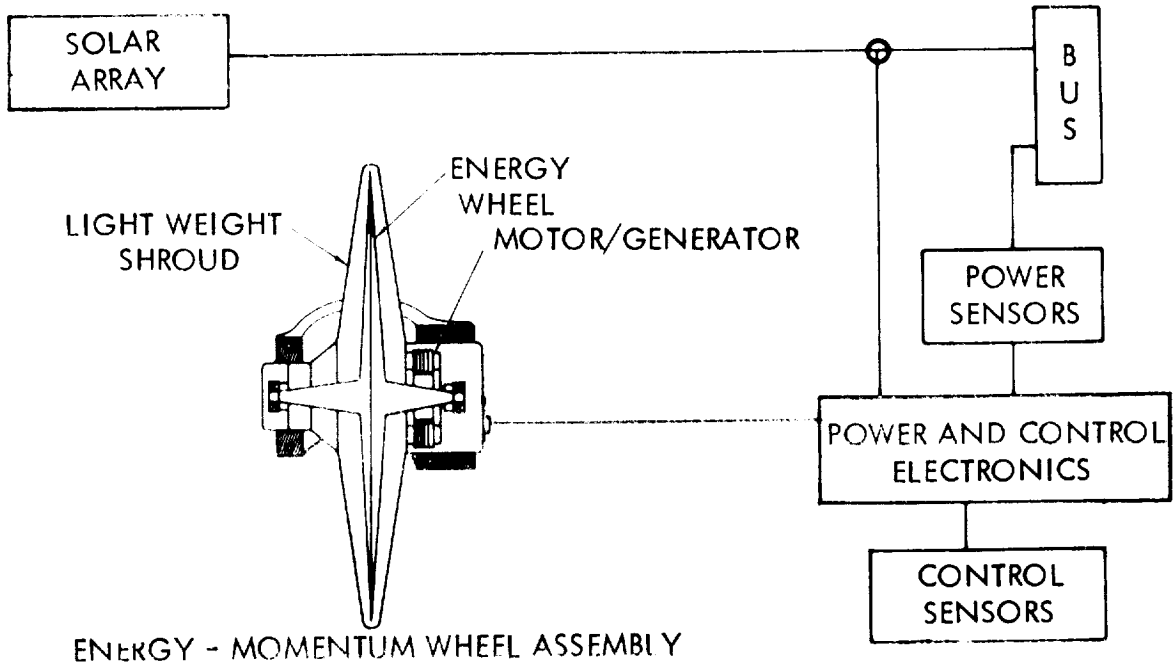

Figure I-1. Integrated Power and Control System Concept

mission/spacecraft were selected as representative for each mission class. The selections were an astronomy mission (A303B) for the research and application module (RAM), the Rockwell modular space station (MSS) design, and the Rockwell 30-day Shuttle sortie mission design. In the unmanned satellite mission class the variety of requirements dictated that more than one mission/spacecraft be studied to typify the class as a whole. In this case, three mission/spacecraft were selected for study: the Rockwell tracking and data relay satellite (TDRS) Phase B design for a geosynchronous satellite; a low earth orbit design for the earth observatory satellite (EOS) mission; and a Rockwell design for the Mariner Jupiter/Saturn (MJS) flyby spacecraft. Each mission/spacecraft selected had previously been defined by extensive contract or research study efforts.

IPACS candidate conceptual designs were developed through component trade and system synthesis studies. These studies established the more efficient components to be used in the flywheel rotating assembly for both current and projected technology. Projected technology developments were analyzed and programs defined. The more efficient flywheel assemblies were then combined in different system configurations and screened for performance. The more efficient systems within each technology classification were then selected and compared with the conventional power and control designs in performance.

Cost-effectiveness studies were performed by comparing system and penalty costs developed for IPACS against the costs determined in the Phase B studies for the competitive systems. Cost studies represented approximately 3 percent of the total effort.

The development of system conceptual designs for the TDRS and RAM missions comprised approximately 50 percent of the contract effort. The system conceptual designs present element sizing, dimensioning, material selection, electronic schematics, system design, spacecraft integration, and dynamic performance studies. The designs define two distinct prototype flywheel energy storage subassemblies. The subassemblies incorporate high energy density isotropic wheels with permanent magnet motor-generators.

The depth of technical analyses and accuracy of data are considered appropriate for the comparisons made between IPACS and competitive systems. Study scope did not permit iterations and optimizations of the IPACS designs. In this respect, design decisions were made such that the IPACS advantages which are predicted in the performance comparisons can be considered conservative and may be improved.

The feasibility study also identified interesting alternative studies which were beyond the scope of the reported effort. Potential areas for further study are discussed in the conclusions and recommendations sections of Volume I.

Report Organization

The report is presented in two volumes, each of which is modularized. The modules contain the results of specific sets of tasks performed to satisfy study objectives. This volume, which presents the IPACS subsystem designs, consists of the following four modules:

(1) Tracking and Data Relay Satellite Conceptual Design

(2) Research and Application Module Conceptual Design

(3) Dynamic Analysis and Simulation

(4) Conclusions

MODULE 1 - TRACKING AND DATA RELAY SATELLITE CONCEPTUAL DESIGN

A conceptual design of an IPACS for the TDRS (tracking and data relay satellite) was prepared to establish the approach for integration of both attitude control and energy storage for this class mission. A description of the TDRS and its baseline electrical power and control subsystem is included in Module 1, Appendix 1-C, Volume I, of this report.

Included here is a description of the baseline TDRS system and mission, the TDRS IPACS, its operation, and a discussion of the energy-momentum wheel design.

TDRS System Description

The objective of the TDRS is to relay information from a multitude of earth-orbiting vehicles to a single ground station. Two TDRS vehicles are placed in synchronous orbit to accomplish real-time continuous data transfer from the user spacecraft to the ground station.

Baseline configuration.- Figure 1-1 illustrates the arrangement of antennas and solar array panels symmetrically grouped around the central spacecraft body. The two medium data rate (MDR) parabolic reflector antennas are supported on struts on each side of the body. The S-band array shown has 32 elements, 28 are receivers and 4 transmitters. The one-degree-of-freedom solar panels are deployed above and below the spacecraft beyond the shadow limits of the antennas. Telemetry and command VHF omni whip antennas located around the rear of the spacecraft are utilized during launch and spacecraft orbital maneuvers prior to deployment of the primary antennas.

Four thermal control louvered shutter assemblies are positioned at north-south extremities of the body such that at least one-half the shutter radiator area is always shadowed from solar radiation. These individually thermal operated louvers are of the overlap design and have high rigidity to withstand launch shock and vibration loads when in their normally-warm open position.

TDRS system operational timeline. - Each TDRS is launched from the Eastern Test Range by a Delta 2914 with a TE-364-4 third stage at a launch azimuth of 1.57 rad (90°). The vehicle lifts into a parking orbit at a nominal altitude of 185 km (100 nm) with an inclination of approximately 0.5 rad (28.3°). The fairing is jettisoned about 36 seconds after Stage II ignition and 4

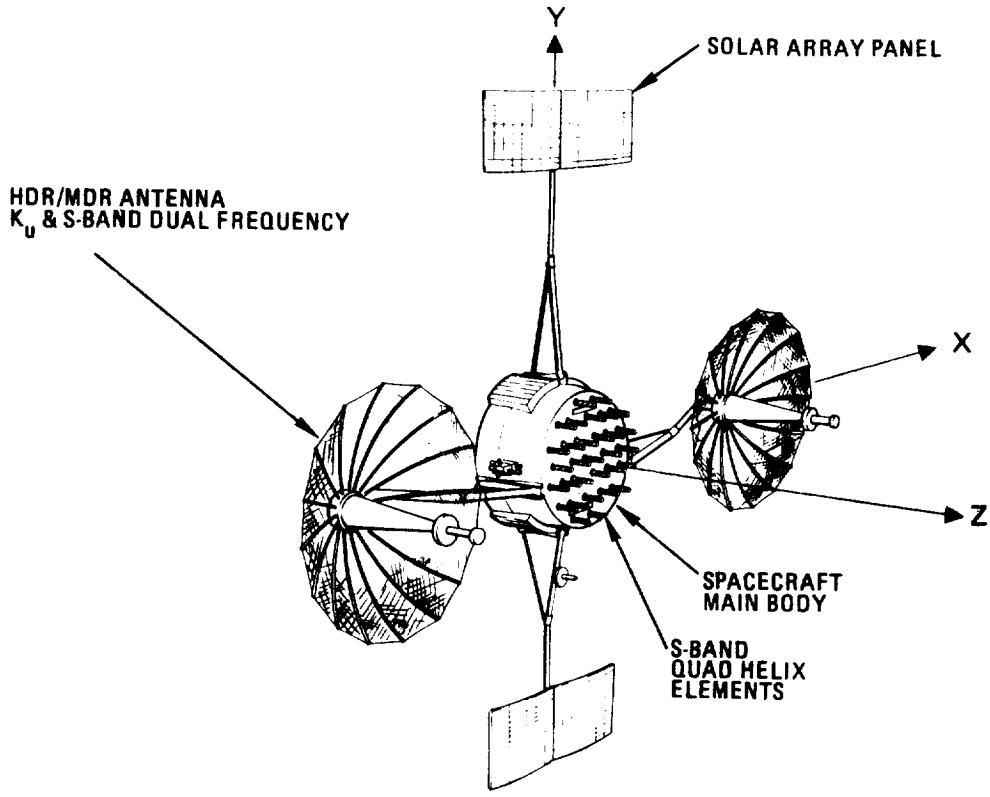

Figure 1-1. Baseline TDRS Configuration

minutes before the first Stage II cutoff command and start of the parking orbit coast phase. Coast lasts 16.22 minutes and concludes when the vehicle reaches the first descending node (first perigee) at 0.052 rad (3°) east longitude. At the node, the second stage restarts and uses its residual energy to inject into the transfer orbit. The second burn of Stage II lasts 28 seconds. After its burnout, the third stage and the TDRS are spun up to 90 rpm, Stage III ignites and burns for 24 seconds to complete transfer orbit insertion. Payload separation occurs two minutes after Stage III burnout, 27 minutes after liftoff and 3 minutes after first descending node injection. The TDRS remains spinning until after insertion into synchronous orbit.

Transfer orbit phase profile: At the first descending node the vehicle is injected into a 0.47 rad (27°) inclination transfer orbit by the solid propellant Delta 2914 third stage which changes the inclination from that of the parking orbit to that of the transfer orbit. After payload separation at 204 km (110 nm) the spacecraft coasts to synchronous altitude in an elliptical 3.14 rad (180°) transfer orbit which combines simplicity of implementation and economy of propellant and has been used successfully in other space missions. The long transit allows time for smoothing and processing of tracking data for reorienting the spacecraft for the apogee motor burn. The transfer orbit transfer time from injection (perigee) to apogee (one-half orbit) is 5.25 hours. During the entire transfer orbit, the spacecraft will be spinning and

will maneuver into appropriate attitudes for attitude determination and measurement, and nutation will be damped out. In this transfer time the spacecraft must also acquire the sun, establish contact with the ground stations, and reorient for apogee maneuver.

The initiation of the vehicle reorientation maneuvers occurs within the first half hour after transfer orbit injection when the spacecraft has come into view of the ground station, so that all systems can be activated and checked out and the reorientation commands given from the ground. The torque vector is applied along an axis normal to the major axis of the transfer orbit, normal to the spin vector, in the plane of the desired precession so that the vehicle is precessed about the major axis of the transfer ellipse (line of nodes). Since the spacecraft is spinning at a rate imparted by the launch vehicle, it is reoriented by means of periodic synchronized precessional torque impulses. The sequence of operations for accomplishing this takes at least one and one-half orbits (15.75 hours) and is provided to obtain data and make the necessary corrections prior to synchronous orbit insertion.

For proper deployment of the spacecraft into the desired longitude location, the east spacecraft is inserted into the synchronous altitude at the second apogee and the west and spare satellites at the third apogee. At the given apogee, the apogee motor fires to change plane and circularize the orbit at synchronous altitude for approach to operational station. This deployment philosophy provides a complete transfer orbit time of approximately 15.75 hours to the second apogee and approximately 26.25 hours to the third apogee, sufficient for all required operations and economic fuel consumption.

Preoperational synchronous orbit phase profile: After apogee motor burnout, the spacecraft is despun and stabilized (momentum wheels energized) in an essentially equatorial orbit. The solar panels are deployed 1.5 hours after spacecraft despin and the antennas are deployed about 20 minutes later. The spacecraft then acquires the sun and earth and receives near-continuous sunlight for the mission at synchronous altitude. The spacecraft drifts to its assigned station. Appropriate post-apogee delta-V maneuvers are performed to correct the spacecraft injection errors and to acquire the proper drift orbit (about 24 hours after apogee motor burnout).

Flight envelope: Two vehicles are nominally operated at synchronous altitude. One is positioned at a longitude of approximately 0.262 rad west (15° west) and the other at a longitude of approximately 2.53 rad west (145° west). The selected orbit inclination is 0.044 rad (2.5°).

Mission duration: The vehicle is designed for a minimum operational life of 5 years.

TDRS IPACS operational requirements.- The IPACS must generate and distribute electrical power required by the TDRS as well as provide spacecraft control.

Attitude control: The control system will provide the capability to execute station change and stationkeeping functions. These maneuvers are executed from the nominal vehicle orientation.

The nominal vehicle flight mode will be local level with the vehicle stabilized about all axes.

Transfer orbit functions to be performed include nutation damping, attitude determination, spin axis precession, and apogee burn control. The vehicle is spin-stabilized during transfer orbit operations.

Performance requirements The vehicle will be controlled so that body-mounted antennas are oriented with an accuracy of 0.0174 rad (1.0°). The pointing accuracy required for the gimballed antennas is approximately 0.0078 rad (0.45°). These overall requirements have been budgeted to allocate 0.0052 rad (0.3°) for the short-term attitude control error and approximately 0.0162 rad (0.93°) for the long-term attitude control error.

Disturbances and momentum storage The predominant environmental disturbance source for this vehicle is solar pressure. Aerodynamic and gravity gradient disturbances are negligible. Magnetic interactions will be controlled through design constraints and onboard magnets. The predominant internal disturbance is reaction torques associated with the motion of gimballed antennas. The momentum storage requirements, including the effect of simultaneously slewing two antennas, are summarized as follows:

H_X = 0.407 N-m-sec (0.3 ft-lb-sec)

H_Y = 0.475 N-m-sec (0.35 ft-lb-sec)

H_Z = 0.271 N-m-sec (0.2 ft-lb-sec)

The vehicle body axes are oriented as follows. The Y axis passes through the solar array shaft. The Z axis is the axis of symmetry of the body (also the local vertical axis) and the X axis completes the orthogonal set.

Electrical power: The IPACS must generate, store, regulate, control, condition, and distribute electrical power required by the TDRS. The IPACS must supply power for the mission life of 5 years in a geosynchronous orbit.

EPS performance requirements Table 1-I summarizes baseline operation electrical power loads. These loads can be varied by the telecommunication services duty cycle. The power shown for the low data rate (LDR) forward link is based on two transmitters operating full time with one providing voice transmission for 25 percent of its duty cycle. Medium data rate (MDR) power required is based on two S-band forward links operating full time. Allocating 48 W for battery charging and 39 W for contingency, an end of life (EOL) solar array power output of 400 W is required. Figure 1-2 shows a typical

Subsystem	Power Requirements (watts)		
	Daylight	Eclipse	Transfer Orbit
Attitude stab. & control	16.5	13.5	5.2
Heaters	2.0	1.0	19.6
TT&C	5.3	5.3	5.3
Telecommunication services			
LDR	113.8	73.5	
MDR #1	40.3	40.3	
MDR #2	40.3	12.7	
TDRS-GS	11.3	11.3	
Freq. source	4.8	4.8	4.8
TDRS tracking	7.9	7.9	
Ku-band acq. beacon	8.3	8.3	
Solar panel drive	6.5	6.5	
EPS central controls	9.2	5.2	5.2
Subtotal	266.2	190.3	40.1
Battery charge	48.0		
Power cond./line losses	46.8	17.6	3.9
Contingency	39.0	22.1	
Array output End of Life	400.0		
Degrad. allow. (5 years)	66.0		
Array output Beginning of Life	466.0		
Battery load		230.0	44.0

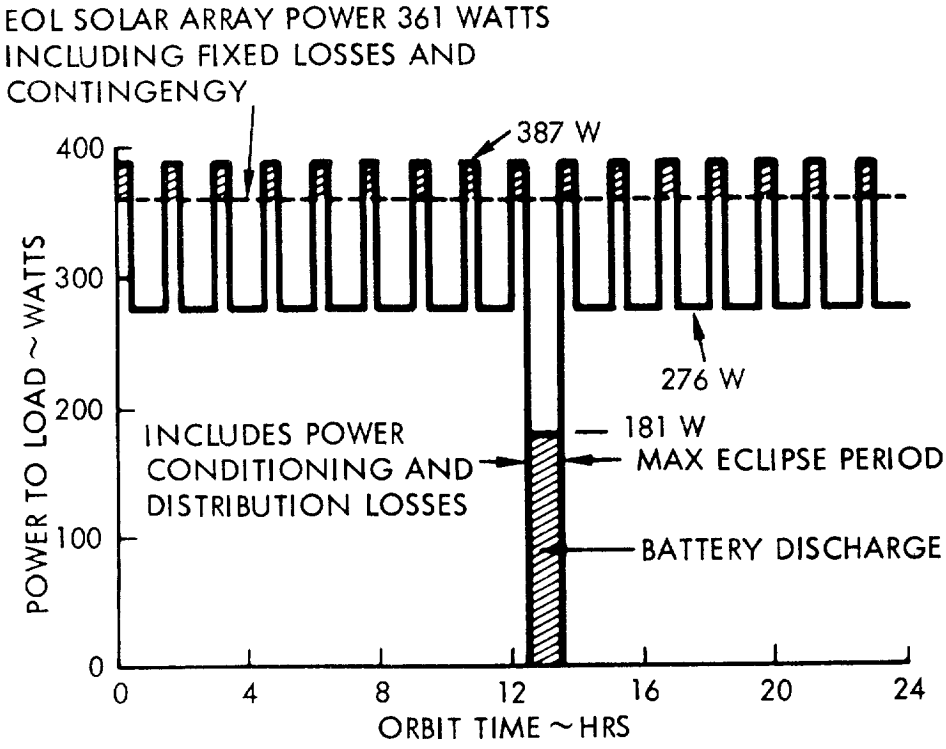

Figure 1-2. TDRS Power Profile

TDRS power profile. The maximum eclipse period is 1.2 hour in duration. Telecommunication services are reduced to one LDR forward link (25-percent voice) and one MDR (S-band) during this period to minimize energy storage weight. As the solar array power degrades to levels where the array cannot meet peaking requirements, the IPACS generators will be used for peaking during daylight.

TDRS IPACS system description.- Major assemblies making up the IPACS are the power source (solar array panels), energy-momentum (E-M) wheel assemblies and associated electronics, central control unit, and the regulated bus.

Functional diagram: Figure 1-3 depicts the mechanization selected for the TDRS IPACS. The scheme shown is based on a minimum modification of the competitive TDRS electrical power subsystem discussed in Module 1, Volume I, of this report. The 4 motor-generator wheel sets replace the two 12-AH (16 cells) nickel cadmium batteries of the competitive EPS.

The electrical power scheme shown is based upon a direct energy transfer mechanization. Power is supplied directly from the solar array to the loads with a central regulated 28 $\pm$ 1.4 V bus. Voltage regulation is accomplished by a shunt regulator operating as a variable load across lower sections of the solar array panels. By shunting only a portion of the solar array and locating the shunts on the array, the net spacecraft thermal dissipation is substantially reduced.

A set of electronics is added for each motor-generator and the TDRS central power control is replaced with an IPACS central control unit.

The central control unit controls the various electrical power and attitude control system operational modes. Electrical power is regulated by detecting the difference between the main bus and reference voltage levels. The difference error is amplified and used to drive the motor generator electronics to either drive current to the bus by back EMF or store power by using excess amounts to torque and subsequently spin up the E-M wheels. Power switching functions are provided by the central control unit.

Energy storage and attitude control is provided by an array of four identical, non-gimbaled, variable-speed E-M units. Each unit includes a permanent magnet brushless dc motor-generator and a constant stress geometry, titanium flywheel. The baseline attitude control sensors are retained with the exception of the horizon sensors used during the normal on-station operation. In the baseline control system the horizon sensors are integrated with the momentum wheels which provide the rotational motion for the scan function. In the IPACS concept a separate solid-state horizon sensor is required due to the inability of the sensor bolometers to respond to the high modulating speeds of the E-M wheels. The logic which governs operation of the attitude control functions is contained in the central control unit.

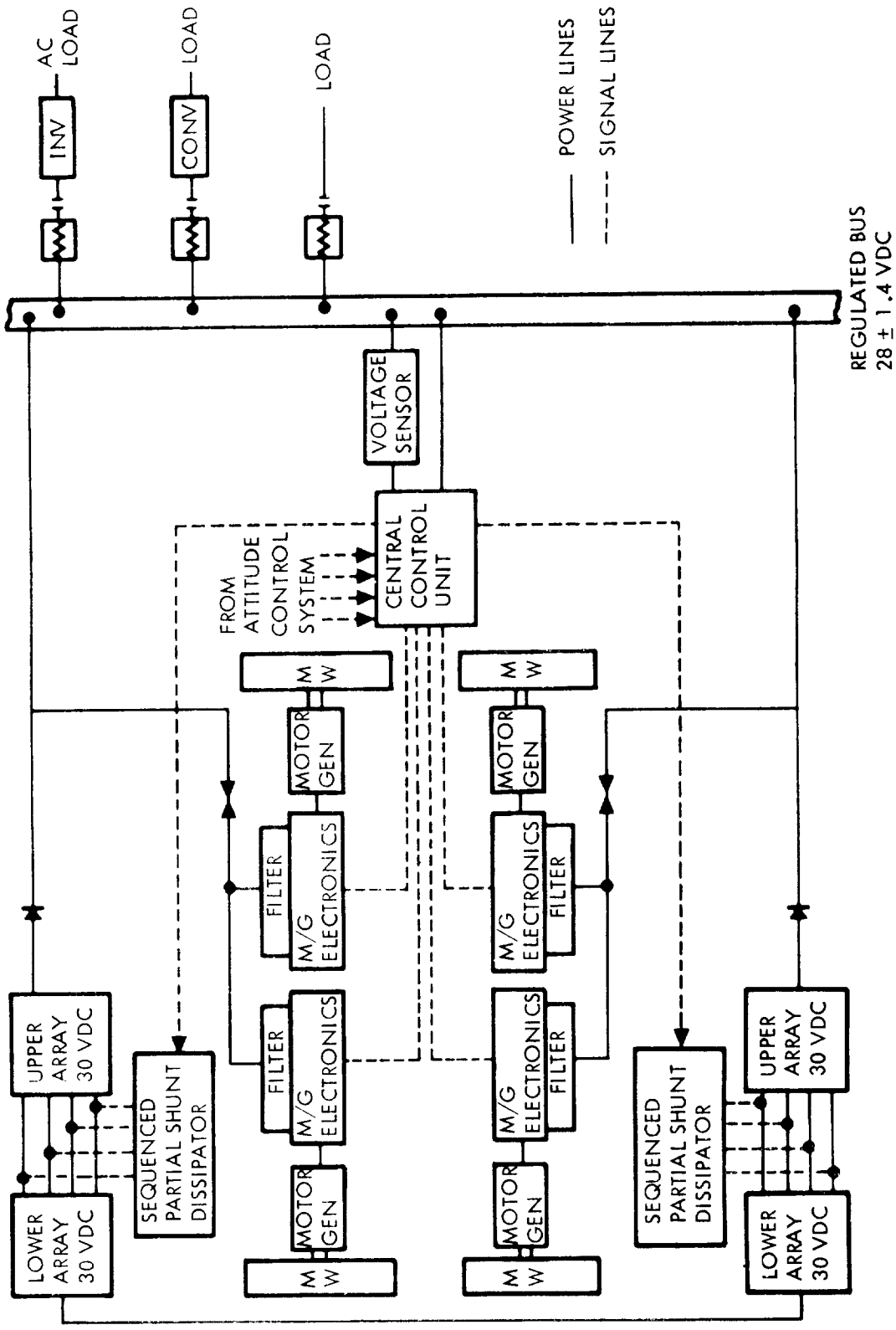

Figure 1-3. TDRS IPACS Electrical Power System Block Diagram

Nominal system operation: The four motor/generator-wheel units are mounted in the vehicle (figure 1-4) in pairs to deliver torques directly along the vehicle pitch and yaw axes. The pitch axis wheels are operated with a momentum bias perpendicular to the plane of the orbit. Energy is stored in both the pitch axis and yaw axis wheels by counter-rotating the wheels. Pitch axis control may be obtained by torquing either or both of the pitch axis wheels. The yaw axis wheels are nominally operated with zero net angular momentum but are torqued to provide active nutation damping.

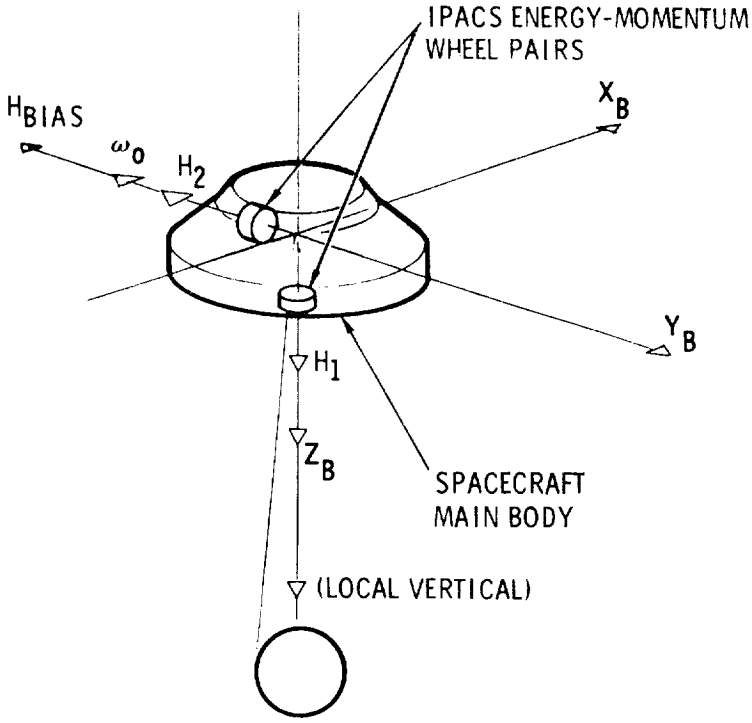

Figure 1-4. TDRS Control Configuration

Under failure mode conditions, where one unit has failed, energy is stored in the pair of units which remain operational. The operative wheel in the failed axis is used for control only. Thus, control performance with one unit failed for IPACS is essentially equivalent to the unfailed baseline system. In the competitive TDRS design, control performance degradation results from a wheel failure.

The power profile shown in figure 1-2 is based on an end of life solar array power (EOL = 5 years). Worst case EOL power requirements as shown exceed solar array capability during short voice communication periods as well as during solar occultation. During both periods, the IPACS provides the energy indicated by the cross-hatched areas.

It should be noted that solar array power at the beginning of the mission of 466 W is adequate for full voice transmission during daylight without an assist from the IPACS energy. Scaling the five-year degradation at 13 W per year indicates that voice transmission can be handled directly from array power for the first three years. During that time power is required of the IPACS only during occultation. For the last two years IPACS supplies power both during occultation and voice periods, which progresses to the worst-case requirement shown in figure 1-2.

The IPACS control is configured to operate in three modes. In the first, control only mode, the IPACS operates as a reaction wheel control system with wheel speeds modulated about a nominal 8250 rpm for control torques. This mode is used for nine months of each of the first three years. As solar array capability degrades below voice transmission requirement levels (387 W) the IPACS is used for control and short power periods with power discharges ranging from the control nominal of 8250 rpm to a minimum of 4900 rpm at end of life. This mode is called the low energy mode and is used for nine months of the remaining two years.

Solar occultation occurs for two 45-day periods a year. The duration of occultation never exceeds 1.2 hours (5 percent of orbit time). During occultation IPACS wheel pairs are discharged sequentially to supply the required power. At the maximum occultation both pairs are discharged through the full speed range of 50 000 to 25 000 rpm. This operation is termed the IPACS high energy mode.

Table 1-II summarizes IPACS operational mode functions and duration.

TABLE 1-II.- IPACS POWER AND CONTROL MODES

Mode designation	E-M wheel functions	Wheel maximum speed range (rpm)	Wheel Array avail. energy w-hr	Mode time (percent of operational life)
Control only	Control torques	Nominal 8250	-	45
Low energy and control	Control torques - Voice power	8250 to 4900	18.4	30
High energy and control	Control torques - Occultation power	50 000 to 25 000	280	25

As can be noted, the IPACS operates in the high energy and control mode for about one quarter of the mission time. For nearly half the time the system operates as a conventional reaction wheel system.

During eclipse periods the TDRS loads require 180 W of electrical power with no voice communication. At geosynchronous altitude maximum eclipse duration is 1.2 hours resulting in a maximum 216 W-hr load demand. Four IPACS rotor assemblies deliver 70 W-hr each (includes discharge circuit losses). The motor/generator sets are sized so that any two wheels operating in pairs can supply required eclipse power.

Figure 1-5 shows a typical charge-discharge profile for IPACS. The common motor/generator is sized to deliver full torque at minimum speed (50 percent) which results in a 250-W rating. During the sunlight portion of the orbit 85 W are available from the solar array for charging (EOL, no voice communication). Allowing for charge circuit losses (feeders, electronics, motor, etc.) 36 W shaft power is available for wheel energy storage. Adding energy to each pair of wheels sequentially results in a total charge time of 4.5 hours. Since the motor torque required for charge is approximately 1/4 that necessary for discharge, the motor/generators are designed to operate at maximum efficiency at 1/3 torque. The motor/generator electronics efficiency (η_{EL}) is based on a nominal 30-volt minimum at the solar array and a 28-V load voltage. The total average charge-discharge efficiency (power out/power in) is 70.0 percent. The comparable charge-discharge efficiency for the TDRS 12-AH NiCd batteries is 61.6 percent (at the available C/10 charge rate and Temp = 65°F). A 100-V solar array and 100-V loads would result in an IPACS charge-discharge efficiency of approximately 78 percent.

Transfer orbit operation: The use of an IPACS concept rather than the TDRS baseline raises the question of power storage through the transfer orbit. The electrical load requirement for the transfer orbit phase is 40.1 W. A brief analysis of the spacecraft sunline relationships and for the case of the baseline curved solar panels indicates that it is possible to perform the transfer orbit profile without the use of batteries, and thus without the need of energy from the IPACS system. In order to provide satisfactory design margins it may be necessary to restrict the minimum spin axis to sun line angle to 20° rather than the current 15°. This imposes no apparent penalty. During the eclipse, which is very brief at these altitudes, the power demand can be: a) left unmet, b) satisfied by further constraining the mission to reduce the eclipse time to zero, c) by the addition of a small battery, or d) operation of the IPACS.

In the current concept, mission launch constraints for sunlight through the transfer orbit appears attainable.

IPACS physical characteristics: The TDRS IPACS component weights are summarized in Table 1-III. The weights shown represent the total required for the spacecraft power and control system.

IPACS physical and performance characteristics are summarized by Table I-IV.

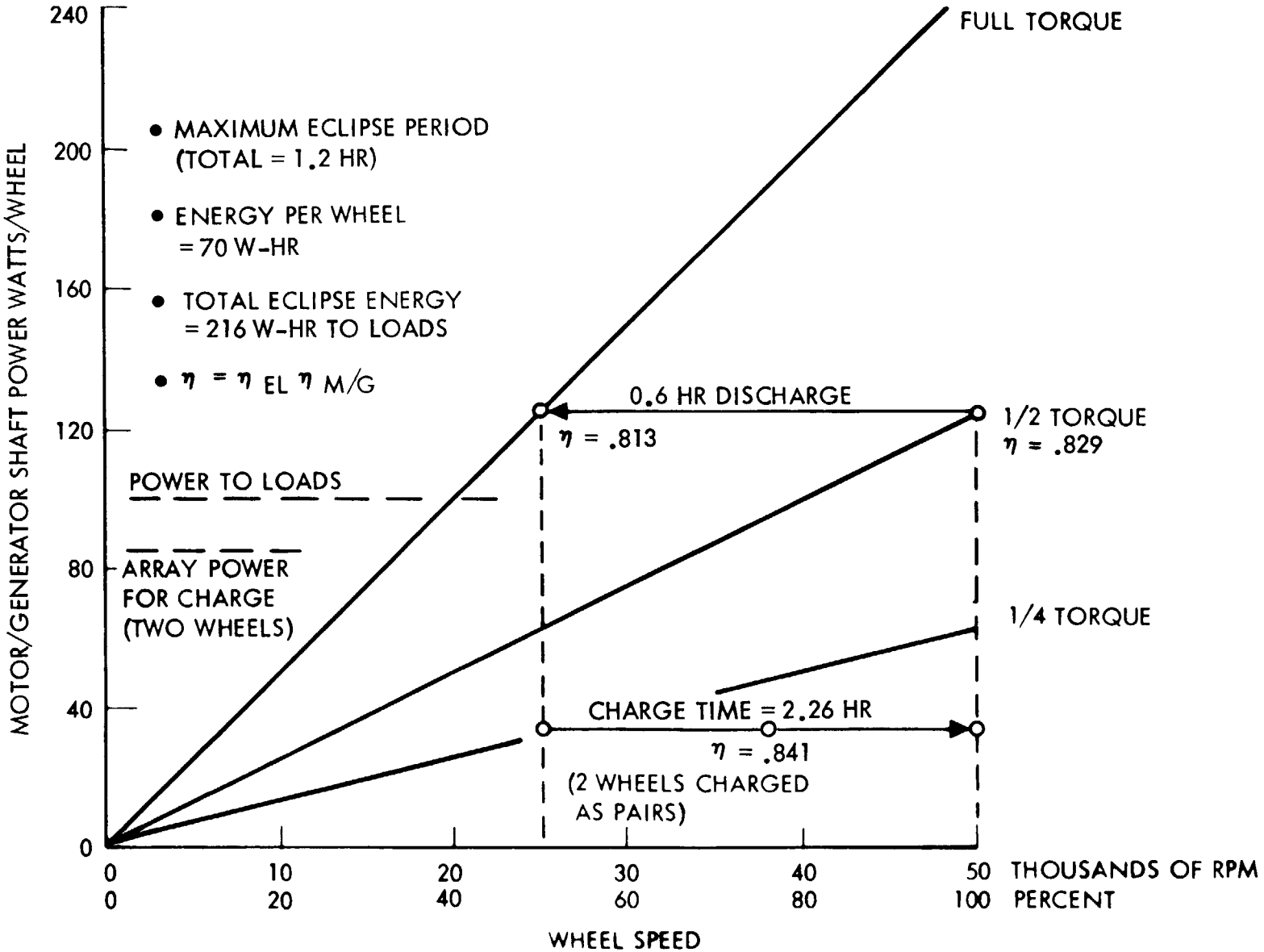

Figure 1-5. TDRS IPACS Charge-Discharge Profile

TABLE 1-III.- TDRS IPACS WEIGHT SUMMARY

Components/assemblies	Weight	
	kg	lb
Solar array	(36.3)	(79.8)
Panels (2)	27.2	59.8
Drive mechanisms (2)	6.8	15.0
Linkage and fittings (2)	2.3	5.0
Power conditioning and distribution	(14.7)	(32.3)
Packaging	2.2	4.9
Shunt dissipators	1.1	2.4
Power conditioner	2.3	5.0
Cabling	9.1	20.0
Central control unit	8.6	19.0
Energy storage/attitude control	(37.7)	(82.7)
Wheel assemblies (4)	22.6	49.6
M/G electronics (4)	4.0	8.8
Horizon sensor	3.3	7.2
Control sensors	7.8	17.1
Total	97.3	213.8

Note - Number in parentheses represents subassembly total weight.

TABLE 1-IV.- TDRS IPACS PHYSICAL AND PERFORMANCE CHARACTERISTICS

Solar Array

Area, total of 2 panels	4.18 m^2 (45.0 ft^2)
Specific power, BOL	111.5 W/m^2 (10.35 W/ft^2)
EOL, 5 years	95.8 W/m^2 (8.9 W/ft^2)
Array power, BOL	466 W
EOL, 5 years	400 W
5-year degradation	14.3%
Power transfer, BOL	16.9 amps (28 Vdc)

Energy Storage

Maximum available energy/wheel*	70 W-hr
Maximum available energy/array*	280 W-hr
Wheel maximum energy speed range	25 000 - 50 000 rpm
Wheel low energy speed range	4900 - 8250 rpm
Generator maximum output	120 W
Line voltage	28 Vdc

Charge-discharge efficiencies (η)

Operating mode	Shaft power watts	Wheel speed rpm	$\eta_{m/g}$	η_{elec}	η_{C-D}
Generator	120	50 000	96.4	86.0	82.9
	120	25 000	92.2	88.2	81.3
Motor	42.5	39 500	96.3	87.4	84.1

Average charge-discharge efficiency 70%

Central Control Unit

Volume	<0.0141 m^3 (<0.50 ft^3)

Attitude Control

Pointing accuracy	0.017 rad (0.9°)
Design control torque/axis	0.0212 N-m (3 in.-oz)
Minimum momentum storage	16.95 N-m-sec (12.5 ft-lb-sec)
Nominal (no energy delivery) Wheel-speeds	8250 rpm

*At 50 percent speed reduction

TDRS IPACS Components

The following TDRS IPACS components are discussed in this section:

(1) Wheel assembly
(2) Motor-generator design
(3) Spin-bearing system
(4) Motor-generator electronics
(5) Horizon sensor
(6) Distribution and regulation

Other power and control components in the TDRS design are not changed by IPACS and therefore remain as described in Module 1, Volume I.

Wheel assembly.- The TDRS wheel assembly is shown in figure 1-6. It consists of a constant stress wheel weighing 3.7 kg (8 lb) and spinning at speeds between 25 000 and 50 000 rpm. Angular momentum varies from 87 to 174 N-m-sec (64 to 128 ft-lb-sec) and kinetic energy from 31.5 to 126 W-hr. The rotor is a high strength to weight ratio titanium alloy.

The rotor is supported on two angular contact ball bearings (38H) built and specially selected for high-speed, long life operation. The bearings are preloaded by a central rod running through a hole in the rotor shaft. The rotor design is such that stress concentrations at the hole are low and do not impact the design.

Centrifugal oilers, having a 7.7-year storage capacity, are used to lubricate the bearings. This oiler provides increased flow at elevated temperatures and at higher speeds.

A single, two-pole permanent magnet type brushless dc motor-generator is used to transfer power in and out the wheel. It can supply 120 W at 28 Vdc over the speed range of 25 000 to 50 000 rpm. Average motor efficiencies are in excess of 96 percent. The motor design is discussed in a subsequent subsection.

The wheel enclosure and support is an aluminum double conical structure for high strength and minimum weight. The wheel assembly is mounted at the rim of the conical enclosure.

Total weight of the wheel assembly is 5.61 kg (12.4 lb). The unit is 37.8 cm (14.85 in) in diameter and 20.6 cm (8.1 in.) maximum along the axis. An additional 1 kg (2.2 lb) is required for the electronic package.

Rotor and shaft: The rotor is a constant stress design and is 34.04 cm (13.4 in.) in diameter. The rotor has an integral shaft with a 0.51 cm (0.200 in.) diameter hole through its center. This hole (which provides

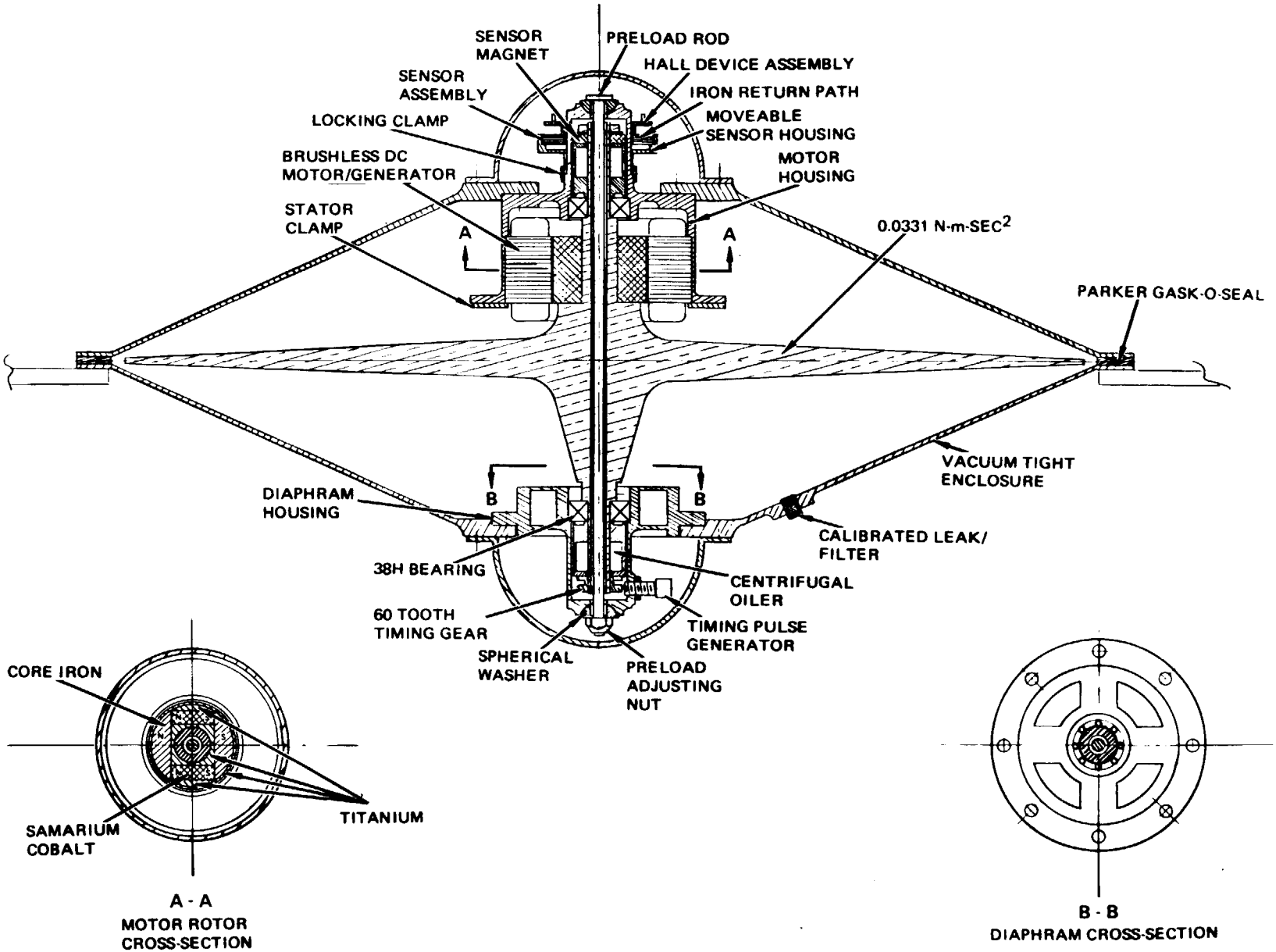

Figure 1-6. TDRS Momentum Wheel

clearance for the spin bearing preload rod) causes a stress concentration which for a disk of uniform cross section would be twice that of the solid disk. However, the oversize shaft and thin rotor cross section reduce the stress concentration at the hole to a value well below the wheel stress level. The motor-generator rotor has a central hole which allows it to be fastened to the shaft as shown in figure 1-6. A 1.27 mm (0.050 in.) thick shrink ring is used to hold the motor rotor magnets and pole pieces together. The rotor is supported on two size 38H spin bearings on 10.8-cm (4.25-in.) centers. A shaft extension provides a mounting for the two centrifugal oilers.

The rotor has a mass moment of inertia of .0332 N-m-sec^2(0.0245 ft-lb-sec^2) about the spin axis and approximately 0.0166 N-m-sec^2 (0.01225 ft-lb-sec^2) about an axis perpendicular to the spin axis.

Spin bearings: The 38H angular contact bearings are press-fitted to the rotor shaft and clamped by the centrifugal oilers. The bearing on the motor-generator side is seated in a housing which supports both the motor stator and spin bearing outer race. The outer race of the second spin bearing is supported in a housing which has low axial stiffness to allow for motion of the conical shell under pressure changes and under load variations. A through rod, having spherical segments and a threaded end, provides axial loading of the bearing outer races. The rod is 3.96 mm (5/32 in.) in diameter and has a 0.56 mm (0.022 in.) radial clearance between shaft and rod.

A simplified sketch of the preload rod method is shown in figure 1-7. Notice that both bearings are axially tied to the frame at side A. The frame on side B is free to move in an axial direction without influencing the preload which is adjusted by the nut and produces tension in the rod.

The spin bearings are lubricated with RL-743 oil by centrifugal oilers.

Details of the spin bearing system appear in a subsequent section of this module.

Bearing housings: The two bearing housings support the spin bearings and are fastened to the conical housings by screws. The housings are fabricated from titanium to minimize weight and still match thermal coefficients with the bearings. Since the conical housing is aluminum, the bearing housings must be designed to prevent excessive interference at the bearing outer race at low temperatures as a result of conical housing shrinkage. One bearing housing also supports the motor-generator stator. Because of the high efficiency of this unit, heating is very low even at full load. The other bearing housing (bearing support ring) is built to have low axial stiffness while still retaining high radial stiffness.

Enclosure: The enclosure serves the function of mounting structure, protective cover, and vacuum enclosure for ground testing. It is designed as a double conical structure of aluminum for axial and radial stiffness and light weight.

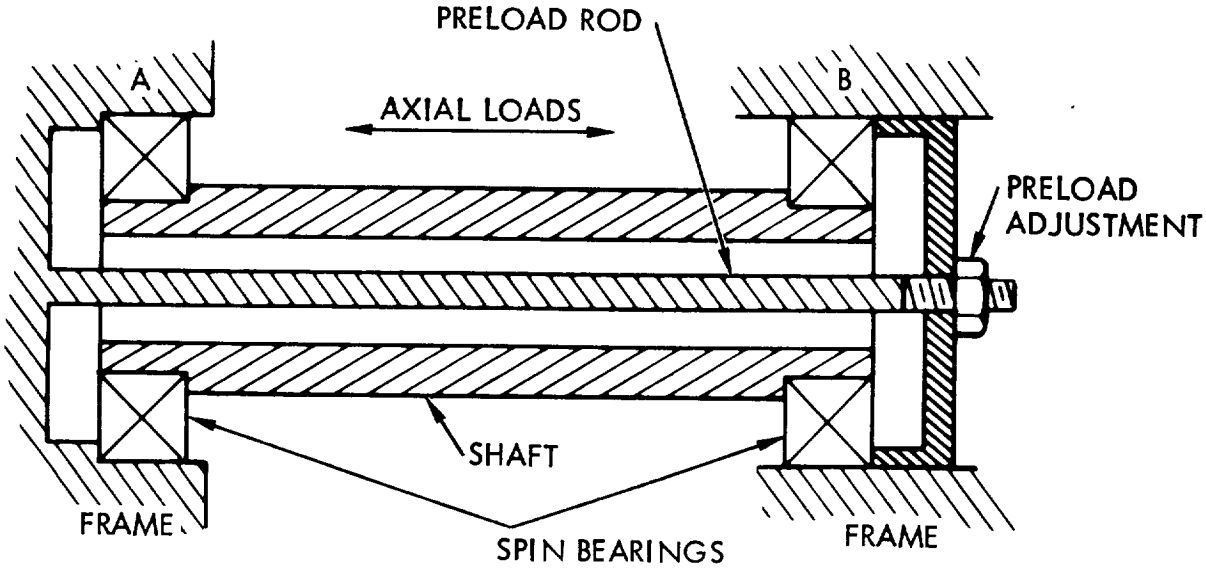

Figure 1-7. Generic Sketch of Preload Rod Method for Spin Bearings

The enclosure comprises two truncated cones with the bases joined by screws spaced 5 cm (2 in.) apart and sealed by a Parker Gask-O-Seal or similar. The truncated portion of the cone terminates in a mounting ring to support the spin bearings and motor. Two small hemispherical covers interface at O-ring surfaces to provide seals at the shaft ends.

The enclosure weighs 0.728 kg (1.6 lb) when designed as a vacuum enclosure suitable for ground test. The weight may be reduced by approximately 25 percent if a vacuum enclosure is not necessary. Structural stiffness will be reduced by about 50 percent. The extra 0.182 kg (0.4 lb) weight to provide the stiffer vacuum enclosure is a relatively small penalty.

Sensors: Three sensor types are used to monitor operation of the wheel assembly:

- Speed sensor
- Temperature sensors
- Vibration sensors

The speed sensor utilizes a magnetic transducer with a permanent magnet bias field to indicate changes in a magnetic path as gear teeth pass under the sensing element. A 60-tooth gear mounted on the rotor would be used to measure wheel speed. The speed sensor is used to monitor and regulate the wheel speed.

Temperature sensors will be mounted at each spin bearing and at the motor-generator stator to monitor these critical temperatures. An accuracy of approximately 2°C is required. An accelerometer would be mounted at each bearing end to monitor vibration induced by the rotor and bearings. Bearing irregularities and balance shifts can be measured.

Mounting: The TDRS unit is mounted on 3 to 4 bosses at the outer rim. If the spin axis is to be parallel to the launch vehicle axis, the preferred orientation is to mount the motor end furthest from the nose of the vehicle.

Structural weights: The weight of the various components comprising the TDRS wheel assembly is given in Table 1-V. All components have been designed to produce minimum practical weight. Reductions can be made in the cover and in the rotor shaft. However, the stiffness would be compromised. At this stage of the design, no further weight reductions are warranted.

TABLE 1-V.- COMPONENT WEIGHTS (TDRS)

Item	Weight	
	kg	lb
Rotor and shaft	3.70	8.16
Bearings (2)	0.027	0.06
Preload rod and spherical washers	0.023	0.05
Motor	0.725	1.60
Motor housing	0.181	0.40
Bearing support ring	0.10	0.22
Enclosure (vacuum)	0.675	1.49
Oilers (2)	0.136	0.30
End covers (2)	0.059	0.13
Total	5.626	12.41

Rotor windage: The constant-stress rotor design is well approximated by a disk. Windage losses in watts are given in Table 1-VI for four values of internal air pressure.

TABLE 1-VI.- ROTOR DRAG LOSSES FROM ENCLOSURE PRESSURE

Air pressure in enclosure		Windage (W)	
N/m^2	Microns	25 000 rpm	50 000 rpm
0.00133	0.01	0.032	0.128
0.01333	0.1	0.32	1.28
0.1333	1.0	3.2	12.8
0.6665	5.0	27.1	140.0

For ground testing, a 0.1333 N/m^2 (1.0 micron) vacuum can be obtained with standard equipment. To obtain 0.01333 N/m^2 (0.1 micron) will require either a high-performance rotary vacuum pump or a diffusion pump. A breather orifice and filter would be provided for orbital operation. When we consider this arrangement and the outgassing within the enclosure, the internal pressure might not drop much below 0.01333 N/m^2 (0.1 micron). An effort must be made to reduce pressure to as low a value as possible without going below the vapor pressure of the lubricant, which is 0.00133 N/m^2 (0.01 micron)at 65.6°C (150°F) and 0.1333 x 10^{-4} N/m^2 (0.0001 micron) at -17.78°C (0°F). Care must be taken in use of shielded bearings, in minimizing sources of outgassing and in minimizing pressure drop through the breather orifice. The calculated windage has by experience been slightly lower than the actual value. Since windage losses at 50 000 rpm could be as high as motor-generator losses under maximum power conditions, the measurement of windage on a development model to verify calculations is important.

Spin up and coast down: The sum of bearing and windage losses at an enclosure pressure 0.2 microns is approximated by the expression:

$$\text{Total Drag } (W_d) = 1 + 2.9 \times 10^{-9} (\text{rpm})^2 \text{ watts}$$

If we operate the motor at its capacity of 120 W for spin up and total drag is W_d, the spin up time is 2.2 hours. The same drag losses will give a coast down time from full speed of 44 hours and 17 hours from half speed where energy storage is 1/4 that at full speed.

Spring mass models: Linear and torsional spring constants were determined for the TDRS wheel assembly as indicated in Table 1-VII. The resulting spring mass models for the three cases (two linear and one torsional) are shown in figures 1-8, 1-9, and 1-10. The simplified two-degree-of-freedom models were solved for undamped natural frequencies. These results are given in Table 1-VIII.

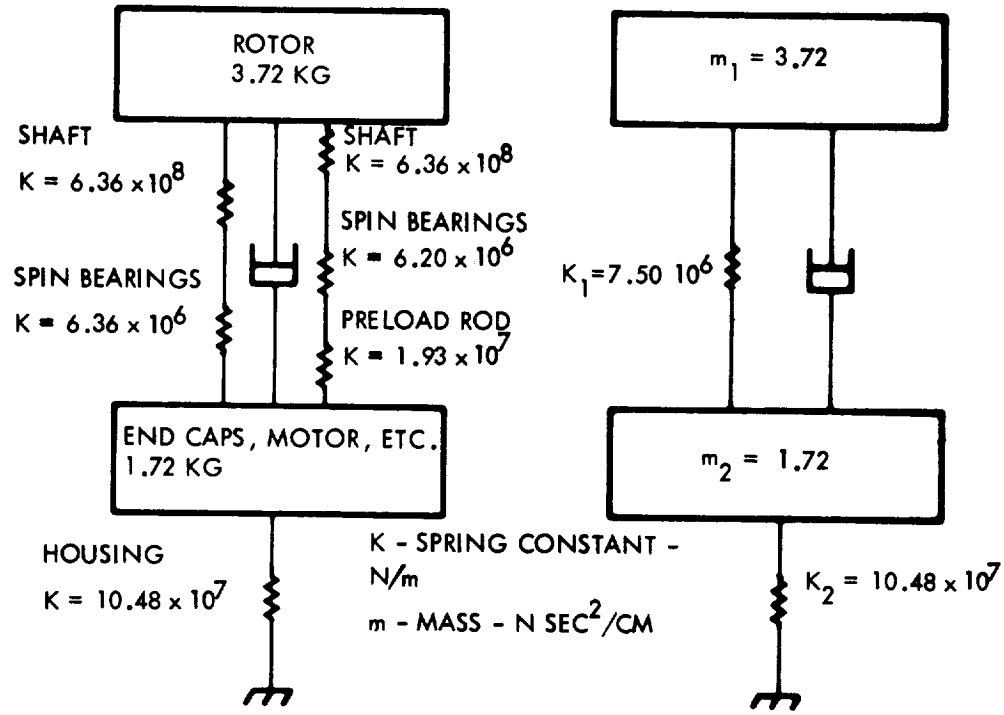

Figure 1-8. Linear Spring Mass Model - Along Spin Axis

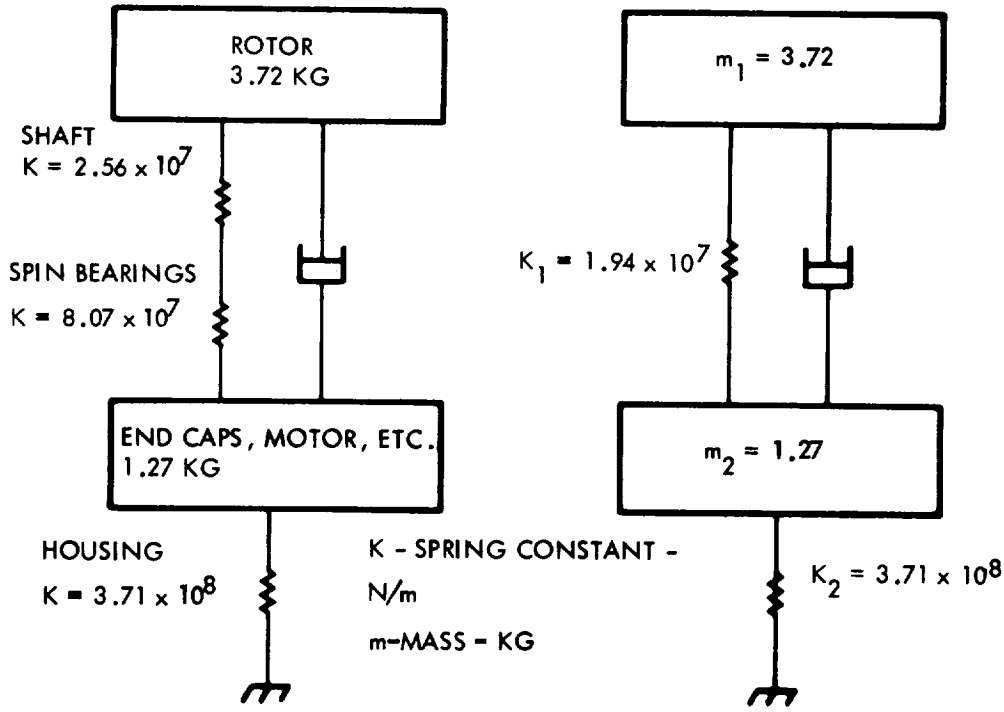

Figure 1-9. Linear Spring Mass Model - Perpendicular to Spin Axis

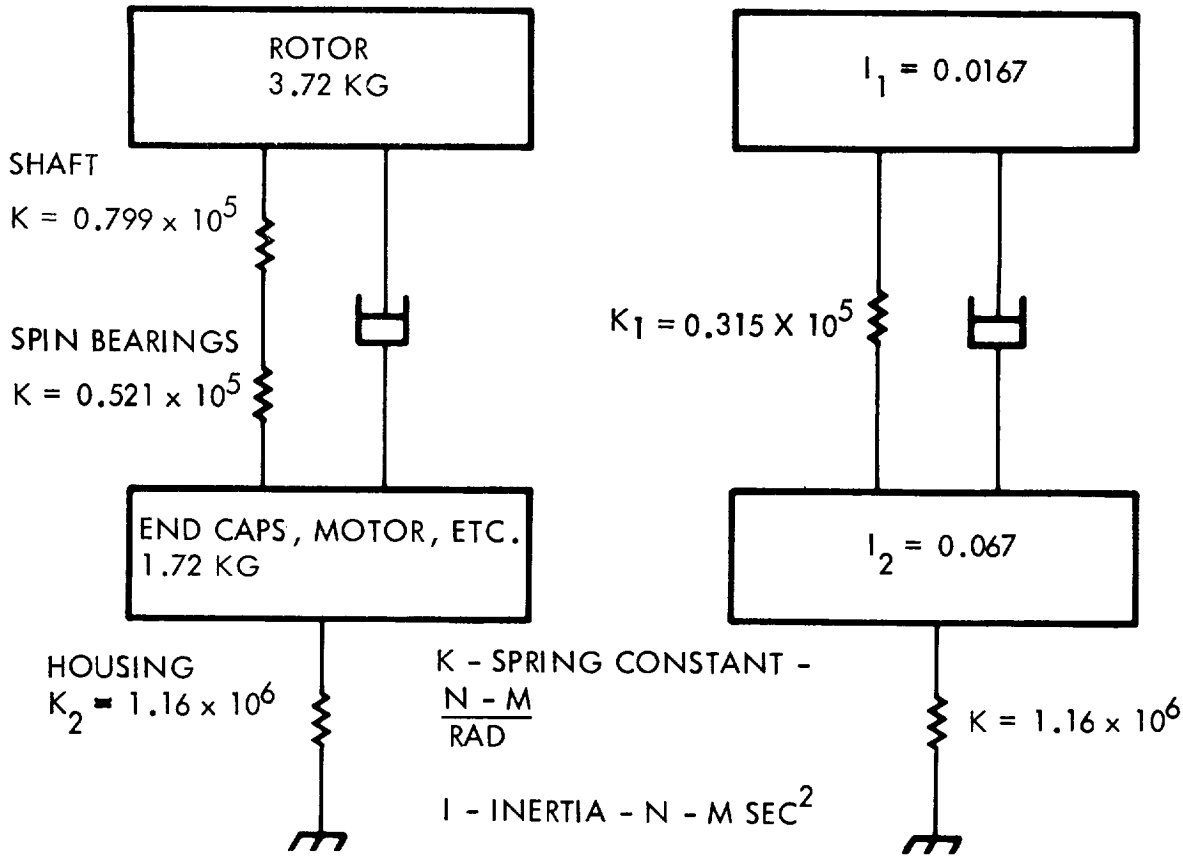

Figure 1-10. Torsional Spring Mass Model - Perpendicular to Spin Axis

TABLE 1-VIII.- WHEEL COMPONENT STIFFNESS CALCULATION METHODS

Spring rate	Method
Shaft	
Linear - along spin axis	$K_L = \frac{AE}{\ell}$
Linear - perpendicular to spin axis	Area Moment Method
Torsional - about axis perpendicular to spin	$K_T = K_L r^2$
Conical Enclosure	
Linear - along spin axis	$K_L = \frac{\pi E t \sin\alpha \sin 2\alpha}{\ln \frac{S}{S_o}}$
Linear - perpendicular to spin axis	$K_L = \frac{\pi E t \cos^3\alpha}{\ln \frac{S}{S_o}}$
Torsional - about axis perpendicular to spin	$K_T = K_L r^2$
Bearings	
Axial	From Barden Bearing Co.
Radial	From Barden Bearing Co.
Preload Rod	
Linear - along spin axis	$K_L = \frac{AE}{\ell}$

K_L = Linear spring rate

K_T = Torsional spring rate

A = Cross-sectional area

E = Youngs modulus

ℓ = Length

r = Radius

t = Thickness

α = Cone angle

S = Cone surface length

S_o = Truncated cone surface length

TABLE 1-VIII.- NATURAL FREQUENCIES OF WHEEL ASSEMBLY

Spring mass model	Natural frequency Lower range rpm
Linear - along spin axis	11 700
Linear - perpendicular to spin axis	18 480
Torsion - perpendicular to spin axis	11 100

Rotor critical frequency analysis: The preceding analysis assumed the rotor assembly to be an inelastic mass. A modal analysis of the elastic wheel shaft assembly was conducted to determine natural frequencies and modal shapes for the first 20 modes under both static and dynamic loading conditions. The critical frequency study was performed digitally using the NASTRAN program. The shaft was modeled using 8 beam elements and the rotor using 20 triangular plate elements. In this analysis assembly members were omitted and the bearings were considered to act as rigid, pinned supports. The frequencies were calculated for three cases, with the wheel static, running at half speed, and running at full speed. The study results are summarized in Table 1-IX. For the static case, there are four plate modes and one bending mode within the operating speed range of the unit. The plate modes are characterised by axial motion of the wheel elements in a direction parallel to the shaft (figure 1-11). The bending mode refers to shaft bending (figure 1-12).

TABLE 1-IX.- FREQUENCIES OF TDRS WHEEL WITH ROTATIONAL SPEED

Mode number	Frequencies (rpm)		
	Natural frequencies (wheel static)	Rotational speed	
		25 000	50 000
1	17 000	18 600*	18 600*
2	18 600*	33 800	59 200
3	27 200	42 600	60 000
4	28 900	53 900	91 500
5	38 300	71 000	119 500
6	55 600	92 000	198 000
7	56 700	93 500	151 000
8	72 500	105 000	154 000
16	205 000 **		

*Denotes first beam bending mode
**Denotes second beam bending mode

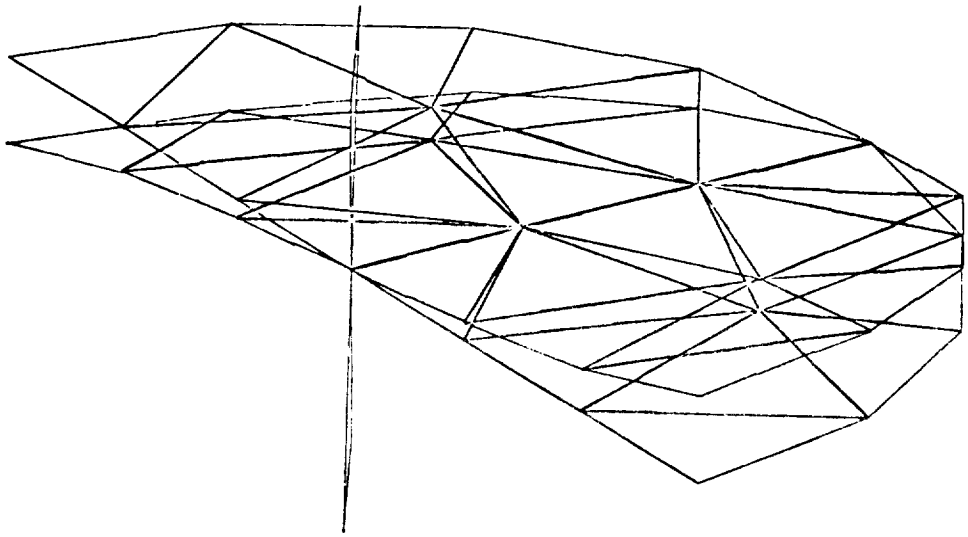

Figure 1-11. TDRS Design Mode No. 1 First Plate Mode Frequency = 17,000 rpm

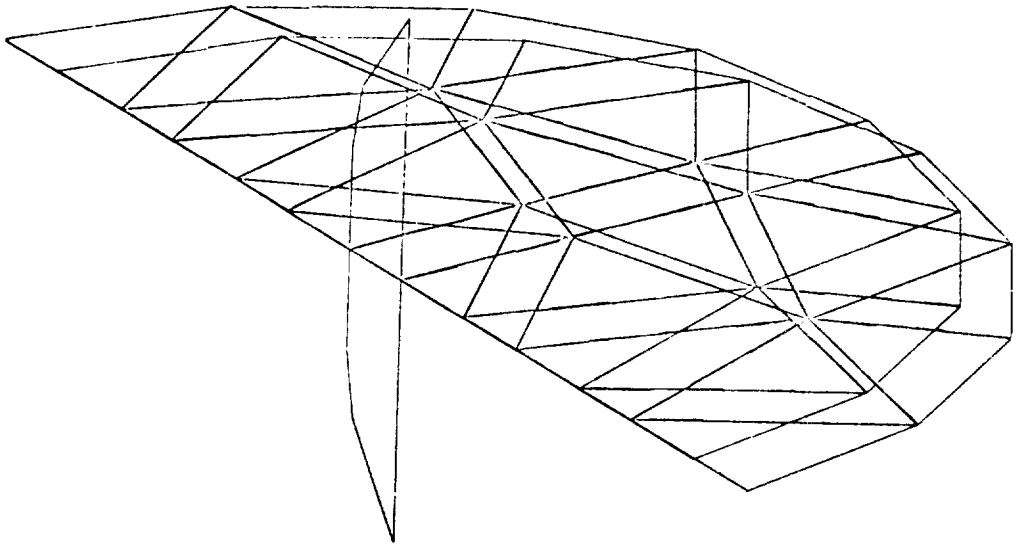

Figure 1-12. TDRS Design Mode No. 2 First Beam Bending Mode Frequency = 18,600 rpm

This table indicates that the frequencies of the TDRS configuration are increased to values greater than the rotational speed of the design for all the plate predominant modes. The first beam bending mode of the TDRS design is below the operational range of the design and is unchanged by the inertial effects of spinning the wheel. This is due to the fact that this bending mode has no rotational contribution from the wheel and so stiffening the wheel by spinning the configuration will not change the frequency of this mode. The plate mode frequencies of the TDRS design are increased to values above the rotational frequencies of the wheel which means that, as the wheel is spun up to its operational speeds, there will be no plate modes in this region of interest. In addition to this, the only way these modes can be excited is by an axial symmetric force down the shaft. There is no apprent way a significant force of this type can be applied to the TDRS design during operation unless the supporting structure for this configuration induces such a loading condition. The second beam bending mode of the TDRS design is 205 000 rpm, which is well above the operational speed of the wheel.

It can be noted that the linear mode of the previous section perpendicular to the spin axis agrees with the first shaft mode calculated by the NASTRAN program. The shaft clearly shows as the more compliant member of the assembly. It can also be noted that plate modes are at factors of 3 to 5 above axial modes of the assembly. Clearly, an integrated modal analysis of the total assembly is required to predict modal interaction accurately. The preliminary studies shown, however, indicate that design stiffness as currently proposed is adequate.

Assembly procedure: The assembly of the TDRS is initiated with the following steps:

- Spin bearings shrunk on shaft.
- Motor rotor (magnet) assembled to spin shaft.
- Motor stator assembled in housing.
- Oilers assembled to spin shaft.
- Housings mounted to enclosure cones.
- Motor sensor and stator are electrically aligned.

The cone (enclosure half) containing the spin motor is fixtured so that the rotor can be lowered into it, taking care that the bearing is properly entered into its housing.

The interface seal, properly oriented with its keying dowels, is placed on the cone. The second cone is then lowered over the first so that the exposed spin bearing properly interfaces with its housing. All assembly screws are then torqued and secured around the cone flanges.

The preload rod may now be inserted and the 5-lb preload established. The magnetic speed pickup device is then adjusted for the prescribed output at the predetermined speed.

Finally, the hemispherical end covers and their elastomer seals can be attached and secured.

Motor-generator design.- The motor-generator requirements for the TDRS are given in Table 1-X.

TABLE 1-X.- TDRS MOTOR-GENERATOR REQUIREMENTS

Speed range:	25 000 - 50 000 rpm
Generator output:	120 W
Average motor power:	42.5 W
Average generator power:	60 W
Average speed (1/2 usable energy point):	39 500 rpm
Line voltage:	28 Vdc
Peak efficiency:	97% or above

The low-power, high-speed requirement makes achievement of 97 percent efficiency difficult even with increased size.

Preliminary considerations: The maximum back EMF should be about 4 V lower than the line voltage. This, then, establishes the back EMF and torque constants K_E and K_T, respectively.

$$K_E = 4.584 \times 10^{-3} \text{ V/rad/sec}$$

$$K_T = 4.58 \times 10^{-3} \text{ N-m/amp } (3.381 \times 10^{-3} \text{ ft-lb/amp})$$

A relatively high current sheet density $\sigma_{A_{max}}$ must be chosen to minimize core losses and maintain high efficiency at the low power levels. A value of $\sigma_{A_{max}}$ = 120 rms ampere conductors per cm was chosen giving a flux density in in the gap of only about 3000 gauss. To minimize core losses at 50 000 rpm, the motor-generator must have only two poles. Therefore, an integral number of slots per pole and phase must be chosen.

Cobalt samarium magnets would be used in the rotor. If the magnet length is one third the pole pitch τ_p, the wave shape of the rotor flux density distribution does not contain harmonics divisible by three but does contain a 20 percent fifth and 14.3 percent seventh harmonic. The fifth harmonic is minimized by a short pitch winding of 0.75 τ_p and the selection of 16 slots.

Winding distribution: The winding distribution factors f_{w_λ} were calculated for a winding of four slots per pole and phase and a six-slot winding pitch. These factors were then used to determine the harmonic content of the EMF wave. Table 1-XI shows results.

TABLE 1-XI.- EMF WAVE RIPPLE AT HARMONIC POINTS

Harmonic	Percent Ripple
1	100.0
3	0
5	-1.4
7	-1.7
9	0
11	0.3

The resulting wave will be very nearly sinusoidal and should not result in additional losses or require smoothing.

Stator design: Selection of the air gap diameter is a compromise between best utilization of winding copper and allowance for a central shaft. A 2.79-cm (1.1-in.) diameter stator bore will produce the former, but a 3.30-cm (1.3-in.) diameter stator is desirable for the central shaft. Subsequent calculations are based on the larger diameter but with the flux density reduced to 2500 gauss. The overall stack length becomes 2.38 cm (0.938 in.).

Allegheny Ludlum AL-4750 or Carpenter 49 iron of 0.0152 cm (0.006 in.) thickness should be used to keep the core losses as low as possible. The stacking factor is 0.935, giving a total number of punchings of 146. Tooth and yoke cross sections are designed to keep flux density in the iron below 5000 gauss (normal flux densities of 10 000 - 13 000 gauss are used). The stator punching is shown in figure 1-13. At the maximum operating speed of 50 000 rpm, a two-pole machine is required for switching and core loss considerations. The two-pole machine as well as the low flux density make a relatively heavy yoke section. The slots are designed to provide sufficient winding cross section to keep copper losses down and at the same time to maintain the low tooth flux density.

The outside diameter of the stator is determined principally by three factors:

- A flux density in the teeth of approximately 5000 gauss.
- A slot cross section large enough to maintain comparable copper and core losses.
- An acceptably low flux density in the yoke or flux return path of the stator. With two poles, mechanical strength is a limiting factor.

The slot cross section is 23.4 mm^2 (0.0363 in^2), and with an assumed slot utilization of 39 percent as reasonable for this size machine, the copper cross section is 9.06 mm^2 (0.014 in^2). Estimated mean turn length is 18.4 cm (7.25 in.).

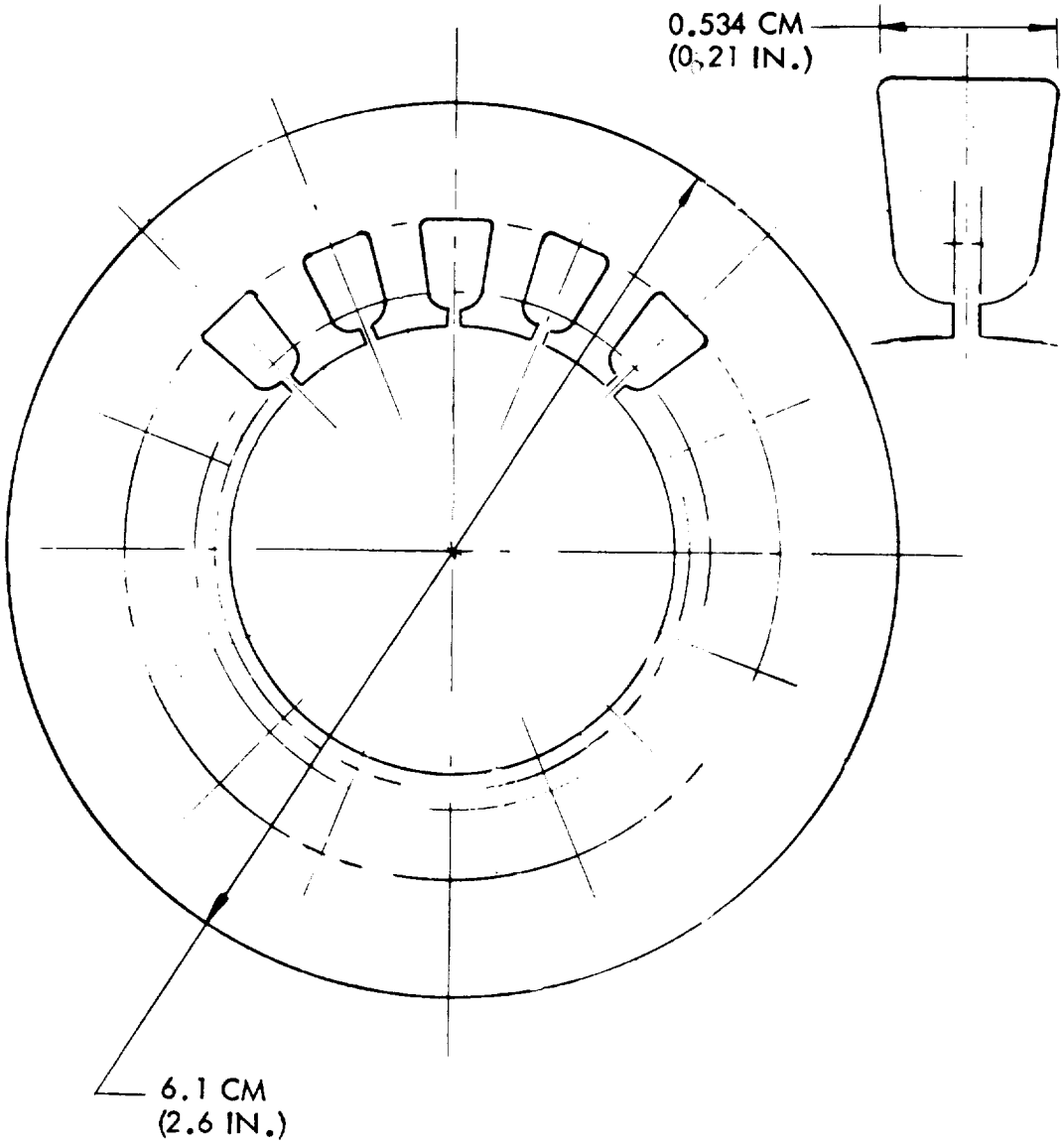

Figure 1-13. Stator Punching--TDRS

The winding diagram is shown in figure 1-14. Each winding section consists of four skeins of seven turns each having 10 parallel wires of AWG No. 29 HML. Winding resistance per phase is 0.0723 ohms (at 25°C) and includes lead resistance.

Rotor design: The rotor cross section is shown in figure 1-15. The rotor is designed to be either shaft-mounted or inserted in a hollow shaft. The overall air gap is 1.524 mm (0.060 in.) radial which would allow for a shrink ring or hollow shaft of 1.27 mm (0.050 in.) wall thickness. Rotor length is 2.38 cm (0.938 in.). Air gap flux density is 2267 gauss with an assumed leakage of 15 percent. Permeance is determined in the next section,

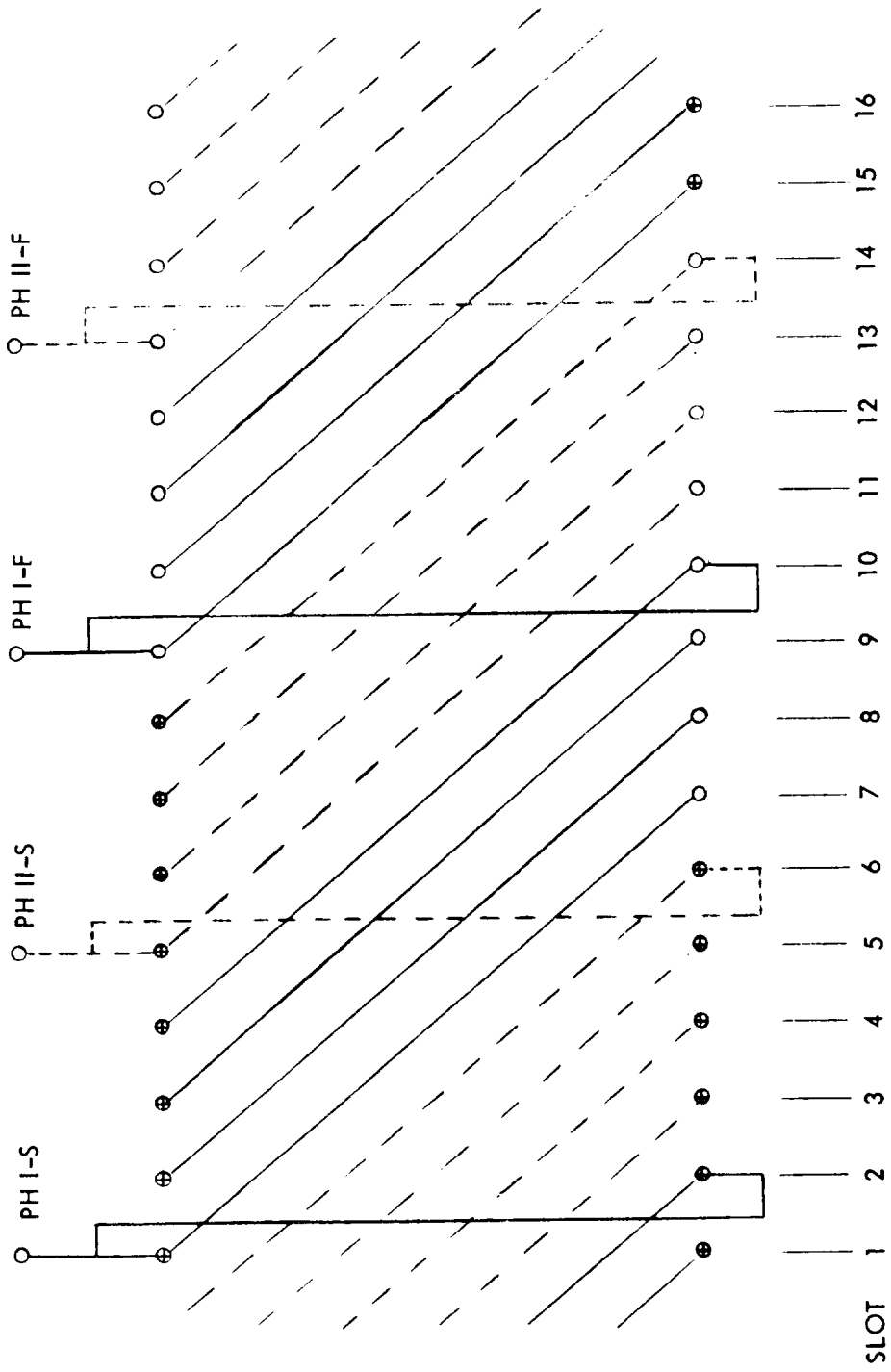

Figure 1-14. Winding Diagram--TDRS

which will yield an exact leakage. Centrifugal forces on the rotor cause a stress of 241 x 10^6 Newton/m^2 (35,000 psi) to appear in the shrink ring at maximum speed.

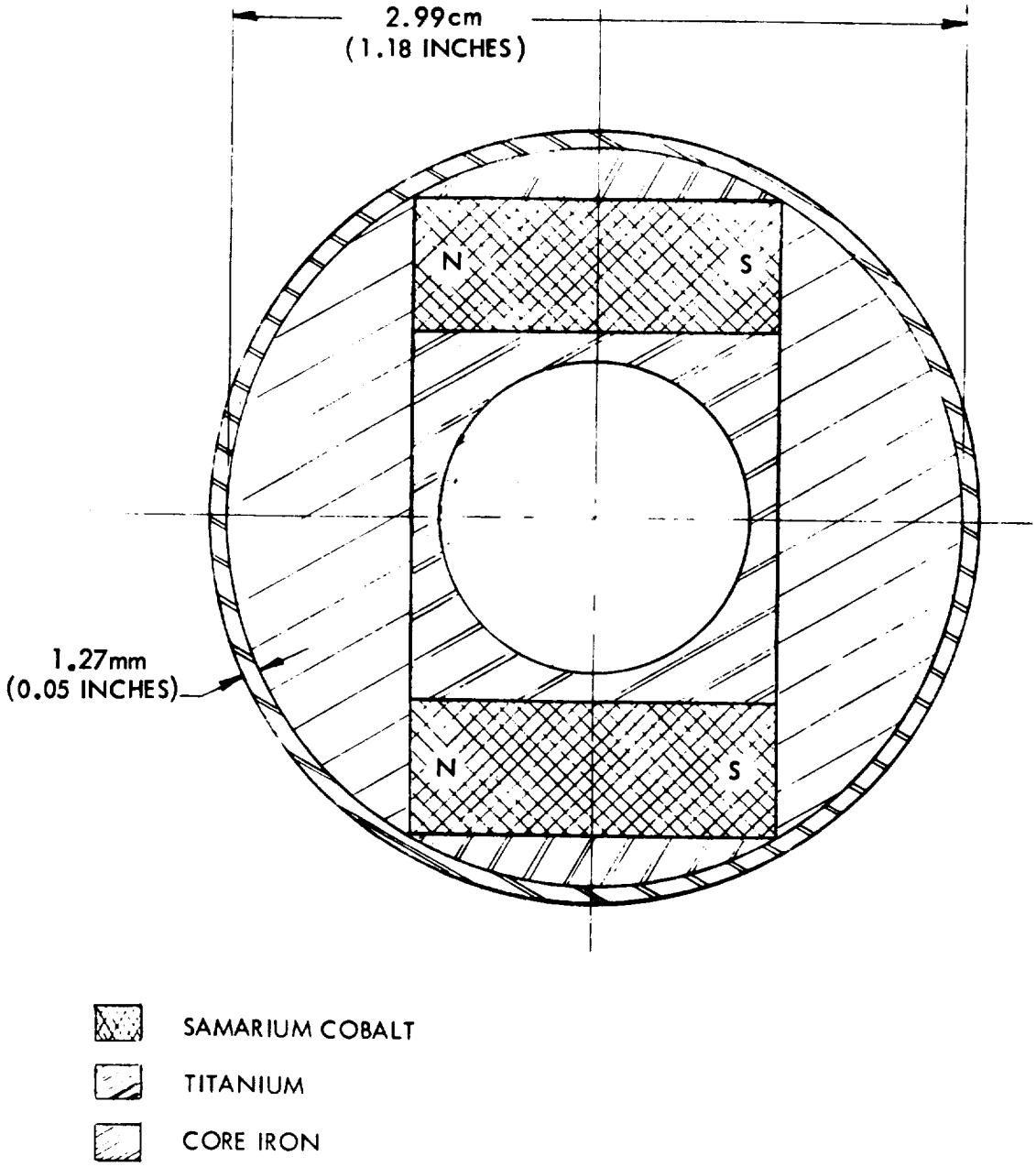

Figure 1-15. Rotor Cross-Section--TDRS

Permeance and winding inductance: The total air gap permeance, including the fringe permeances at the pole piece edges, is calculated to be 13.82 cm (5.44 in.). The total rotor permeance consists of the air gap permeance plus leakage permeances as given in Table 1-XII.

TABLE 1-XII.- TOTAL ROTOR PERMEANCE

Source	Permeance	
	cm	in
Total air gap	13.82	5.44
Leakage between pole pieces inside rotor	1.19	0.468
Leakage between pole piece edges	0.39	0.154
Rotor to stator leakage	1.76	0.693
Total	17.16	6.755

The resultant leakage flux is then $\frac{3.34}{17.16} \approx 19.5$ percent which is higher than estimated. The permeance coefficient is:

$$19.65 \frac{\text{Gauss}}{\text{Oersted}}$$

Figure 1-16 shows the $(B/H)_c$ line plotted on the demagnetization curve for samarium cobalt; the flux density in the neutral zone of the rotor magnet is 9000 gauss (8400 gauss was assumed initially). The pole flux is therefore, 1.5 percent higher than the first iteration, indicating the design is satisfactory with this safety margin.

The winding diagram shows that there are four fully-occupied slots per phase and each four slots have conductors either at the bottom or top of the slot. The total inductance of the winding is summarized in Table 1-XIII. The electrical time constant is: 2.05 milliseconds.

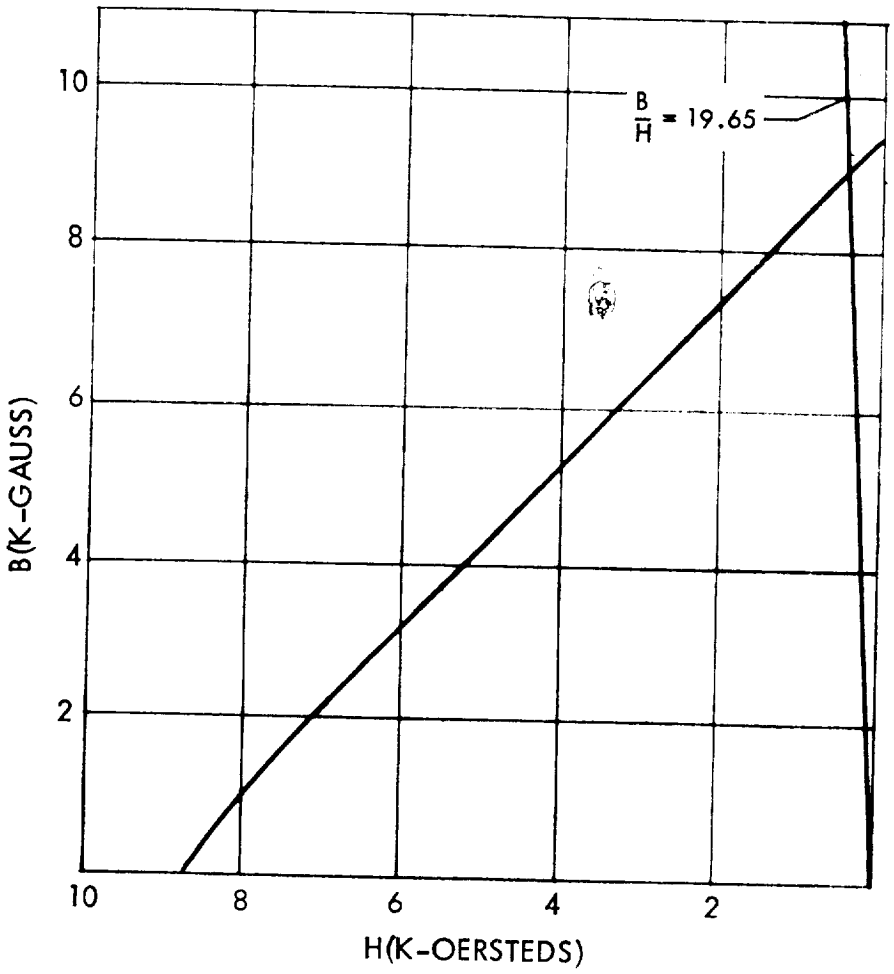

Figure 1-16. Demagnetization Curve--Samarium Cobalt

TABLE 1-XIII.- WINDING INDUCTANCE

Component	Inductance*
Slot leakage	18.8
Tooth head leakage	6.7
End turn leakage	24.4
Armature reaction	98.4
Total	148.3

*Microhenries

Core losses: The core loss is the sum of tooth and yoke losses. At the maximum efficiency point (39,500 rpm) f ≈ 660 Hz, the specific loss is 2.2 W per kg (1.0 W per lb) at 4840 gauss in the teeth. The flux density in the stator yoke is 4720 gauss, and the specific loss is 2.094 W per kg (0.95 W per lb) for the AL-4750 punchings. In prior designs, the specific core loss has been doubled to account for losses due to harmonics and increased losses due to strain in assembly. Losses have, in practice, been lower than those assumed, so the design is conservative. Using these higher specific losses:

Tooth loss = 0.4 W

Yoke loss = 1.2 W

Total = 1.6 W (1.7 W assumed)

The core losses are about 50 percent of the above at 25 000 rpm and 140 percent of the above at 50 000 rpm. With assumed pole face losses of 0.25 W at low speed due to armature reaction and 0.30 W loss at maximum speed due to higher frequencies, the core losses are:

1.10 W at 25 000 rpm

1.70 W at 39 500 rpm

2.70 W at 50 000 rpm

Efficiencies - Losses in the motor-generator consist of copper and core losses. The core losses are given above and copper losses are readily calculated knowing the winding resistance and current associated with the motor-generator load. Table 1-XIV summarizes losses and efficiencies for critical operating conditions. Efficiencies are also given for core losses as quoted by the material suppliers. In order to achieve the 97 percent efficiency goal, the motor must be very carefully built and a second design iteration probably would be desirable.

TABLE 1-XIV.- LOSSES AND EFFICIENCIES FOR TDRS MOTOR-GENERATOR

	Power (W)	Speed (rpm)	Core Loss (W)	Copper Loss (W)	Efficiency %	Efficiency % (1/2 core loss)
Motor	42.5	39 500	1.70	0.38	96.3	97.2
Generator	60.0	39 500	1.70	0.72	96.1	97.5
Generator	120.0	25 000	1.10	9.10	92.2	95.5
Generator	120.0	50 000	2.70	1.76	96.4	97.5

Motor-generator characteristics: The motor-generator design characteristics are summarized in Table 1-XV. The stator punching is shown in figure 1-13, the winding diagram appears in figure 1-14, and the rotor cross section in figure 1-15. For performance under various load and speed conditions, refer to Table 1-XIV.

TABLE 1-XV.- TDRS MOTOR-GENERATOR DESIGN CHARACTERISTICS

Physical characteristics	
Outside diameter	6.604 cm (2.600 in.)
Overall length	4.419 cm (1.74 in.)
Stator material	AL-4750 0.015 cm (0.006 in.) thick
Stack length	2.375 cm (0.935 in.)
Stator bore	3.302 cm (1.300 in.)
Number of slots	16
Iron to iron gap	0.152 cm (0.060 in.)
Rotor material	Core iron - cobalt samarium
Rotor diameter	2.997 cm (1.180 in.)
Rotor length	2.375 cm (0.935 in.)
Number of poles	2
Stator weight	0.567 kg (1.25 lb)
Rotor weight	0.158 kg (0.35 lb)
Total motor weight	0.726 kg (1.60 lb)
Winding characteristics	
Number of phases	2
Pitch	6 slots
Slots per pole and phase	4
Wire size	No. 29 HML
Slot utilization (bare Cu)	39%
Winding	4 skeins, 7 turns each having 10 parallel wires
Approximate turn length	18.41 cm (7.25 in.)
Electrical characteristics	
Rated output	120 W
Speed range	25 000 - 50 000 rpm
Voltage	28 Vdc
Back EMF constant, K_E	4.584×10^{-3} V/rad/sec
Torque constant, K_T	4.58×10^{-3} N-m/amps (3.381×10^{-3} ft-lb/amp)
Winding resistance per phase	0.0723 ohm
Winding inductance per phase	148 μH
Electrical time constant	2.05 milliseconds

Spin bearing system.- The spin bearing system consists of the two spin bearings, the methods for preloading these bearings, and a means to lubricate the bearings during their lifetime. The TDRS design uses conventional ball bearings of moderate precision for high-speed, long life application.

Bearing selection: In the selection of the spin bearings for the TDRS wheel the considerations include:

- Static load capability under launch conditions
- Bearing life
- Bearing losses
- Bearing stiffness

The launch loading is 365 N (82 lb) at 10g and 1824 N (410 lb) total at 50g. The launch load is expected to be at some point between these values. If we take the higher value, the maximum radial load will be 912 N (205 lb) and the thrust load 1824 N (410 lb). The 38H bearing is selected on the basis of both launch load survival and life.

For the TDRS, five ball bearing types were selected for consideration. These are listed in Table 1-XVI. The L_{10} life requirement was originally estimated to be 186 300 hours. The reliability analysis shows that the spin bearings are a major source of failure if redundancy is utilized in the electronics. It is therefore possible to accept a lower L_{10} life from the spin bearings and meet the overall reliability requirement. At a revised estimate of R = 0.985 for 5 years for a spin bearing, $L_{1.5}$ = 43 800 hours and L_{10} = 148 500 hours.

TABLE 1-XVI.- SPIN BEARING SELECTION FOR TDRS

Bearing	Static Load Rating- N (lb)				L_{10}-Life (hrs) at 50 000 rpm*
	Radial		Thrust		
R-4	312	(70)	253	(125)	1 810
R-36	507	(114)	388	(192)	4 620
Z-114	498	(112)	376	(186)	4 620
38BX2	743	(167)	1339	(301)	28 400
38H	1379	(310)	3204	(720)	160 000

*At 22.2 N (5-lb) preload

Conventional bearings are considered adequate for the TDRS design. Life ratings, DN ratings, and bearing design have all been defined conservatively.

As can be noted in Table 1-XVI L_{10} life was calculated for a case of 50 000 rpm for the total 5-year operational life. As shown in Table 1-II, IPACS units are operated at maximum speed for only a quarter of mission

life. Three quarters of the time operation is at 8250 rpm maximum. The L_{10} life value would significantly exceed 160 000 hours when calculated for actual operating speeds. L_{10} rating is only considered indicative of bearing operation at values above 100 000 hours so refined calculations are considered somewhat superfluous.

The DN rating of the bearing also indicates the suitability of a conventional bearing design. DN is a speed factor used to gauge the suitability of rolling element bearings to high-speed applications; it is the bore diameter D in millimeters, multiplied by the shaft rotation speed N in rpm. The DN numbers are thus surface speed values and are affected by bearing design characteristics, which include surface finishes, retainer strength, friction properties, and internal clearances. Each "standard" bearing could therefore be assigned a DN value which establishes its upper speed limit. Table 1-XVII lists general DN limits for ball bearings with oiler lubrication (reference 1-1).

TABLE 1-XVII.- SPEED LIMITS FOR BALL AND ROLLER BEARINGS

Lubrication	DN Limit (mm x rpm)
OIL	
Conventional bearing designs	300 000 to 350 000
Special finishes and separators	1 000 000 to 1 500 000

For a quarter of its operational life the IPACS operates at an average DN of 300 000. The remainder of the time DN values are less than 65 000.

A life safety margin is attainable by specifying special precision bearings to, or above, ABEC 7 levels with consumed electrode vacuum melt (CEVM) M-50 tool steel materials and low race waviness. An improvement in life by a factor of 5 to 10 is considered possible.

The other consideration in bearing selection is loss at operating speed. The two bearings which most closely meet the launch and life requirements are the 38BX2 and 38H bearings. Bearing losses at 50 000 rpm are included in Table 1-XVIII. Since the 38H bearing is superior on all three counts (static load, life, friction), it was chosen. The TDRS motor-generator size is relatively small so that the bearing losses become a significant portion of the total charging or discharge wattage at maximum speed. For this reason, the smallest bearing which will meet load and life requirements must be selected since this bearing will produce the minimum drag losses.

An angular contact bearing is used to provide adequate bearing stiffness values. Natural frequencies must be above 100 Hz to meet vibration test requirements.

TABLE 1-XVIII.- SPIN BEARING LOSSES AT 50 000 RPM

Item	38BX2 Bearings	38H Bearings
Applied load friction - N-cm (in.oz).	0.09371(0.133)	0.0725 (0.103)
Viscous drag - N-cm (in. oz.)	0.0295 (0.042)	0.029 (0.042)
Total drag - N-cm (in. oz.)	0.123 (0.175)	0.102 (0.145)
Total drag power - W	6.46	5.37

Preload methods - In the selection of the spin bearing preload method, four approaches were investigated:

- Preloading across frame
- Preload rod
- Spring loading
- Centrifugal preloader

The first was rejected because of the weight penalty incurred in obtaining the stiffness required. The centrifugal preloader (figure 1-17) was discarded because of the slide fit necessary for the inner race of the bearing. This would cause dynamic balance uncertainties.

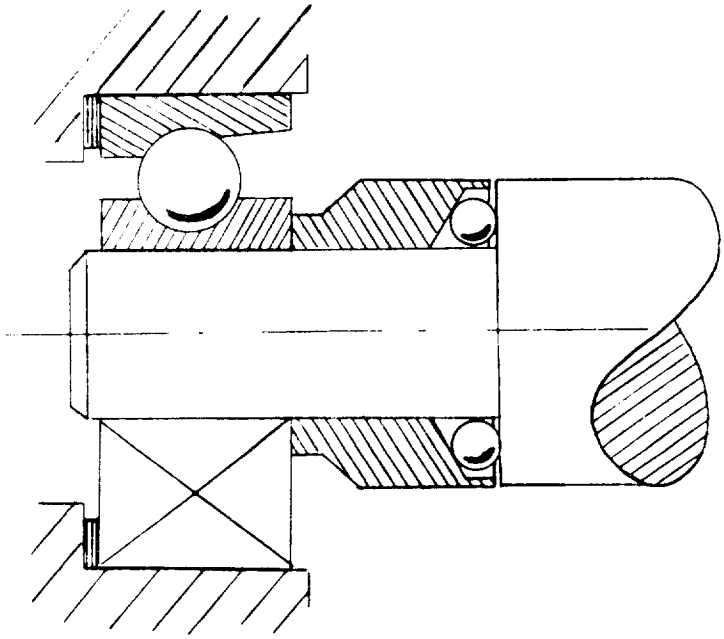

Figure 1-17. Centrifugal Preloader

Both the preload rod approach and the spring loading method are feasible candidates. The preload rod was picked for the TDRS since it was possible to provide a central hole in the shaft without developing an excessive stress concentration in the wheel. The spring preload also could be used for the TDRS but the extra complexity of a launch lock mechanism is required. This approach is used in the RAM and is discussed there.

Preload method selected for TDRS: The spin bearings are preloaded at 22.2 N (5 lb) by a rod extending through a hole in the rotor shaft. This rod ties the outer races of both bearings together and axially loads the bearings by applying pressure through the outer races to the bearing balls and then to the inner races and through the shaft. The axial stiffness of rod and shaft and their thermal similarity make this preload method advantageous when a hole can be placed through the shaft. This preload method eliminates the need for a launch lock (as required in the RAM design) and minimizes the effects of thermal and pressure changes in the enclosure.

Tension in the rod supplies the preload through an adjustable nut on one end of the rod. Each end of the rod is terminated at a ball joint to prevent misalignment loads on the bearings. Small changes in preload, due to dimensional changes of the enclosure, are reduced by a bearing support ring which permits one bearing to be freely supported in the axial direction.

To maintain constant spin bearing preload, the bearings must be isolated from axial motion of the conical enclosure which may be as much as $\pm$ 0.127 mm ($\pm$ 0.005 in.). This is accomplished by the combined use of the preload rod and the design of a bearing support member which provides high radial stiffness and low axial stiffness. This bearing support ring is shown in figure 1-18. It consists of two coupled four-spoke members with each spoke 12.7 x .127 mm (0.50 x 0.005 in.). Characteristics of this bearing support ring are:

Axial stiffness	- 14 639 N/m (83 lb/in.)
Radial stiffness	- 7.14×10^7 N/m (407,000 lb/in.)
$\frac{\text{Radial}}{\text{Axial}}$ stiffness	- 4900
Maximum radial load (at 68.9×10^7 N/m^2)	- 2220 N (500 lb)
Worst case preload change	- 8.3%

The worst case preload change of 8.3% or 1.84 N (0.415 lb) is based on an enclosure motion of $\pm$0.127 mm ($\pm$0.005 in.). Since this condition is only realized with one atmosphere of pressure differential between outside and inside the wheel enclosure it will not be obtained under normal operating conditions.

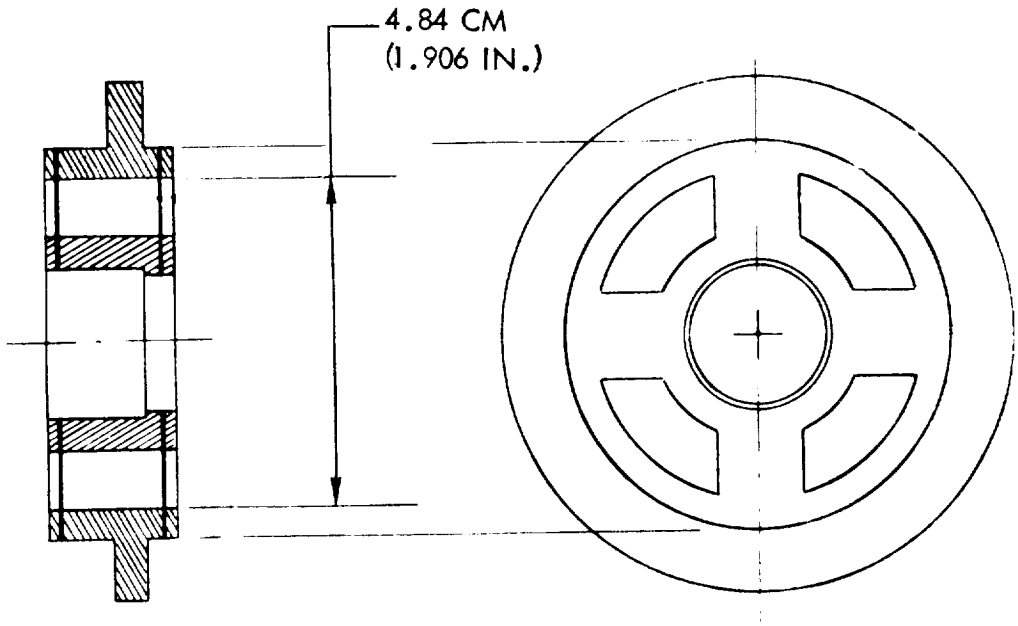

Figure 1-18. Bearing Support Ring--TDRS

Spin bearing lubrication: The spin bearings must be lubricated during the five-year life. This lubrication should be sufficient but not excessive. Excessive lubrication will increase the viscous drag component of the bearing power loss and at 50 000 rpm this would amount to about one-half the total power.

The lubricant chosen is RL-743. Evaluation tests on spin bearings using grease and various oils have shown that RL-743 oil is superior. This oil has low drag under vacuum conditions and is readily stored and metered into the bearings.

Centrifugal oilers are used to meter the oil to each bearing. The oilers are attached to the ends of the spin shaft adjacent to bearings. The cylindrical storage chamber contains felt (SAE-F10) saturated with 1.05 cc of oil. The oil is metered at 3.1×10^{-6} cc per hour at 23.9°C (75°F) through a calibrated leak. The metering device (calibrated leak)is a small threaded cylinder of sintered material .32 cm (1/8 in.) in diameter by .645 cm (1/4 in.) long. Porosity is selected to provide the desired flow rate. The centrifugal forces generate a pressure of 324×10^3 N/m^2 (47 psi) to force the oil through the calibrated leak. A peripheral lip carries the oil to the bearing race. The flow rate will vary from 0.34×10^{-6} cc per hour at -6.7°C (20°F) to 15.5×10^{-6} cc per hour at 60°C (140°F). Enough oil is contained to lubricate the bearings for 7.7 years at the highest flow rate. During storage periods, the oil flow is zero. The centrifugal oiler in general provides oil flow as required by the operating conditions. Flow is high at elevated temperatures and at high speeds where additional lubrication is needed. Also, if bearings become heavily loaded then temperature increases and oil flow increases.

The centrifugal oiler reservoir contains a felt which allows filling to 75-percent capacity. Deaerated oil is used and trapped air is avoided by bottom to top filling. The oilers are stored in a vacuum environment prior to use.

At assembly, the oilers are slipped on the rotor shaft extensions and secured with a lock nut. The oiler is a close sliding fit on the shaft. A small orifice near the shaft permits equalization of internal pressure. The metered flow is through a calibrated orifice at the maximum centrifugal pressure point.

Physical and performance characteristics.- Physical characteristics of the TDRS wheel assembly and components are given in Table 1-XIX. Performance characteristics of the TDRS wheel assembly and components are given in Table 1-XX.

TABLE 1-XIX.- TDRS WHEEL ASSEMBLY CHARACTERISTICS SUMMARY

Wheel assembly	
Total weight	5.61 kg (12.4 lb)
Maximum diameter	37.8 cm (14.85 in.)
Axial length	20.6 cm (8.10 in.)
Mounting	at rim of enclosure
Internal vacuum	<0.1 micron
Rotor	
Diameter	34.04 cm (13.4 in.)
Weight	3.72 kg (8.2 lb)
Inertia	0.0332 N-m-sec^2 (0.0245 ft-lb-sec^2)
Material	Titanium alloy 6AL-6V-2SN
Spin bearings	
Size	38H angular contact
Material	vacuum melt M-50 tool steel
Lubricant	RL-743 oil
Preload	22.2 N (5 lb)
Weight (2)	0.0272 kg (0.06 lb)
Centrifugal oiler	
Size	1.905 cm diam. x 1.905 cm long (0.75 in. diam. x 0.75 in. long)
Weight (2)	0.136 kg (0.30 lb)
Reservoir	1.05 cc
Motor-generator	
Type	DC permanent magnet, brushless
Size	6.60 cm diam. x 4.45 cm long (2.6 in. diam. x 1.75 in. long)
Number of poles	2
Number of phases	2
Rated voltage	28 V dc
Total weight	0.725 kg (1.60 lb)
Enclosure	
Material and thickness	Aluminum alloy 1.40 mm (0.055 in.)
Type	Truncated cones suitable for vacuum
Seal	Gask-O-Seal
Venting	Breather hole with filter
Weight	0.675 kg (1.49 lb)

TABLE 1-XX.- TDRS WHEEL ASSEMBLY PERFORMANCE CHARACTERISTICS

Wheel assembly	
Maximum input/output power	120 W
Voltage	28 V
Minimum natural frequency	
Linear - along spin axis	195 Hz
Linear - perpendicular to spin axis	308 Hz
Torsional - perpendicular to spin axis	185 Hz
Rotor	
Operating speed range	25 000 - 50 000 rpm
Maximum angular momentum	174 N-m-sec (128 ft-lb-sec)
Maximum energy storage	126 W-hr
Minimum spin-up time	2.2 hr
Maximum coast down-time	44 hr
Dynamic balance	0.254 micro meters (10 microinches)
Spin Bearings	
Static load rating (radial)	1375 N (310 lb)
(axial)	3195 N (720 lb)
Bearing drag at 50 000 rpm (2 bearings)	5.4 W
L_{10} Life	160 000 to 800 000 hr
Axial stiffness	62.4×10^5 N/m (35 400 lb/in.)
Radial stiffness	40.6×10^5 N/m (230 500 lb/in.)
Centrifugal oiler	
Oil flow rate at 6.67°C (20°F)	0.34×10^{-6} cc/hr
Oil flow rate at 60°C (140°F)	15.5×10^{-6} cc/hr
Worst case lubricating capacity	7.7 years
Motor-generator	
Input/output voltage	28 V dc
Back EMF constant	0.00458 V/rad/sec
Torque constant	4.58×10^{-3} N-m/amp (0.00338 ft lb/amp)
Maximum input/output	120 W
Electrical time constant	0.00205 sec
Efficiency (average)	96%

TABLE 1-XX.- TDRS WHEEL ASSEMBLY PERFORMANCE CHARACTERISTICS - Concluded

Enclosure	
Vacuum ground test	$<.4$ N/m^2 <3 microns
Vacuum orbit	$<.14$ N/m^2 <1 micron
Leak/outgassing rate	$<.014$ N/m^2/hr < 0.1 micron/hr
Linear stiffness along spin axis	1.05×10^8 N/m (5.98×10^5 lb/in.)
Linear stiffness perpendicular to spin axis	3.73×10^8 N/m (2.12×10^6 lb/in.)
Torsional stiffness perpendicular to spin axis	1.16×10^6 N-m/rad (10.3×10^6 in.lb/rad)
Sensors	
Speed	
Type	Magnetic
Pulses per revolution	60
Output (at minimum speed)	6 V p.p.
Temperature	
Type	Thermistor
Range	0-100°C
Accuracy	2°C
Vibration	
Type	Accelerometer
Output in millivolts/g	100

Electronics.- The electronics for the IPACS will drive the permanent magnet brushless motor to spin up the momentum/energy storage wheel. The same electronics and motor will act as a generation system to return power to the line. The requirements and interfaces for the electronics are given in Table 1-XXI. Symbols used in this subsection are defined as follows:

I_C - Motor coil current, amps

I_L - Load current, amps

I_m - Total current to motor/generator electronics, amps

I_S - Solar array current, amps

I_w - Rotor inertia, N-m-sec^2

K_I	-	Current feedback loop amplifier, 1/amps
K_T	-	Motor torque constant
K_V	-	Motor generator constant, V/rad/sec
L_C	-	Motor coil inductance, henries
n	-	DC transformer ratio
PG	-	Power ground
R_C	-	Coil resistance, ohms
R_{L_1}, R_{L_2}	-	Load resistance, ohms
R_S	-	Shunt resistance, ohms (motor coil current measurement
V_C	-	Voltage across motor coil, V
V_L	-	Load voltage, volts
ω	-	Rotor speed, rad/sec

TABLE 1-XXI.- TDRS ELECTRONICS REQUIREMENTS

Number of phases	2
Input voltage	28 Vdc
Maximum motor input power	120 W
Average motor input power	42.5 W
Maximum generator output	120 W
Average generator output	60 W
Operating speed range	25 000 - 50 000 rpm
Motor-generator winding resistance per phase	0.072 ohms
Motor-generator winding inductance per phase	148 μH
Motor control - spin up	constant torque
Motor control - charging	constant power
Generator control - discharging	constant line voltage
Efficiency of electronics at maximum output	85.5%
Electronic size	<820 cm^3 (< 50 $in.^3$)
Electronic weight	<1.0 kg (<2.2 lb)
Failure rate per 10^6 hours	<2.88
Ambient temperature range	-6.67°C - 60°C (20°F - 140°F)

Functional block diagram: There are three energy modes of operation of the wheel assembly:

- Spin up - Constant torque is applied to the wheel by monitoring current through a feedback resistor in the motor winding.
- Charging - Energy is added to the wheel from 25 000 to 50 000 rpm by a constant power circuit which monitors both torque and speed.
- Discharging - Energy is removed from the wheel at command from the voltage regulator circuit operating on the 28 Vdc bus.

Overriding operating limits are established for:

- Overspeed
- Minimum power return speed
- Over current protection
- Motor-generator overheating

A functional block diagram of the electronics is shown in figure 1-19. It can be noted that identical electronics are used for the spin motors of the RAM assembly. The RAM units are rated at 52 V but do not change in design or function.

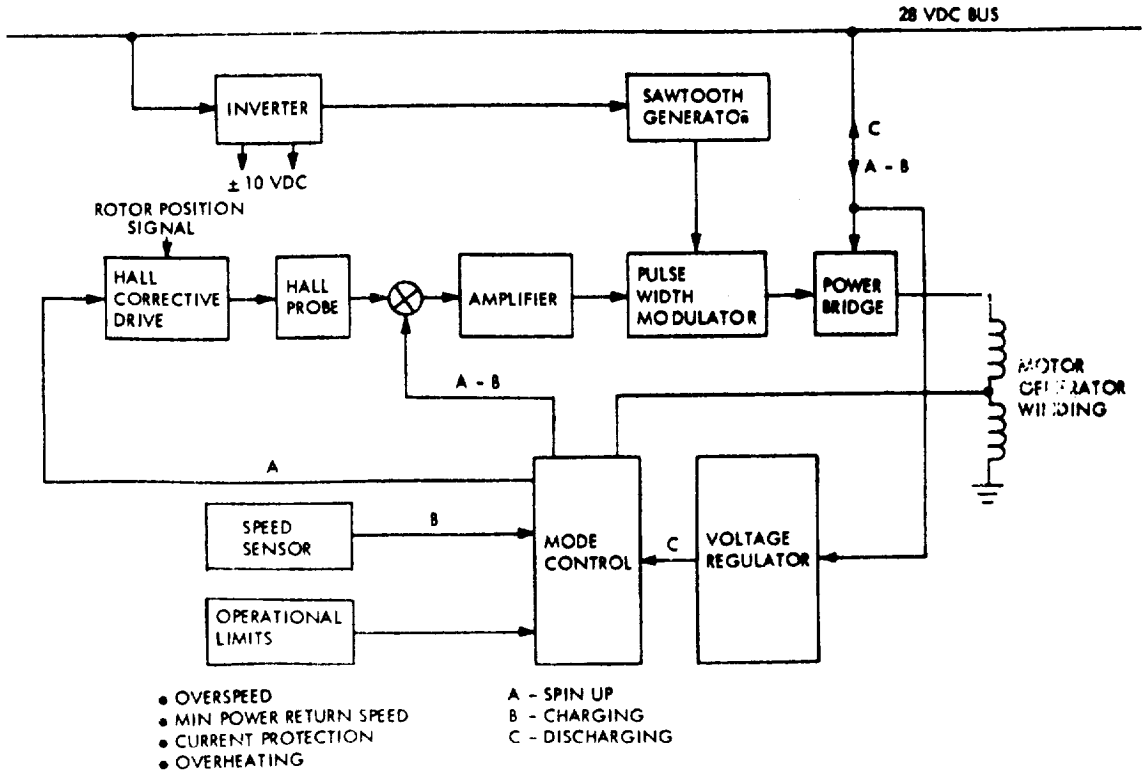

Figure 1-19. Motor/Generator Electronics Functional Block Diagram

Circuit model: Figure 1-20 is the IPACS circuit model which best represents the operation of the dc motor/generator and electronics. The key element is the dc transformer with a controllable transfer ratio which shows the dual operation (charge-discharge) of the motor and electronics. It represents the function of the high frequency (20 KHz) pulse-width modulat power amplifiers used to drive and commutate the two-phase motor. The transfer ratio, n, is controlled by the current feedback loop and any other outer loops to maintain the motor torque at the desired level.

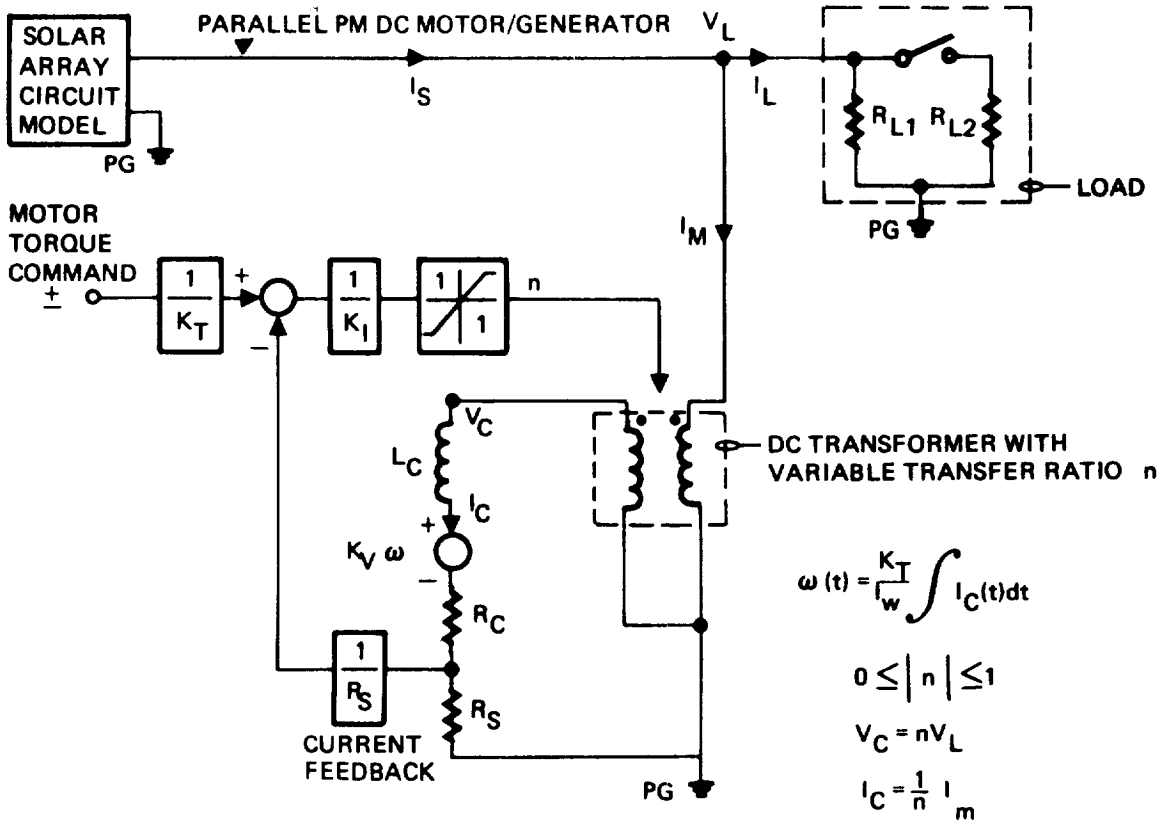

Figure 1-20. IPACS Circuit Model

In a more sophisticated model, power losses would be represented by

(1) DC transformer efficiency < 100%

(2) Changes in K_T and K_V with speed

Figure 1-21 shows a schematic of the power bridge used for the brushless dc motor/generator. One bridge is required for each motor phase. The bridge

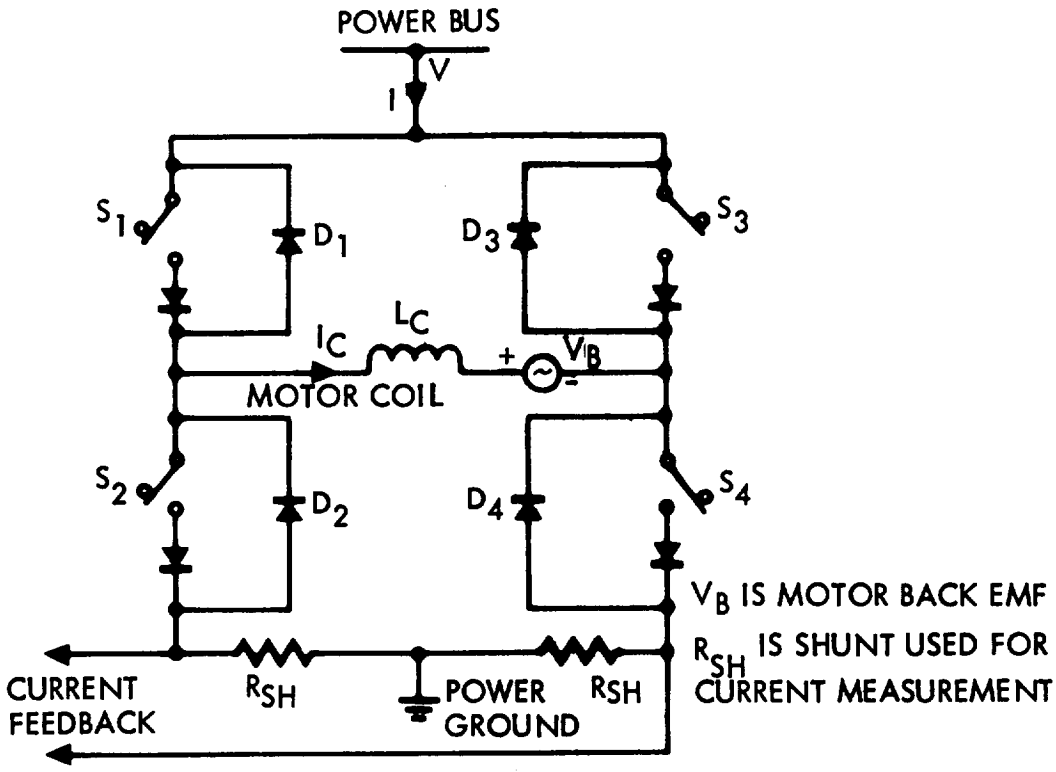

Figure 1-21. Motor/Generator Electronics Power Bridge

is time-ratio controlled at a high frequency (10-20 KHz) to deliver a given average current through the motor coil. Switches S1 through S4 are two-transistor Darlingtons.

The modes of operation of the bridge are as follows:

(1) Charge - Apply torque to rotor to spin up. If the back EMF, V_B, is the polarity shown, then S3 is always open and S4 is always closed. S1 and S2 are time ratio controlled.

- S1 closed, S2 open. Current flows through the coil in the direction shown and through the current measuring shunt to ground

- S1 open, S2 closed. Free wheeling, current flows through D2 from ground, through coil in the same direction and through S4 to the ground.

When the polarity of the back EMF changes, the other side of the bridge is used in the same manner as above.

S1 open always
S2 closed always
S3, S4 time-ratio controlled

(2) Discharge - Apply torque to rotor to spin down. If the back EMF is the polarity shown, then again S3 is always open and S4 always closed. S1 and S2 are time-ratio controlled.

- S2 closed, S1 open. Current flows from ground through D4 through the coil and to ground through S2.

- S2 open, S1 closed. Current flows from ground through D4, through the coil, and to the power bus through D1 (power return). Power return can be described as a high-frequency "inductive kick" produced by a current which is the result of the back EMF.

The only difference between the efficiency in the charge-discharge cycles is the difference in power required to use the diodes compared to the saturated transistors.

Schematic: A typical schematic is shown in figure 1-22. The pulse width modulator, power bridge, and predrivers are hybrid circuits.

Electronic efficiencies: The efficiency of the electronics when operating in the motor or generator mode is approximated by the expression

$$E = \frac{100}{1 + \frac{3}{V} + \frac{W_s}{10^6} + \frac{0.05P_o}{V^2} + 0.005}$$

where

E = efficiency in %

P_o = electronic output power, W

V = line voltage

W_s = wheel speed in rpm

The efficiencies for the TDRS electronics are plotted in figure 1-23 for the maximum and minimum operating speeds and the mean energy wheel speed.

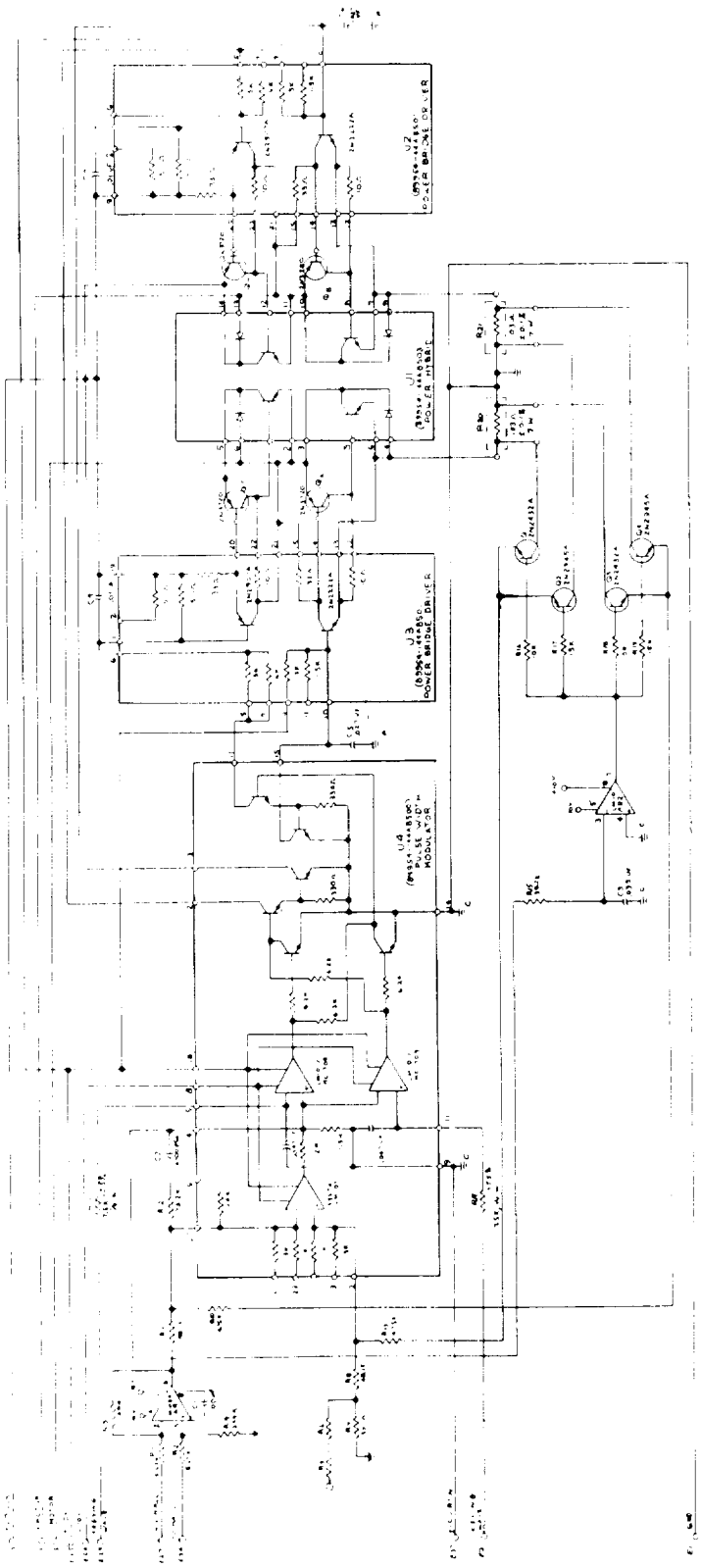

Figure 1-22. Power Amplifier Electrical Schematic

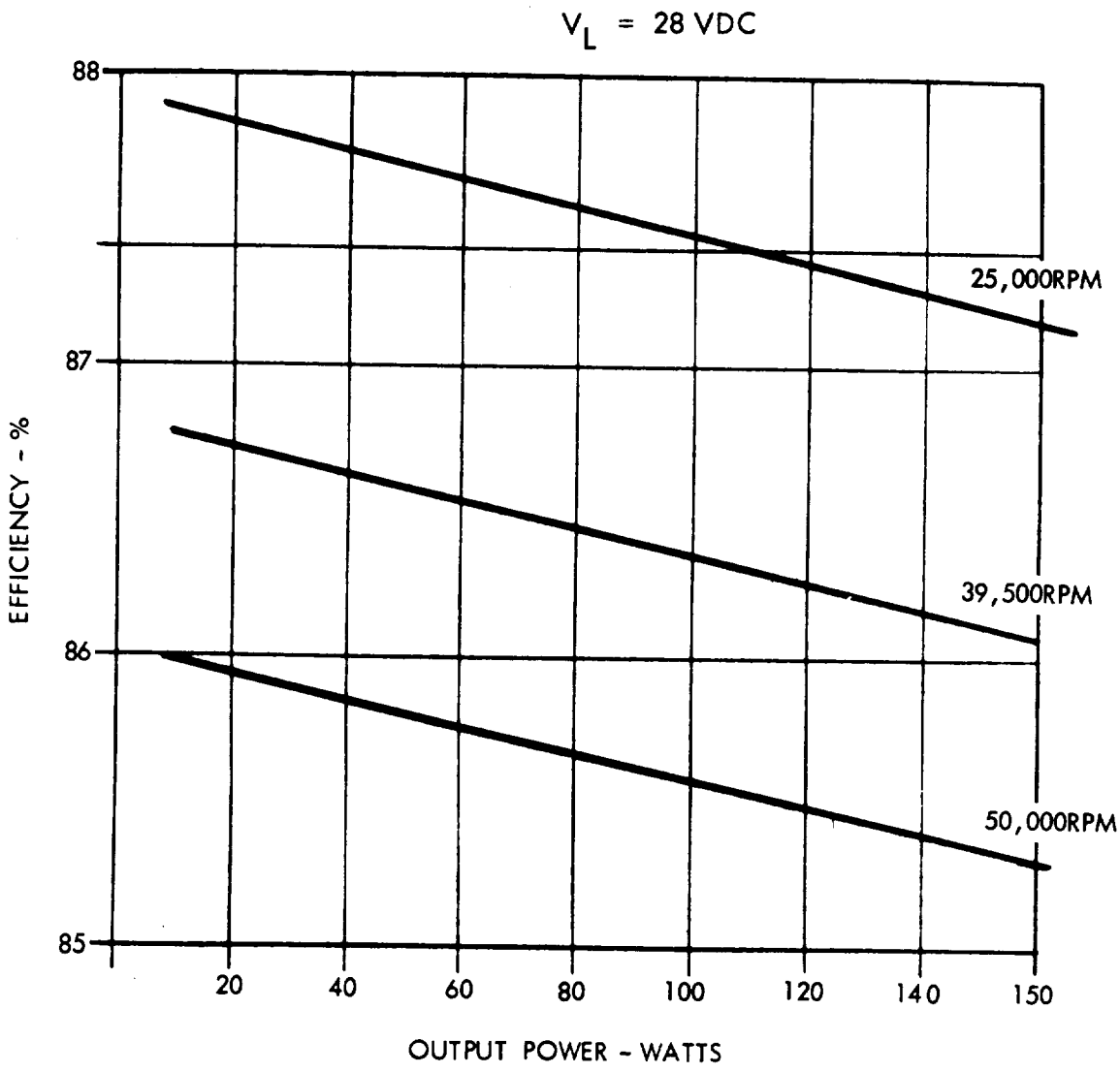

Figure 1-23. TDRS Electronic Efficiencies

Horizon sensor.- The baseline system design for the TDRS spacecraft locates the horizon sensors on the momentum wheels. The wheels thus perform the scanning function for the horizon measurements. Because of the high wheel speeds in the IPACS concept the horizon sensor must be separate from the wheels. Table 1-XXII shows three sensors considered. The selection criteria were based on a desire to include a sensor that is representative of a flight-qualified unit which is capable of meeting the performance requirements of the competitive system. The Unit C was rejected because it is not presently flight-qualified. The Unit A was selected because of superior physical characteristics and lower cost. The function of the selected unit in this analysis was only to have representative data on cost, weight, and volume penalties of the IPACS concept relative to the competitive baseline.

TABLE 1-XXII.- HORIZON SENSOR TRADE FOR TDRS

Factor	Unit characteristics		
	Unit A	Unit B	Unit C
Weight, kg (lb)	3.27 (7.2)	5.46 (12.04)	1.8 (4)
Power, W	2.0	6.5	5
Size or volume, m^3 ($in.^3$)	0.0048 (293)	0.0078 (479)	0.0022 (134)
Accuracy rad (deg)	$\pm$0.00175 ($\pm$0.1°)	$\pm$0.00052 ($\pm$0.03°)3	$\pm$0.00087 ($\pm$0.05)
Components	Single unit	2 heads + electronics	Single unit
Comments	1. Flight-qualified 2. Analog output 3. MTBF = 533 000 hr 4. No moving parts	1. Flight units contracted 2. Digital output 3. Offset point capability	1. Adaptation of existing qualified unit 2. MTBF = 250 000 hr 3. Uses torsion bar, resonant, scanning mirror

Distribution and regulation.- Figure 1-3 shows the TDRS IPACS electrical block diagram. The solar array output voltage at beginning of life is 30 to 34 V depending on temperature. In order to maintain bus voltage to 28 $\pm$ 5% Vdc, all excess energy is utilized by the IPACS energy storage wheels until maximum speed is reached. The shunt dissipators are then activated sequentially until the voltage has dropped to within allowable limits. In this manner overvoltage conditions are controlled. Should the loads become excessive or the array enter an eclipse, the bus voltage will drop below 26.6 V at which time the IPACS units will be switched to generate mode and supply power to the bus. To provide proper voltage regulation, the IPACS unit must be designed to provide power at 28 $\pm$ 1.4 V over the speed range of 25 000 to 50 000 rpm and 8250 to 4900 rpm with variable load conditions. The motor/generator electronics include amplifiers and inverters which cause transients in output power and induce line interference in the 10 to 15 kHz frequency range. Also, to control voltage within the required limits over the speed range, control within the IPACS electronics units or separate voltage control probably will be necessary. The most efficient type of pulse width modulation (PWM) regulator generates high-frequency ripple in voltage and current which may be as high as 5 percent of the operating level. This interference can add to the lower frequency stator switching transients and harmonics of 2 to 3 percent to produce higher amplitude spikes. This interference can be filtered with the required attenuation with losses of less than 2 percent. This filter will be included in the TDRS IPACS motor-generator electronics units.

TDRS IPACS Design Characteristics

The reliability, safety, vibration and acoustic noise, and maintainability characteristics discussed in this section relate primarily to the IPACS wheel assembly. In other subassemblies or components these factors do not differ from those of the conventional design.

Reliability.- IPACS and power and control system reliability are estimated in the following paragraphs.

IPACS reliability: A preliminary reliability analysis was performed for the TDRS IPACS wheel assembly and electronics and a model was developed. Failure rates of electronic parts are principally from RADC Reliability Notebook TR 67-108 using high reliability burn-in parts operating at low stress levels. For hybrid and monolithic integrated circuits, a GE-developed failure model was used.

Failure rates for mechanical and electromechanical components are not as well documented and have been obtained from various General Electric, General Dynamics, and Martin reports. Operation of these components is in a light-duty cycle.

The failure rates for electronics and wheel assembly are given in Table 1-XXIII. Note that the principal failure rates are electronic components and the spin bearings. Use of redundant electronics will improve reliability at minimum expense. The resulting reliability diagram is shown in figure 1-24. The single remaining critical component is the spin bearing and this must be emphasized in the design since we now have both power as well as attitude control dependent on the operation of the spin bearing. Since spin bearing redundancy within the wheel assembly unit is not easily achieved, the redundancy, if necessary, will be in additional wheel assemblies.

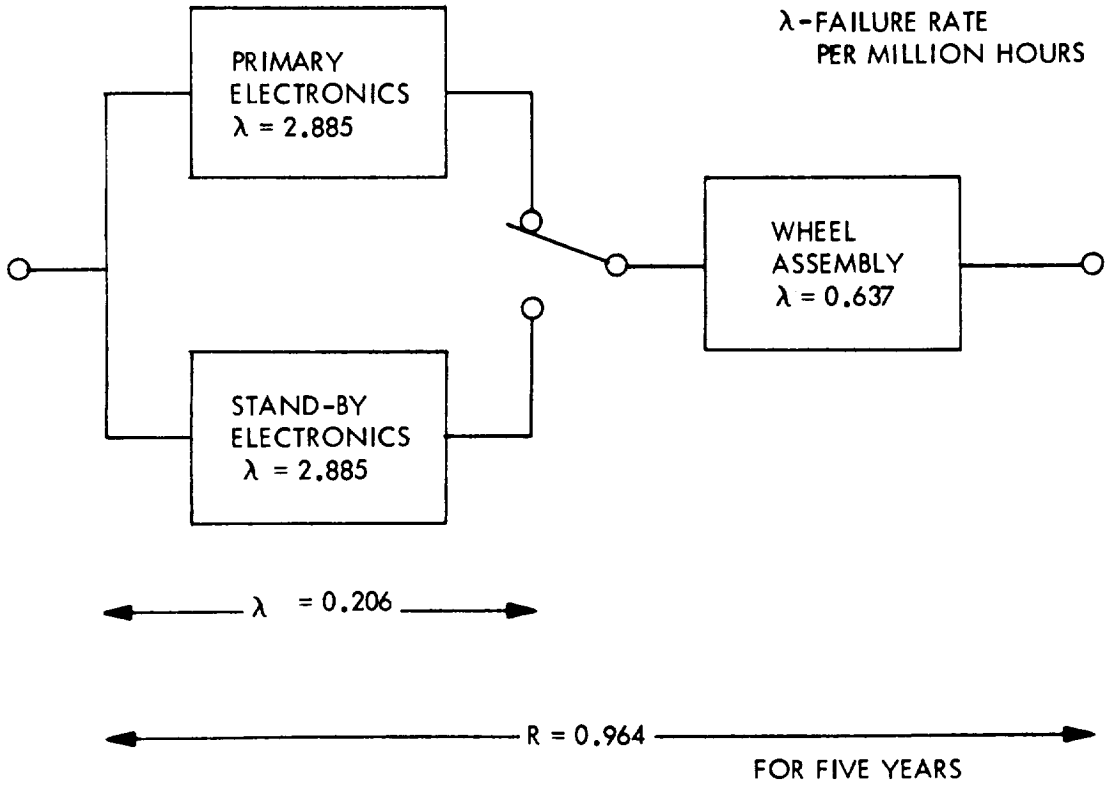

Figure 1-24. Reliability Diagram for IPACS Components--TDRS

Power and control system reliability: Of significance in the TDRS design is the reliability of the total power and control system with an IPACS design. Table 1-XXIV presents the subsystem reliability allocations and analytical predictions for TDRS. In figure 1-25 the electrical power system reliability diagram for the conventional system is presented. Figure 1-26 presents the same data for the control system.

TABLE 1-XXIII.- FAILURE RATES OF IPACS COMPONENTS FOR TDRS

Item	No. of failures per 10^6 hr
Electronics - λ_T = 2.885	
2 Hall probes at 0.100	0.200
2 LM 107 at 0.06064	0.121
7 LM 108A at 0.05443	0.381
1 NM 002 at 0.06644	0.066
4 hybrid predrivers at 0.06917	0.277
2 hybrid PWM at 0.08543	0.171
2 hybrid power amps at 0.2083	0.417
8 2N3720 at 0.04133	0.330
4 2N2432 at 0.01767	0.071
4 2N2925 at 0.02245	0.090
29 capacitors at 0.00474	0.137
71 resistors at 0.00355	0.252
4 Zener diodes at 0.04008	0.160
Connections	0.212
Wheel Assembly - λ_T = 0.637	
2 spin bearings - 38H	0.600
2 centrifugal oilers	0.008
Brushless motor-generator	0.008
Seals	0.017
Magnetic speed pickup	0.004

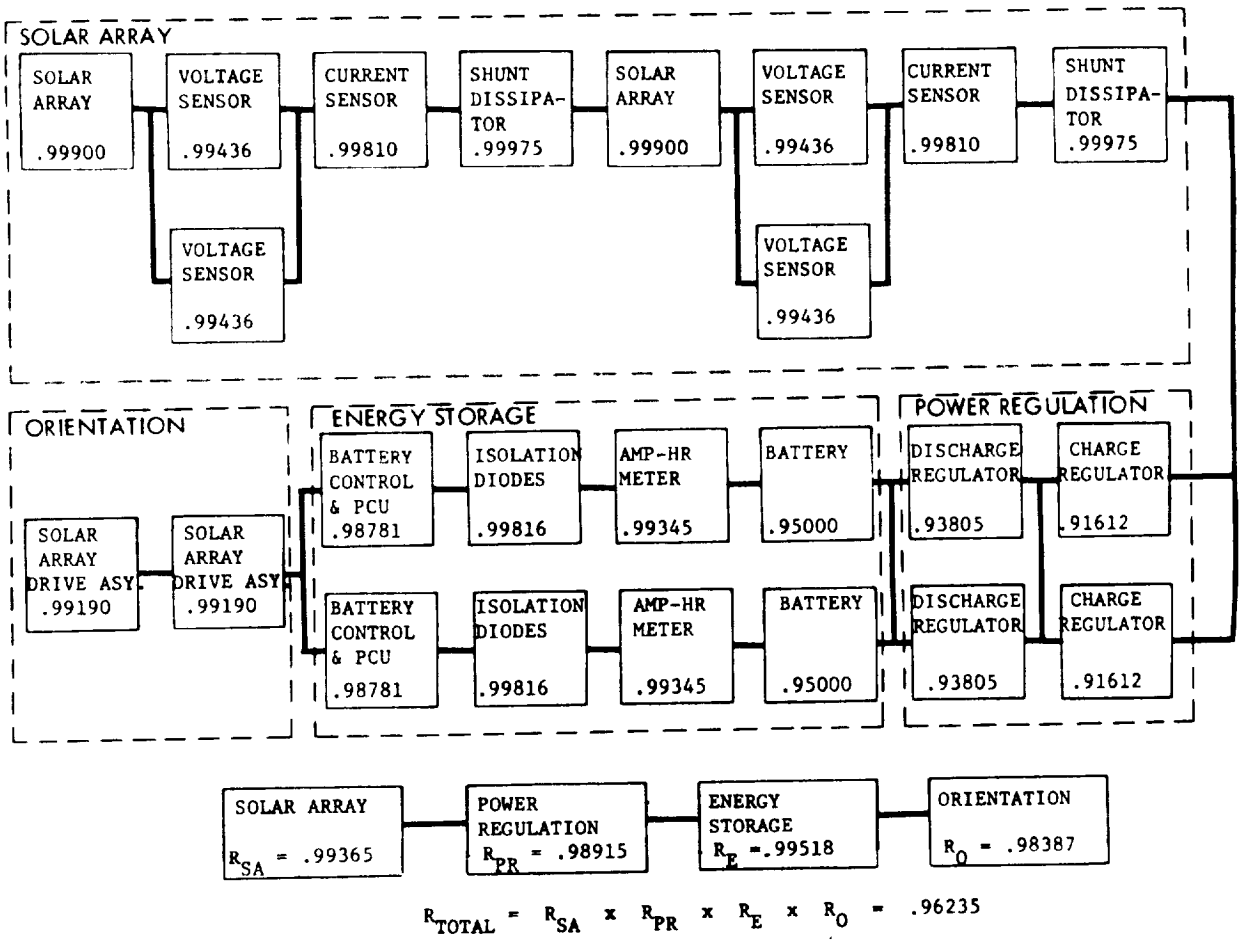

Figure 1-25. Reliability Logic Diagram - Conventional TDRS Electrical Power System

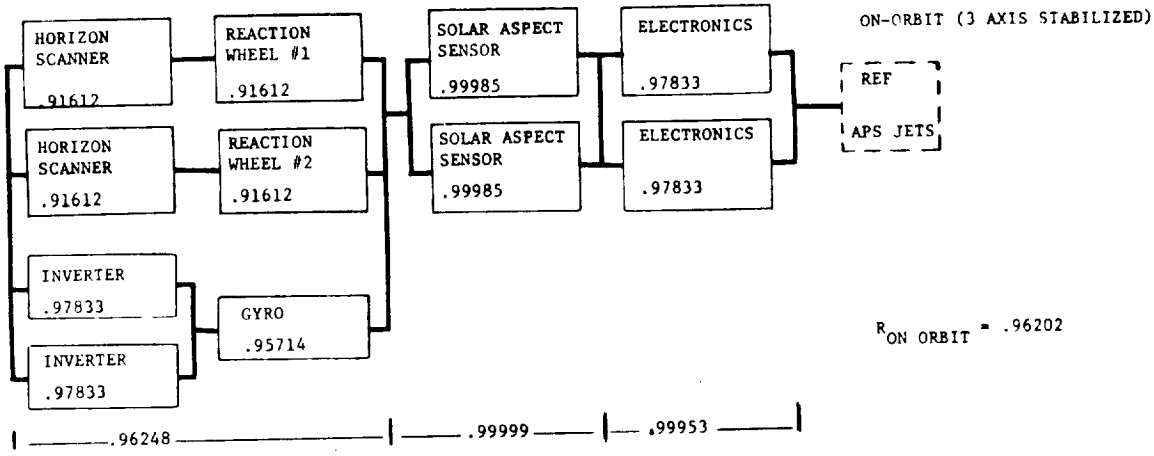

Figure 1-26. Reliability Logic Diagram - Conventional TDRS Attitude Control Subsystem

TABLE 1-XXIV.- TDRS SUBSYSTEM RELIABILITY GOALS

Subsystem	Initial allocation
Tracking, telemetry, & command	0.96
Communications	0.96
Structure & mechanisms	0.98
Attitude control	0.96
Auxiliary propulsion	0.98
Electrical power	0.95
Thermal control	0.99
Total satellite	0.80

Combined power and control system reliability for the conventional system is seen to be 0.92579. Since IPACS wheel assemblies perform dual functions a revised reliability diagram would appear as in figure 1-27, which meets the 0.912 combined power and control reliability apportionment (product of power and attitude control goals).

TDRS safety.- A brief generalized discussion of IPACS safety considerations is presented in Volume I, Module 1. Specific comments regarding the IPACS design for TDRS are presented here.

The safety problem is confined to the development, manufacturing, assembly, and test phases of the program, which are the only phases where personnel come in contact with the hardware.

The working stress for the titanium rotor was selected to provide adequate design margin and assure rotor integrity. For this mission fatigue cycling is essentially negligible.

Vibration and acoustic noise.- The TDRS design was analyzed under a static unbalance loading condition, a dynamic unbalance loading condition, and under the combined effects of the static and dynamic unbalance. The static unbalance used was a 5×10^{-7} cm shift in the location of the c.g. (center of gravity) of the wheels. To analyze this type of c.g. shift under a rotational loading condition, the axis of rotation was moved 5×10^{-7} cm from the axis of symmetry and then the bearing loads computed for spin rates in the operational range of respective designs. The dynamic unbalance loading was set equal in magnitude to the static unbalance.

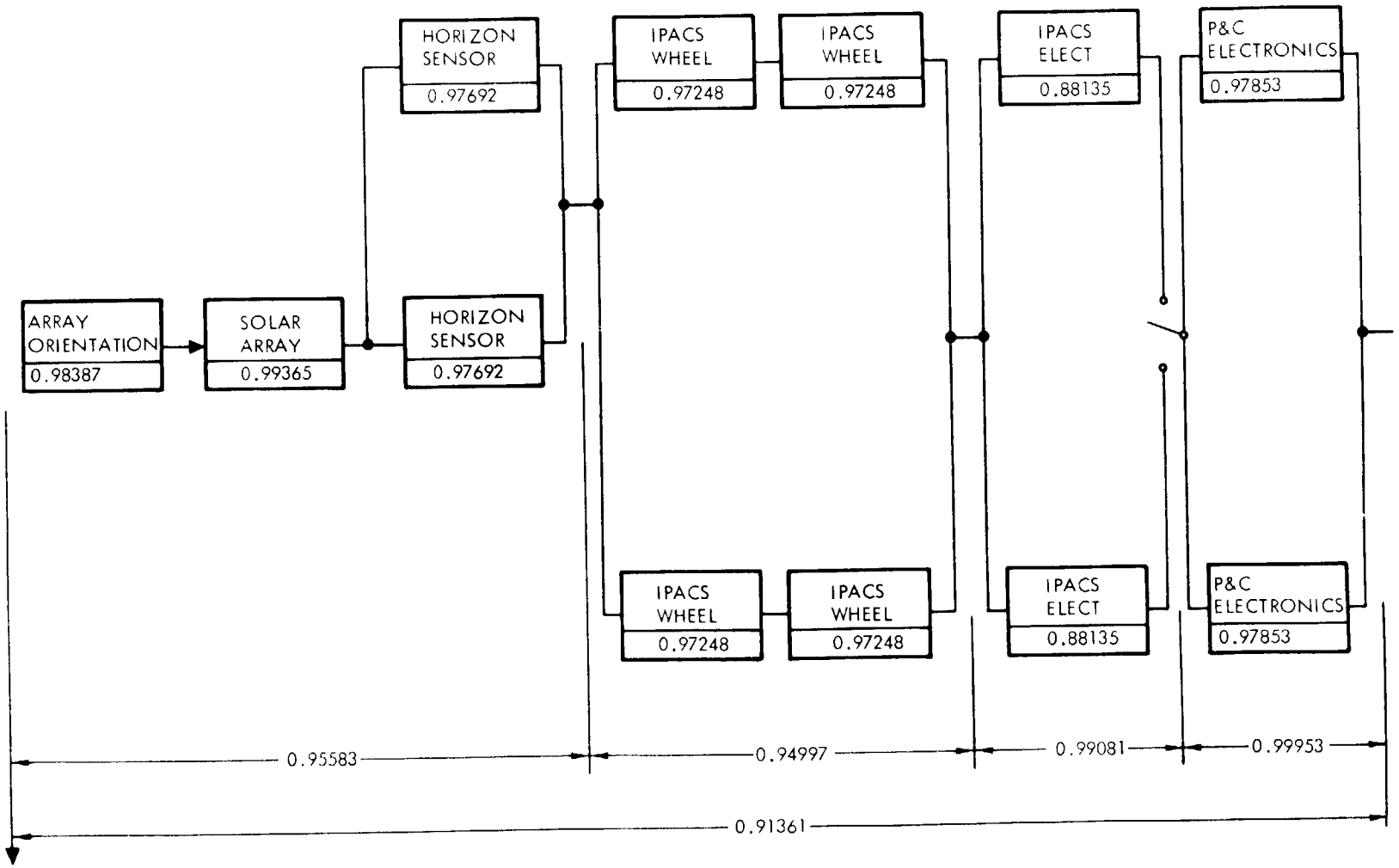

Figure 1-27. IPACS Reliability - Energy and Control Mode

The dynamic unbalance is applied to the system by placing concentrated masses at the edge of the wheel. The masses to be added are determined as a function of the radial location of the mass and the thickness of the wheel at the location of the concentrated mass.

The configuration was analyzed under the static, dynamic, and combination of static and dynamic loading conditions at the limits of the operational speeds. Figure 1-28 shows the results of the bearing loads analyses for the TDRS design. The load is shown as a function of the rotational speed of the wheel ω for both bearings 1 and 2. The loading conditions analyzed assume a c.g. shift which was not symmetrical with respect to the location of the small masses used in the dynamic unbalance condition. This results in different bearing loads as indicated. At Bearing 1, the loads due to static and dynamic unbalance subtract from each other, while at Bearing 2 these loads are additive. The loads due to the static unbalance vary linearly with the value of ϵ, the c.g. offset used. Since a value of 5×10^{-7} cm was selected, this means if loads for a 2.5×10^{-7} cm offset are wanted, 1/2 of the loads shown for the static case only would be used. These loads also vary as the square of the rotation frequency ω. The values shown for the dynamic loading condition will vary linearly, as a function of ϵ, since the mass values vary linearly with ϵ. It should be noted that this can only be used for masses located as shown in figure 1-28.

The loads shown in figure 1-28 are conservative as rotor balance requirements are to be maintained to less than 2.5×10^{-7} cm, reducing the loads by half. The loads of figure 1-28 cannot be expected to affect bearing life calculations and therefore will contribute only to noise and low-level high frequency vibration. Shock mounting of the IPACS units may be desirable if other systems within the vehicle are found to be sensitive to vibrations within the IPACS operating spectrum of 400 to 800 Hz.

Acoustic noise for TDRS is considered significant only with regard to ground testing. Isolation mounts may be useful in minimizing acoustic noise in test areas. The problem is best left to resolution when development units are built and operated.

TDRS maintainability.- The IPACS concept for TDRS is representative of the designs that might be applied to relatively small satellites which operate unmanned. Orbital maintenance for vehicles of this type would be restricted either to return of the entire vehicle to the ground for servicing or replacement of spacecraft modules on orbit. In the latter case, a module might consist of an entire spacecraft subsystem or major portions thereof (perhaps all four IPACS energy storage/momentum units). The modules would be returned to ground for refurbishment and reuse.

For either of the above concepts, it is envisioned that a failed IPACS energy/momentum unit would be returned to the vendor for refurbishment. The refurbishment operation would include disassembly of the unit to the point

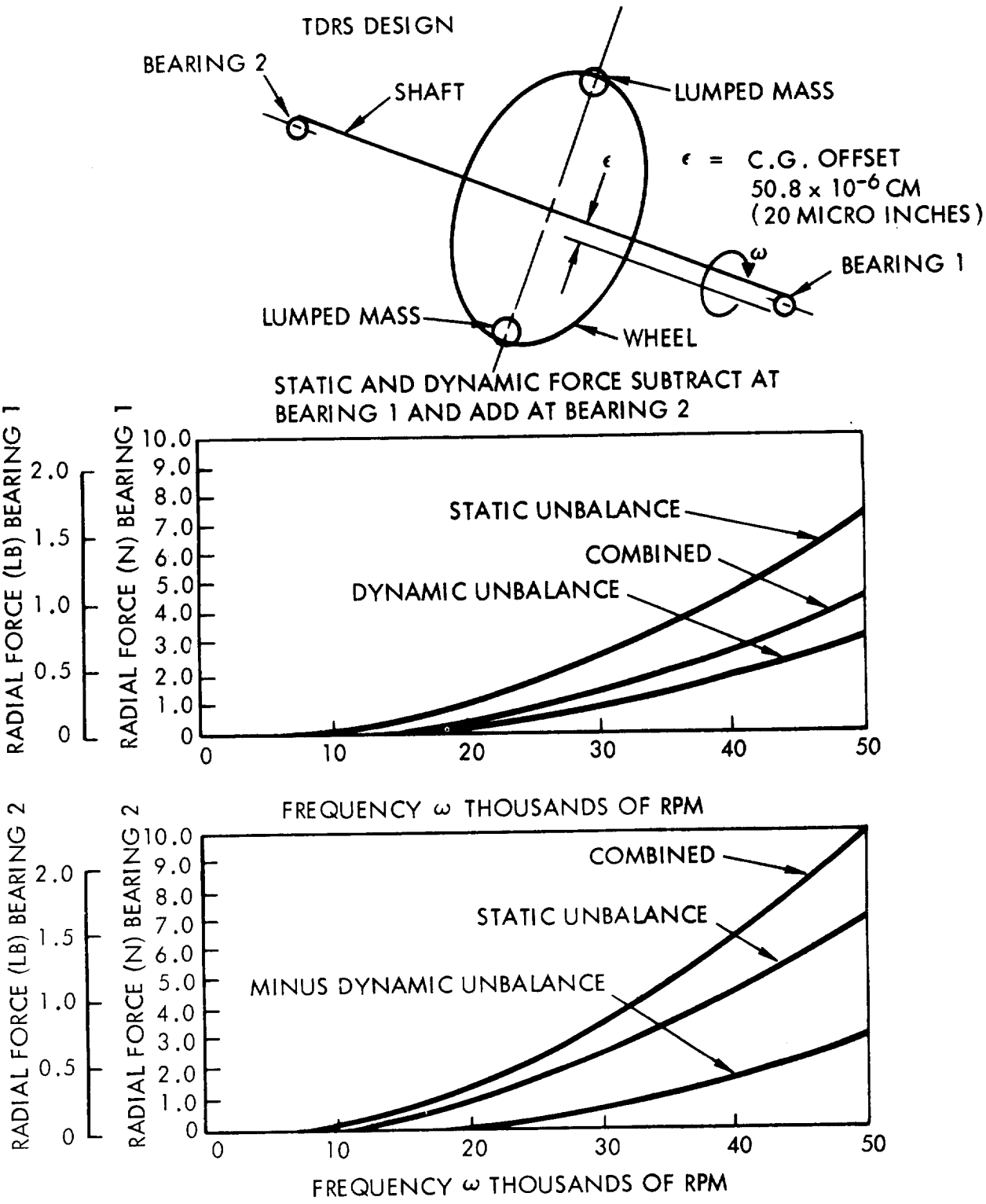

Figure 1-28. Radial Forces at Bearings

where individual components could be inspected and tested. Corrective action would depend on the cause of failure. The following operations would be conducted in the case of a bearing failure (note that the bearings would be replaced even if they were not the source of failure):

- Disassemble
- Replace bearings
- Rebalance rotor assembly (trim)
- Refill oilers (store in vacuum environment prior to use)
- Adjust preload
- Check motor/generator commutation
- Check or replace electronics
- Conduct full acceptance tests

It is estimated that the cost to refurbish one unit would be in the range of 7-10 percent of the cost of a new unit, assuming a failure such as a bearing failure. Failures requiring the replacement of other components would increase the cost.

System data link requirements.- Table 1-XXV shows up-down data link requirements for the IPACS.

References

1-1. Bower, E. R., "Rolling and Sliding Bearings," Production Engineering (April 27, 1969).

1-2. Integrated Power/Attitude Control System (IPACS) Study, Vehicle/Mission Selection Report. North American Rockwell, Space Division, SD72-SA-0144 (Aug. 10, 1972).

TABLE 1-XXV.- UP-LINK/DOWN-LINK REQUIREMENTS (TDRS)

Parameter	Number	Information flow
ANC accelerometer	2	Down
Horizon sensor (spinning)	2	D
Sun sensor	2	D
Pitch jet command	2	D
Reaction jet commands	8	D
Attitude commands	6	D
Horizon sensors	2	D
Solar aspect sensors	4	D
Rotor speed	4	D
Spin bearing temperature	8	D
Bearing induced acceleration	8	D
Current: solar array to bus	2	D
Bus voltage	1	D
Panel temperature	2	D
Orientation motor: temp	4	D
voltage	4	D
current	4	D
Main bus current	1	D
Shunt dissipation base plate temperature	2	D
Attitude commands	3	U_p
Panel orientation commands	2	U
Wheel speed override	1	U
Power commands	2	U

MODULE 2 - RESEARCH AND APPLICATION
MODULE FREE-FLYER CONCEPTUAL DESIGN

A conceptual design of an IPACS for the free flying RAM (research and application module) was formulated to determine the approach for integration of both attitude control and energy storage for this class mission. This module includes a description of the resulting IPACS and its operation. A description of the baseline mission and spacecraft and its associated electrical power and control subsystem is taken from reference 1. Additional material on the baseline mission and spacecraft may be found in Module 1, Volume I, of this report.

RAM System Description

The objective of free-flying RAM A303B mission is to accomplish solar astronomy observations. Experiments include photoheliograph, UV spectroheliograph, solar X-ray telescope, and solar coronograph experiments. These experiments were assigned to free-flyer accommodation to (1) provide the necessary stability and fine pointing capability, (2) remove the experiment from the potentially contaminating environment around the Shuttle or space station, (3) provide long-duration operation with only periodic manned servicing, and (4) provide selective orbit capability.

Baseline configuration. - The configuration of the A303B free flyer is shown in figure 2-1. The primary structure consists of a 3.4m (11.25 ft) inside diameter pressure shell 5.5m (18 feet) long, a 0.785 rad (45 deg) truncated transition cone to a 2.59m (8.5 ft) diameter, a 0.61m (2 ft) long cylindrical utilities section at 2.59m (8.5 ft) diameter, and a standard docking assembly that is 2.59m (8.5 ft) in diameter by 0.38m (1.25 ft) long. All structural components are welded together to minimize atmosphere leakage (except the docking assembly which has a bolt and elastomer seal joint).

The detached mode of operation of the free-flying RAM dictates a self-contained electrical power subsystem (EPS) capable of supplying average and peak power demands of experiments and subsystems. This long-term power is provided by four flexible roll out solar cell arrays. The solar cell area is $98.5m^2$ ($1060\ ft^2$). Nickel-cadmium batteries provide the required energy storage with long life and high cycle capability. Location of major EPS assemblies is shown in figure 2-2.

The solar arrays are attached near the aft end of the free-flying RAM and lie forward along the side of the vehicle in the stowed position. During deployment, the masts are erected and the arrays rolled out to the extended positions. End of life solar array power output is 6890 W.

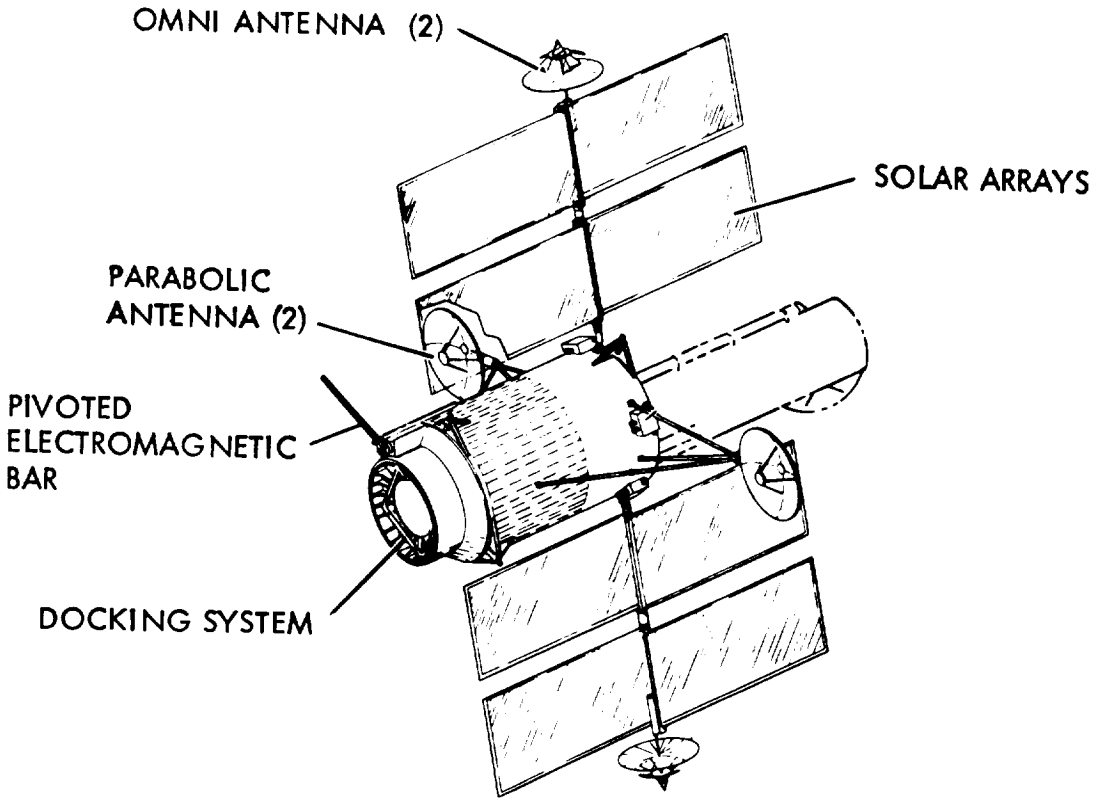

Figure 2-1. Free-Flying RAM General Arrangement

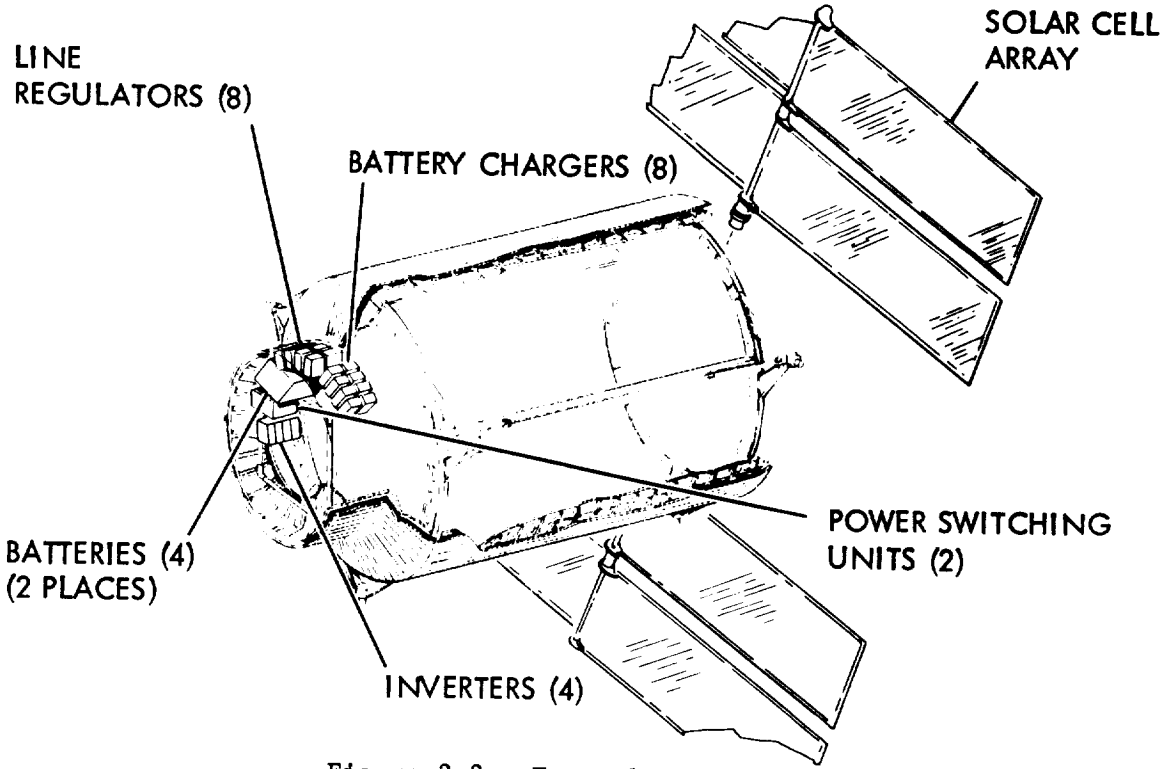

Figure 2-2. Free-Flying RAM EPS

The propulsion/reaction control subsystem (RCS) operates with the guidance, navigation, and control (GN&C) subsystem and provides the propulsive capability for vehicle orientation, stationkeeping, rendezvous, and docking/undocking as needed by the associated operating mode. Twenty-four 111N (25-lb) thrust hydrazine thrusters provide all axis translation and rotation to the free-flying RAM in the Shuttle-supported mode.

The RCS on the Shuttle-supported free-flying RAM consists of four independent replaceable packaged tank and thruster units spaced each 90 degrees near the solar arrays and antenna mounts. This arrangement provides minimum plume impingement on the solar array, antenna, and orbiter support fitting installations.

Astronomy payloads require precise pointing accuracy and stability. The GN&C subsystem will provide a precise pointing accuracy of $\pm 4.85 \times 10^{-6}$ rad (± 1 arc-sec) and a stability of 2.42×10^{-6} to 4.85×10^{-6} rad (0.5 to 1.0 arc sec) per observation period. This satisfies the pointing accuracy requirements but does not meet stability requirements of two reference payloads: 2.42×10^{-8} rad and 8.25×10^{-8} rad (0.005 and 0.017 arc sec) per observation. Improvements in stability characteristics are the payloads' responsibility.

The vehicle is controlled by three double-gimballed CMG's. Sensors include star trackers, sun sensor, IMU, and magnetometers. An electromagnetic torque bar for momentum desaturation of the CMG's is located at the docking end to place the induced magnetic field furthest from sensitive focal point instruments. The bar is provided with a three-degree-of-freedom mount for alignment relative to the earth's magnetic field.

Free-flying RAM's operate in an unpressurized condition. When man-tended, as for servicing, the repressurization and environmental control/life support (EC/LS) functions are provided by the servicing vehicle. The free-flying RAM provides only air distribution and circulation. The free-flying RAM provides work positions, mobility aids, and restraints for two to four men.

RAM system operational timeline.- Flight operations are summarized by describing the basic operations involved in Shuttle delivery of a free-flying RAM to operational orbit and performance of on-orbit checkout of subsystem and payload systems.

The delivery operations begin with the Shuttle launch. The free-flying RAM delivery crew monitors the payload from the orbiter during ascent; the RAM payloads are generally inactive except for thermal control and caution and warning. In orbit, the RAM payload crew performs a preliminary post-boost checkout of the free-flying RAM prior to deployment from the orbiter cargo bay.

After deployment and interconnect verification (if manipulators are used) and after the proper functioning of subsystems is verified, the crew enters the free-flying RAM. First, the crew performs a preliminary post-boost/deployment electrical circuit check to verify EPS functioning. Next, the free-flying RAM communication antennas are extended and the TDRS telemetry and command link from the ground to the free-flying RAM is established. From this point on, the on-orbit checkout of the free-flying RAM is ground-aided through the TDRS communication link. The solar arrays are extended to provide electrical power for subsequent checkout operations.

The next checkout period is eight hours long; two hours are required to spin up the CMG's. The checkout operations include all systems, but emphasize those required to deploy and retrieve the free-flying RAM. Following checkout, the interface connections between the orbiter and the free-flying RAM are broken manually prior to depressurization. Electrical power during depressurization of the free-flying RAM is provided from the solar panels or from the orbiter through an umbilical connection on the manipulators. The solar arrays are locked (electrically disabled) to prevent interference with manipulator operations during depressurization and undocking. After the two hours estimated for depressurization, a final check of all systems is made and free-flying RAM controls are set for remote operations.

The orbiter now undocks and stands off from the free-flying RAM (no ΔV requirement on free-flying RAM), which is stabilized by its CMG system under automatic programmer control. The ground then takes over control (with the orbiter monitoring and having RF override capability) and remotely checks out the command communication link. With the free-flying RAM properly stabilized, the solar arrays (orientation mechanism) are unlocked (enabled). A one and one-half hour period for CMG control system checkout is followed by an equal period for checkout of the data communication link. Two hours are allocated for a remote auto-checkout of all subsystems and the payload.

All operations and checkouts up to this point have been conducted with the optical sensor (telescope) closed to protect the contamination-sensitive instruments. A period of 36 to 48 hours (from the start of depressurization) is estimated for contamination clearing and thermal equilibrium before the telescope lens covers are opened. Once the telescope is opened, a series of observations of celestial objects is conducted to provide an end-to-end checkout of the free-flying RAM subsystems and payload. With satisfactory completion of this last checkout, the orbiter returns to earth (nominal four-hour return operation indicated) with landing occurring for a nominal mission at 98 hours elapsed time from launch.

A final 48-hour period for contamination clearing to obtain scientific quality observation data is indicated on the timeline. Telescope observations are monitored on the ground and scientific observations begin whenever proper data quality is obtained.

Free-flying RAM delivery mission flight operations which affect RAM subsystems are summarized in this paragraph. The EPS is off from launch to the start of RAM checkout, with the orbiter supplying the limited power needed early in the checkout procedure. RAM solar arrays are soon deployed, however, to satisfy the increased power requirements as the checkout procedure progresses The EC/LS system includes two blowers that circulate air when the delivery crew is inside the free-flying RAM. The thermal system operates continuously and provides thermal control while the free-flying RAM is located in the orbiter cargo bay or in a space environment. The GN&C system is off until CMG spin-up during on-orbit checkout while the RAM is attached to the Shuttle. CMG's are the primary method of RAM attitude control after release. Controls and displays support manned operations in the RAM. The communication and data management system (CDMS) operates continuously during the mission. Communications links are compatible with the TDRS and the ground network. The structures and mechanical subsystem is compatible with boost flight loads and manipulator or pivoted methods of free-flying RAM deployment. The RCS acts as a backup to the free-flying RAM CMG's. The crew and habitability subsystem provides for two crewmen in a free-flying RAM. Maintaining proper cleanliness of sensitive payload equipment is important and is controlled locally by special integration equipment which includes breathing masks and lint-free garments.

IPACS implication: If the IPACS concept is employed on the free-flying RAM the only impact to the timeline may be in the area of the IPACS control and energy momentum gyros (CEMG's). Because of the size of the CEMG's used for this mission it will be necessary to have them secured during the launch. This will be done via a lock mechanism that will increase the bearing preload during launch by air pressure on a piston which compresses the preload spring and makes contact with the movable outer race of one spin bearing. The mechanism is pressurized prior to mounting in the vehicle. A sublimating solid is used to seal a small piston-operated valve. Under the vacuum of space the solid sublimates and allows this piston to move under the internal pressure and vent the pressurized chamber to space, thus releasing the launch lock automatically. In the event of a failure a manual override is provided to the mechanism, which constitutes the only deviation from the timeline previously described.

RAM IPACS operational requirements.- The IPACS must generate and distribute electrical power required by the RAM as well as provide spacecraft control.

General requirements: The vehicle is delivered to orbit by the Shuttle. The desired orbit is circular with an inclination of less than 0.17 rad (10 deg) and an altitude of 740 km (400 nm). Acceptable orbit characteristics are a circular orbit with an inclination between 0.785 rad (45 deg) and 0.96 rad (55 deg) and an altitude of 500 km (270 nm). Mission duration is 5 years.

All critical subsystems/functions (hardware whose failure results in loss of crew or loss of module) will be designed for any credible combination of two component failures. Conservative factors of safety will be provided where critical single failure points cannot be eliminated (pressure vessels, plumbing, etc.). As a goal, free-flying RAM's will be designed to facilitate their retrieval and recovery by the Shuttle in case of the failure of critical onboard systems. The vehicle will be designed for on-orbit maintenance in a shirtsleeve environment with a nominal service interval of six months. The vehicle is manned periodically for on-orbit servicing but nominally operates unmanned.

Attitude control requirements:

Functional requirements The nominal vehicle flight mode will be solar inertial with the longitudinal axis of the vehicle oriented toward the sun. Experiment-integral sensing will be provided. The aspect or error signal so obtained will be used for vehicle control.

There is no requirement for an integral orbit-keeping capability. That function will be performed as required by the orbiter. The orbiter will be active during rendezvous and docking operations. The RAM is required to maintain a stable orientation to support docking operations.

Performance requirements The vehicle will be controlled to a pointing accuracy of 4.85×10^{-6} rad (1 arc sec). Pointing accuracy is defined as the maximum deviation from perfect pointing. Pointing stability is defined as the maximum deviation from a time average over the observation period. The experiment required pointing stability is 8.25×10^{-8} rad (0.017 arc sec) over the observation period which is considered as 0.75 hours. It is acceptable for the vehicle to be controlled to a stability of 2.42×10^{-6} rad (0.5 arc sec) with the experiment providing the finer stability.

During experiment observations, the experiment must not be subjected to acceleration levels greater than 1×10^{-4} g's.

A control torque 9.35 N-m (7 ft-lb) per torquer is required.

Disturbances and momentum storage The predominant external disturbances for this vehicle are aerodynamic and gravity gradient. The momentum storage requirement is shown in Table 2-I and was developed by scaling the 9080-kg (20 000-lb) spacecraft data to represent the 18 160-kg (40 000-lb) growth size vehicle with pitch and yaw inertias on the order of 406 000 $kg\text{-}m^2$ (300 000 $sl\text{-}ft^2$).

TABLE 2-I.- MOMENTUM STORAGE REQUIREMENTS (ATTITUDE CONTROL)

Item	Requirement	
	N-m-sec	ft-lb-sec
React gravity gradient	1262	930
React aero drag	64	47
Maneuvers	712	524
Total (worst case)	2038	1501

Electrical power requirements:

Functional requirements The IPACS must generate, store, regulate, control, condition, and distribute electrical power required by the free-flying RAM for the full duration of its mission. The RAM will be serviced periodically by the Shuttle. During the period the RAM is attached to the Shuttle, power will be supplied by the Shuttle.

In the case of primary power generation failure, sufficient backup power will be required for Shuttle recovery of the RAM. Solar arrays are used for prime power generation.

Performance requirements Table 2-II summarizes payload electrical power requirements and power profiles are shown by figure 2-3.

TABLE 2-II.- A303B PAYLOAD POWER REQUIREMENTS

Item	Mode of operation	
	Simultaneous	Sequential
Power average (on)	2180 W	540 W standby
Peak	+ 450 W	See figure 2-3
Duration	5 peaks of 40 sec ea	3 test periods of 0.06 hr 2 observation periods
kW hr/day	52.3	

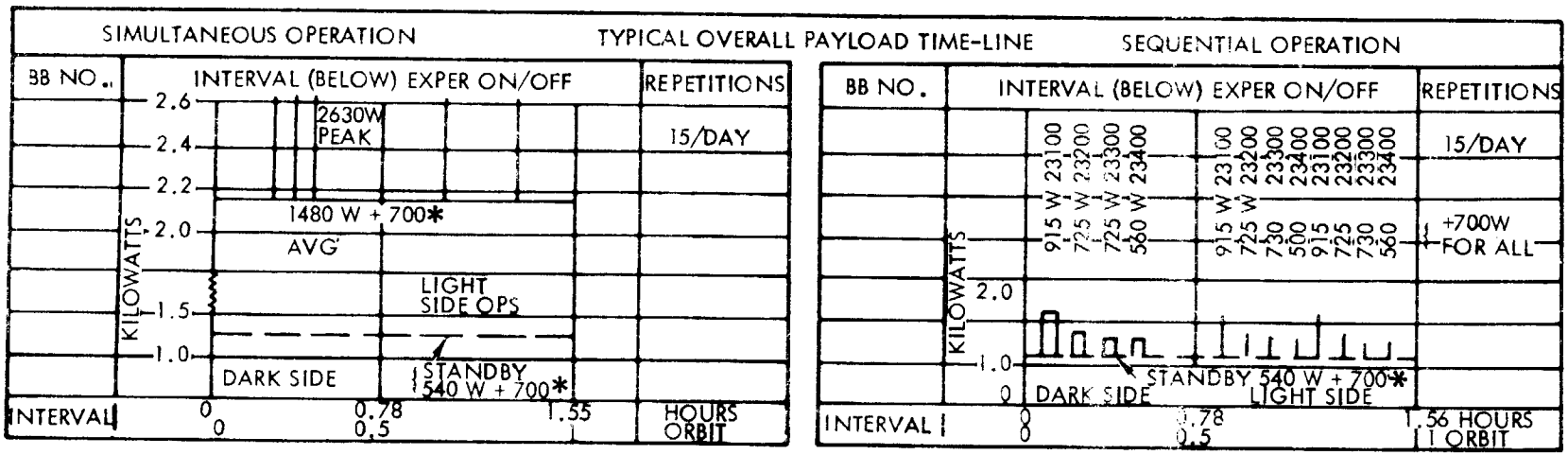

Figure 2-3. Payload Power Profile, A303B

Total power requirements are obtained by adding payload and subsystem (1020 W) requirements. An average total load power of 3400 W is shown by the RAM Phase B study for the A303B payload.

At an orbit altitude of 500 km (270 nm) the eclipse energy required by the spacecraft is 2010 W-hr. This is based on an eclipse period of 0.591 hour.

Table 2-III shows subsystem voltage and regulation requirements (experiment requirements are undefined). Peak powers required for sizing power-conditioning and distribution equipment also are shown in Table 2-III. Subsystem average power (1220 W) is obtained by subtracting the payload average power of 2180 W from the 3400 W average total power load. The experiment load voltage regulation requirements for the free-flying payloads were not defined by the RAM studies. However, to provide flexibility and because of commonality with subsystem power form, a basic requirement was established to provide the experiment loads with at least 1000 VA of 115/200 Vac power and 1.5 kW of $\pm$5 percent regulated 28 Vdc power.

The emergency loads for the free-flying RAM, if it must be operated powered-down, total 841 W. Two subsystems must be operated normally and these consume the major portion of the power: the communication and data management subsystem at 394 W average and the thermal control subsystem at 300 W average. The GN&C subsystem is operated with only the rate gyro package and three star trackers on and requires 84 W of power total. Average power for propulsion is estimated at 10 W, and EPS conditioning consumes an additional 53 W.

RAM IPACS system description.- Major assemblies making up the RAM IPACS are the power source (solar array panels), motor-generator wheel assemblies and associated electronics, central control unit, and the regulated bus.

Functional diagram: Figure 2-4 shows the mechanization selected for the RAM IPACS. The scheme is based on a minimum modification of the competitive RAM electrical power subsystem discussed in Module 1, Volume I, of this report. The three motor-generator wheel sets replace the eight 36-AH (24-cell) nickel-cadmium batteries of the competitive EPS. A set of electronics is added for each brushless dc motor-generator set. A new power and momentum controller is added. The original RAM buck regulators are replaced by two larger units. The original RAM double bus with fault isolation and bus-to-bus switching capability is retained. Dual three-phase inverters supply the ac loads from either dc bus.

Any two of the three double-gimbaled momentum wheels can meet normal RAM eclipse power requirements. Any one of the three units can be connected to either main power bus.

The baseline solar array sections are connected to provide 75 V dc (52 V minimum) power output. This voltage is utilized in the IPACS to improve efficiencies. Voltage is reduced to 28 and controlled to within $\pm$5 percent by buck regulators. Although the block diagram shows one regulator for each bus, this could be increased as required by availability of existing components

TABLE 2-III.- FREE-FLYING RAM POWER, VOLTAGE/REGULATION REQUIREMENTS

(WATTS)

Subsystems	Voltage and regulation*		
	28 Vdc ± 15%	28 Vdc ± 5%	115/200 Vac, 400 Hz ± 5%
OCS			
Stimuli generator	-	15	-
Thermal control			
Freon pump	-	-	110
Water pump	-	-	115
Controls	75	-	-
Data management			
Computer, multiplexing,etc.	150	-	-
Tape recorder	220	-	-
Communications			
Ku band	445	-	-
S band/VHF	150	-	-
GN&C			
DG-CMG system	-	75	-
Reaction wheels	-	30	-
Star trackers	-	31	-
IMU	-	70	-
Magnetometer	-	2	-
Magnetic torquer	-	60	-
Propulsion	360	-	-
Peak power requirements	1400	283	225

*Peak power demands are listed under each voltage type.

and power rating. For redundancy the regulator to one bus should be capable of carrying the total load in case of failure of the other regulator and use of the bus tie power switching.

Power switching functions are performed by the power and momentum controller. Computational functions performed within this unit are supplemented by those performed within the centralized RAM digital processor.

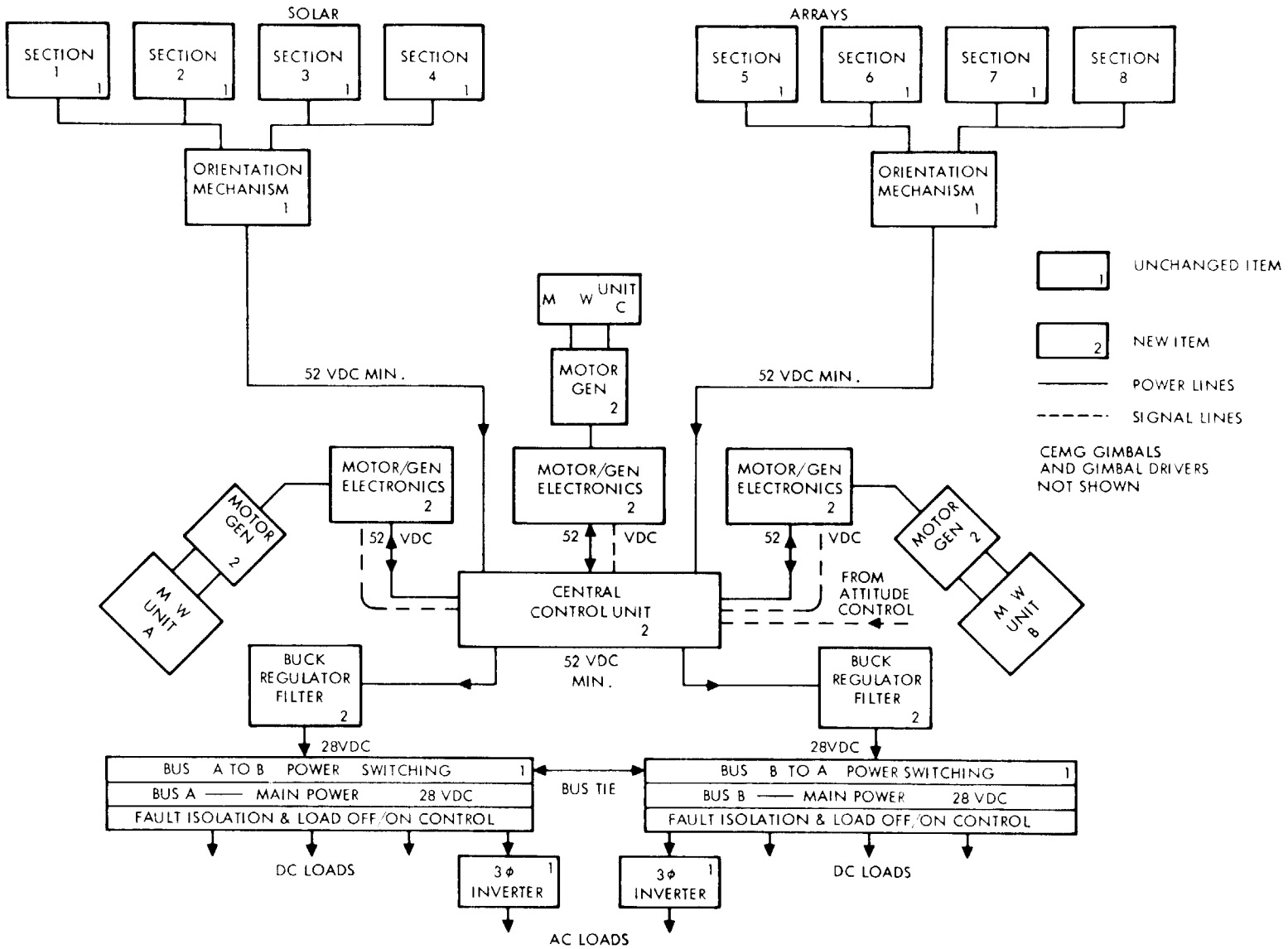

Figure 2-4. Free-Flying RAM IPACS (Electrical Power System) Block Diagram

The three double-gimbaled energy/momentum units replace the three double-gimbaled CMG's in the competitive attitude control design. The remainder of the baseline control concept is retained including the sensors, RCS, magnetic torquers for desaturation, and reaction wheels for precision control.

IPACS interfaces with other spacecraft components are discussed in the last section of this module. The motor-generator electronics are discussed in Module 1 of this report.

Nominal system operation: The three energy units are mounted in the vehicle as a planar array with the outer gimbal axes parallel and aligned with the longitudinal axis of the vehicle which is the minor inertia axis. Thus the three outer gimbal torques act in parallel. The deliverable torque about the transverse axes is dependent upon the instantaneous gimbal configuration but in general will be equal to or greater than the output of a single torquer.

Energy is stored in all three wheels under normal operating conditions. The gimbals are torqued to minimize the effects of torques produced by rotor speed changes. Under failure mode conditions, the two remaining units are slewed to a position where the spin axes of the rotors are collinear. The rotors are counter-rotated to provide torque-free energy storage. The primary attitude control function is assumed by the reaction control system supplemented by the energy units where possible.

When power demand exceeds solar array capability (daylight peaking or orbit eclipse periods) the bus voltage will start to drop below the nominal value of 28 V dc. The power control unit will modulate the IPACS generator electronics to supply the additional power needed. During daylight periods when solar array power exceeds load requirements, the power control unit will apply power to the CEMG motors to increase rotor speed, if they are not already at maximum rpm (45 000). During eclipse periods the RAM loads require 3400 W of electrical power.

The energy storage discharge-only circuit efficiency is 0.767 as calculated from:

Motor/generator and electronics efficiency	=	85%
Buck regulator efficiency	=	92%
Transmission efficiency	=	98%

The eclipse power required from the generators including bearing losses is 4440 W. This can be supplied by two CEMG's with generators operating at about 93 percent of full output (2400 W wheel). Figure 2-5 shows a typical charge/discharge profile for the RAM CEMG. The efficiencies shown include both motor/generator and electronics. A minimum of two CEMG's are required to meet eclipse power requirements. However, all three CEMG's will be needed to

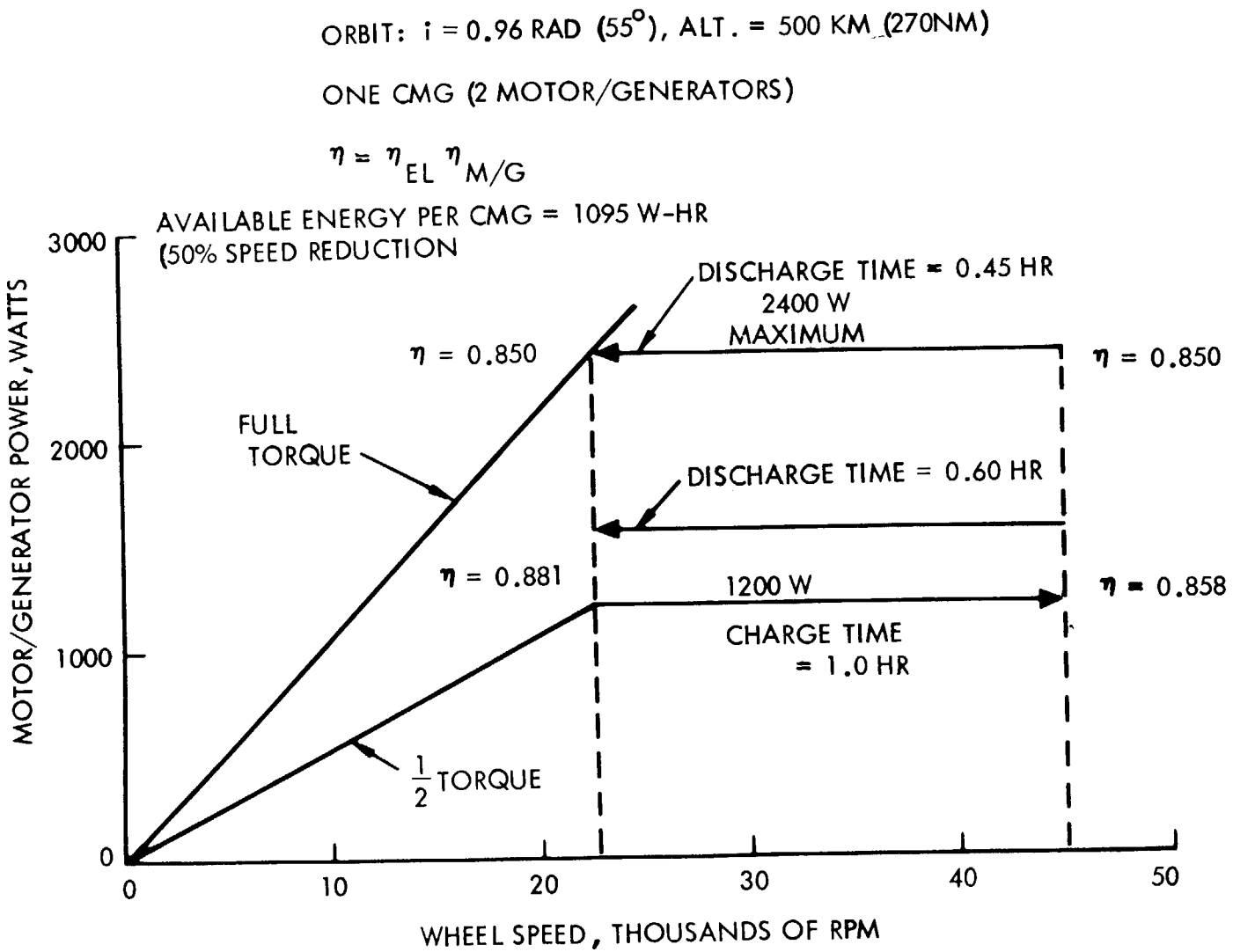

Figure 2-5. RAM IPACS Charge-Discharge Profile

meet eclipse energy requirements. Total eclipse energy requirements from the array is 2743 W-hrs. Available energy from all three CEMG's is 3285 W-hr (for a speed reduction from 45 000 to 22 500 rpm). Therefore 87 percent of total stored available energy is used to meet eclipse power requirements. All three CEMG's will operate simultaneously to deliver eclipse power at 1540 W/wheel.

During the eclipse period, 5 peak power loads of 3850 W lasting 40 seconds each occur. The generator power required to meet these loads is 1790 W per CEMG.

Launch operation There is no requirement for RAM operation during a Shuttle launch. The free-flying RAM is in the orbiter cargo bay. RAM payloads are generally inactive except for thermal control and caution and warning. During this period power is supplied to RAM by the orbiter. The solar arrays are extended to provide electrical power before the orbiter undocks and stands off from the free-flying RAM.

IPACS physical and performance characteristics: RAM IPACS weights are summarized in Table 2-IV. The baseline solar arrays, load busses, and power conditioning equipment are retained. Items retained from the baseline guidance and control system total 180 kg (397 lb): a sun sensor, fixed head star tracker, target/stadiometer, magnetic torquer, and magnetometer. Three energy momentum units weigh 216 kg (475.8 lb). These are further delineated by Table XXIV. Installation hardware weight from the baseline power system is retained. Total IPACS weight to meet both electrical power and attitude control requirements is 1115 kg (2458 lb).

RAM IPACS physical and performance characteristics are summarized by Table 2-V. A detailed description of the CEMG physical and performance characteristics is presented in a later section.

TABLE 2-IV.- RAM IPACS WEIGHT SUMMARY

Components/assemblies	Weight	
	Kg	lb
Solar array	(255.9)	(564)
Panels (2)	223.1	492
Sun sensor	0.9	2
Orientation mech. (2)	22.7	50
Orient. cont. elec.	9.1	20
Power conditioning and distr.	(150.6)	(332)
Power switch unit (2)	31.8	70
Inverters (4)	18.1	40
Line regulators (2)	50.8	112
Docking interface conn.	9.1	20
Manipulator conn. PN6	9.1	20
Ground conn. PNL	4.5	10
Busses	18.1	40
Outlets	9.1	20
Power and momentum controller	9.8	21.7
Energy storage/attitude control	(220.6)	(486.3)
Energy momentum unit (3)	215.8	475.8
M/G electronics (3)	4.8	10.5
Baseline guidance and control retained	180.1	397.0
Electrical wiring	248.6	548.0
Installation hardware	49.4	109.0
Total	1115	2458

Note: Number in parantheses represents subassembly total weight

TABLE 2-V.- RAM IPACS PHYSICAL AND PERFORMANCE CHARACTERISTICS

Solar array	
Area, total of 8 panels	$105.8 m^2$ ($1114 ft^2$)
Specific power (BOL)	$87.48 W/m^2$ ($8.13 W/ft^2$)
(EOL) (5 years)	$69.94 W/m^2$ ($6.5 W/ft^2$)
Array power (BOL)	9317 W
(EOL)	7450 W
10-year degradation	20%
Min. voltage	52 V dc
Power transfer (BOL)	179.2 amps
(EOL)	143.3 amps
Energy storage	
Available energy/CEMG	1095 W-hr
Total available energy	3285 W-hr
Wheel speed range	22 500 - 45 000 rpm
Generator output (max)	2400 W/wheel
Charge/discharge voltage	52 V dc
Charge and discharge efficiencies*	

Operating mode	Shaft power (W)	Wheel speed (rpm)	$\eta_{m/g}$ (%)	η_{elec} (%)	η_{c-d} (%)
Motor	1200	22 500	97.6	90.3	88.1
Motor	1200	45 000	97.0	88.5	85.8
Generator	2400	45 000	97.9	86.8	85.0
Generator	2400	22 500	96.1	88.5	85.0

Charge/discharge cycle eff. (avg)	73.9%
Charge-discharge cycles, 5 years	27 800
Power & momentum controller, volume	$< 0.028 m^3$ ($< 1 ft^3$)
Attitude control	
Pointing accuracy	4.8×10^{-6} rad (1 arc sec)
Design control torque/torquer	9.49 N-m (7 ft lb)
Minimum momentum storage (total)	3343 N-m-sec (2466 ft-lb-sec)
Rate control	8.25×10^{-8} rad/.75 hr(.017 sec/.75 hr)

*Does not include bearing losses

RAM IPACS Components

The following RAM IPACS subassemblies and components are discussed in this section:

Inner gimbal assembly
Motor-generator design
Spin bearing system
Torquer unit
Sensor unit
Outer gimbal
CMG/energy storage assembly
Solar array
Distribution and regulation

The motor-generator electronics and control are discussed in Module 1 of this volume. In principle the electronics and central control unit will function in a similar manner to the TDRS IPACS for energy modes.

Inner gimbal assembly.- The RAM inner gimbal assembly is shown in cross section in figure 2-6. The constant stress wheel is fabricated of steel with a titanium shaft, weight 44 kg (97 lb), and operates over speed range of 22 500 to 45 000 rpm. Angular momentum varies from 1114 to 2229 N-m-sec (822 to 1644 ft-lb-sec) and stored energy from 365 to 1460 W-hr over this speed range.

The rotor is supported on two angular contact ball bearings (206H) built and specially selected for high-speed, long-life operation. The bearings are preloaded by a long travel spring. The preload method differs from the TDRS (which uses a central preload rod) since a hole through the shaft of the RAM rotor would produce unacceptable stress concentration and loss of energy storage capacity.

Centrifugal oilers, having a 5 year storage capacity, are used to lubricate the spin bearings.

To provide a maximum of 2400 W output from the rotor, two permanent magnet type brushless dc motor-generator units are used. These are identical, two-pole machines especially designed for high efficiency (97 percent). The motor-generator rotor is contained within the shaft of the wheel and utilizes rare earth magnets of high coercive force.

The wheel enclosure and inner gimbal is an aluminum double conical structure giving high stiffness and minimum weight. A central ring supports the gimbal shafts and provides the mounting surface for each gimbal cone. Electronics for the motor-generator are mounted on the inner gimbal assembly to minimize the number of flexible leads.

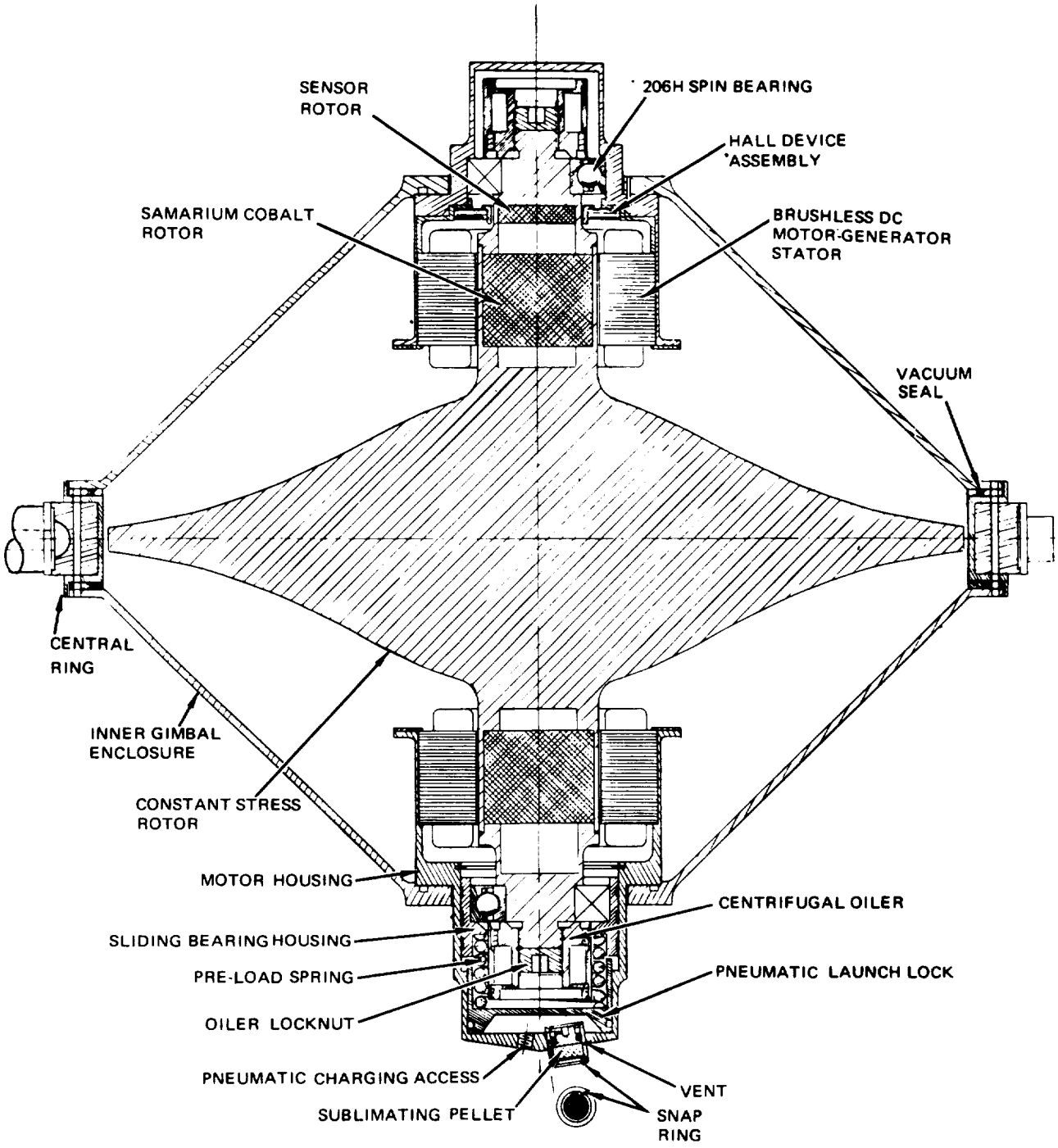

Figure 2-6. RAM Inner Gimbal Assembly

The total weight of the inner gimbal assembly is 56.1 kg (123.6 lb). The assembly unit is 41.9 cm (16.5 in.) in diameter and 44.2 cm (17.4 in.) maximum along the spin axis. The electronic package for the motor-generator would weigh 1.6 kg (3.5 lb).

A launch lock device is provided to lock the CMG rotor.

Rotor and shaft: The rotor is a constant stress design 37.8 cm (14.9 in.) in diameter. Rotor and shaft are integral. Placement of a hole through the wheel was acceptable for the TDRS design due to the thin cross section of its rotor. However, the stress concentration in the RAM wheel cross section at a central hole would impose too high a penalty on the design. Therefore, it was decided to use a different preload approach.

One motor-generator unit is located at each end of the wheel shaft with the two-pole rotor mounted in the center of the hollow shaft. The stub shafts are pressed into the ends of the hollow shafts and electron beam welded. The shaft wall is 0.23 cm (0.090 in.) thick which gives a sheer stress of 29.64×10^6 N/m^2 (4300 lb/square in.) at the worst-case condition of 50g. Centrifugal forces from the motor rotor cause a stress of 344.73×10^6 N/m^2 (50 000 lb/square in.) in the shaft wall at maximum speed.

The rotor is supported on two size 206H angular contact spin bearings on 32.3 cm (12.7-in.) centers. The centrifugal oilers are mounted on a shaft extension.

The rotor has a mass moment of inertia of 0.473 N-m-sec^2 (0.349 ft-lb-sec^2) about the spin axis and approximately 0.237 N-m-sec^2 (0.175 ft-lb-sec^2) about an axis perpendicular to the spin axis.

Spin bearings: The 206H angular contact spin bearings are press-fit to the rotor shaft and the inner races are clamped by the nut holding the centrifugal oilers. The bearing on the motor-generator sensor side is seated in the housing which supports both the stator and the spin bearing outer race. The outer race of the second spin bearing is supported in a housing which is free to slide in an axial direction. The preload force of 134 N (30 lb) is applied through a long travel spring to the movable bearing housing. Motions of the enclosure have a minimum effect on the bearing preload due to this approach. Axial friction in the movable bearing housing is reduced by a good finish on the surfaces and by venting the oil leakage from the spin bearings to this area.

The spin bearings are lubricated with RL-743 oil by centrifugal oilers.

Details of the spin bearing system appear in a subsequent part of this module.

Bearing housings: The two bearing housings support the spin bearings and motor generator stators and are fastened to the conical housings by screws. Labyrinth seals attached to the motor housing prevent lubricating oil from entering the motor area. The bearing housings are fabricated from steel to match the thermal coefficient with that of the spin bearings. Since the conical housings are aluminum for light weight and high stiffness, the bearing housings must be designed to prevent interference at the bearing outer race at low temperatures as a result of conical housing shrinkage. Therefore a clearance is provided between the main body of the bearing housing and the main bore of the truncated cone. The bearing housing is axially positioned by the outer diameter where radial stiffness in the bearing housing is high.

The bearing housings also support the motor-generator stators. Because of the high efficiency of these units, heating is low even at full load.

Conical shell: The conical shell serves the function of mounting structure, gimbal, protective cover, and vacuum enclosure for ground testing. A double conical structure of aluminum is used for light weight and high axial and radial stiffness.

The enclosure is composed of two truncated cones joined to a central ring by screws spaced 5.08 cm (2 in.) apart and sealed by a Parker Gask-O-Seal or similar. The truncated portion of the cones terminate in a mounting ring to support the spin bearings and motor through the bearing housings. The bearing housing - cone seal is by an O-ring. The conical shells and central ring weigh 3.21 kg (7.08 lb).

Two flat diametrically opposite mounting surfaces and centering holes are provided on the central ring for the inner gimbal shafts.

Sensors: Three sensor types are used to monitor operation of the wheel assembly:

- Speed sensor
- Temperature sensors
- Vibration sensors

The speed sensor utilizes a magnetic transducer with a permanent magnet bias field. Changes in the magnetic field are produced by gear teeth as they pass under the sensor element. This induces a voltage in the coil of the transducer. A 60-tooth gear mounted on the rotor measures the wheel speed.

Temperature sensors will be mounted at each spin bearing and at the motor-generator stators to monitor these critical temperatures to an accuracy of 2°C or better.

Accelerometers would be mounted at each bearing end to monitor vibration induced by rotor and/or bearings. Bearing irregularities and balance shifts can be measured.

Rotor windage: The constant stress rotor contour was approximated by a disk and cylindrical section. Preliminary calculations indicated that the range of pressures must be in the 0.013 to 0.13 N/m^2 (0.1 to 1.0 micron-Hg) range to keep windage losses within acceptable limits. Windage losses are given in Table 2-VI for three values of internal air pressure.

TABLE 2-VI.- ROTOR DRAG LOSSES FROM ATMOSPHERE IN ENCLOSURE

Air pressure in enclosure		Windage (W)	
N/m^2	Microns	22 500 rpm	45 000 rpm
0.013	0.1	0.45	1.78
0.133	1.0	4.45	17.80
0.666	5.0	50.90	239.00

At pressures of 0.013 to 0.13 N/m^2 (0.1 and 1.0 microns) the mean free path of the remaining gas molecules is on the order of the characteristic length of the rotor (radius) and windage equations are those suitable for the free molecular flow region. At 0.666 N/m^2 (5.0 microns), operation is in the transition region between free molecular flow and laminar flow. Windage in this region was determined by averaging the two calculations. However, operation would be unacceptable in the 0.666 N/m^2 (5.0 micron) region so that the error resulting from the above averaging process will not be serious.

For ground testing the enclosure pressures must be kept to 0.133 N/m^2 (1.0 micron) or less. This can be accomplished by a good rotary vacuum pump or by the use of a 5.08 cm (2-in.) diffusion pump. The latter would give a 2 - 3 order of magnitude improvement over the rotary pump.

A breather orifice and filter would be provided for orbital operation. With this arrangement, and considering an outgassing rate of 0.033 to 0.133 N/m^2 (0.25 to 1.0 micron) per hour, the internal pressure might not drop much below 0.1 micron. The vapor pressure of the spin bearing lubricant, which is 0.0013 N/m^2 (0.01 micron) at 65.5°C (150°F) and 0.1333×10^{-4} N/m^2 (0.0001 micron) at -17.8°C (0°F) will also limit the vacuum. While a low vacuum is not as critical as the TDRS design, the final design must consider shielding of bearings, minimizing sources of outgassing, and reducing the pressure drop through the breather orifice. When we consider the losses in the spin bearings

(approximately 93 W at 45 000 rpm), the windage losses of 17.8 W at 0.133 N/m^2 (1.0 micron) are probably acceptable.

Breather orifice, filter, and vacuum valve would be located on the central ring of the inner gimbal.

Spin-up and coast-down times: The sum of bearing and windage losses at an enclosure pressure of 0.133 N/m^2 (1 micron) is approximated by the expression

$$\text{Bearing and windage drag (watts)} = 10 + 4.98 \times 10^{-8} (\text{rpm})^2$$

When the motors are operated at constant torque at a maximum capacity of 2400 W at 45 000 rpm the spin-up time from zero speed is 1.25 hours, when drag W_d is considered.

The same drag losses will give a coast-down time from full speed of 29.5 hours and 13.5 hours from half speed (22 500 rpm).

Thermal characteristics: Heating in each motor-generator unit may be 36 W per unit for 40-second peaks or 21.2 W for a 35-minute period for a 97-percent efficient motor. Table 2-VII indicates the temperature rise resulting from the two conditions above and also with the transfer of all normally usable energy between 22 500 and 45 000 rpm. Thermal losses from the inner gimbal are ignored.

TABLE 2-VII.- MOTOR/GENERATOR UNIT HEAT GENERATION
(No Thermal Losses)

Energy transfer	Temperature rise (no losses from inner gimbal - 97% efficient)					
	Motor only		Inner gimbal (less rotor)		Inner gimbal	
	°C	°F	°C	°F	°C	°F
2400 W for 40 sec	2.3	4.1	0.45	0.81		
1417 W for 35 min			13.9	25.0	3.1	5.6
45 000 - 22 500 rpm (1095 W-hr)			22.3	40.1	5.0	9.0

If the average power (1417 W) is assumed to be continuously either transfered into or from the wheel the steady-state temperature rise in the inner gimbal, assuming only radiation losses from the inner gimbal, would be 10°C (18°F).

The relatively low motor generator heating in the inner gimbal assembly is attributable to the high efficiency of the motor generator units.

If we now consider all the losses within the inner gimbal we have:

36.8 W average motor-generator losses

70.0 W average bearing loss

10.0 W average windage at 0.133 N/m^2 (1.0 Micron)

116.8 W total

Again assuming only radiation losses, the temperature rise in the inner gimbal will be 39°C (70.2°F). The actual rise will be less than this due to some conduction losses through gimbal shafts and bearings. A rise of 30 - 35°C (54°F - 63°F) might be more reasonable.

To determine the bearing temperature rise above that of the inner gimbal, measurements on the 206H bearing in a CMG were reviewed. In tests where bearing losses were 16.5 W, a temperature rise at the outer race of the bearing of 7.2°C (13°F) was measured. If we now generate 70 W in this same bearing the temperature rise with the same surrounding structure would be:

$$\frac{70}{16.5} \times 13 = 55°F = 30.6°C$$

(the actual rise would be less than this value).

This rise would be above that of the inner gimbal. Since 60 percent of the heat is generated in the spin bearings, an effort should be made in subsequent work to optimize wheel speed and bearing preload.

Motor-generator design for RAM.- A high efficiency motor-generator unit is required to transfer power into and from a high-speed energy storage wheel with a speed range of one half to full speed. The motor-generator also must be compatible with the two-gimbal configuration selected in the feasibility study (Volume I of this report). Table 2-VIII partially summarizes design requirements.

TABLE 2-VIII.- RAM MOTOR-GENERATOR ELECTRICAL DESIGN REQUIREMENTS

Peak generator output:	2400 W
Operating speed range:	22 500 - 45 000 rpm
Average power at mean energy storage point (35 600 rpm):	
Motor:	1040 W
Generator:	1417 W
Line voltage:	52 V
Efficiency at average power point:	97% min

Initial considerations: Preliminary calculations indicated a motor stack length of 8.18 cm (3.2 in.) and an rms current of 76 amps at the minimum speed of 22 500 rpm. The high current and relatively long stack length indicated that the use of two units, one on each side of the constant stress wheel, would be more reasonable. Therefore, the subsequent design is for a motor-generator unit of 1200 W maximum with average power of 520 W (motor) and 718 W generator.

Stator design: An initial selection of 20 slots was made. With 20 slots there can only be 10 or 15 turns per phase with either two or three conductors per slot, respectively. Assuming 15 turns, five slots per pole and phase, two phases, and eight-slot winding pitch, the harmonic content is shown in Table 2-IX. Ripple is very low with the voltage almost ideally sinusoidal.

TABLE 2-IX.- HARMONICS OF EMF WAVE

Harmonic	Percent Fundamental
1	100.0
3	0
5	0
7	-1.26
9	0
11	-0.826
13	+0.366
15	0

The stator punching is shown in figure 2-7. The slot has a circular cross section at the bottom, which is a result of several preliminary designs. The overall slot cross section is increased by this circular section resulting in decreased copper losses. The peak flux density in the yoke will become locally higher, but the overall yoke losses will be only slightly higher and will be more than balanced by decreased copper losses.

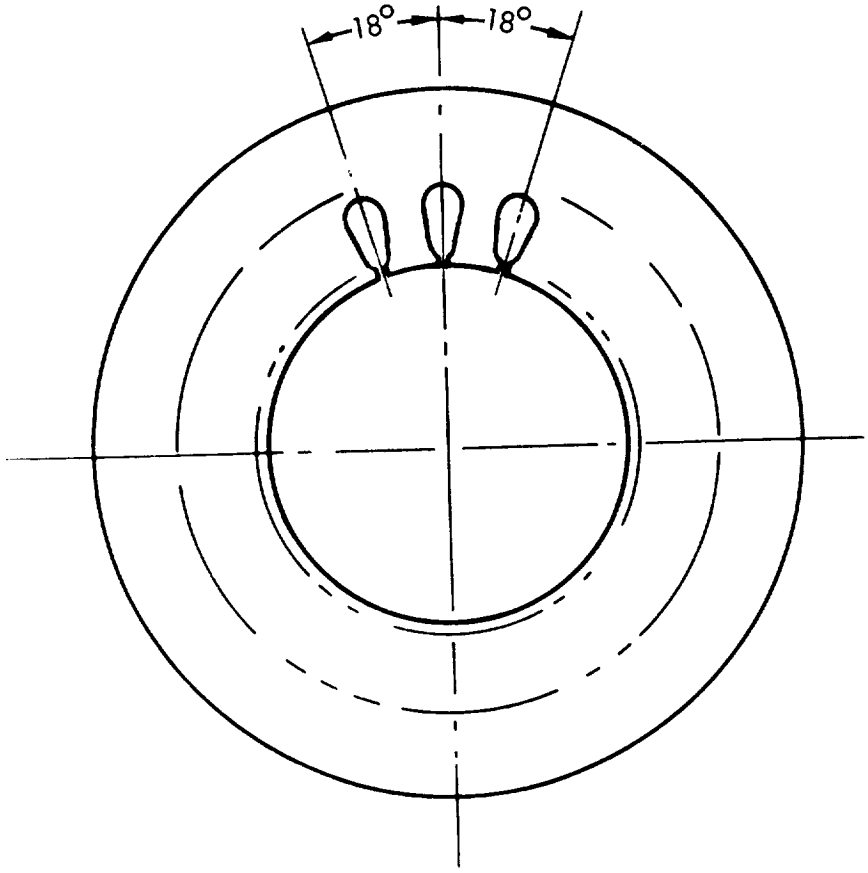

Figure 2-7. Motor-Generator Stator Punching for RAM

To keep core losses low, the maximum average air gap flux density at the stator surface is B_{ave} = 3266 gauss, and the maximum iron flux density is taken at B_{fe} = 5800 gauss. This, then, determines the tooth and yoke cross section. Stator mass will be somewhat higher than a conventional design due to high speed and efficiency requirements.

The slot cross section is 39.9 mm^2 (0.0618 $in.^2$), and with 40 percent utilization the bare copper cross section is 15.99 mm^2 (0.0248 $in.^2$). Mean turn length is 0.305 m (12.0 in.).

The stator punchings are AL-4750, 0.152 mm (0.006 in.) thick with a total stack length of 40.5 mm (1.595 in.).

The winding diagram is shown in figure 2-8. Each winding section consists

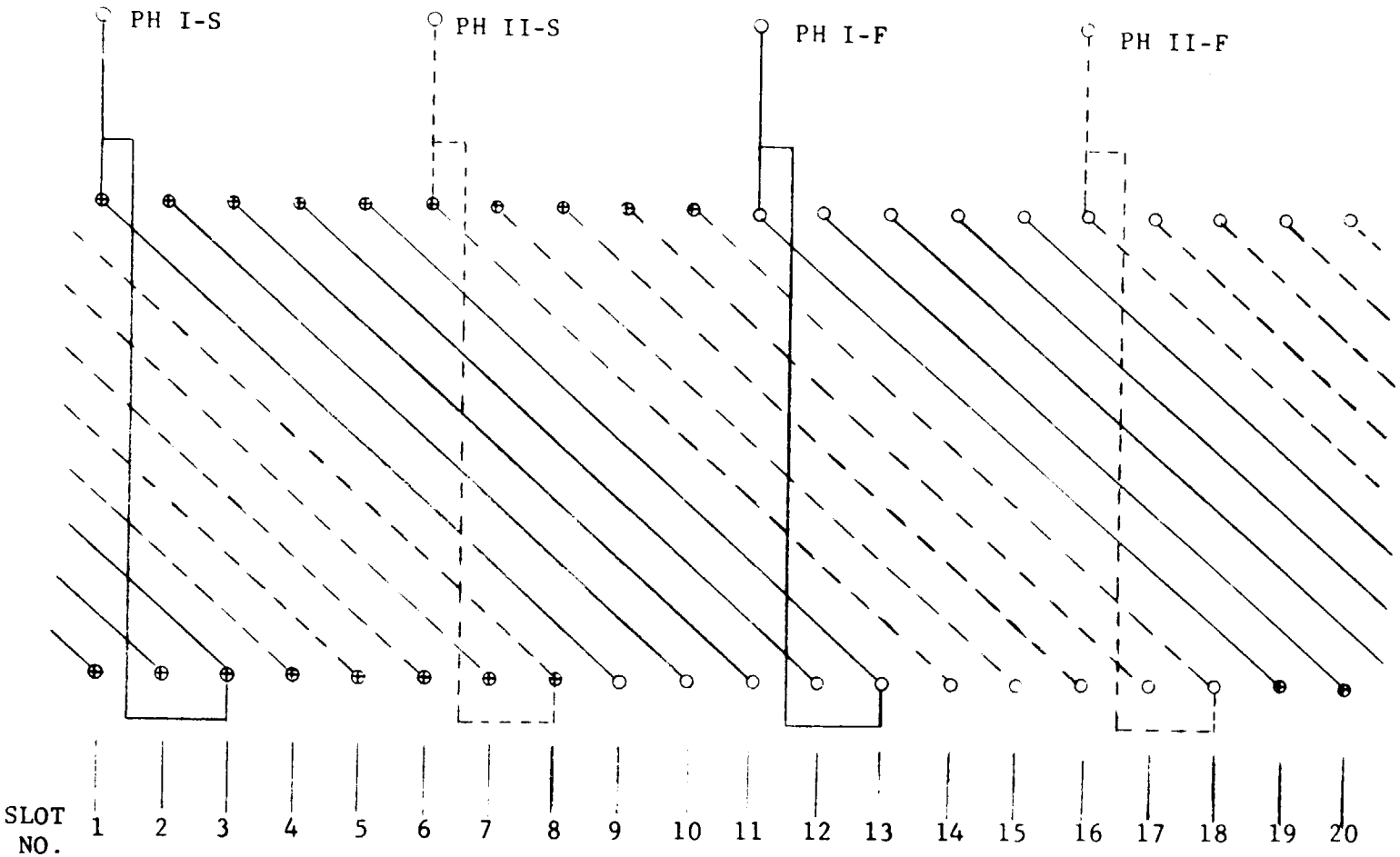

Figure 2-8. Wiring Diagram - RAM

of five skeins of three turns each having 13 parallel wires of AWG No. 24 HML. Resistance of each phase, including leads, is 0.0156 ohms at 25°C (77°F).

Rotor design: The cross section of the rotor is shown in figure 2-9. The rotor is contained in the hollow nonmagnetic shaft of the constant stress wheel. The overall air gap is 2.54 mm (0.100 in.) with a 2.28 mm (0.090-in.) shaft wall. The rotor is two-pole and consists of two pieces of core iron with two central samarium cobalt magnets. The rotor is 3.746 cm (1.475 in.) long and is .510 mm (0.020 in.) shorter than the stator stack. Pole flux is 3266 gauss with an assumed leakage of 18 percent. Permenance calculations are made in the next section. Centrifugal forces on the rotor cause a stress of 34.470×10^7 N/m^2 (50 000 psi) to appear in the shaft shell at maximum speed.

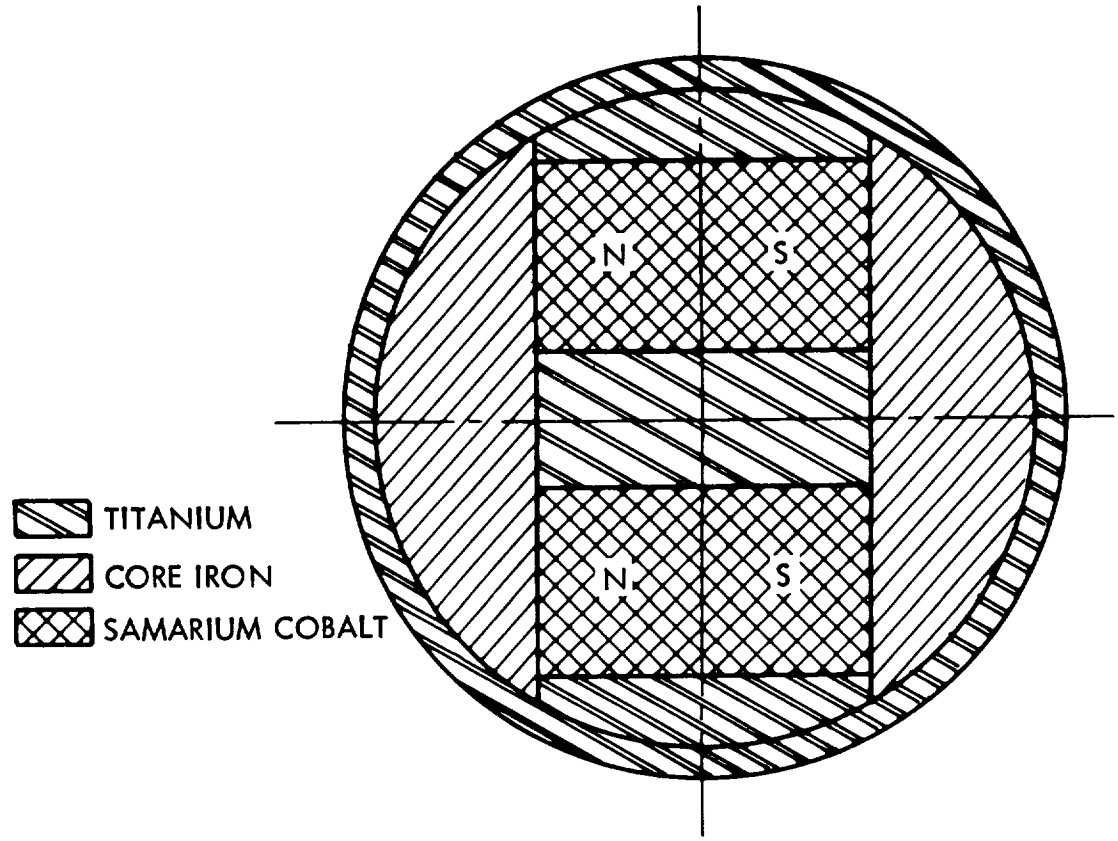

Figure 2-9. RAM Rotor Cross Section

Permeance and winding inductance: The total air gap permeance (Table 2-X) is the sum of the gap and fringe permeance around the pole edges. The fringe permeance consists of the end fringing from rotor to stator and the pole edge fringing.

TABLE 2-X.- MOTOR/GENERATOR ROTOR AIR GAP PERMEANCE

Source	Permeance	
	cm	in.
Air gap	19.86	7.82
End fringing	0.96	0.38
Pole edge fringing	1.42	0.56
Total	22.24	8.76

The total rotor permeance consists of the air gap permeance plus leakage permeances (Table 2-XI).

TABLE 2-XI.- MOTOR/GENERATOR ROTOR TOTAL PERMEANCE

Source	Permeance	
	cm	in.
Total air gap	22.24	8.76
Leakage between magnets	0.77	0.30
Leakage between inner pole piece edges	0.99	0.39
Leakage from axial pole piece faces - inner path	0.21	0.08
Leakage from axial pole piece faces - outer path	2.18	0.86
Total	26.39	10.39

The resulting leakage flux is 15.8 percent and is lower than originally estimated (18%). The permeance coefficient now becomes:

$$12.44 \frac{\text{Gauss}}{\text{Oersted}}$$

Figure 2-10 shows the permeance coefficient $(B/H)_C$ line plotted on the demagnetization curve for samarium cobalt. This gives a flux in the neutral zone of the rotor magnet as 8750 gauss and the pole flux becomes 77 064 maxwells. This is a 2.3 percent increase in flux over the design value of 75 310 maxwells. The 2.3 percent improvement may be considered as a safety factor, or the air gap may be increased by 0.508 mm (0.020 in.) to increase the wall thickness of the shaft to 2.794 mm (0.110 in.).

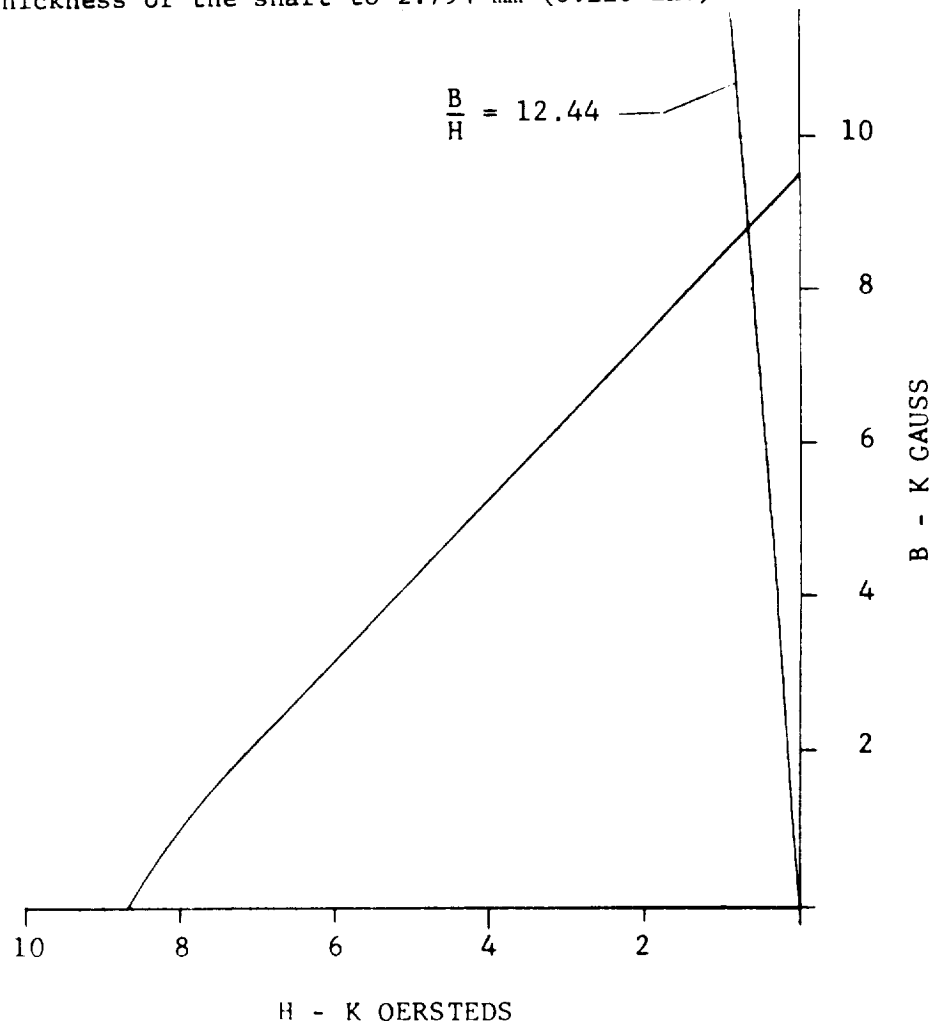

Figure 2-10. Demagnetization Curve for Samarium Cobalt

The winding diagram shows that there are six fully-occupied slots per phase and four slots with conductors either at the bottom or top of the slot. The total inductance of the winding is summarized in Table 2-XII.

TABLE 2-XII.- MOTOR/GENERATOR WINDING INDUCTANCE

Component	Inductance (microhenries)
Slot leakage	8.7
Tooth head leakage	2.5
End turn leakage	12.9
Armature reaction	44.4
Total	68.5

The electrical time constant now becomes 4.4 millisecond.

Efficiencies: Losses in the motor-generator consist of copper and core losses. The copper losses are readily calculated knowing the winding resistance and the current associated with the motor-generator load. The core loss is a function of the amount and type of stator material, punching thickness, wheel speed, and armature reaction. At 36 500 rpm the material selected gives 6.05 W loss per kg (2.75 W loss per lb), for a total of 8.59 W for the 1.42 kg (3.12 lb) of stator material used.

Table 2-XIII summarizes losses and efficiencies for critical operating conditions. Specific core losses for a flux density of 6000 gauss are 2.64 W per kg (1.2 W per lb) at 22 500 rpm, 5.72 W per kg (2.6 W per lb) at 36 500 rpm, and 8.14 W per kg (3.7 W per lb) at 45 000 rpm.

TABLE 2-XIII.- LOSSES AND EFFICIENCIES FOR RAM MOTOR-GENERATOR

	Power (W)	Speed (rpm)	Core loss (W)	Copper loss (W)	Percent efficiency
Motor	520	22 500	5.6	7.3	97.6
	520	36 500	10.9	2.8	97.4
	520	45 000	15.4	1.8	97.0
Generator	708.5	22 500	5.6	14.2	97.2
	708.5	36 500	10.9	5.4	97.8
	708.5	45 000	15.4	3.5	97.3
Generator	1200	22 500	6.2	42.3	96.1
	1200	36 500	11.5	16.1	97.7
	1200	45 000	15.8	10.2	97.9

The core loss used in the efficiency calculation is twice the value given above to allow for strain in the punchings and to provide a safety factor.

Note that the efficiency only drops below 97 percent at the point where speed is low and power and current are high. At this point copper losses are relatively high. Fortunately, the duty cycle at this point is low since wheel energy has dropped off to one-fourth and a relatively small amount of motor or generator power will remove the wheel from this extreme energy boundary.

Efficiency calculations in all cases have been conservative and detailed enough to have considered all significant losses. A motor-generator carefully built to this design would be expected to have efficiencies at least as high as indicated in Table 2-XIII. However, some additional work will be required during the final design stage to establish sensor configurations and perform optimization.

Motor-generator characteristics: The motor-generator design characteristics are summarized in Table 2-XIV.

Spin Bearing System.- The spin bearing system for the RAM consists of the two spin bearings, the method for preloading these bearings, and a means for providing the correct amount of lubrication during the 5-year lifetime. The RAM design uses standard size ball bearings which are specially built for high speed and long life.

TABLE 2-XIV.- MOTOR-GENERATOR DESIGN CHARACTERISTICS FOR RAM

Physical characteristics		
Outside diameter	10.67 cm	(4.200 in.)
Overall length	6.09 cm	(2.40 in.)
Stator material	AL-4750	0.152 mm (0.006 in.) thick
Stack length	4.05 cm	(1.595 in.)
Stator bore	5.43 cm	(2.140 in.)
Number of slots	20	
Iron to iron gap	0.254 cm	(0.100 in.)
Rotor material	4.92 cm	(1.940 in.)
Rotor length	(3.74)cm	(1.475 in.)
Number of poles	2	
Stator weight	2.65 kg	(5.85 lb)
Rotor weight	0.508 kg	(1.12 lb)
Total motor weight	3.16 kg	(6.97 lb)
Winding characteristics		
Number of phases	2	
Pitch	8 slots	
Slots per pole and phase	5	
Wire size	AWG No. 24 HML	
Slot utilization (bare copper)	40%	
Winding	5 skeins, 3 turns each having 13 parallel wires	
Approximate turn length	30.48 cm	(12 in.)
Electrical characteristics		
Rated output	1200 W	
Speed range	22 500 - 45 000 rpm	
Voltage	52 Vdc	
Back EMF constant, K_E	0.01019 V/rad/sec	
Torque constant, K_T	0.0102 N-m/amp (0.007513 ft-lb/amp)	
Winding resistance per phase	0.0156 ohms at 25°C	
Winding inductance per phase	68.5 microhenries	
Electrical time constant	4.4 milliseconds	

Bearing selection: In selection of the spin bearings for the RAM inner gimbal, four factors must be considered:

Static load capability under launch conditions

Bearing life

Losses at operating speeds

Bearing stiffness

For the RAM, four ball bearing types were selected for consideration. These are listed in Table 2-XV along with the first two items listed above. The L_{10} life requirements were estimated to be 73 000 hours. From the life standpoint either the 206H or the 207H bearing would meet the life requirement at a 222-N (50-lb) preload.

The launch loading is approximately 4000 N (900 lb) thrust load at 10g and 20 000 N (4500 lb) thrust load at 50g. The dynamic launch load is expected to be at some point between these values. For the RAM, one or more of the gyros may take a radial load 2000 N (450 lb) at 10g, and 10 000 N (2250 lb) at 50g per bearing. Of the four bearings, only the 204H would be rejected due to loads.

TABLE 2-XV.- SPIN BEARING SELECTION FOR RAM

Bearing	Static load rating				L_{10} Life (hr) at 45 000 rpm (222 N preload)
	Radial		Thrust		
	N	lb	N	lb	
204H	7 117	1600	16 902	3 800	17 600
206H	13 789	3100	36 829	8 280	74 500
207H	18 815	4230	49 818	11 200	147 000
304H	11 386	2560	29 891	6 720	34 800

Based on the load and life factors, either the 206H or 207H bearing could be used. We must now consider bearing losses at operating speeds. Table 2-XVI gives spin bearing losses at 45 000 rpm for the two remaining candidates. The 206H bearing has about 15-percent lower drag torque at operating speed. Another

factor to consider is the high bearing losses of both bearings at 222-N (50 lb) preload. By reducing the preload to 133-N (30 lb) (probably the minimum acceptable is 111 N (25 lb)) the drag torque is reduced to 60 percent of the loss, which is 93 W for the two 206H bearings.

TABLE 2-XVI.- SPIN BEARING LOSSES AT 45 000 RPM

	206H Bearings	207H Bearings
Applied load friction, N-m (in. oz)	0.0249 (3.53)	0.0263 (3.73)
Viscous drag, N-m (in. oz)	0.00797(1.14)	0.0124 (1.76)
Total drag, N-m (in. oz)	0.0329 (4.66)	0.0387 (5.49)
Total drag power, W	154.0	181.0
Note: Two bearings and 222 N (50 lb) preload		

The 206H bearing selected for the RAM application would be operated at 33 N (30 lb) preload and within a speed range of 22 500 to 45 000 rpm. This new preload would increase the L_{10} life from 74 500 to 330 000 hours which is adequate for the estimated requirement of 73 000 hours.

In determining the bearing life, conventional bearings have been considered. A safety margin is obtained by use of (1) vacuum melt M-50 tool steel and (2) selected low race waviness and eccentricity $<1.27 \times 10^{-4}$ cm ($<50 \times 10^{-6}$ in.). An improvement factor of 5 to 10 is possible with these precautions.

An angular contact spin bearing is used to provide adequate bearing stiffness. Natural frequencies should be above 100 Hz to meet vibration test requirements. The RAM stiffness analysis is included in the CMG assembly section.

The initial four bearing factors are given in Table 2-XVII for the 206H bearing.

TABLE 2-XVII.- 206H BEARING FACTORS

Static load	
Axial	36 829 N (8280 lb)
Radial	13 788 N (3100 lb)
L_{10} life	330 000 hr
Bearing losses (for 2 bearings)	93 W at 45 000 rpm 36 W at 22 500 rpm
Stiffness	
Axial	0.42×10^8 N/m (0.240×10^6 lb/in.)
Radial	2.43×10^8 N/m (1.39×10^6 lb/in.)

Preloading methods: Preloading is a parasitic axial load introduced when mounting bearings, and is employed to eliminate radial and end play, reduce non-repetitive runout, and increase system rigidity. There are three basic methods of achieving preloads:

- Spring preloading
- Axial adjustment, either using preload rod or across the frame
- Duplex bearings

A fourth method, also considered for RAM, makes use of a centrifugal preloader. This is described in the TDRS conceptual design section (Module 1, Volume II).

Axial adjustment across the frame was rejected due to the weight penalty necessary for the required stiffness and the objectionable preload variation from thermal and pressure developed dimensional changes.

The preload rod method of axial adjustment requires a hole through rotor and shaft. Such a hole would cause objectionable stress concentrations in the rotor. It, too, was rejected.

The centrifugal preload method also was discarded because the sliding fit necessary at the inner race of the bearing would cause uncertainties in dynamic balance.

Both the spring loading and duplex pair methods are feasible candidates. However, use of duplex pairs would greatly increase bearing drag and present difficulties in lifetime lubration methods negating its use in the RAM design.

The spring preloading method selected offers several advantages:

- Preloading is more uniform than other systems.
- It is less sensitive to differential expansion.
- It offers more accommodation to minor misalignment.

Preloading selected for RAM: The spin bearings are preloaded at 133.4N (30 lb) across the conical enclosure. This enclosure ties both bearings together and a helical spring, placed between the enclosure and one bearing, is deflected to provide the desired force. The preloading force is through the outer races to the bearing balls, then to the inner races through the shaft.

The low gradient of the spring 1.49×10^4 N/m (85 lb/inch) allows only small changes in preload due to thermal and pressure changes in the enclosure. A sliding sleeve concentric with one bearing permits it to move with the spring load as dimensional changes occur. The enclosure may have an axial motion at the worst case of ± 0.127 mm (± 0.005 in.) causing a change in preload which is not greater than 1.4 percent or 1.89 N (0.425 lb). Since this condition occurs only at one atmosphere of differential pressure between inside and outside of the inner gimbal, it will not occur under normal orbital conditions.

Differential expansion, over the operating temperature of -6.67°C to 60°C (+20°F to 140°F) will cause a maximum change in preload of 1.1 percent or 1.15 N (0.34 lb).

The preload method, by itself, has one disadvantage. The low spring rate of 1.49×10^4 N/m (85 lb/in.) presents opportunity for impact damage to bearings under launch vibration environment. To prevent such damage, a launch lock must be used in conjunction with the spring preload. This lock must be activated prior to launch and deactivated in orbit.

Launch lock: The launch lock mechanism shown in figure 2-6 will increase preload during launch by air pressure on a piston which compresses the preload spring and makes contact with the movable outer race of one spin bearing. Expansion and contraction of the conical housing can still occur without any appreciable change in preload. The launch lock is pressurized prior to mounting in the vehicle. A sublimating solid is used to seal a small piston operated valve. Under the vacuum of space the solid sublimates and allows this piston to move under the internal pressure and vent the pressurized chamber to space, thus releasing the launch lock automatically.

An organic solid such as hexachlorethane or acetophenone could be used. The gas in the launch lock chamber is exhausted through the vent and the bearing preload drops to 133.4 N (30 lb) for orbital operation.

A preload of 2224 N (500 lb) would be sufficient and would require a gas pressure of 67.56×10^4 N/m^2 (98 psi). If the spin axis is placed parallel to the launch vehicle axis, the launch lock mechanism should be in the direction of the nose of the vehicle.

Preload adjustment: The preload is established by the overall dimensions and by selection of the spring. The preload must have a gradient of 1.49×10^4 N/m (85 lb per in.) and an overall length which will allow a deflection of 0.897 cm (0.353 in.) during assembly. This deflection will produce a sustaining force of 133.4 N (30 lb) on the spin bearings.

Bearing lubrication: The spin bearings require lubrication replenishment during the 5-year life. The rate of replenishment must be adequate but not excessive as the viscous drag component of bearing loss at rated speed would approach 25 percent of the total power.

The lubricant chosen is RL-743. Evaluation tests on spin bearings have shown RL-743 oil superior to other greases and oils. This oil exhibits low drag under vacuum conditions and is easily stored and metered into the bearings.

Centrifugal oilers are used to meter oil into each bearing. The oilers are attached to the ends of the spin shaft adjacent to the bearings. The cylindrical storage chamber contains felt (SAE-F10) saturated with 20.7 cc (1.26 in.^{3}) of usable oil. The oil is metered at 100×10^{-6} cc per hour (at 75°F or 23.9°C) through calibrated leaks.

The centrifugal force generates a maximum pressure of 3.37×10^6 N/m^2 (490 psi) to force the oil through the calibrated leak. A peripheral lip carries the oil to the bearing ball retainer and then on to each ball. The flow rate will vary from 11.0×10^{-6} cc (0.67 in.^{3}) per hour at -6.67°C (20°F) to 500×10^{-6} cc (30.5×10^{-6} in.^{3}) per hour at 60°C (140°F). Enough oil is contained to lubricate the bearing for 4.75 years at the highest flow rate. The average flow rate will be considerably below this value.

During storage periods the oil flow rate is zero. During these periods capillary forces in the felt prevent oil seepage through the pressure-equalizing orifice. This orifice is provided to prevent air or vacuum pressure differential between the inside and outside of the oil reservoir from varying the flow rate. The orifice is located so that centrifugal force drives the oil away from it.

In general, the centrifugal oiler provides oil flow commensurate with operating conditions. Flow is high at elevated temperatures and high speeds where additional oil is required. Excess bearing lubricant is absorbed in a sintered material collector located in the bearing housing (not shown in the drawings).

The metering device (calibrated leak) is a small threaded cylinder containing sintered material. It is approximately 3.175 mm (1/8 in.) in diameter and 6.35 mm (1/4 in.) long and is located at a point where centrifugal pressure is maximum. Porosity is selected to provide the desired flow rate.

Torquer unit.-

Selection: The torque requirements for both inner and outer gimbals do not exceed 9.49 N-m (7 ft-lb) as estimated for disturbing torques, maneuvering the spacecraft, and for servo response. The highest torque and, fortunately, the torque with the light duty cycle is that required for maneuvering.

A direct-drive torque motor was selected over the geared unit for the following reasons:

- Torque and average power requirements are acceptably low.
- Breakaway friction is minimized.
- Improved response is obtained.
- Reliability is superior to geared drive.
- High stiffness is achieved.

A 9.49 N-m (7.0 ft-lb) torquer with dimensions of 18.29 cm (7.2 in.) diameter by 4.13 cm (1.625 in.) long and weighing 3.17 kg (7.0 lb) was selected. The design can be a conventional off-the-shelf unit or may be an advanced design which would require non-recurring development costs.

A torque motor of advanced design using rare earth magnets with high energy product and optimized for minimum I^2R losses can provide an appreciable saving in power over the more conventional design. This is evidenced by figures 2-11 and 2-12 where motor power and weight are plotted for the 9.49 N-m (7.0 ft-lb) and 20.33 N-m (15 ft-lb) sizes. Notice that, if we are willing to accept a higher weight torquer, the power is reduced considerably. Generally a compromise is made where the torquer weight in pounds is approximately equal to the maximum torque in ft-lbs. For this case, Table 2-XVIII indicates the comparison between the conventional and the advanced design.

For the RAM application, the torque motor duty cycle at rated torque is low. The disturbing torques are sinusoidal and require a torque of approximately 1.36 N-m (1.0 ft-lb). The maneuvering torque requirements will not exceed 8.13 N-m or (6 ft-lb) if we assume that the vehicle rate of .0017 rad/sec (6°/min) must be established within 1-1/2 minutes and will be of short duration and infrequently. Table 2-XVIII indicates the peak power for the motor selected as 133 watts or 98 watts for an output torque of 8.13 N-m (6 ft-lb).

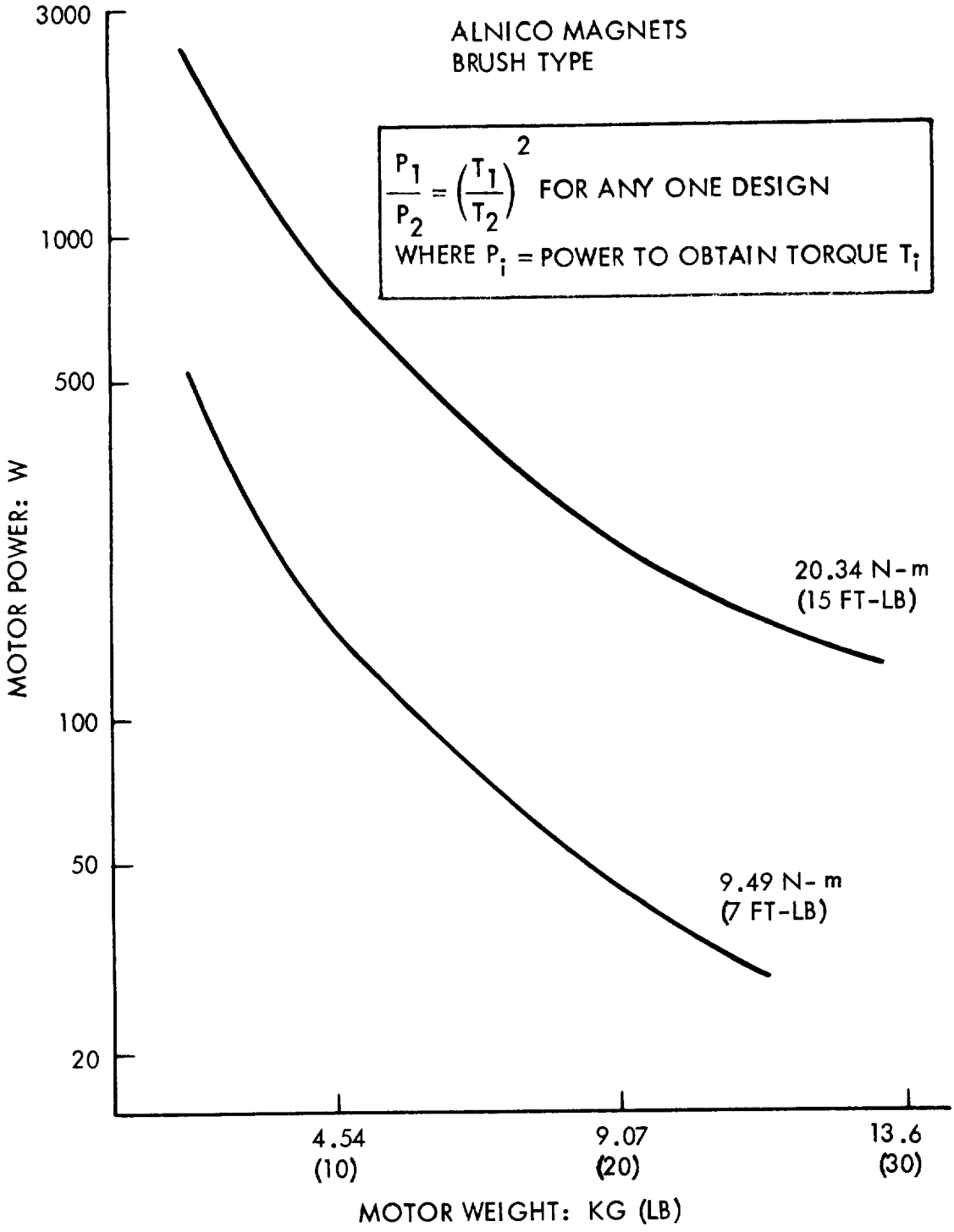

Figure 2-11. Conventional Torque Motor Weight-Power.

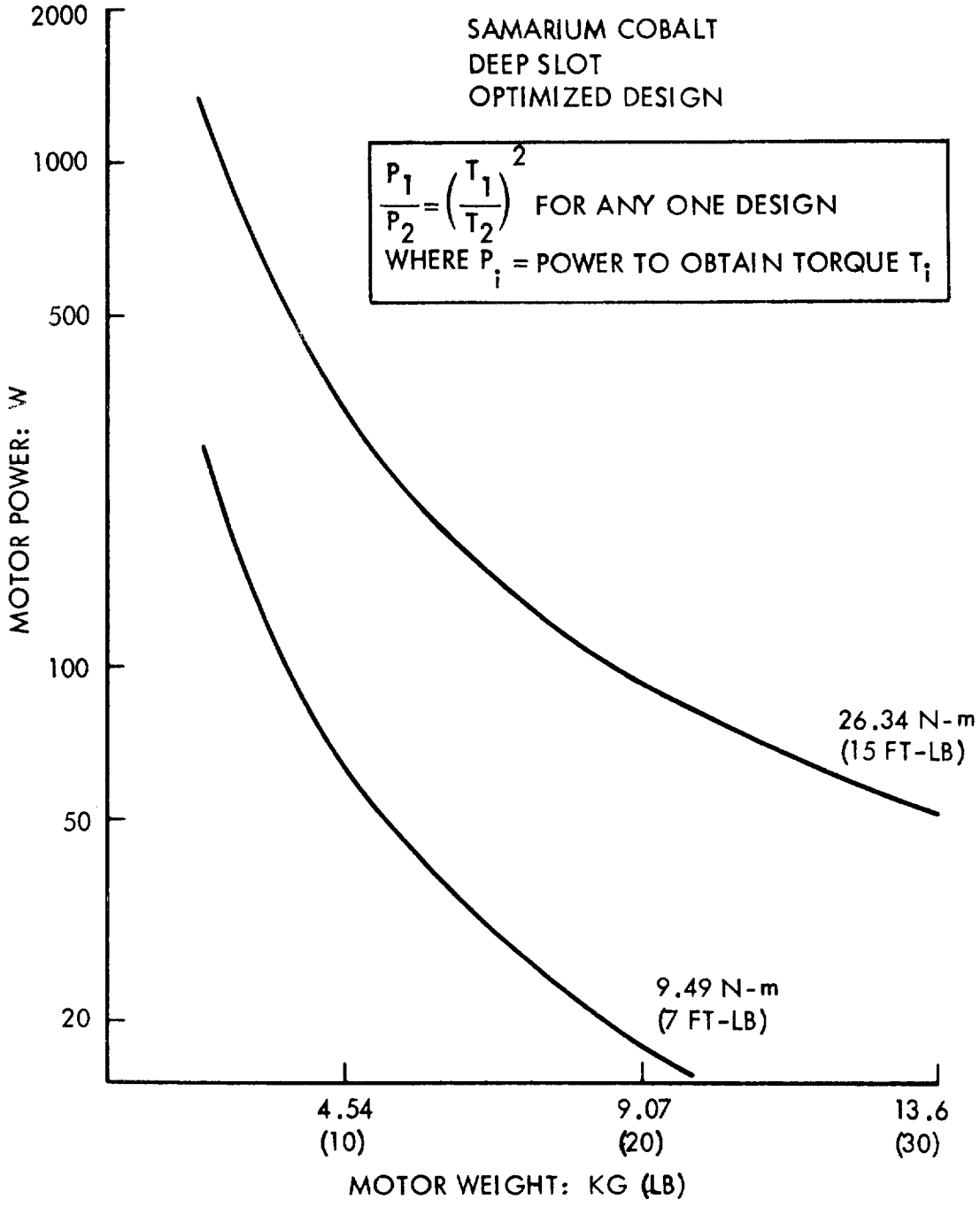

Figure 2-12. Advanced Torque Motor Weight-Power

TABLE 2-XVIII.- COMPARISON OF CONVENTIONAL AND ADVANCED TORQUE MOTORS

Torque motor weight-kg(lb)		Torque output N-m	(ft-lb)	Power (W) Conventional	Advanced
3.2	(7)	4.65	(3.5)	66	33
3.2	(7)	8.13	(6.0)	196	98
3.2	(7)	9.49	(7*)	265	133
3.2	(7)	14.24	(10.5)	596	299
6.8	(15)	10.17	(7.5)	96	37.5
6.8	(15)	20.34	(15)	385	150
6.8	(15)	30.51	(22.5)	866	338

* Normal maximum output torque for the machine size indicated.

Characteristics: The cross section of the torquer unit is shown in figure 2-13. The torque motor is mounted in an aluminum alloy housing 21.59 cm (8.5 in.) in diameter which is flange-mounted to the gimbal or support. The gimbal shaft is supported by a preloaded pair of A541T ball bearings. The bearings are arranged in the DF configuration as this form of mounting is less sensitive to misalignment. The torque motor rotor is keyed to the gimbal shaft (refer to figure 2-6).

Table 2-XIX summarizes the characteristics of the torquer unit.

TABLE 2-XIX.- CHARACTERISTICS OF RAM TORQUER UNIT

Size	21.6 cm diam x 5.72 cm long (8.5 in. diam x 2.25 in. long)
Weight	5.13 kg (11.32 lb)
Mounting	Flange
Gimbal bearings	Duplex pair (A541T)
Torque motor (advanced design)	
Size	18.3 cm diam x 4.13 cm long (7.2 in. diam x 1.625 in. long)
Weight	3.18 kg (7 lb)
Rated torque of motor	9.49 N-m (7 ft-lb)
Maximum RAM torquer power	133 W
Torque sensitivity	1.76 N-m/amp (1.3 ft-lb/amp)
Input volts (to electronics)	52 V
Friction	0.027 N-m (0.02 ft-lb)

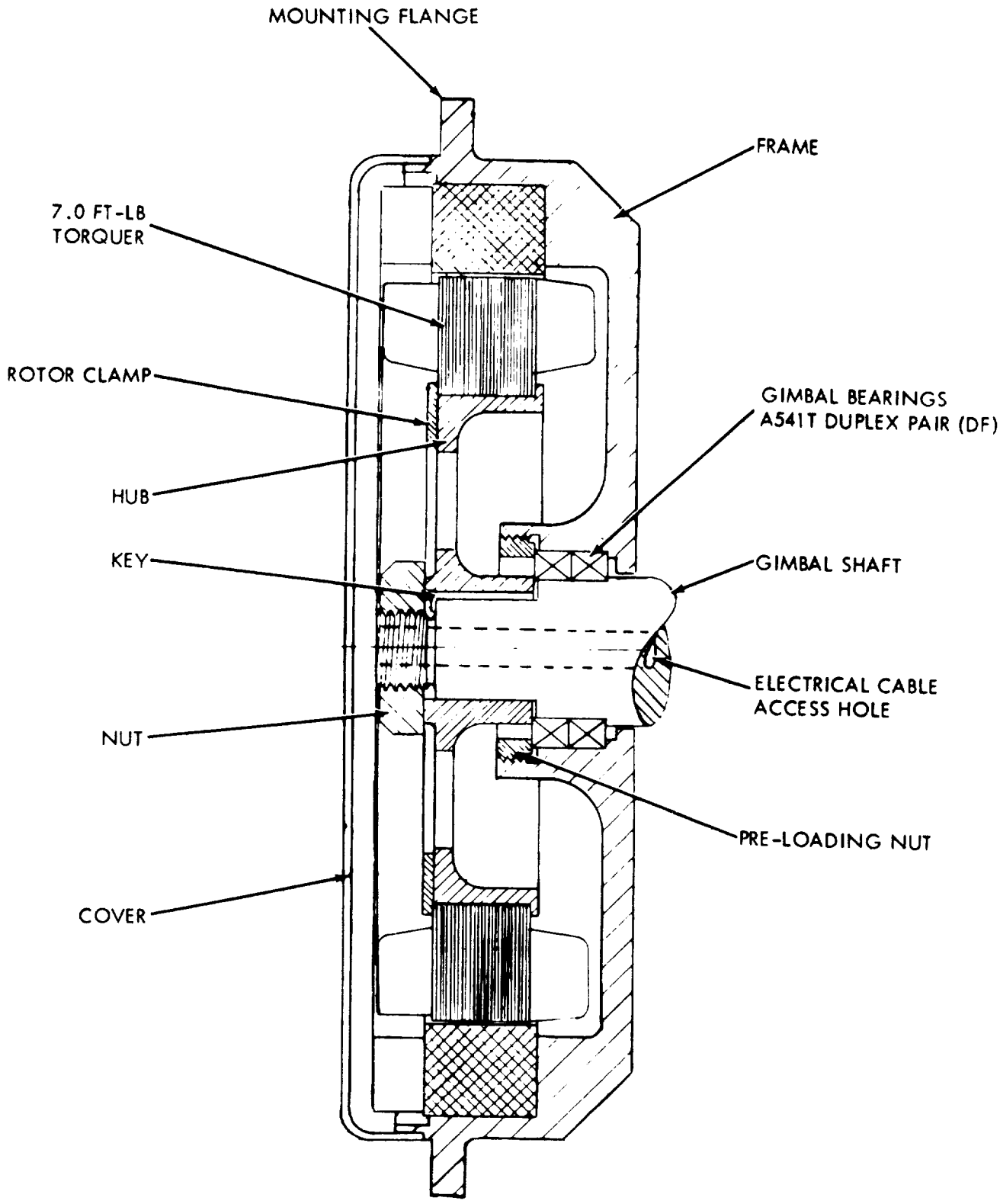

Figure 2-13. RAM Torquer Module

Sensor unit.- The sensor unit provides gimbal position and rate information and supports one side of the gimbal. A cross sectional view is shown in figure 2-14. It consists of a resolver and a tachometer mounted on a cantilevered shaft. The shaft contains an internal spline coupling to provide a stress relief joint for the gimbal axis. The spline minimizes effects of misalignments and thermal expansion. Spline backlash is 0.00029 rad (1 arc min) but this can be reduced to zero by a preload element.

The sensor shaft and gimbal is supported by a preloaded pair of A543T bearings whose ball race center-to-center distance is increased to 0.889 cm (0.350 in.). This increase is effected by locating two match ground spacers between the bearings.

The bearings are arranged in the DB configuration to provide a high moment rigidity.

The tachometer, used for rate feedback for accurate speed control, is an Inland dc device (TG-2913D). Table 2-XX exhibits pertinent data for the tachometer. As an alternative, a brushless tachometer could be used within the envelope shown. The brushless unit would have better life characteristics but require additional electronics and a limited development effort.

TABLE 2-XX.- RAM TORQUER TACHOMETER CHARACTERISTICS

Friction torque	0.019 N-m (0.014 ft-lb)
Ripple voltage, average to peak	4%
Sensitivity	3.2 V/rad/sec
Resolution	8.72×10^{-5} rad/sec (.005°/sec)
Weight	0.68 kg (1.5 lb)
Maximum diameter	9.47 cm (3.73 in.)
Maximum width	2.77 cm (1.09 in.)

Position error is detected by a General Precision size two resolver. It is a rotary transformer type providing both sine and cosine functions as outputs. Table 2-XXI lists its characteristics.

TABLE 2-XXI.- RAM TORQUER RESOLVER CHARACTERISTICS

Input	22 Vac, 400 Hz
Output	22 Vac, 400 Hz
Null	30 mV
Maximum error	4.4×10^{-3} rad (15 $\widehat{\text{min}}$)
Phase shift	0.069 rad (4°)

The sensor unit is flange-mounted to the gimbal and is 13.84 cm (5.45 in.) in diameter and 8.64 cm (3.4 in.) long and weighs 2.75 kg (6.06 lb).

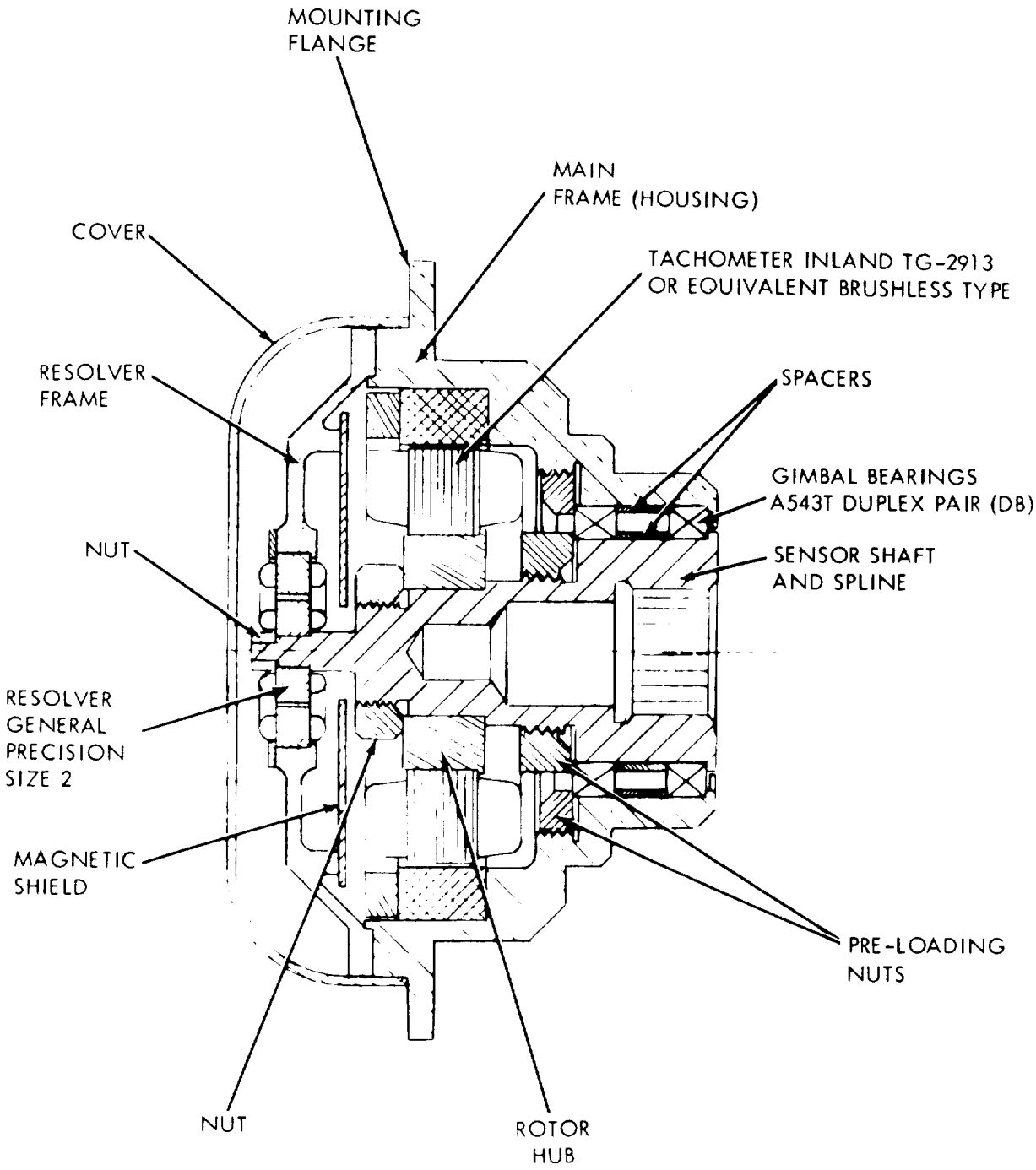

Figure 2-14. RAM Sensor Module

Outer gimbal: The outer gimbal is fabricated from aluminum alloy with a box-type cross section 5.08 cm (2 in.) by 7.62 cm (3 in.) with a 0.254 cm (0.1 in.) thick wall. This structure weighs 17.9 kg/m (0.1 lb/in.) and has an inertia of 50.24 cm^4 (1.207 $in.^4$). Heavier sections are required at the axes to both strengthen and provide mounting surfaces for the torquer and sensor units. The gimbal has an approximate outside diameter of 56.39 cm (22.2 in.) and an inside diameter of 46.23 cm (18.2 in.). The total weight is 7.03 kg (15.5 lb).

Torsional stiffness inner gimbal axis to outer gimbal axis is 0.531 x 10^6 N-m/rad (4.7 x 10^6 in. lb/rad). Linear stiffness is 8.58 x 10^8 N/m (4.9 x 10^6 lb/in.). With a 22.2 N (5 lb) unbalance load at 10g, the maximum stress level is less than 4.32 x 10^6 N/m^2 (700 psi).

CEMG/energy storage assembly.-

Description: The inner gimbal assembly provides both the energy storage and transfer capability for the RAM power system and the angular momentum for the control energy moment gyro (CEMG) attitude control system. The attitude control system design for this study utilizes three double-gimbal CEMG's in a 3-PM configuration. The 3-PM configuration is one in which the outer gimbals of each of the 3 CEMG's are parallel to each other and parallel to the minor axis of inertia (or roll axis) of the spacecraft. The inner gimbals of the gyros are slaved together and move through small angles since roll axis momentum requirements are low.

The design of each CEMG is modularized having an inner gimbal, two sensor units, two torquer units, and an outer gimbal. Each of the two gimbal axes has both a sensor and torquer unit which also contains the gimbal pivots (refer to figure 2-15).

The maximum angular motion of each gimbal axis is limited to relatively small angles. If we consider worst-case conditions (adding all momentum storage requirements, considering the most unfavorable CEMG orientations, and having all CEMG at their lower speeds), the inner gimbal angles will be less than $\pm$0.052 rad ($\pm$3°) and the outer gimbals will rotate less than $\pm$2.006 rad ($\pm$115°). Therefore, it will be possible to use flex leads rather than slip rings. This will improve reliability significantly since peak current of 50 amps may occur.

The CEMG assembly is shown in outline form in figure 2-16. The assembly would be flange mounted to the spacecraft structure or a separate frame designed to mount the three assemblies of the IPACS. Enough clearance space must be provided to swing a 31.75 cm (12.5 in.) radius about the outer gimbal axis.

The electronics packages (4 units), two for each phase, are shown mounted to the inner gimbal. This arrangement will reduce the number of flexible leads and will keep all critical motor-generator signal leads within the inner gimbal unit.

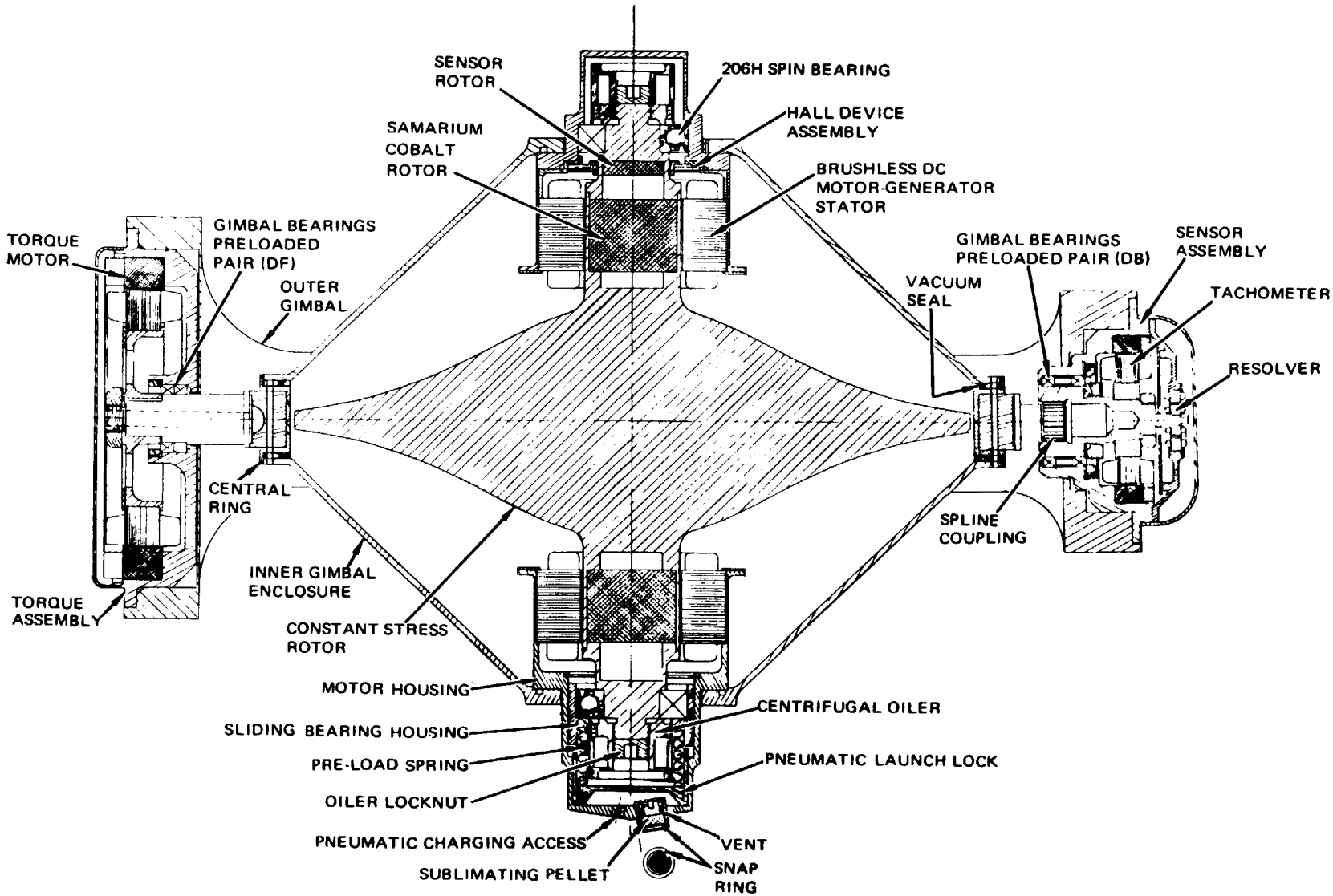

Figure 2-15. RAM Gimbal Assembly

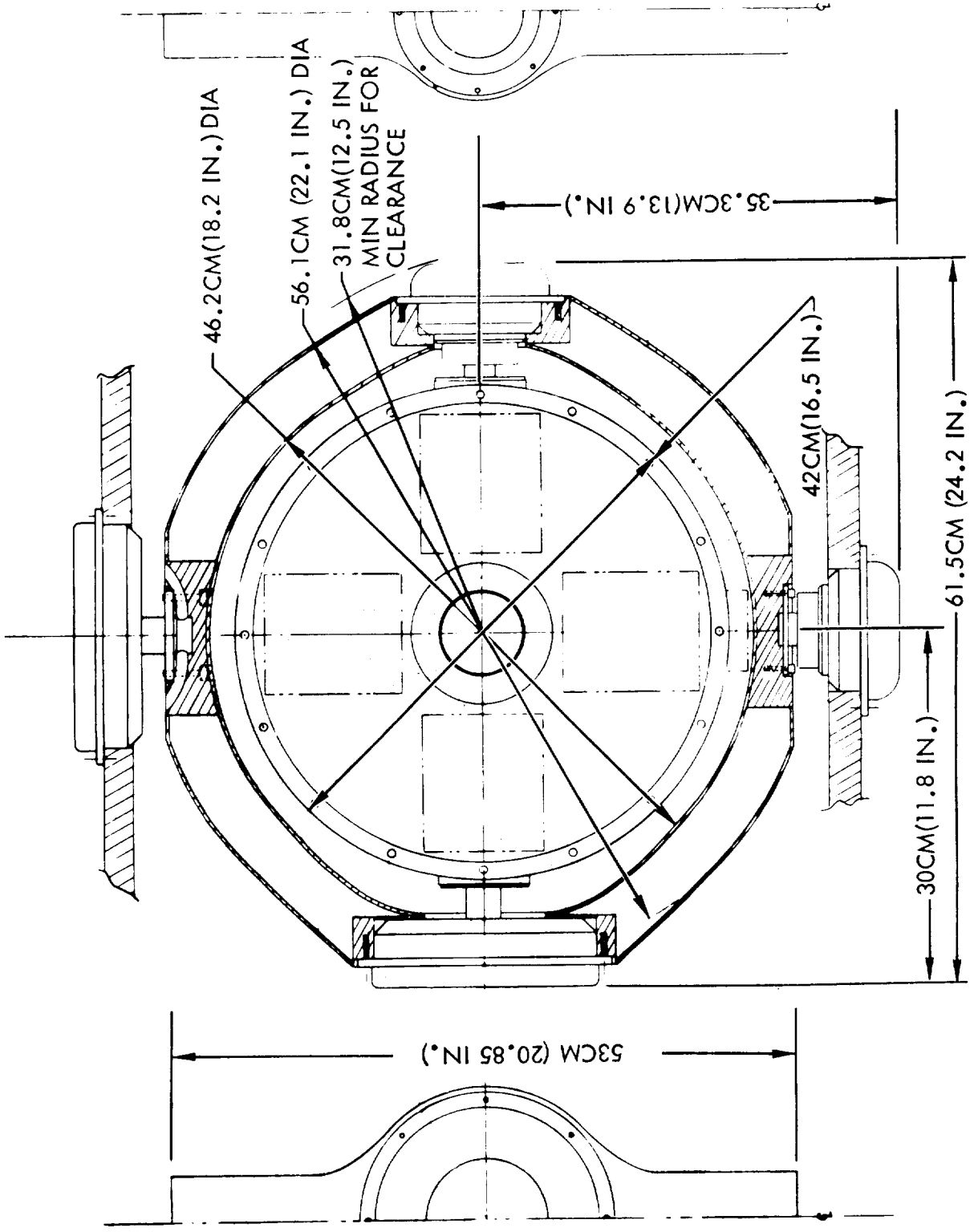

Figure 2-16. RAM Inner Gimbal Assembly

Differential thermal expansion, minor misalignments, and dimensional tolerances are handled by an internal spline coupling which is provided as part of the sensor unit. This feature also facilitates assembly and disassembly.

Both inner and outer gimbal axes use duplex ball bearings. These bearings are located in the sensor and torquer units and are part of these subassemblies. Therefore, all critical assemblies are confined to the individual modules and the final assembly and disassembly can be performed in a less critical environment (as to cleanliness and temperature).

Since the angular motion is small about the inner gimbal axis $<\pm 0.052$ rad ($<\pm 3°$), a small loop in the wires as they cross to the outer gimbal is sufficient. At the outer gimbals where motion is ± 2.006 rad ($\pm 115°$) maximum, the leads will be brought out through the center of the torque motor shaft, shaped as a spiral, and clamped at the outer diameter.

Since the CMG/energy storage assembly must survive launch conditions and have no low resonant frequencies, this factor controls the design. The peak stress levels will be relatively low with the exception of the rotor where maximum energy storage is required.

The gimbals will be balanced within 0.027 N-m (0.02 ft-lb) about each axis. At a 10g launch acceleration this is 0.27 N-m (0.2 ft-lb) which can be nulled by a position loop including resolver, tachometer, and torque motor in each gimbal axis. This will eliminate the necessity for a mechanical lock and its lower reliability.

Spring mass models: Spring mass models have been established for the RAM two-gimbal CMG/energy storage assembly. The five models are:

Linear motion along spin axis	- Figure 2-17
Linear motion along outer gimbal axis	- Figure 2-18
Linear motion along inner gimbal axis	- Figure 2-19
Torsional motion about the outer gimbal axis	- Figure 2-20
Torsional motion about the inner gimbal axis	- Figure 2-21

The terms included in these preliminary models are indicated in figure 2-22.

An approximate minimum natural frequency is listed in Table 2-XXII for each model.

Preliminary dynamics analyses were conducted to estimate critical frequencies for the RAM rotor. The type of analysis was similar to that described previously for the TDRS rotor. The shaft was modeled as a solid shaft with 16 beam elements and the wheel portion with 74 triangular plate elements. The results of the analysis are presented in Table 2-XXIII.

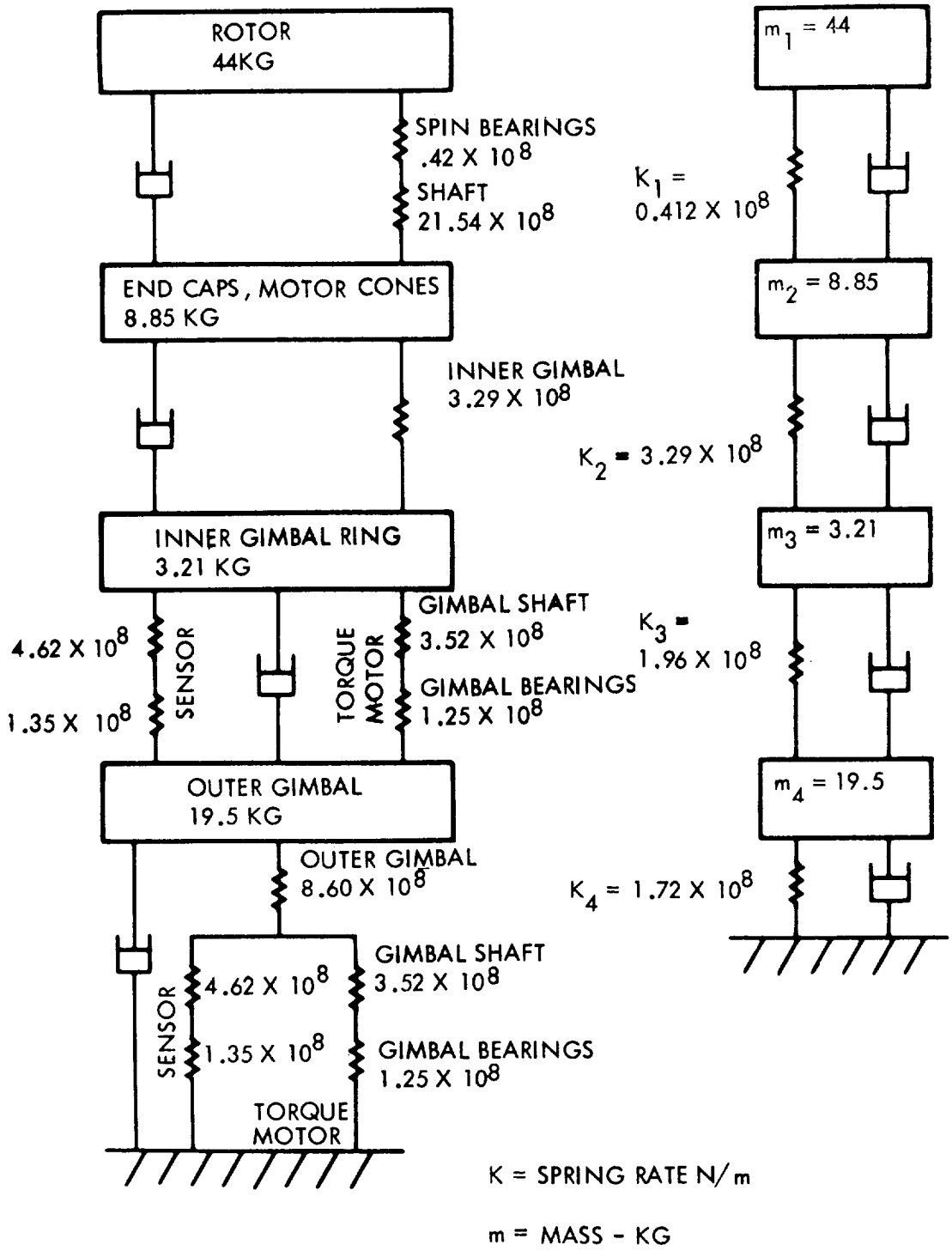

Figure 2-17. RAM Spring Mass Model - Linear Motion Along Spin Axis

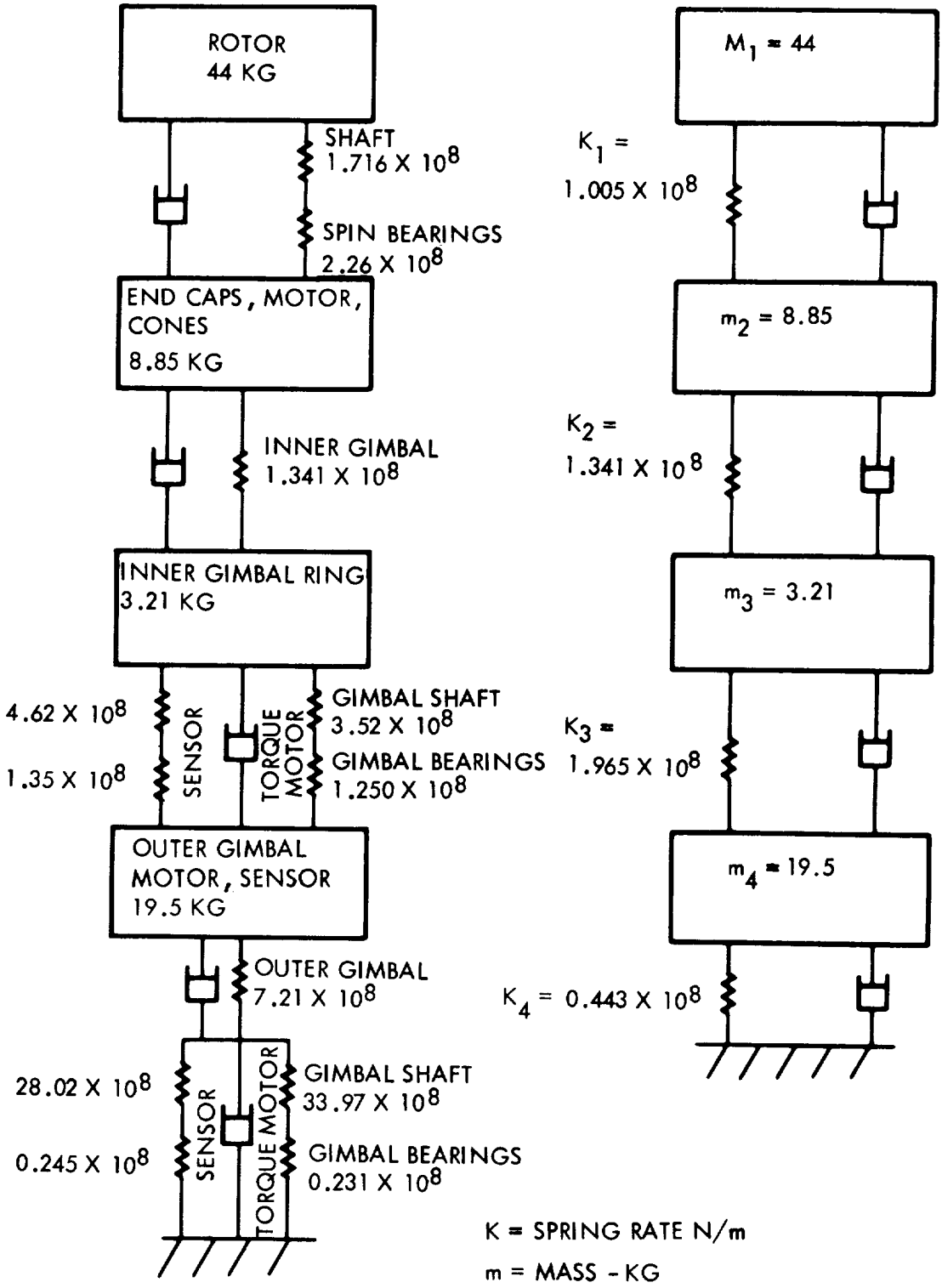

Figure 2-18. RAM Spring Mass Model - Linear Motion Along Outer Gimbal Axis

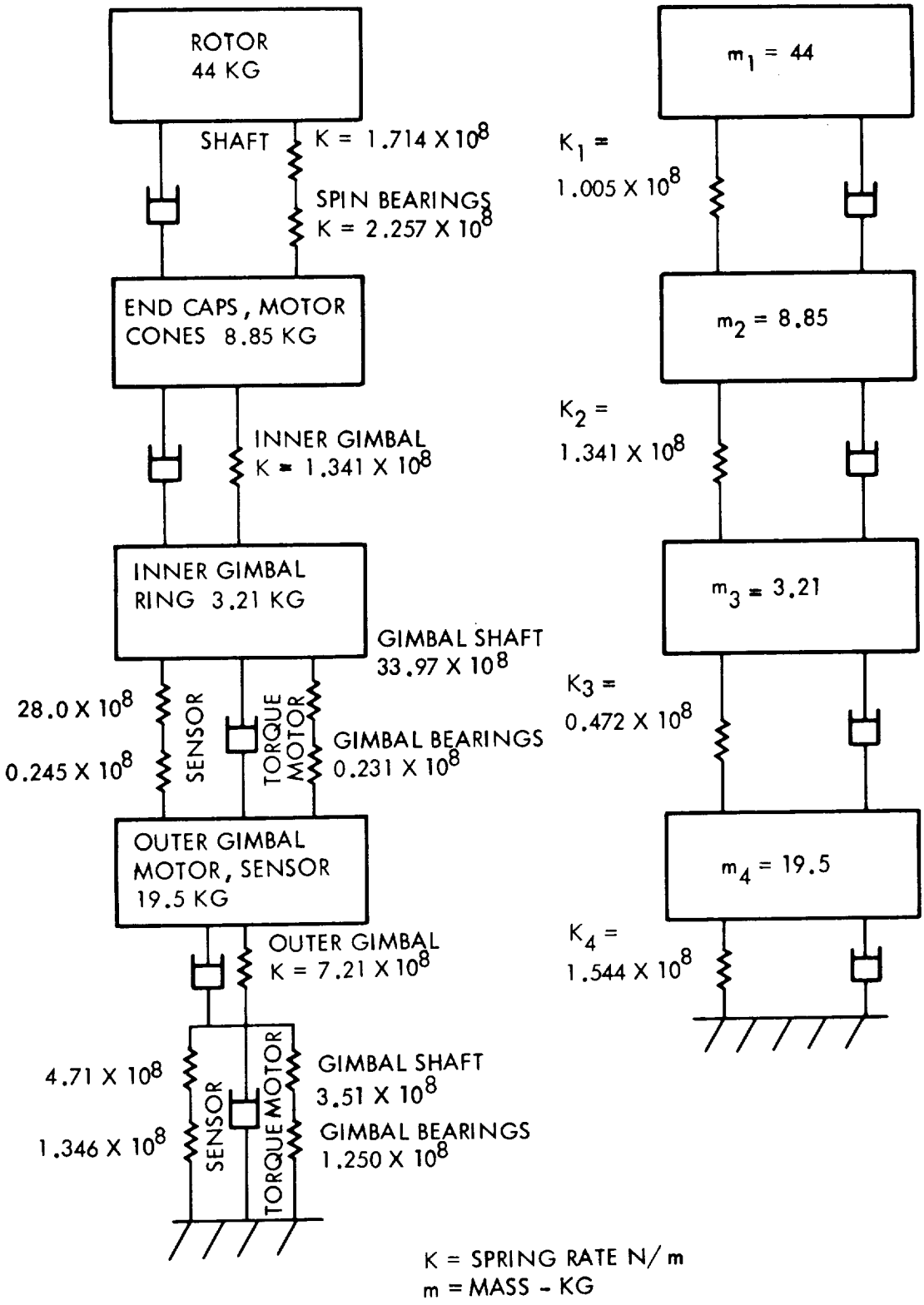

Figure 2-19. Ram Spring Mass Model - Linear Motion Along Inner Gimbal Axis

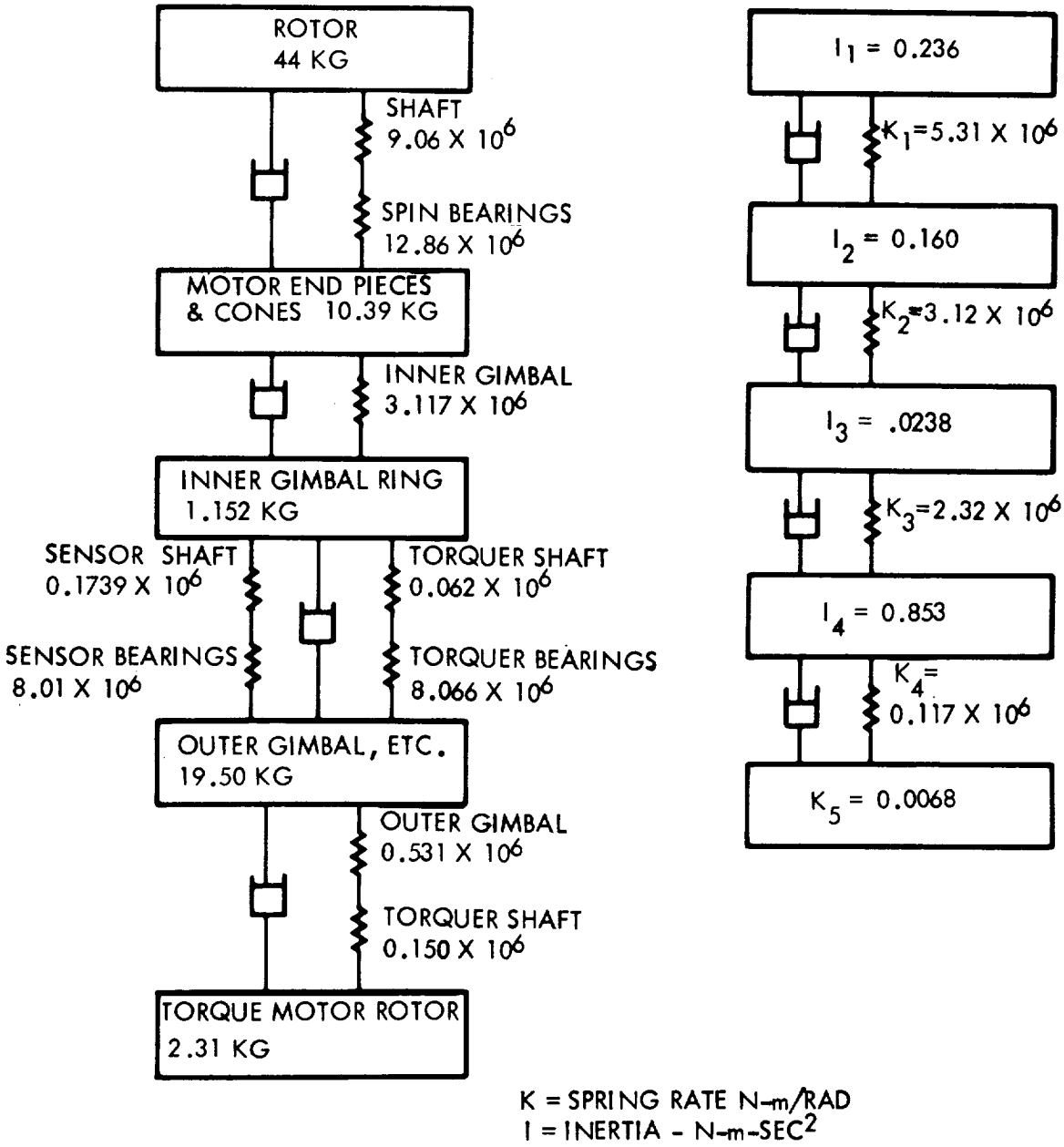

Figure 2-20. RAM Spring Mass Model - Torsional Motion About Outer Gimbal Axis

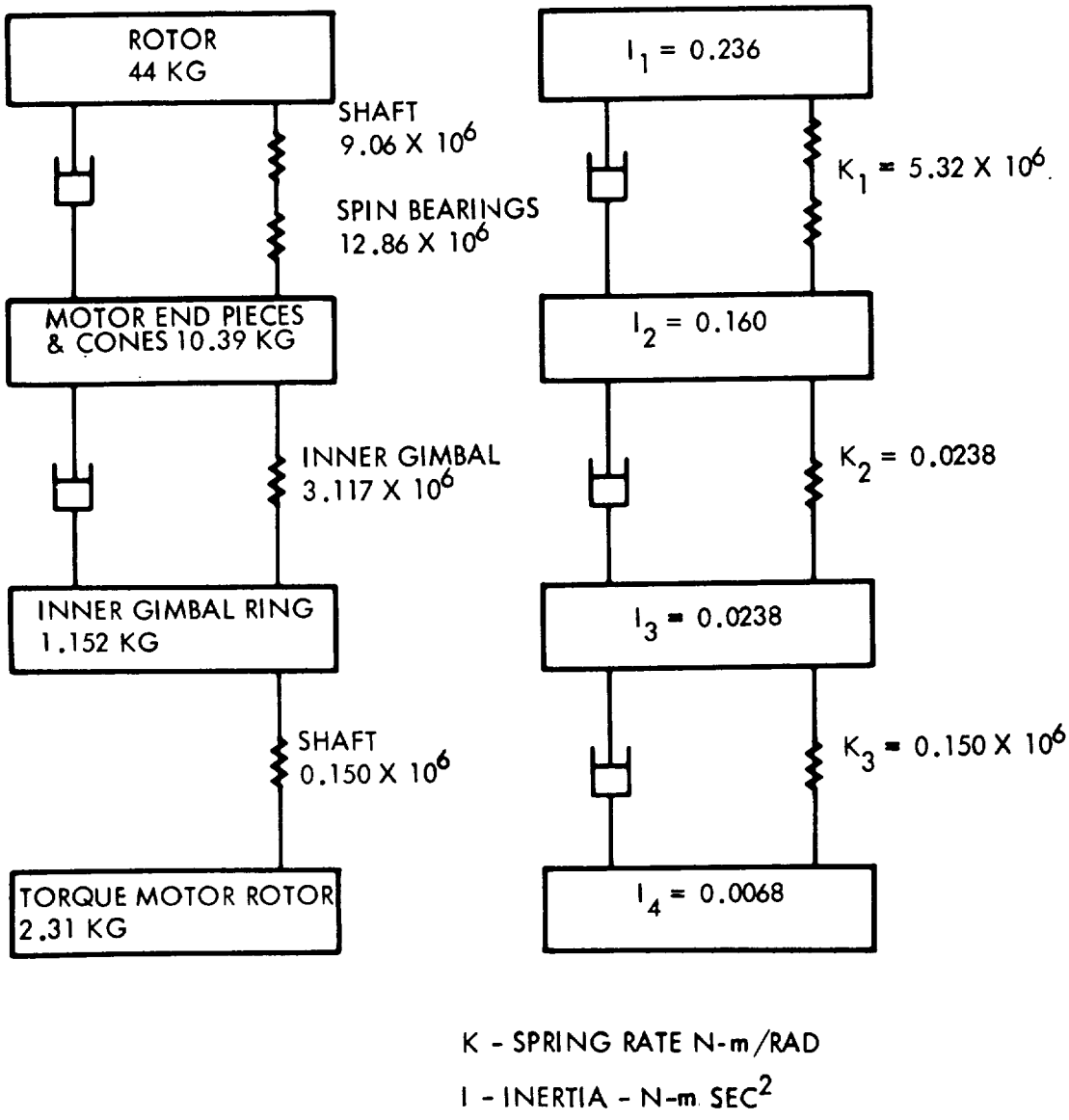

Figure 2-21. RAM Spring Mass Model - Torsional Motion About Inner Gimbal Axis

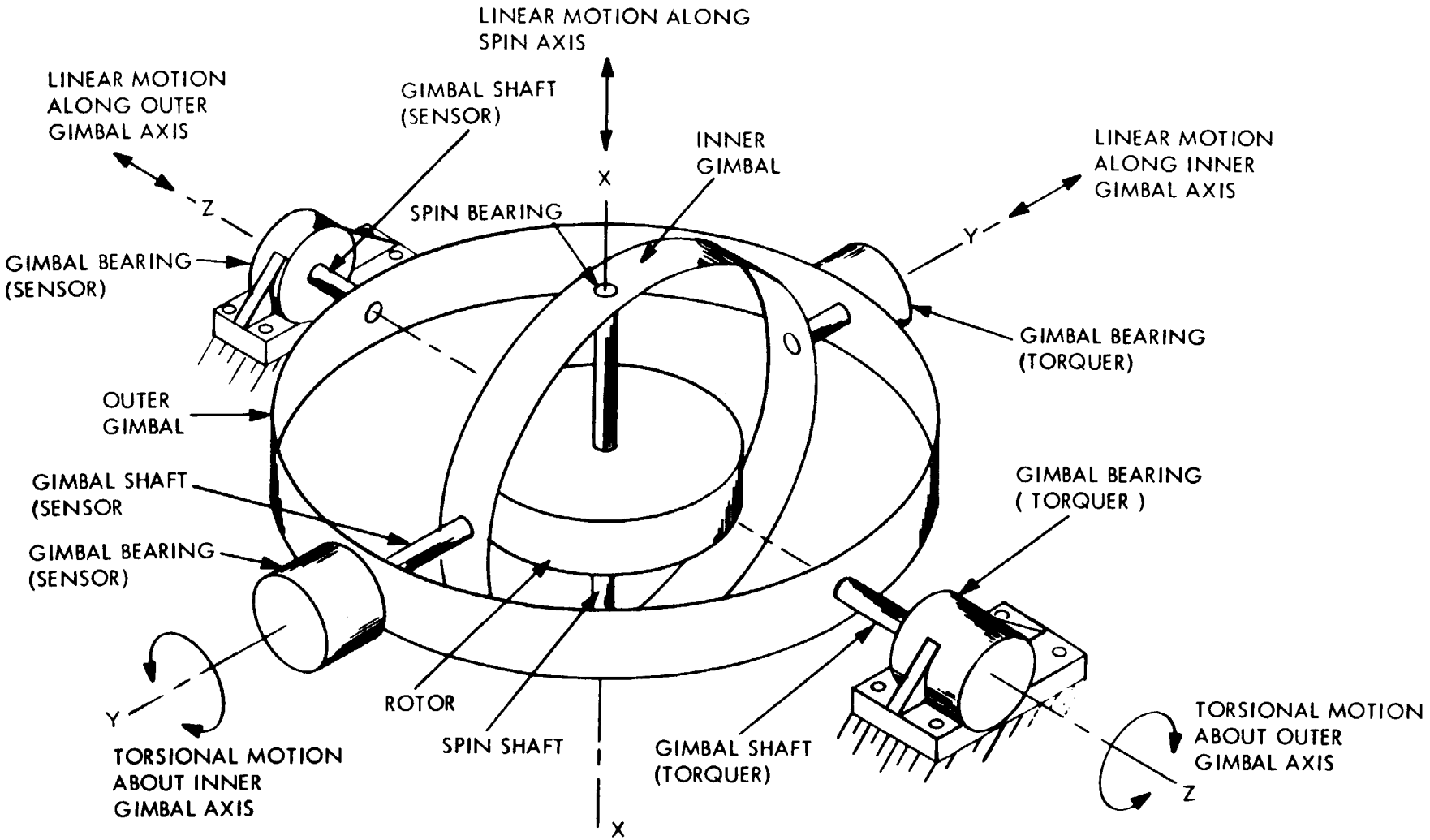

Figure 2-22. CMG Terms for Spring Mass Models

TABLE 2-XXII.- ESTIMATED RAM CMG MINIMUM NATURAL FREQUENCIES

Figure	Model	Minimum natural frequency (Hz)
2-17	Linear - along spin axis	98
2-18	Linear - along outer gimbal axis	126
2-19	Linear - along inner gimbal axis	131
2-20	Torsional - about outer gimbal axis	152
2-21	Torsional - about inner gimbal axis	755

TABLE 2-XXIII.- FREQUENCIES OF RAM FLYWHEEL

Mode number	Frequencies		
	Natural frequencies (wheel static)	Rotational speed	
		22 500	45 000
1	12 600	14 400	15 100*
2	38 700	52 600	67 600
3	67 400	67 500	79 700**
4	209 000	231 000	269 000

* Denotes first beam bending mode.

** Denotes second beam bending mode.

The results are constrained by the assumption of a hollow motor rotor section of about double nominal wall thickness. This was to approximate the shaft design with core iron and samarium cobalt inserted in a shrink fit. Of significance is that critical frequencies do not appear in the operating speed range. It can also be noted that the first plate frequency, unlike the thinner TDRS design, is well above the operating range. Further studies are required to model completely the shaft with motor rotor inserts.

Assembly procedure: The assembly of the RAM CMG/energy storage unit is summarized in this subsection. A detailed description is not warranted at this stage of the design. The following preassembly is first accomplished:

(1) Oilers assembled and filled

(2) Torquer assembly complete

(3) Hall probe ring assembled and wired

(4) Sensor assembly complete

(5) Preloading device assembled into its proper motor housing

Inner gimbal: Rotor stress and bearing load considerations dictate the spin bearings to be of greater diameter than the spin motor rotor. This creates some problems in assembly so that the following procedure must be adhered to:

(1) Fixture momentum rotor with spin shaft vertical, sensor end up.

(2) Slip stator clamp, motor stator, and Hall device assembly over the top shaft.

(3) Shrink fit spin bearing to shaft.

(4) Assemble oiler to shaft and secure with lock nut.

(5) Slide housing over bearing, Hall ring assembly, and motor stator taking caution to properly align Hall ring assembly with its keying device. Secure motor stator with its clamp ring.

(6) Carefully invert momentum rotor in its fixture to assemble No. 2 spin motor, bearing, and oiler to its shaft in the manner outlined above. (This end does not have a Hall device assembly.)

(7) Slide remaining housing over bearing and motor stator as before. Secure stator with its clamp ring.

(8) Place assembled spin assembly in motor alignment fixture and align Hall probe ring with its adjacent motor (No. 1) and index.

(9) Align motor No. 2 to motor No. 1 and index.

(10) Place one cone cover in a fixture, small end down, and carefully lower spin assembly into it to properly mate the cone to its motor housing, aligning index marks.

(11) Place the two Gask-O-Seals and central ring around momentum rotor.

(12) Place remaining cover over assembly and, after aligning motor index mark to cone index, secure all bolts and screws.

Careful alignment of all index marks is necessary to maintain electrical alignment in the spin motor system. This completes assembly of the inner gimbal.

Inner gimbal to outer gimbal assembly:

(1) Attach splined shaft to inner gimbal.

(2) Fixture inner gimbal and outer gimbals so that the gimbal axis is approximately aligned.

(3) Insert sensor assembly into outer gimbal carefully mating the spline coupling. Secure sensor to gimbal with proper screws.

(4) Insert torquer assembly into outer gimbal taking care that its output shaft mates properly at inner gimbal interface. Secure shaft flange to inner gimbal with screws. Then secure torquer assembly to outer gimbal with proper screws.

(5) Outer gimbal torquer and sensor assemblies are attached similarly when mounting momentum assembly to the vehicle mounting structure.

RAM CEMG characteristics.- The physical characteristics of the RAM CEMG assembly and components are given in Table 2-XXIV and the performance characteristics in Table 2-XXV.

RAM IPACS solar array.- In order to minimize the impact of integrating IPACS into the baseline free-flying RAM, the competitive solar array design is retained (reference 2-2). The array is based on a flexible rollout type assembly developed by Hughes (FRUSA). A prototype of this array has been flight tested.

Figure 2-23 shows the prototype rollout array system. Illustrated are the storage drum mechanism and the two flexible solar arrays. The arrays are wound on the storage drum during launch and deployed after the spacecraft attain orbit. Deployment is accomplished by means of boom assemblies mounted on the storage drum structure. The drum mechanism also has the ability to retract the solar panels while in orbit. The solar cells are 2 x 4 cm, 2 ohm-cm, 0.203 mm (0.008 inch) N/P silicon. The coverglass is 0.153 mm (0.006 in.) fused silica with anti-reflection and blue filter coatings. The solar array substrate consists of a 0.0254 mm (0.001 in.) Dupont Kapton H-film bonded to a 0.0254 mm (0.001-in.) type 108 fiberglass. A two-part epoxy is used to bond the solar cells to the substrate. A 0.0508-mm (0.002-inch) embossed Kapton cushion is used to protect the solar cells during the launch vibration.

TABLE 2-XXIV.- RAM CEMG PHYSICAL CHARACTERISTICS

CMG assembly		
Total weight	71.94 kg	(158.6 lb)
Maximum diameter	61.5 cm	(24.2 in.)
Maximum axial length	69.9 cm	(27.5 in.)
Mounting	Trunion	
Inner gimbal		
Total weight	56.06 kg	(123.6 lb)
Maximum diameter	41.9 cm	(16.5 in.)
Axial length	44.2 cm	(17.4 in.)
Internal vacuum	0.0133 to 0.0666 N/m^2	(0.1 to 0.5 micron)
Rotor		
Diameter	37.8 cm	(14.9 in.)
Weight (including motor rotor)	44 kg	(97 lb)
Inertia	0.474 N-m-sec^2	(0.349 ft-lb-sec^2)
Material	Republic H9-4-45 steel with nonmagnetic shafts	
Spin bearings		
Size	206H	
Material	Vacuum melt M-50 steel	
Lubricant	RL 743-E oil	
Preload	133.4 N	(30 lb)
Weight (2)	0.4536 kg	(1.0 lb)
Centrifugal oiler		
Size	4.57 cm diam by 3.56 cm long (1.8 in. diam by 1.4 in. long)	
Weight (2)	0.431 kg	(0.95 lb)
Capacity (usable oil)	20.7 cc	(1.25 $in.^3$)
Motor-generator		
Type	dc permanent magnet, brushless	
Size	10.67 cm diam x 6.10 cm long (4.2 in. diam x 2.4 in. long)	
Number of poles	2	
Rated voltage	56 Vdc	
Total weight (2 stators)	5.31 kg	(11.70 lb)
Enclosure		
Material	Aluminum alloy 0.127 cm (0.050 in.) thick	
Type	Truncated cones	
Scale	Gask-O-Seal	
Total weight	5.85 kg	(12.9 lb)

TABLE 2-XXIV.- RAM CEMG PHYSICAL CHARACTERISTICS - Concluded

Outer gimbal		
Total weight	7.71 kg	(17 lb)
Maximum diameter	56.38 cm	(22.2 in.)
Width	7.62 cm	(3 in.)
Mounting	Trunion	
Material	Aluminum alloy	
Interia about gimbal axis	0.274 N-m sec^2	(2.424 in.-lb sec^2)
Inertia about gimbal axis, including sensor and torquer assembly	0.853 N-m sec^2	(7.55 in.-lb sec^2)
Torque motor assembly		
Enclosure		
Material	Aluminum alloy	
Weight	1.85 kg	(4.07 lb)
Mounting	Flange	
Bearings		
Type	D-F preloaded pair	
Size	A541T	
Torque motor		
Type	Advanced brushless dc	
Size	18.3 cm diam x 4.13 cm long (7.2 in. diam x 1.625 in. long)	
Weight	3.29 kg	(7.25 lb)
Sensor assembly		
Enclosure		
Material	Aluminum alloy	
Weight	1.84 kg	(4.06 lb)
Mounting	Flange	
Bearings		
Type	D-B preloaded pair	
Size	A543T	
Tachometer		
Type	Brushless, dc, permanent magnet	
Size	9.47 cm diam x 2.77 cm long (3.73 in. diam x 1.09 in. long)	
Weight	0.68 kg	(1.5 lb)
Resolver		
Type	Rotary transformer	
Size	5.59 cm diam x 1.47 cm long (2.2 in. diam x 0.58 in. long)	
Weight	0.227 kg	(0.5 lb)

TABLE 2-XXV.- RAM CEMG PERFORMANCE CHARACTERISTICS

CMG assembly	
Maximum input/output power	2400 W
Line voltage	52 Vdc
Linear natural frequency (minimum)	
Along X axis (spin axis)	98.2 Hz
Along Y axis (inner gimbal axis)	131 Hz
Along Z axis (outer gimbal axis)	126 Hz
Torsional natural frequency (minimum)	
About Y axis	755 Hz
About Z axis	152 Hz
Position accuracy	0.484×10^{-6} rad - 4.84×10^{-6} rad (0.1 - 1.0 arc-sec)
Reliability	0.822 for 5 years
Rotor	
Operating range	22 500 - 45 000 rpm
Maximum angular momentum	2229 N-m-sec (1644 ft-lb-sec)
Maximum energy storage	1460 W-hr
Minimum spinup time	1.25 hr
Maximum coast down time	29.5 hr
Dynamic balance	$<2.54 \times 10^{-5}$ cm (<10 microinch)
Spin bearings	
Static load rating	
Axial	36 900 N (8280 lb)
Radial	13 800 N (3100 lb)
L_{10} life	333 000 hr
Axial stiffness	0.420×10^{8} N/m (0.240×10^{6} lb/in.)
Radial stiffness	2.434×10^{8} N/m (1.39×10^{6} lb/in.)
Loss at 45 000 rpm (2 brgs)	93 W
Centrifugal oilers	
Flow rate at 20°F	11×10^{-6} cc/hr (0.67×10^{-6} in.^{3}/hr)
Flow rate at 140°F	500×10^{-6} cc/hr (30.5×10^{-6} in.^{3}/hr)
Worst case lubricating capacity	4.75 years
Motor-generator	
Input voltage	52 Vdc
Torque constant	0.0102 N-m/amp (0.00751 ft lb/amp)
Maximum input/output per unit	1200 W

TABLE 2-XXV.- RAM CEMG PERFORMANCE CHARACTERISTICS - Concluded

Electrical time constant	4.4 millisec	
Efficiency (one)	97%	
Inner gimbal		
Vacuum - ground test	<0.133 N/m^2	(<1 micron)
Vacuum - orbit	<0.0266 N/m^2	(<0.2 micron)
Leak/outgassing rate	<0.0266 N/m^2-hr	(<0.2 micron/hr)
Linear stiffness along spin axis	1.644×10^8 N/m	(0.939×10^6 lb/in.)
Linear stiffness perpendicular spin axis	0.6701×10^8 N/m	(0.383×10^6 lb/in.)
Torsional stiffness (spin to output axis)	2.55×10^6 N-m/rad	(22.2×10^6 in. lb/rad)
Sensors		
Speed		
Type	Magnetic	
Pulses per revolution	60	
Output	6 volts P-P	
Temperature		
Type	Thermistor	
Range	0 - 100°C	(32 - 212°F)
Accuracy	2°C	(3.6°F)
Vibration		
Type	Accelerometer	
Output, millivolts/g	100	
Torque motor		
Peak torque	9.49 N-m	(7.0 lb-ft)
Friction torque	0.0237 N-m	(0.0175 lb-ft)
Amps at peak torque	5.4	
Volts at peak torque	45.7	
Torque sensitivity	1.76 N-m/amp (1.3 ft-lb/amp)	
Tachometer		
Sensitivity	3.2 V/rad/sec	
Resolution	8.7×10^{-5} rad/sec	(0.005°/sec)
Friction torque	0.019 N-m	(0.014 lb-ft)
Ripple voltage, peak to peak	4%	
Resolver		
Frequency	400 Hz	
Input	22 Vac	
Output	22 Vac	
Maximum error	4.36×10^{-4} rad	(1.5 arc-min)
Null	30 milliradians	

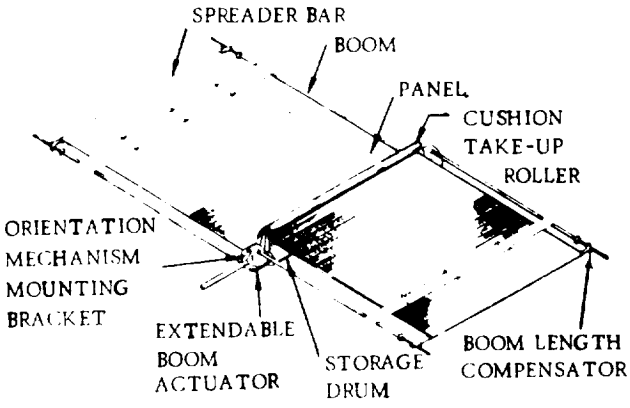

Figure 2-23. Hughes Rollout Array System

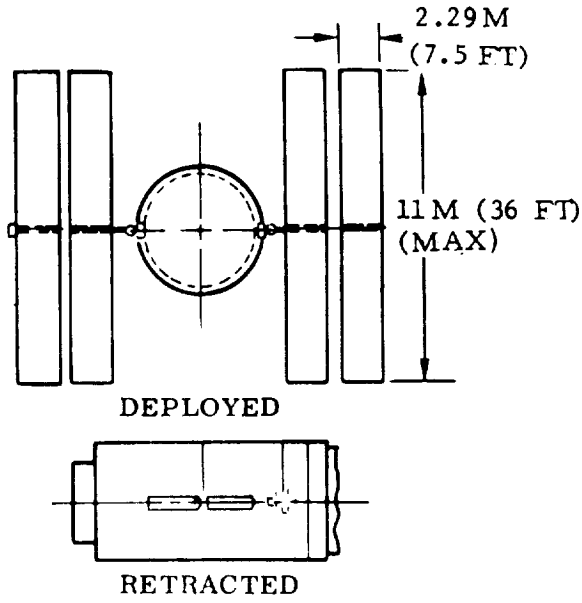

Figure 2-24. Solar Array Configuration

Figure 2-24 illustrates the retracted and deployed array configurations. Reference 2-2 indicates that the different free-flying RAM's required solar arrays varying in area from 47.4 m^2 to 93.9 m^2 (510 to 1010 ft^2). The array panels are divided into subpanels of 0.97 by 2.29 m (3.18 by 7.5 ft) so that incremental changes in array power can be performed without major redesign of the baseline array. Drum size, boom length, and orientation mechanisms are common for all free-flying RAM's to minimize redesign.

A minimum array voltage of 52 Vdc was selected so that it would be compatible with the Skylab airlock module (AM) conditioning equipment. The power conditioning equipment was chosen on the basis of availability or minumum cost (reference 2-3). The nominal voltage of the developed FRUSA is 34 Vdc at operating temperature.

Using the conditioning and battery efficiencies from reference 2-3, the competitive power system requires a solar array power of 7450 W. Including bearing losses, the RAM IPACS requires 7242 W from the solar array (52 Vdc array output). For an EOL array specific power of 69.94 W/m^2 (6.5 W/ft^2) at 88°C, the RAM IPACS requires 2.97 m^2 (32 ft^2) less solar array area than the competitive power system. This is based on the efficiencies shown in Table 2-V. If the array were designed to deliver 100 V, the increase in IPACS efficiency would result in an array size 9.67 m^2 (104 ft^2) smaller than the competitive power system array.

Distribution and regulation.- The solar array is designed to provide an output voltage of 52 Vdc minimum. Under beginning of life conditions and at low temperatures, output voltage will be 75 to 80 V. This array design was not changed from the General Dynamics RAM studies. The IPACS electronics and motor/generator units will be designed to operate at the 50 to 80-V input levels. Array power is connected to a central control unit which directs power to the bus regulators and the IPACS units. When IPACS wheels are at maximum speed, sensors signal the controller which selectively cuts off power to the saturated wheel motor. When array voltage drops below 52 V, the central controller switches IPACS units to the generator/output mode which provides 52 to 80 V to the bus regulators.

This voltage is utilized in the IPACS to improve efficiencies. Voltage is reduced to 28 and controlled to within $\pm$ 5 percent by buck regulators. Although the block diagram shows one regulator for each bus, this could be increased as required by availability of existing components and power rating. For redundancy the regulator to one bus should be capable of carrying the total load in case of failure of the other regulator and use of the bus tie power switching.

The buck regulators operate on the pulse width modulation principle which switches the input power on and off at a high frequency with off-on ratio adjusted to provide the desired average voltage output level. This type regulator provides high efficiencies with good control provided input voltage exceeds output level. In order to meet specification quality requirements a filter will be required in order to attenuate induced high-frequency interference ripple from switching transients. In some regulator designs, this filter is included in the basic regulator circuitry and packaging. Since filter and regulator are necessary at the bus input point, the motor-generator electronics can be simplified by eliminating filters and regulators.

Reference 2-3 indicates that the Skylab regulator will operate over an input voltage of 33 to 125 Vdc and will deliver up to 1500 W of power. The use of two regulators with the RAM IPACS will require uprating of the Skylab units or development of a new regulator. Another approach is to use four of the Skylab type regulators.

RAM IPACS Design Characteristics

Design characteristics which can be expected to differ between IPACS and a conventional CMG are considered. Subjects include reliability, safety, vibration, maintenance, and system interfaces.

Reliability.- A preliminary reliability analysis was performed for the RAM CMG/energy storage assembly including electronics.

Failure rates of electronic parts are principally from RADC Reliability Notebook TR 67-108 using high reliability, burn-in parts operating at low stress levels characteristic of orbital environments. For hybrid and monolithic integrated circuits, a General Electric-developed failure model was used.

Failure rates for mechanical and electromechanical components are not as well documented and have been obtained from various General Electric, General Dynamics, and Martin reports. Operation of these components in a light duty cycle environment is assumed.

Results of a failure analysis on space systems of the late 1960's indicate that a significant percentage of the failures are due to design defects (up to 50 percent) and that these could be corrected with sufficient redesign and test. Thus, a well-engineered system could have failure rates below the quoted values.

The failure rates for electronics and rotor assembly are given in Table 2-XXVI. Principal failure rates are in electronics components and the spin and gimbal bearings. Use of redundant electronics will improve reliability at minimum expense. The resulting reliability diagram is shown in figure 2-25. When standby redundancy is used for the electronics, the single remaining critical component is the spin bearing. The failure rate used for this bearing is conservative based on the calculated L_{10} life of 330 000 hours. The failure rate of 2.4 per 10^6 hours is equivalent to an L_{10} life of 95 000 hours, indicating a safety factor of 3.48. In the subsequent design the spin bearing will be the single most critical factor since reliability and power losses are dependent on the selection of the bearing and its operational speed. Since spin bearing redundancy within the IPACS unit is not easily achieved, this redundancy, if necessary, will be obtained in additional wheel assemblies.

The calculated reliability shown in figure 2-25 is for a 5-year period, not considering the six-month service interval. As presented in Module 1, Volume I, the reliability of an IPACS constructed of latest technology parts is calculated to equal or exceed conventional CMG reliability. Further, one element, namely the battery and battery charger electronics reliability, is deleted from the power and control reliability chain. IPACS is, therefore, expected to meet the same RAM requirements as the conventional system.

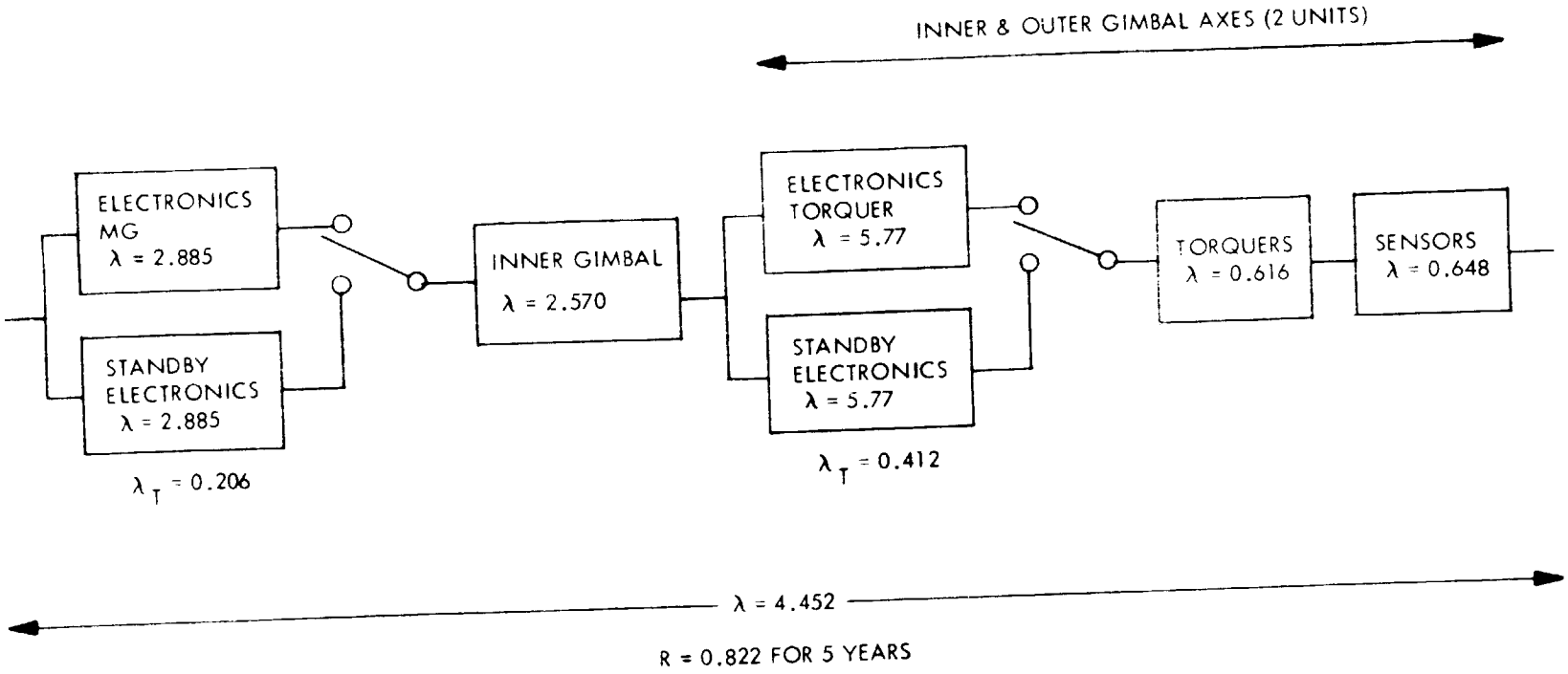

Figure 2-25. CMG Reliability Model for RAM

TABLE 2-XXVI.- FAILURE RATES FOR IPACS COMPONENTS FOR RAM

Item	λ Number of failures per 10^6 hours
Electronics - λ_T = 2.885	
2 Hall probes at 0.100	0.200
2 LM 107 at 0.06064	0.121
7 LM 108A at 0.05443	0.381
1 NH 002 at 0.06644	0.066
4 hybrid predrivers at 0.06917	0.277
2 hybrid PWM at 0.08543	0.171
2 hybrid power amps at 0.2083	0.417
8 2N3720 at 0.04133	0.330
4 2N2432 at 0.01767	0.071
4 2N2925 at 0.02245	0.090
29 capacitors at 0.00474	0.137
71 resistors at 0.00355	0.252
4 Zener diodes at 0.04008	0.160
Connections	0.212
Inner gimbal - λ_T = 2.570	
2 spin bearings - 206H	2.400
2 centrifugal oilers	0.016
2 brushless motor-generators	0.016
4 seals	0.034
Magnetic pickup	0.004
Launch lock (est.)	0.100
Torquer unit - λ_T = 0.308	
Torque motor	0.008
2 gimbal bearings	0.300
Sensor unit - λ_T = 0.324	
Tachometer (brushless)	0.008
Resolver	0.016
2 gimbal bearings	0.300

The reliability calculations are qualified by questions as to the validity of using L_{10} life criteria for bearings operated with a minimum oil film at DN values of 1.5 million as proposed in the current RAM design. The operational regime is considered on the upper limit of DN values for oil-lubricated ball bearings. The resolution of the life question must be resolved through detailed design and test. Current art preliminary design calculations affirm the IPACS reliability presented.

Safety.- The reader is referred to Volume I, Module 1, for a brief generalized discussion of IPACS safety considerations and to Module 1 of this volume for a discussion of TDRS safety considerations.

Specific comments for the RAM design are presented here. The safety problem for RAM is more significant than that for TDRS in that the flight vehicle is periodically manned for servicing. During manned servicing operations, it may be desirable to limit the IPACS units to operation in the lower portion of their speed range which would significantly increase the factor of safety for the rotor. It can be expected that under these conditions, Shuttle will provide some portion of the RAM power demands. An alternative concept would be to completely despin the IPACS rotors; this may be required from a control system interaction standpoint.

The development testing, manufacturing and acceptance testing, and facility provision considerations presented for TDRS are equally applicable for RAM. In addition, fatigue cycling will be an important consideration in the establishment of an allowable working stress for the rotor material.

Vibration. Centrifugal force due to mass imbalance is the major force on the bearings at nominal spin speeds. Figure 2-26 illustrates the effect of a $(5.1 \times 10^{-5}$cm) (20 microinch) offset in center of gravity of the rotating assembly from the spin axis. A specification of 30 to 40 N for allowable bearing force due to imbalance on conventional CMG's is not uncommon. To meet these criteria, the RAM IPACS rotating assembly will require balancing to within 1.16×10^{-5} cm (4.6 microinch). As discussed in Module 2, Volume I, this level of balancing is considered a critical development for IPACS units of RAM size which can be achieved by special processes within the current art.

Acoustic noise.- Acoustic noise for the RAM IPACS must be considered for flight operations as well as ground testing. The vehicle is designed to be serviced on-orbit with a service crew in a pressurized cabin. Maintenance access considerations can be expected to place the units in the vehicle where structural borne noise will occur. Acoustic noise should, therefore, be considered in the detail design of the units and the design of the vehicle installation.

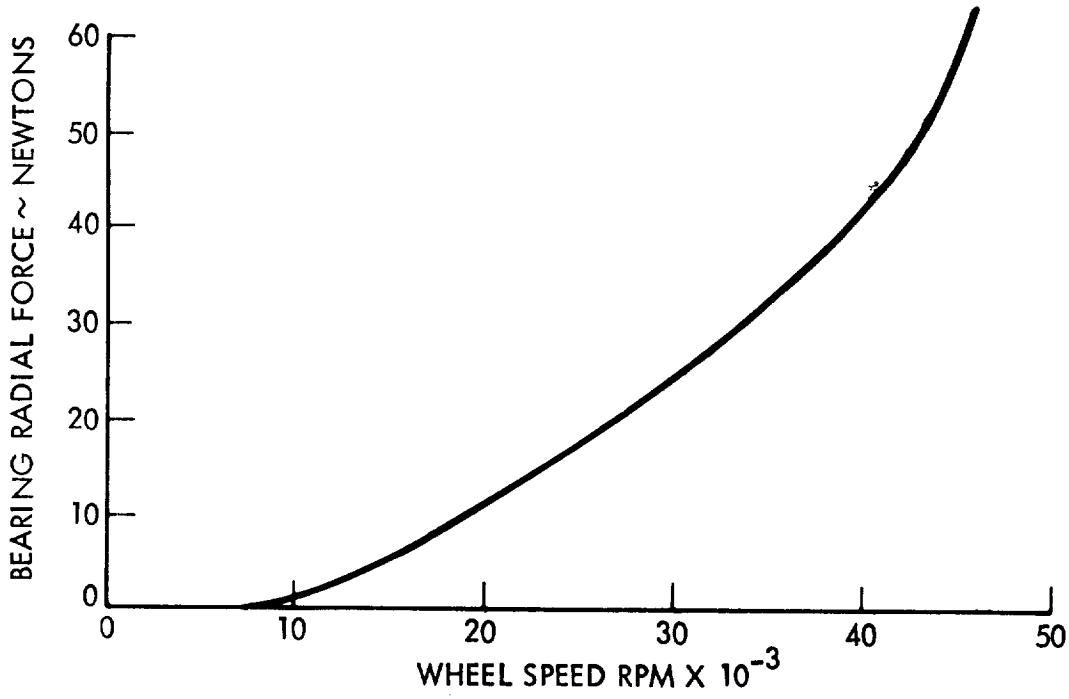

Figure 2-26. Imbalance Force Versus Spin Speed

The acoustic energy of a RAM IPACS is affected by so many variables (housing design and material, bearing noise, retainer resonances, to name a few) that quantization of expected acoustic energy is not possible. The fabrication and test of a unit which reflects care in bearing selection and housing design is considered the best indication of expected noise levels for production units.

Maintainability.- The free-flying RAM is designed to operate unmanned with service on-orbit by a maintenance crew brought up in the Shuttle. Six months is the anticipated service interval.

The IPACS energy/momentum units are designed to facilitate either of two maintenance concepts. In the first concept, modules of a unit would be replaced on-orbit. Representative modules include the electronics package, the inner gimbal assembly, the gimbal drive assembly, and the sensor assembly. The replacement time is estimated to range from less than one hour for the simplest case (replacement of an electronics package) to about three hours for the most complex (replacement of an inner gimbal assembly). One crewman would be able to perform any of the replacements with the exception of the inner gimbal assembly, where two crewmen and some handling equipment would be needed.

In the second maintenance concept, the orbital maintenance crew would replace the failed unit with an operable unit. The failed unit is then returned to the ground for refurbishment. On the ground, module replacement could be performed as described above. Failed modules would be either discarded or returned to the vendor for refurbishment, whichever is less costly. In this case, spare modules would be maintained at a mission support depot. A possible alternative would entail sparing at the unit level and returning an entire unit to the vendor for refurbishment. It is estimated that the cost to refurbish an entire unit is on the order of 5 to 7 percent of the cost of a new unit. This estimate assumes that the torquer and sensor modules are checked and returned to service. Typical refurbishment operations might include the following:

a. Inner gimbal assembly

- Replace bearings
- Rebalance rotor assembly (trim)
- Refill oilers
- Adjust preload
- Check motor/generator commutation
- Check or replace electronics

b. Gimbal drive assembly

- Check bearing friction
- Check commutation

c. Sensor assembly

- Check bearing friction
- Disassemble and test tachometer
- Align resolver

d. Testing

- Operational checks
- Acceptance tests

System interfaces.- The block diagram for the IPACS mechanization of the free-flying RAM is shown in figure 2-27. Unlike the TDRS system, the solar power output is at 52 V rather than 28 V, which means that it must be reduced by the buck regulators. The GEMG's however, operate off the higher voltage.

The functions performed by the major electronics assemblies are summarized in Table 2-XXVII. The system reflects a design concept that will allow the IPACS function to be checked out independently of the centralized digital processor. The telemetry normally interfaces with the processor but this does not preclude provisions for telemetry directly with the subassemblies.

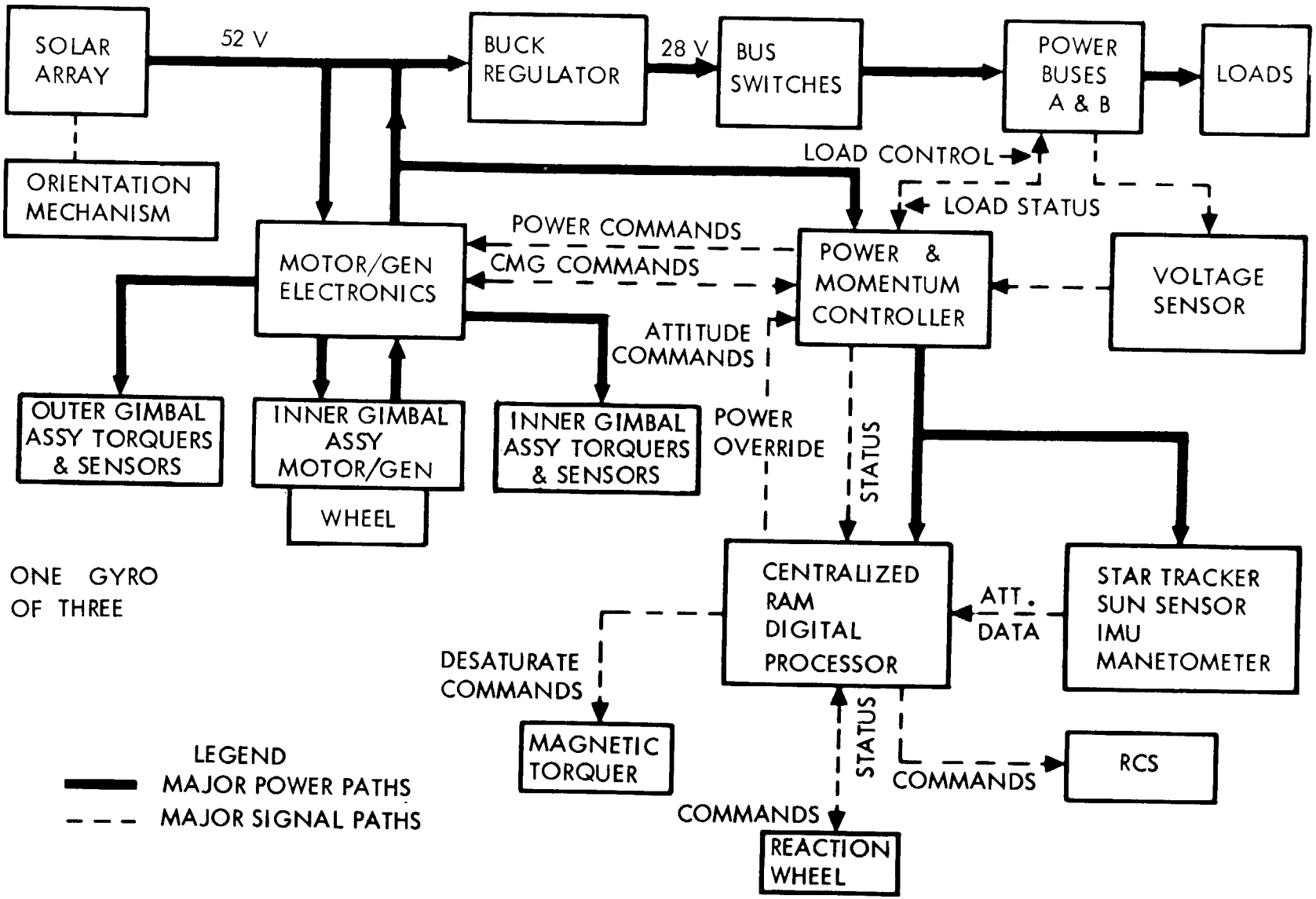

Figure 2-27. RAM Interface Block Diagram

TABLE 2-XXVII.- FUNCTIONS OF MAJOR RAM ASSEMBLIES

Motor-generator electronics	
Hall effect circuits	Telemetry interface
Mode control	Power switches
Wheel speed control	Power overload circuits
Gimbal angle circuits	
Power and momentum control	
Generate individual CMG commands	Power switching commands
Stabilize outer control loops	Power failure detection
Desaturation logic	
Centralized computer	
Attitude determination	Mode control commands
Attitude command generation	Solar panel commands
Failure detection	Antenna steering
TM up and down link communication	

Table 2-XXVIII is an estimated list of telemetry requirements.

When the free-flying RAM is attached to the Shuttle, they will be power-dependent. The power allocations are as follows:

Shuttle power allocation: (Transfer to and from orbit only)	Voltage - nominal	28 Vdc
	Power - average	500 W
	peak	800 W
	Energy - total	50 kW-hr

The RAM EPS must incorporate the necessary interface connector to accept this power. In addition, design of the RAM power conditioning and distribution system must accommodate the type and quantity power available.

TABLE 2-XXVIII.- RAM UP-LINK/DOWN LINK REQUIREMENTS

Parameter	Number	Information flow*
Reaction jet commands	16	D
Attitude commands	3	D
Star Tracker	2	D
Sun sensor	1	D
IMU	6	D
Magnetometer	1	D
Reaction wheel speeds	3	D
Magnetic torquer commands	1	D
Spin bearing temperatures	6	D
Rotor speeds	3	D
Bearing induced acceleration	6	D
Outer gimbal position	3	D
Outer gimbal rate	3	D
Inner gimbal position	3	D
Inner gimbal rate	3	D
CMG commands	3	D
Panel temperatures	2	D
Orientation motor: temperature	1	D
voltage	1	D
current	1	D
Bus voltage A	1	D
Bus voltage B	1	D
Bus switch status	2	D
Bus switch override	2	U
Attitude commands	3	U
Wheel speed override	3	U
Power commands	2	U

*D = Down, U = Up

References

2-1. Integrated Power/Attitude Control System (IPACS) Study, Vehicle/Mission Selection Report. North American Rockwell, Space Division, Report No. SD 72-SA-0144 (August 10, 1972).

2-2. Research and Application Modules (RAM) Phase B Study, Volume III - 4.4 Preliminary Design - Book 1 - Configurations and Subsystems. General Dynamics, Convair Aerospace Division, Report No. GDCA-DDA72-006 (12 May 1972).

2-3. Research and Applications Modules (RAM) Phase B Study, Volume III - 4.4 Preliminary Design, Appendix A - Trade and Special Studies (I-XIX). General Dynamics, Convair Aerospace Division, Report No. GDCA-DDA72-006 (12 May 1972).

MODULE 3 - DYNAMIC ANALYSIS AND SIMULATION

Digital computer models of the RAM and TDRS IPACS applications were formulated and exercised to determine their dynamic performance characteristics for dual attitude control and energy transfer operations. The simulation comprised the attitude control system and IPACS motor/generator models which were interfaced with each other for IPACS dual mode operation. Primary study objectives were to:

(1) Determine stability and transient response characteristics of the IPACS motor/generator assembly during periods of energy transfer to and from the energy momentum (E-M) wheels of the RAM and TDRS IPACS.

(2) Determine the impact of energy transfer commands from the IPACS motor/generator (M/G) assembly on spacecraft attitude control performance.

Preliminary analysis indicated that the response of the IPACS M/G is almost instantaneous in comparison to the spacecraft/E-M wheel response; thus separate simulations of M/G and spacecraft system dynamics are permitted. This separation, while being dependent on the actual interface with the power source and load (regulation), was assumed to represent a design that had insignificant coupling between control and power. Separate spacecraft simulations of the RAM and TDRS spacecraft and their E-M wheel assemblies were used, however, because of the difference in spacecraft physical properties and the use of momentum control devices. Descriptions and results of these three simulations are reported in the sections which follow.

RAM Analysis and Simulation

The energy storage/attitude control system studied for RAM IPACS application utilizes three double-gimbal, control-moment gyros (CMG) in a parallel mounted configuration. The outer gimbals of each CMG are mutually parallel to each other and aligned along the vehicle direction with least momentum requirement. Inner gimbals are slaved together to minimize the maximum single gimbal movement. The inner gimbal rotors of the three CMG's provide the angular momentum for spacecraft attitude control and also the capability for energy storage and transfer for the vehicle power system.

Torque feedback with modified transpose gain distribution for generating gimbal rate commands was selected as the control law to be used with the three planar-mounted CMG configuration. It meets general control law objectives of

(1) predictable and acceptable system transient response, and (2) maximum utilization of gyro momentum. The torque feedback law is representative of a generic class of control laws such as pseudo-inverse and H-feedback, and similar results could be expected for these laws with respect to IPACS performance.

A single energy storage distribution law was investigated; namely, energy is stored equally in each CMG rotor. Simulation of energy transfer thus requires a three-axis attitude control simulation. Attitude control system response characteristics, however, are selectable and can be verified via simple single-axis control models.

RAM simulation activities fall in the following sequence: 1) set control system gains for equal response about each control axis using a linear system model; 2) determine effect of E-M wheel assembly nonlinearities on system response; 3) determine effects of energy charge/discharge commands on attitud control pointing accuracy, gimbal motor torque, and gimbal angles.

Modeling and control laws.- The RAM simulation model is divided functionally into four parts: (1) double gimbal CMG model with precession and compensation loops, (2) torque control laws, (3) attitude control loops, and (4) energy control law.

Gyro model: The three CMG planar array, shown in Figure 3-1, is aligned with its X, Y, and Z axes collinear with vehicle X, Y, and Z axes. This alignment orients the three outer gimbal axes normal to the major momentum plane (X, Y). Momentum transfer to the X, Y plane is obtained by outer gimbal motion, while small equal angle motion of the inner gimbals provides momentum along the Z axis (low moment of inertia axis of the RAM). The nominal zero momentum state occurs when inner and outer gimbal angles ($\gamma(I)$ and $\alpha(I)$ where I is the gyro number) are set to zero. Gyro mounting angles, measured counterclockwise from the Y-axis of the spacecraft, are: $0, 2\pi/3, 4\pi/3$ radians for Gyros 1,2,3.

The mathematical model for Gyro 1 is presented in Figure 3-2. Models for Gyros 2 and 3 are identical except for gyro subscripts. The gyro simulation model includes the significant rigid body effects of friction and gyro dynamics. Gimbal static and running friction are simulated by a nonlinear gimbal force logic routine. If nonlinear friction and spacecraft angular rates are considered negligible, then gyro dynamics can be expressed as follows:

Gimbal motor torques

$$TM1(I) = KM1\left[\dot{\gamma}_D(I)-\dot{\gamma}(I)-A_\gamma(I)\right] - \overset{\circ}{\alpha}(I)\, H(I) \cos\gamma(I)$$

$$TM2(I) = KM2\left[\dot{\alpha}_D(I)-\dot{\alpha}(I)\right] + \overset{\circ}{\gamma}(I)\, H(I) \cos\gamma(I)$$

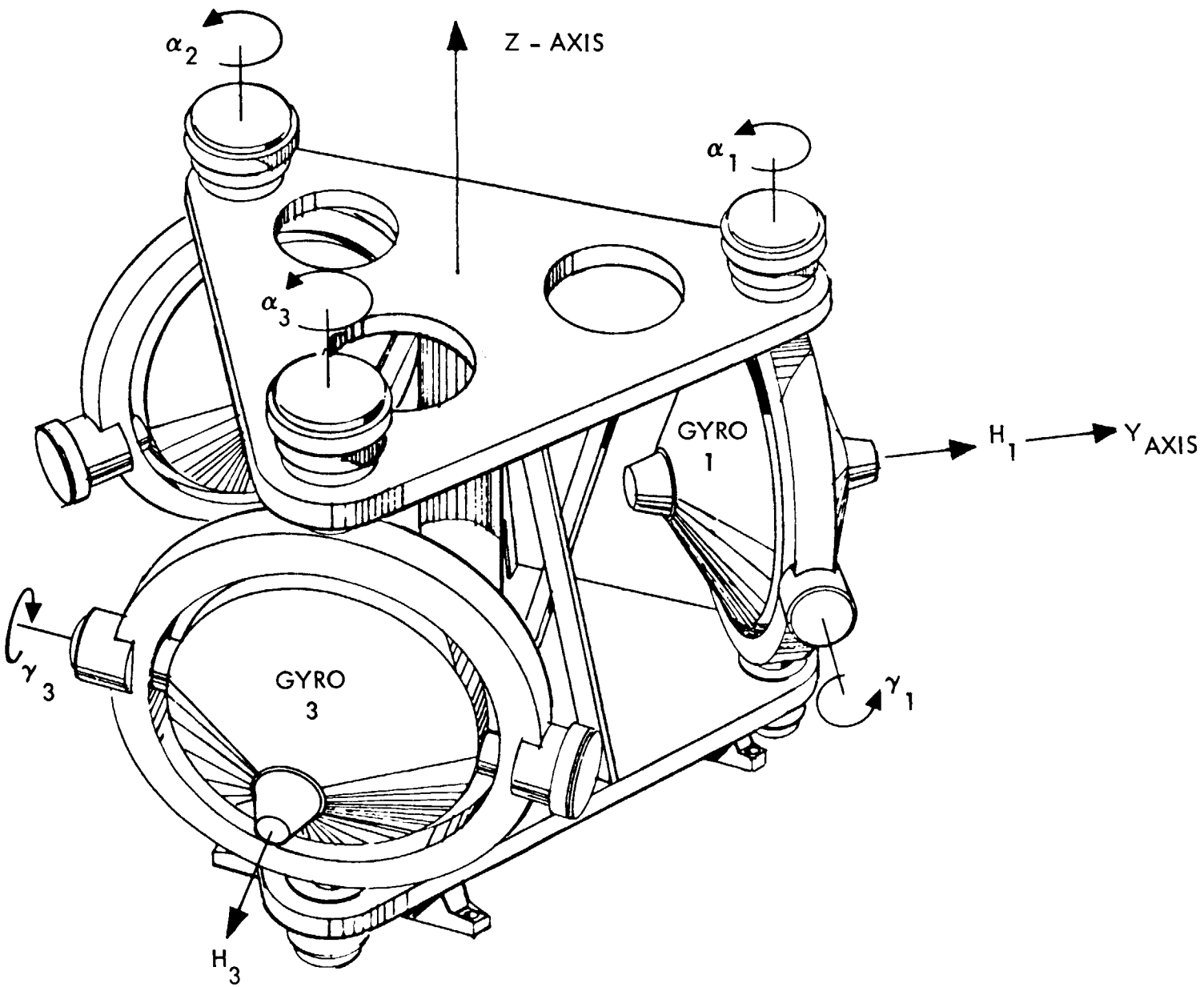

Figure 3-1. Three PM Control Moment Gyro Array

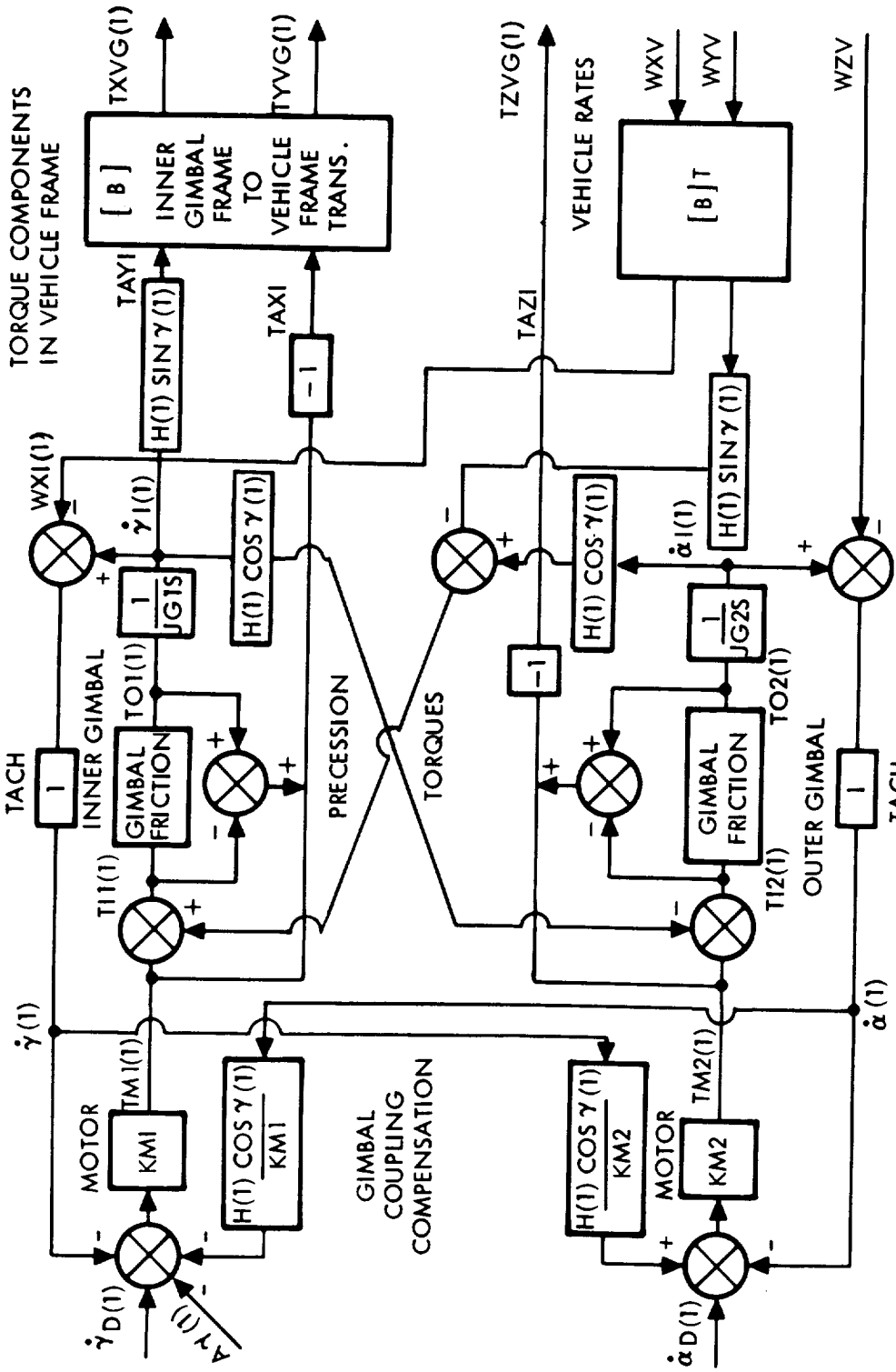

Figure 3-2. Analytical Model of Gyro 1

where TM1(I) and TM2(I) are the inner and outer gimbal motor torques developed in response to commanded inner and outer gimbal rates $\dot{\gamma}_D(I)$ and $\dot{\alpha}_D(I)$. H(I) is the individual gyro momentum. Inner and outer gimbal tachometer feedback is given by $\dot{\gamma}(I)$ and $\dot{\alpha}(I)$. Gimbal torque motors are represented as straight gains KM1 and KM2, and the inner gimbal slaving feedback is formed as:

$$A_\gamma(I) = \Sigma\dot{\gamma}(I)/3$$

The second terms on the right hand side of the gimbal motor torque equations are hard wired networks which feed gained outputs of gimbal tachometers to gimbal motor command signals. These terms, in the perfect sense, act to null precession torques due to gimbal rates and thereby decouple inner and outer gimbal motion.

Gimbal torques

$$TO1(I) = TM1(I) + \dot{\alpha}(I)\, H(I) \cos\gamma(I) = KM1\left[\dot{\gamma}_D(I) - \dot{\gamma}(I) - A_\gamma(I)\right]$$

$$TO2(I) = TM2(I) - \dot{\gamma}(I)\, H(I) \cos\gamma(I) = KM2\left[\dot{\alpha}_D(I) - \dot{\alpha}(I)\right]$$

where TO1(I) and TO2(I) are the developed inner and outer gimbal torques. The first and second terms on the right side of each equation are the torques developed by the gimbal motor and due to precession between inner and outer gimbal motion respectively.

Gimbal accelerations

$$\ddot{\gamma}_I(I) = TO1(I)/JG1$$

$$\ddot{\alpha}_I(I) = TO2(I)/JG2$$

where $\ddot{\gamma}_I(I)$ and $\ddot{\alpha}_I(I)$ are the inertial inner and outer gimbal accelerations, and JG1 and JG2 are the inner gimbal inertia and the equivalent inertia acting on outer gimbal torque.

Gyro torques on the spacecraft

$$TAXI = -TM1(I)$$

$$TAYI = \dot{\gamma}(I)\, H(I) \sin\gamma(I)$$

$$TAZI = -TM2(I)$$

where TAXI, TAYI, TAZI are the torques developed by the gyro in inner gimbal coordinates. These torques are transformed to torques acting on the spacecraft, expressed in spacecraft coordinates as follows:

$$TXV = \Sigma\ (TAXI \cdot \cos \Theta(I) - TAYI \cdot \sin \Theta(I)] = \Sigma\ TXVG(I)$$

$$TYV = \Sigma\ (TAXI \cdot \sin \Theta(I) + TAYI \cdot \cos \Theta(I)] = \Sigma\ TYVG(I)$$

$$TZV = \Sigma\ TAZI = \Sigma\ TZVG(I)$$

where $\Theta(I)$ are the gyro planar orientations given by

$$\Theta(1) = \alpha(1)$$

$$\Theta(2) = \alpha(2) + 2\pi/3$$

$$\Theta(3) = \alpha(3) + 4\pi/3$$

and TXVG(I), TYVG(I), TZVG(I) are the torque contributions of gyro I about the spacecraft roll, pitch, and yaw axes. The torque summations give the total gyro torque components (TXV, TYV, TZV) in spacecraft coordinates.

Torque control law: The desired operation of the gyro array is to make its vector rate of change of angular momentum coincident with the commanded torque vector. Using the conventional torque control concept, Figure 3-3 illustrates the control requirement on the CMG array.

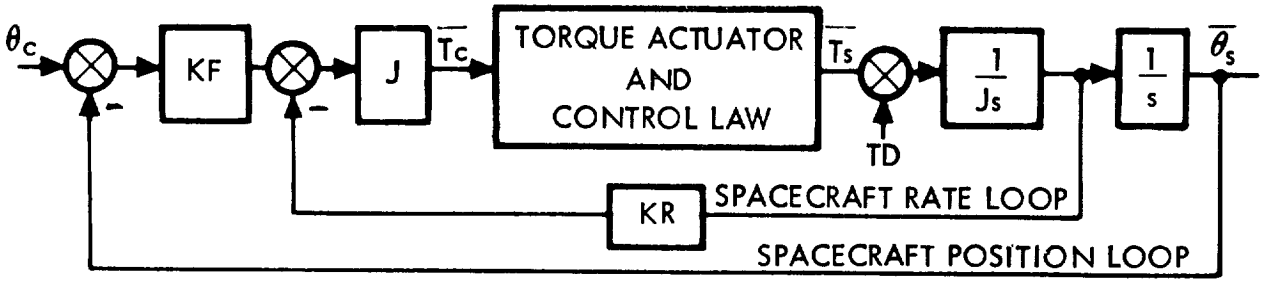

Figure 3-3.- Torque Control Concept

For the RAM gyro model and a torque feedback control law, the torque control operation between the commanded torque, $\overline{Tc}$, and developed torque, $\overline{Ts}$, of Figure 3-3 is further defined in Figure 3-4.

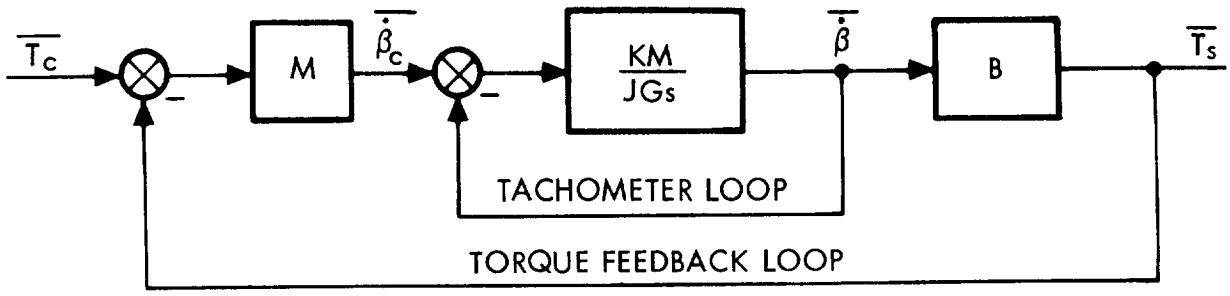

Figure 3-4.- Torque Control Law

In Figures 3-3 and 3-4:

Θ_c = attitude command

K_F = position loop gain

J = wheel inertia

TD = disturbance torque

KR = rate loop gain

M = command distribution matrix

$\dot{\beta}_c$ = gimbal rate command

$\dot{\beta}$ = gimbal rate

B = matrix relating gimbal rates to applied torque

KM = torque motor gain

Torque command errors are operated on by the transpose of the gimbal angle transformation matrix to generate gimbal rate commands. Achieved gimbal rate commands are transformed to obtain gyro torque on the spacecraft.

Tachometer feedback.- A foreseeable problem which is solved by a gimbal rate feedback is gimbal angle wander without torque delivery to the vehicle. This gimbal drift is occasioned by the effect of gimbal system nonlinearities; main causes of which are gimbal friction forces (static-sticktion and running-drag). In order to minimize these nonlinear effects, the motor-tachometer loop should be made as fast as possible; i.e., make the gimbal motor gain large. This, however, causes a problem in that increasing KM causes a decreasing low frequency gain of the torque loop. The selected solution is to

insert an integrator at the input to the command distribution matrix. With this fix, KM can be set sufficiently large to increase the motor-tachometer loop crossover frequency such that its effects are negligible; i.e., no interaction with outer loop crossover frequencies.

Torque feedback This is functionally equivalent to an angular acceleration feedback and thus augments the stabilization and control operation of the spacecraft feedback loops. It is analytically preferable to an alternate approximation, a shaping network in the spacecraft rate feedback loop. With torque feedback, the spacecraft response frequency and damping ratio can be set as desired via a simple analytical relationship between system gain parameters. This is presented and demonstrated in the linear transient response discussion.

Command Distribution Matrix. The objective in selecting the command distribution matrix M is to make the torque error as small as possible over a specified bandwidth and to stabilize the torque feedback loop. The matrix B, which relates gimbal rates and applied torque to the spacecraft, has elements which depend on sines and cosines of the various gimbal angles and thus change. Of necessity then, to keep the gains in the torque feedback loop relatively constant, the elements of M must also vary.

From Figure 3-4, the relationship between $\bar{T}_s$ and $\bar{T}_e$ is

$$\bar{T}_s = BM\bar{T}_e \text{ if } \dot{\bar{\beta}} = \dot{\beta}_c$$

where B and M can be non-square matrices. Also,

$$\bar{T}_s = (I + BM)^{-1} BM\, \bar{T}_c$$

where I is the identity matrix.

If M is selected such that

$$(I + BM)^{-1} \approx (BM)^{-1}$$

then $\bar{T}_s \approx \bar{T}_c$ and the torque error is small.

It can be shown that the selection of M to be

$$M = B^T K$$

where

$$BB^T = \begin{bmatrix} A_{11} & A_{12} \\ A_{21} & A_{22} \end{bmatrix}, \quad K = \begin{bmatrix} K_T & \frac{GCX}{S} & 0 \\ 0 & & K_T \ \frac{GCY}{S} \end{bmatrix}$$

and

$$GCX = \frac{1}{A_{11}}$$

$$GCY = \frac{1}{A_{22}}$$

satisfies the above approximation and sets the bandwidth of the torque feedback loop to K_T.

For the above

$$BM = BB^T K = \frac{K_T}{S} \begin{bmatrix} 1 & \frac{A_{12}}{A_{11}} \\ \frac{A_{21}}{A_{22}} & 1 \end{bmatrix}$$

and $\frac{A_{12}}{A_{11}} = \frac{A_{21}}{A_{22}} << 1$ for small gimbal angles.

Torque control model - Applying the gain corrector to the RAM CMG model and incorporating the forward loop integrator, the simulation model RAM torque control is formed as shown in Figure 3-5. Torque commands (TXC,TYC, TZC) to the gyros, expressed in spacecraft control coordinates, are seen to be:

$$TXC = \frac{KT}{GCX} \int (TXD - TXVC)dt$$

$$TYC = \frac{KT}{GCY} \int (TYD - TYVC)dt$$

$$TZC = KT \int (TZD - TZVC)dt$$

where the integrator acts on the difference between the attitude control commands (TXD,TYD,TZD) computed from spacecraft angular motion measurements and the computed gyro torque (TXVC,TYVC,TZVC) used for torque feedback. The simplified gain distribution matrix is composed of a torquer loop gain constant (KT) and the gain modifier terms (GCX,GCY). These, for the three planar mounted array, are

$$GCX = \Sigma \cos^2 \theta(I)$$

$$GCY = \Sigma \sin^2 \theta(I)$$

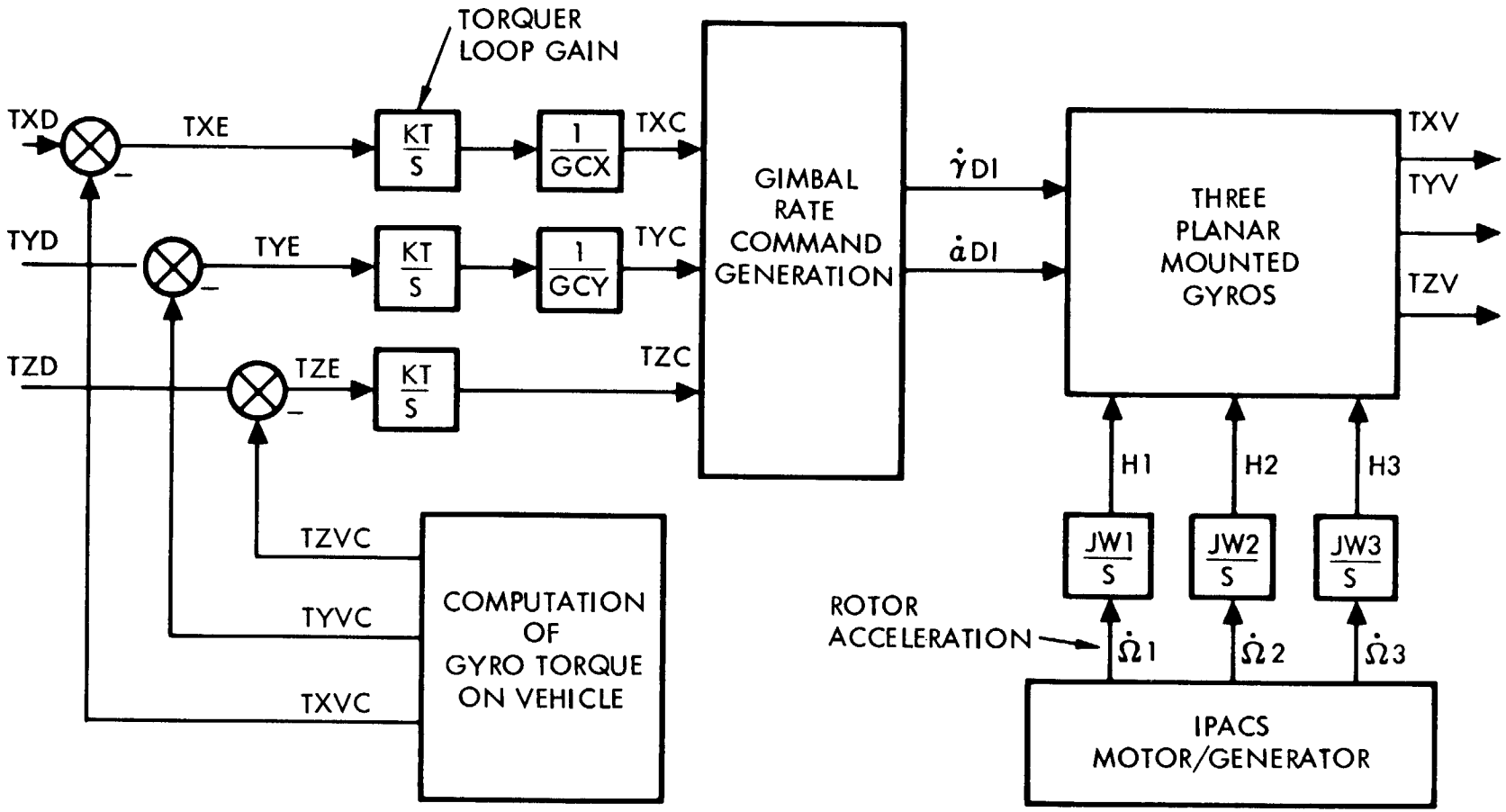

Figure 3-5. RAM Torque and Energy Control Model

Gimbal angle combinations that give zero values to GCX or GCY constitute "gimbal hangup" conditions; obviously, an undesirable state. Since the gain modifiers are formed mathematically, their minimum values can be limited to some suitable value and thus eliminate computational singularities. Gimbal hangup, however, is also a physical problem, and occurs when the momentum vector of one CMG lies opposite to the direction of the commanded momentum vector and when the remaining CMG vectors are symmetrically distributed about the commanded momentum vector.

Hangup for the planar gyro array is a less complex problem to solve than for other CMG configurations. Various simple methods for avoiding hangup can be envisioned; e.g., command gimbal rates to minimize the angle between the individual momentum vector and the momentum vector of the CMG array. Analysis of anti-hangup methods has not been included in the study, since the emphasis is on attitude control considered concurrently with gyro wheel energy transfer.

Torque commands are transmitted to the gyros in the form of gimbal rate commands $[\dot{\gamma}_D(I), \dot{\alpha}_D(I)]$, as seen in Figure 3-2. The gimbal rate commands are formed as follows:

$$\dot{\gamma}_D(I) = -TZC/\,[3H(I)\cos\gamma\,(I)]$$

$$\dot{\alpha}_D(I) = [TXC \cdot \cos\Theta\,(I) + TYC \cdot \sin\Theta\,(I)]/[H(I)\cos\gamma(I)]$$

where $\dot{\gamma}_D(I)$ and $\dot{\alpha}_D(I)$ are the inner and outer gimbal rate commands to the CMG array. The gyro orientation angle, $\theta(I)$, transforms the commanded torque in vehicle axes to gimbal rate commands in inner gimbal space.

Attitude control: To complete the spacecraft attitude control, it remains to define the outer control loops. These are expressed by the following equations.

Vehicle loops

$$TXD = -IXX\,[KR \cdot WXV + KF\,(AX-AXC)]$$

$$TYD = -IYY\,[KR \cdot WYV + KF\,(AY-AYC)]$$

$$TZD = -IZZ\,[KRZ \cdot WZV + KFZ\,(AZ-AZC)]$$

where TXD,TYD, and TZD are commanded vehicle torques. IXX,IYY, and IZZ are vehicle inertias. AXC,AYC, and AZC are commanded vehicle angular orientations. WXV,WYV, and WZV are vehicle rates. AX,AY, and AZ are vehicle attitude angles. The gains KR,KF, KRZ, and KFZ are selected to obtain the desired transient response characteristics for a specific vehicle.

Spacecraft angular rates and attitude

$$WXV = \int (TXV + HDX + TDX)/IXX \, dt$$

$$WYV = \int (TYV + HDY + TDY)/IYY \, dt$$

$$WZV = \int (TZV + HDZ + TDZ)/IZZ \, dt$$

$$AX = \int WXV \, dt$$

$$AY = \int WYV \, dt$$

$$AZ = \int WZV \, dt$$

where TXV,TYV, and TZV are gyro array torques for control with constant wheel speed. HDX,HDY, and HDZ are gyro array torques due to wheel acceleration. TDX,TDY, and TDZ are external disturbance torques on vehicle.

Although the equations are for a simplified vehicle, they are in a form that accommodates incorporation of flexible body equations, cross products of inertia, and additional system nonlinearities with little, if any, simulation model reformulation.

Energy control law: Energy transfer into or out of the control system is effected by changing the rotational energy of the gyro wheels. The energy command function is performed by the IPACS motor/generator assembly (M/G) for each gyro wheel via an interface with spacecraft power system. Ideally the power and attitude control dynamics would be combined in the same simulation model in order to investigate all possible interfacing and operational conditions. This is a goal for the future, when the detailed design of the IPACS system becomes more definitive. For the present, a simple, economical, and still effective simulation approach is taken; i.e., separate simulations of attitude control and power control systems. This is practical, since the motor/generator transient response is virtually instantaneous when compared to attitude control dynamic characteristics.

Relationships between electrical transfer rate demands imposed via the M/G and resultant wheel energy transfer are depicted in Figure 3-5 and are expressed by the following energy control law

$$\dot{\Omega}_W(I) = \frac{\dot{E}}{3H(I)}$$

where $\dot{E}$ is the demanded electrical transfer rate in watts, H(I) is the momentum of the wheel of gyro number I in N-m sec, and $\dot{\Omega}_W$ (I) is the angular acceleration/decleration of the gyro wheel in radians/second^2. The formulation presumes the energy transfer rate is equally distributed between the wheels of the three gyros. Other energy distribution rules were not studied at this time, nor was a consideration of wheel speed limiting at the maximum speed and error effects.

The wheel acceleration/deceleration commands give rise to torques upon the spacecraft. Equations used to represent the net gyro array torque about each spacecraft control axis are:

$$HDX = -J_W \Sigma \left[\dot{\Omega}_W(I) \cos \gamma(I) \sin \theta(I) \right]$$

$$HDY = J_W \Sigma \left[\dot{\Omega}_W(I) \cos \gamma(I) \cos \theta(I) \right]$$

$$HDZ = J_W \Sigma \left[\dot{\Omega}_W(I) \sin \gamma(I) \right]$$

where J_W are the wheel inertias, assumed equal for this study, and HDX,HDY, and HDZ are the gyro torques due to energy transfer. These torque terms can be computed in a manner similar to the zero energy torque terms and also used for torque feedback. Thus torque feedback is the sum of two terms:

$$TXVC = TXV + HDX$$

$$TYVC = TYV + HDY$$

$$TZVC = TZV + HDZ$$

Simulation results.- The mathematical model of the planar CMG array, torque control mechanization, and energy control law was digitally simulated for the RAM IPACS application to determine system energy storage and attitude control performance based upon representative RAM spacecraft/gyro properties. These physical properties and system control requirements are listed in Table 3-I. Before testing the RAM IPACS for the most stringent operation conditions, maximum energy charge/discharge rates, it was necessary to determine control system gain settings for a stable and responsive attitude control system. Consequently the simulation results are divided into two parts: (1) single axis simulation used to check the computer model accuracy and the linear and nonlinear system response characteristics; and (2) three axis simulation to determine the effects of energy transfer commands upon system performance.

Linear system response: Conditions useful for obtaining single axis response from the three axis model are listed in Table 3-II. These conditions obtain the common single axis control diagram presented in Figure 3-6, where IV and JG are the spacecraft and gyro gimbal inertias. The other parameters are constants set to obtain desired response characteristics of the spacecraft attitude A to a commanded attitude Ac. System response is seen to be dependent, then, upon the parameters KP, KT, KF, and KR, where KF can arbitrarily be chosen equal to KR.

Gain values, listed in Figure 3-6, were chosen to satisfy the following design criteria: (1) single axis response shall be identical for all three axes and (2) single axis response shall approximate a second order system with a $\sqrt{2}/2$ damping ratio.

TABLE 3-I.- RAM IPACS DATA BASE

IPACS performance requirements:			
Pointing accuracy - (1 arc-sec) 4.85×10^{-6} radians Maximum energy charge rate - 7220 watts Maximum energy discharge rate - 4820 watts			
Spacecraft properties:			
Control axis convention		Vehicle moments of inertia N-m sec^2 (slug-ft^2) (simulation axes)	
RAM system	RAM simulation		
X-axis	Z-axis (yaw)	IZZ	29 950 (22 090)
Y-axis	X-axis (roll)	IXX	159 850 (117 900)
Z-axis	Y-axis (pitch)	IYY	163 100 (120 300)
Gyro properties:			
Gyro moments of inertia N-m sec^2 (slug-ft^2)			
Gyro wheel	JWL		.4730 (.3489)
Inner gimbal	JG1		.2712 (.2000)
Equivalent outer gimbal	JG2		.3545 (.2615)

TABLE 3-II.- SELECTED CONDITIONS FOR SINGLE AXIS CONTROL

Control axes	Pitch	Yaw	Roll
Vehicle torques	TXV = 0 TYV ≠ 0 TZV = 0	TXV = 0 TYV = 0 TZV ≠ 0	TXV ≠ 0 TYV = 0 TZV = 0
Initial gimbal angles	$\gamma(I) = 0$ and $\alpha(I) = 0$		
Initial inner gimbal rates	$\dot{\gamma}(I) = 0$	$\dot{\gamma}(I) \neq 0$	$\dot{\gamma}(I) = 0$
Initial outer gimbal rates	$\dot{\alpha}(1) = 0$ $\dot{\alpha}(2) = -\dot{\alpha}(3)$	$\dot{\alpha}(I) = 0$	$\dot{\alpha}(2) = \dot{\alpha}(3)$ $\dot{\alpha}(1) = -2\dot{\alpha}(2)$

EQUIVALENT SINGLE AXIS CONTROL SYSTEM

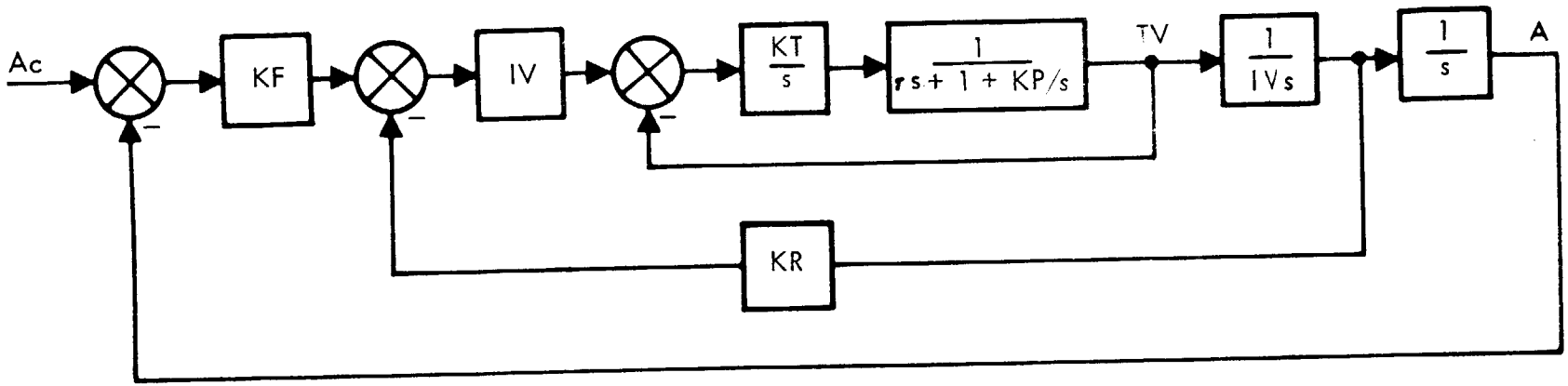

$$\frac{A}{Ac} = \frac{KF \cdot KT}{\tau s^4 + s^3 + (KP + KT)s^2 + KR \cdot KTs + KF \cdot KT}$$

WHERE τ = JG/KM

CONTROL SYSTEM GAIN SETTINGS

CONTROL LOOPS				
CONTROL AXIS	KP	KT	KF	KR
PITCH	0	25	2	2
YAW	1	24	2.083	2.083
ROLL	0	25	2	2

GYRO LOOPS		
τ	.02	SEC
	13.558	N-m -SEC
KM1	(10.)	(FT-LB-SEC)
	17.890	N-m -SEC
KM2	(13.195)	(FT-LB-SEC)

Figure 3-6. RAM Single Axis Control Diagram

Along with these design criteria, the break frequency of the tachometer loop was set at 50 radians/second; i.e., $T = .02$ seconds. As previously mentioned, a fast inner loop is needed to minimize the effect of gimbal motion nonlinearities. For simulation purposes, $T = .02$ satisfies this criterion without causing a computational problem; i.e., an uneconomically small integration stepsize required for computational fidelity. Control frequencies of the system gain settings are approximately 1 and 24 radians/second, which is adequate separation from the 50 radian/second inner loop.

Simulation runs confirmed analytical predictions of identical single axis attitude response for each control axis. The observed gimbal motion behaved as defined in Table 3-II, and the simulation program integration method showed a high enough degree of accuracy not to compromise attitude control accuracy determinations.

Nonlinear system response: Before effects of gimbal friction upon system response are discussed, torque and gimbal motion equations are redefined to include gimbal static and running friction forces and distinction between rates of the gimbal case and gimbal rates measured with respect to the case. These equations are:

Commanded gimbal torques

$$TI1(I) = TM1(I) + \dot{\alpha}_I(I)\, H(I) \cos \gamma(I) - WXY(I)\, H(I) \sin \gamma(I)$$

$$TI2(I) = TM2(I) - \dot{\gamma}_I(I)\, H(I) \cos \gamma(I)$$

$$WXY(I) = WYV \cdot \cos \Theta(I) - WXV \cdot \sin \Theta(I)$$

where $TI1(I)$ and $TI2(I)$ are the inner and outer gimbal command torques. $\dot{\gamma}_I(I)$ and $\dot{\alpha}_I(I)$ are the inner and outer gimbal rates, while WXV and WYV are the vehicle rates about the X and Y axes.

Achieved gimbal torques

$$TO1(I) = STKTON\ (SF1,\ RF1,\ TI1(I),\ \dot{\gamma}(I),\ G1(I))$$

$$TO2(I) = STKTON\ (SF2,\ RF2,\ TI2(I),\ \dot{\alpha}(I),\ G2(I))$$

where TO1(I) and TO2(I) are the developed inner and outer gimbal torques which differ from the commanded torques due to friction effects.

The computer subroutine STKTON is designed to compute the effect of static and running friction on a rotating gimbal of a gyro where the gyro case may be moving. Input and output torque are TI and TO. Static and running friction are SF and RF; subscripts 1 and 2 indicate inner and outer gimbal systems. The gimbal rate with respect to the gyro case is the fourth argument,

$\dot{\gamma}(I)$ or $\dot{\alpha}(I)$, in the STKTON call statement. The last argument, G1(I) or G2(I), is a memory variable for the relative gimbal rate. Static friction acts as a breakout force threshold for gimbal motion and thus functions as an on-off deadband for output torque. Running friction acts as a braking force on the relative gimbal motion.

Gyro torque on the spacecraft

$$TAXI = \Sigma\ [TM1(I) - TO1(I) + TI1(I)]$$

$$TAYI = \Sigma[\overset{\circ}{\gamma}(I)\ H(I)\ \sin\ \gamma(I)]$$

$$TAZI = \Sigma\ [-TM2(I) - TO2(I) + TI2(I)]$$

where TAXI and TAZI are the actual torques acting on the vehicle and are functions of gimbal motor torques and gimbal accelerating torques. The arithmetic difference between commanded and achieved gimbal acceleration torque is due to the effect of friction. Gimbal viscous damping is not represented in the friction model since its effect is negligible.

Gimbal acceleration

$$\overset{\circ\circ}{\gamma}_I(I) = TO1(I)/JG1$$

$$\overset{\circ\circ}{\alpha}_I(I) = TO2(I)/JG2$$

Gimbal rates

$$\overset{\circ}{\gamma}_I(I) = \int \overset{\circ\circ}{\gamma}_I(I)\ dt \qquad \text{if } TO1(I) \neq 0$$

$$= WXV \cdot \cos\ \theta(I) + WYV \cdot \sin\ \theta(I) \qquad = 0$$

$$\overset{\circ}{\alpha}_I(I) = \int \overset{\circ\circ}{\alpha}_I(I)\ dt \qquad \text{if } TO2(I) \neq 0$$

$$= WZV \qquad = 0$$

where the logic indicates that when the achieved gimbal torque is zero, then the respective gimbal moves with the gimbal case at the indicated spacecraft rate. The subscript I denotes inertial frame. The relative gimbal rates with respect to the spacecraft are thus given by the following equations:

$$\overset{\circ}{\gamma}(I) = \overset{\circ}{\gamma}_I(I) - WXV \cdot \cos\ \theta(I) - WYV \cdot \sin\ \theta(I)$$

$$\overset{\circ}{\alpha}(I) = \overset{\circ}{\alpha}_I(I) - WZV$$

where the inner and outer gimbal rates reflect the effect of gimbal stiction and describe gimbal motion due to gimbal torque and also with respect to the gyro case. $\overset{\circ}{\gamma}(I)$ and $\overset{\circ}{\alpha}(I)$ are the gimbal rates measured by the inner and outer gimbal tachometers.

Nonlinear system simulation runs, using the linear system gains and initial conditions, were made to determine the effects of friction on single axis response. Values of .0237 N-m (.0175 ft-lb) were used as estimates of static and running friction torques for RAM IPACS gyro units with direct drive brushless gimbal torque motors. Comparison of like linear and nonlinear system characteristics indicate that gimbal friction of these magnitudes have virtually no effect on spacecraft attitude response. However, nonlinearities are evidenced in vehicle torque and other inner loop variables. As expected, nonlinearities are especially noticeable whenever zero gimbal rate condition exists; i.e., the gimbal motion is inhibited by the static friction breakout torque. Peak values of mission critical variables, notably gimbal motor torques, are not significantly increased by the effects of gimbal friction.

Effects of energy charge/discharge rates: Two energy transfer conditions were selected to test the effects of energy transfer upon control system response: (1) maximum charge rate when the gyro wheels are at the low end of the speed range and (2) maximum discharge rate when the wheels are at their maximum speed.

Torque on the vehicle due to the effect of wheel acceleration/deceleration and the distribution of such torque about individual vehicle control axes is dependent upon the gimbal angle of the gyros as well as the wheel acceleration/deceleration magnitude. The gyro array momentum at any time is dependent upon the previous system time history (attitude maneuvers commands, external disturbance torques, energy charge/discharge cycles); therefore the typical array momentum is virtually a random variable.

Initial conditions for the energy transfer runs are listed in Table 3-III.

A first point of interest is whether the energy charge/discharge torque should be summed with gyro array control torque for torque feedback. Analytical diagrams and resultant transfer functions for the $\dot{H}$ feedback or no $\dot{H}$ feedback options are shown in Figure 3-7. It is of interest to note that the energy charge/discharge torque is functionally equivalent to an external torque source. Torque feedback treats the torque source as a known and measurable quantity; whereas the other option treats the external torque as a random variable.

Short period response characteristics for both torque feedback options are nearly identical, but $\dot{H}$ feedback obtains a zero steady state value whereas the no $\dot{H}$ feedback option tends toward a non-zero steady-state value. Thus $\dot{H}$ feedback is the selected mechanization since the other option results in a vehicle attitude error due to wheel accelerations/decelerations, which could compromise attitude control pointing accuracy capability.

ENERGY TORQUE FEEDBACK

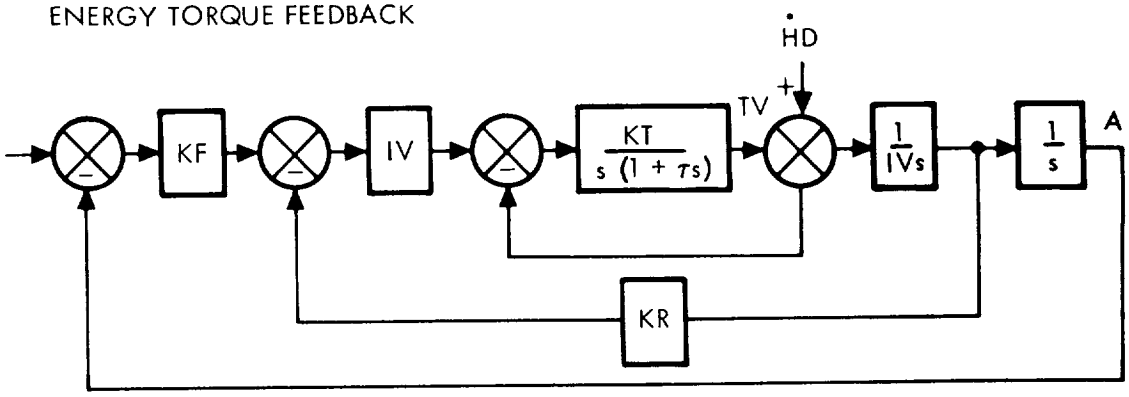

$$\frac{A}{\dot{H}_D} = \frac{s(1+\tau s)}{IV\left[KF \cdot KT + KR \cdot KTs + KTs^2 + s^3 + \tau s^4\right]}$$

NO ENERGY TORQUE FEEDBACK

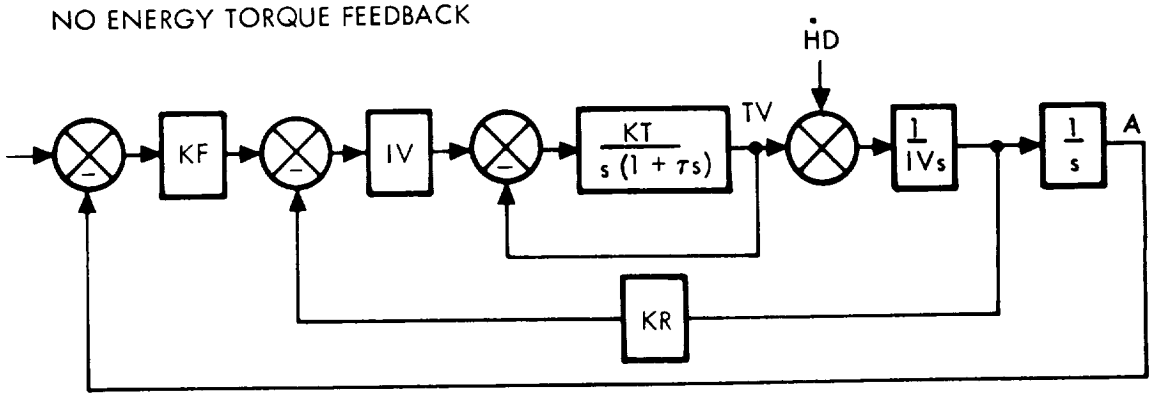

$$\frac{A}{\dot{H}_D} = \frac{s(1+\tau s)+KT}{IV\left[KF \cdot KT + KR \cdot KTs + KTs^2 + s^3 + \tau s^4\right]}$$

Figure 3-7. Energy Torque Feedback Concepts

TABLE 3-III.- ENERGY TRANSFER SIMULATION CONDITIONS

Energy transfer condition	$\dot{E}$ watts	$\Omega_W(I)$ RPM	H(I) N-m sec (ft-lb-sec)	$\dot{\Omega}_W(I)$ rad/sec^2
Maximum charge rate	7220	22 500	1 114 (822)	2.1596
Maximum discharge rate	-4820	45 000	2229 (1644)	-.7209

Energy transfer condition	Array momentum N-m sec (ft-lb sec)			Gimbal angles radians (degrees)				Array torques N-m (ft-lb)		
	HZ	HY	HZ	α_1	α_2	α_3	γ	HDX	HDY	HDZ
Maximum charge rate	0	2034 (1500)	407 (300)	0	-.956 (-54.8)	.956 54.8	.122 (7.0)	0	1.865 (1.375)	.373 (.275)
Maximum discharge rate	0	2034 (1500)	407 (300)	0	-.480 (-27.5)	.480 (27.5)	.061 (3.5)	0	-.310 (-.229)	-.062 (-.046)

Maximum energy transfer response Simulation results for the two sets of conditions defined in Table 3-III are presented in Figures 3-8 through 3-12 for the maximum energy charge rate conditions and Figures 3-13 through 3-18. The gimbal motor torque never exceeded 15 percent of the total available torque for either energy transfer condition.

Based upon these data, the outer gimbal angle change in going from minimum to maximum wheel energy could be approximately .785 radians (45 degrees). This assumes an equivalent wheel acceleration rate equal to 3/4 the maximum rate which yields an equivalent outer gimbal rate of 8.72 x 10-4 radians/sec.

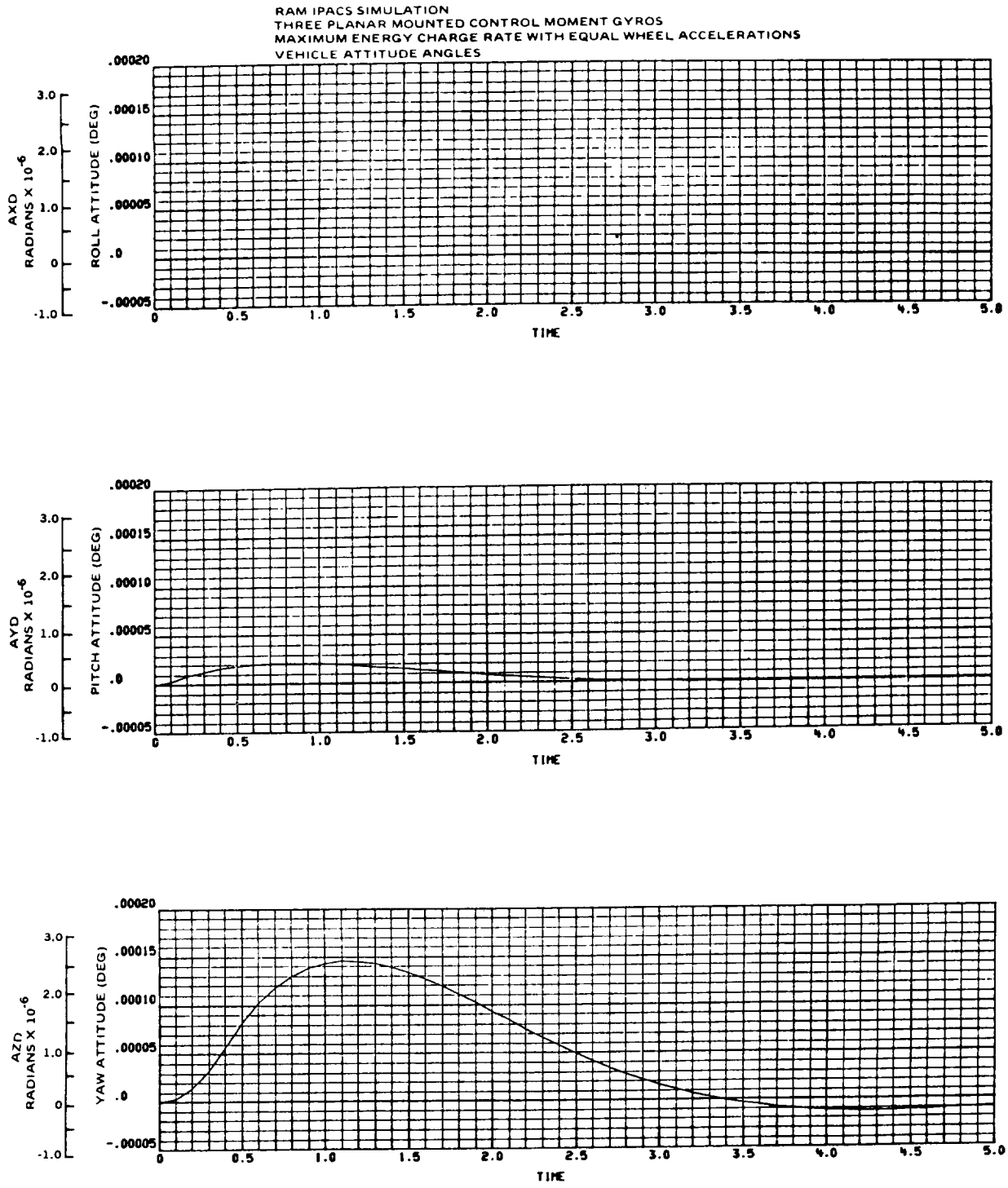

Figure 3-8. RAM-Max Energy Charge Rate Response - Vehicle Attitude Angles

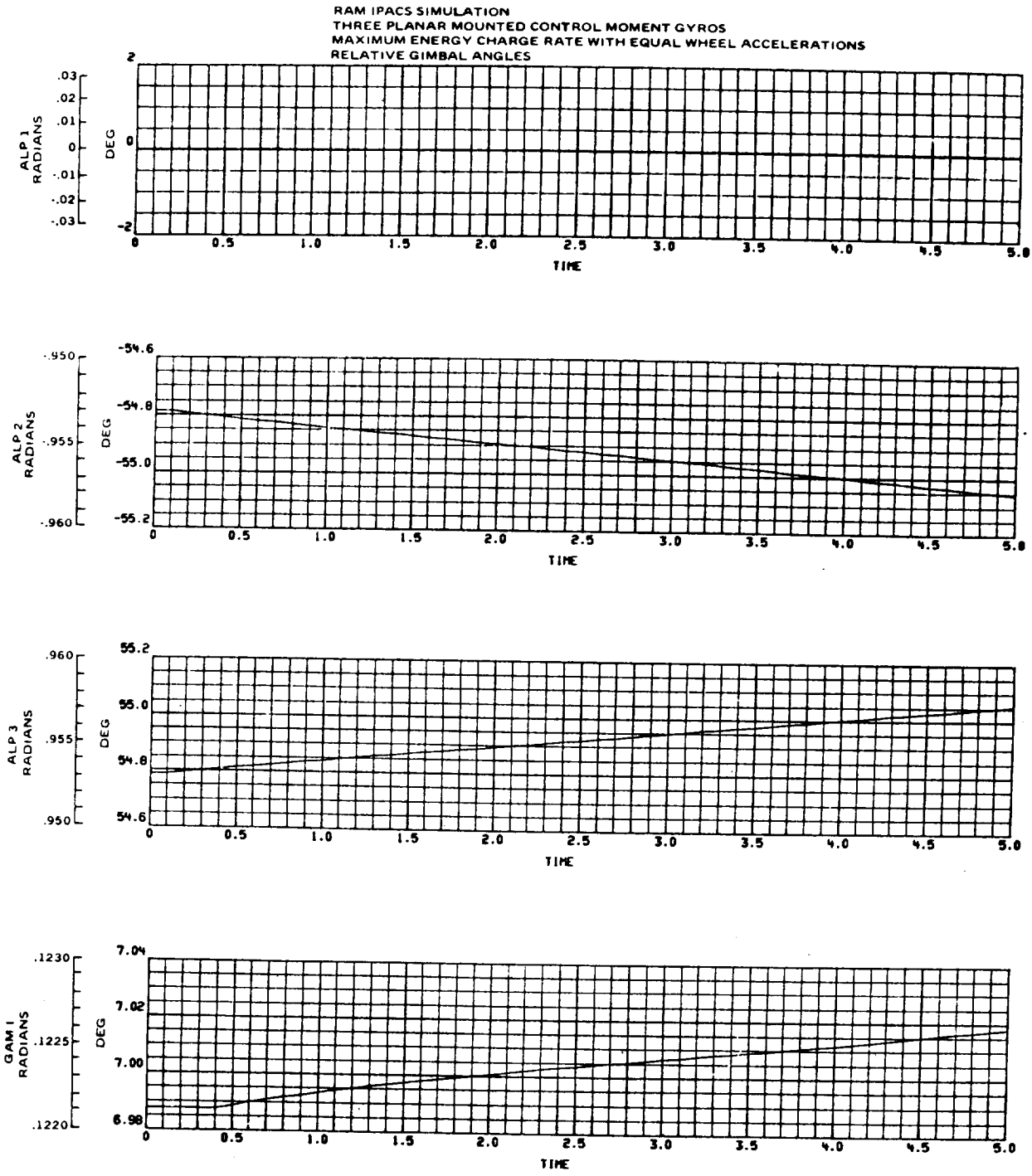

Figure 3-9. RAM-Max Energy Charge Rate Response - Relative Gimbal Angles

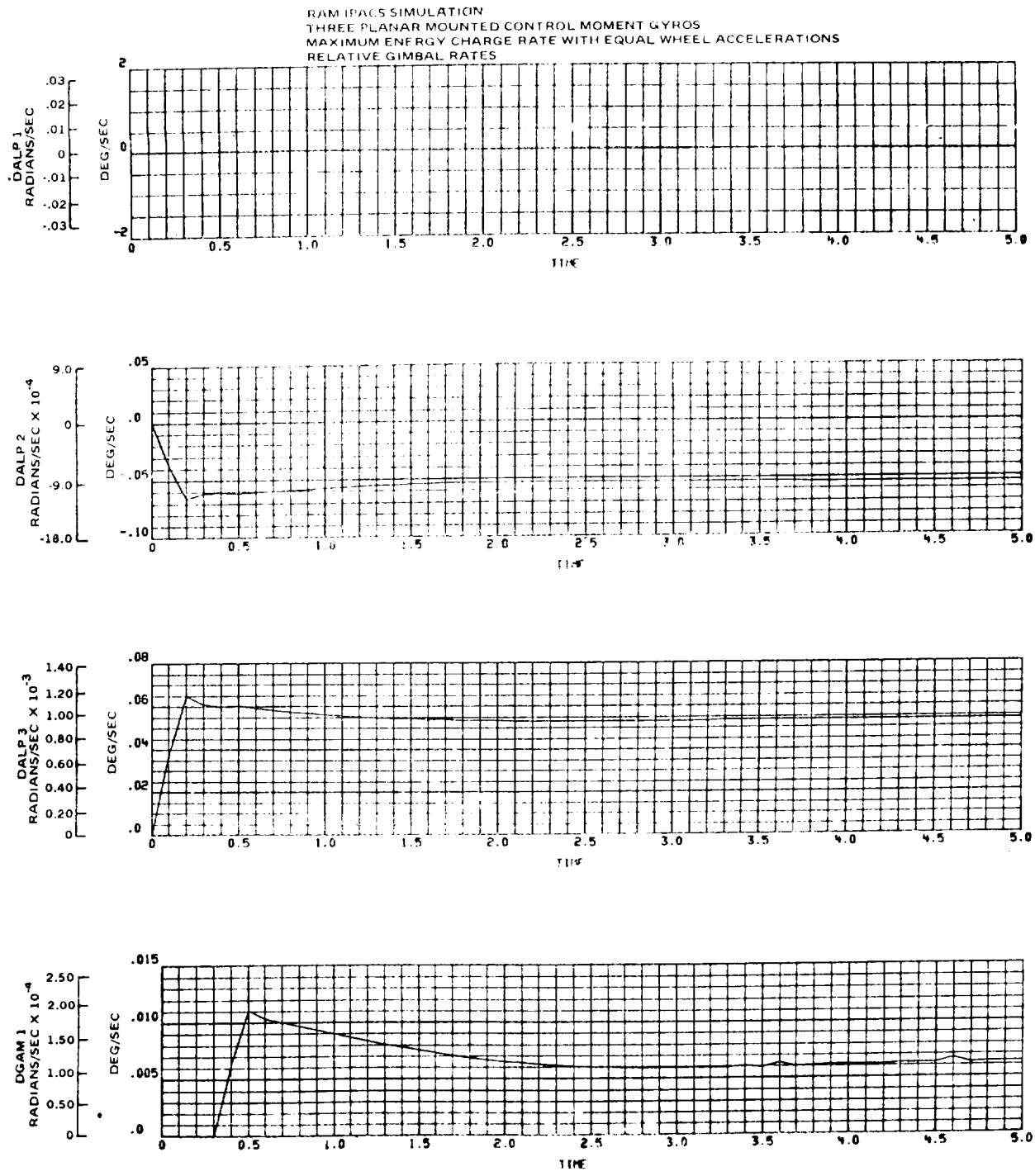

Figure 3-10. RAM-Max Energy Charge Rate Response - Relative Gimbal Rates

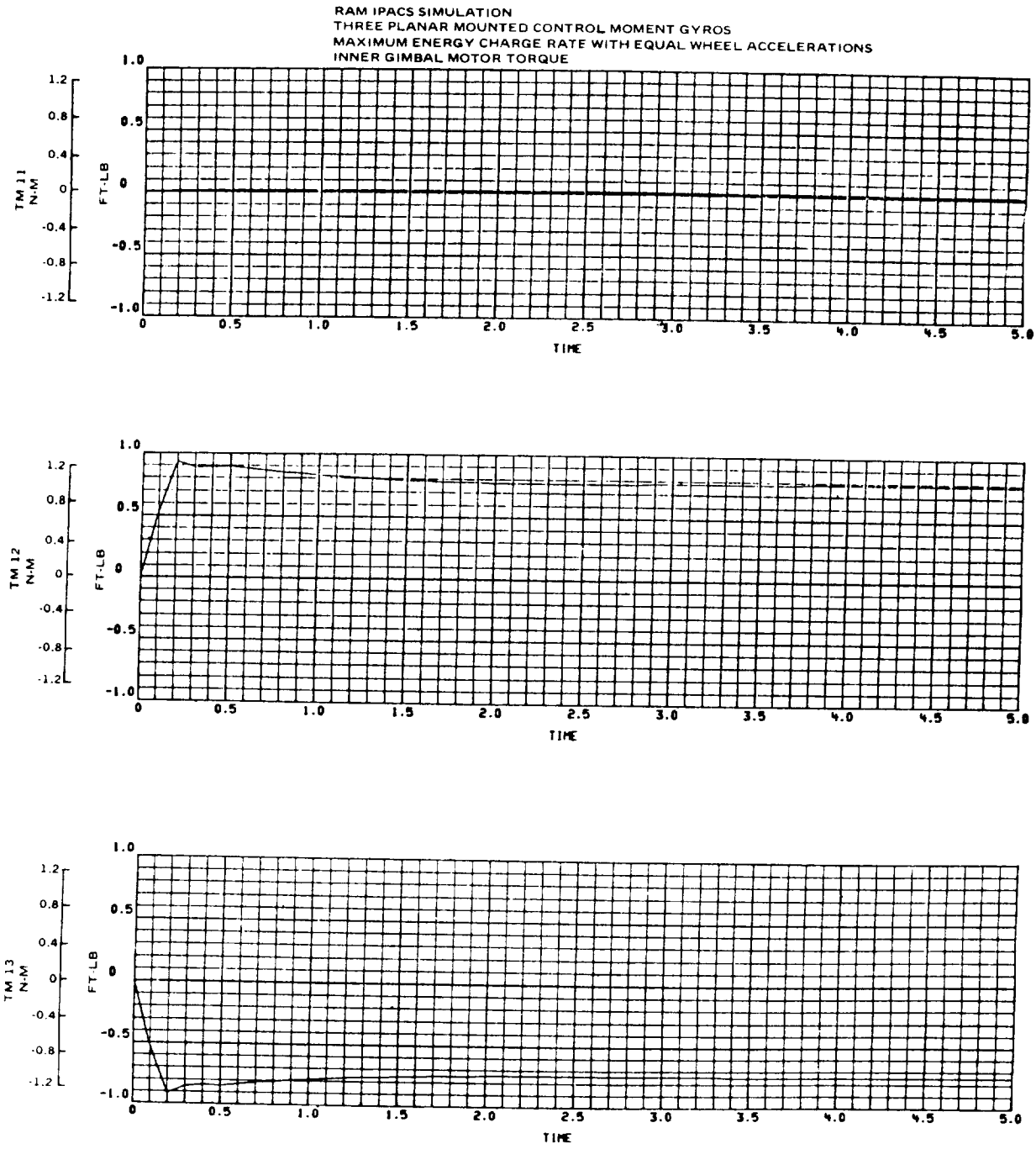

Figure 3-11. RAM-Max Energy Charge Rate Response - Inner Gimbal Motor Torques

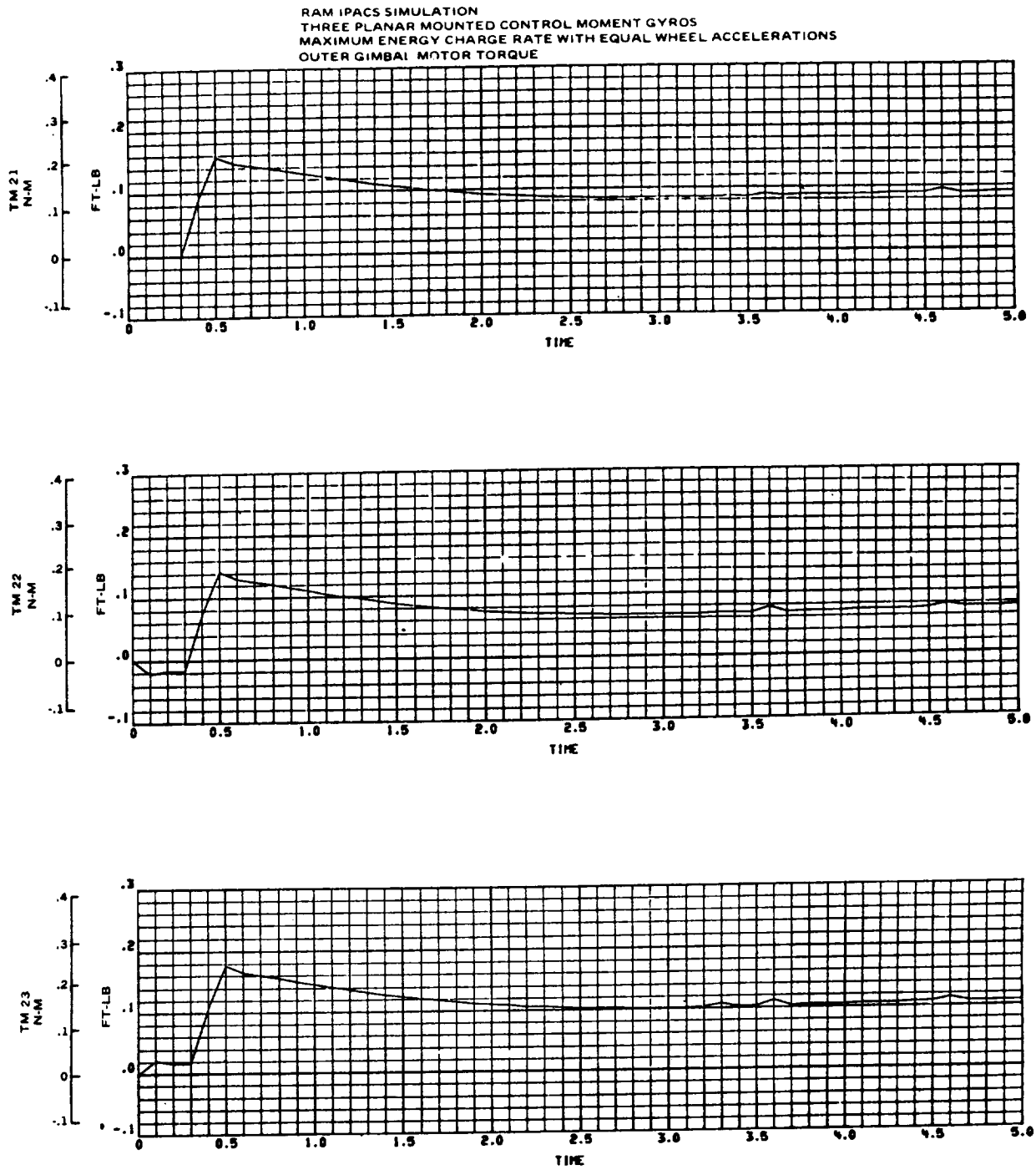

Figure 3-12. RAM-Max Energy Charge Rate Response - Outer Gimbal Motor Torques

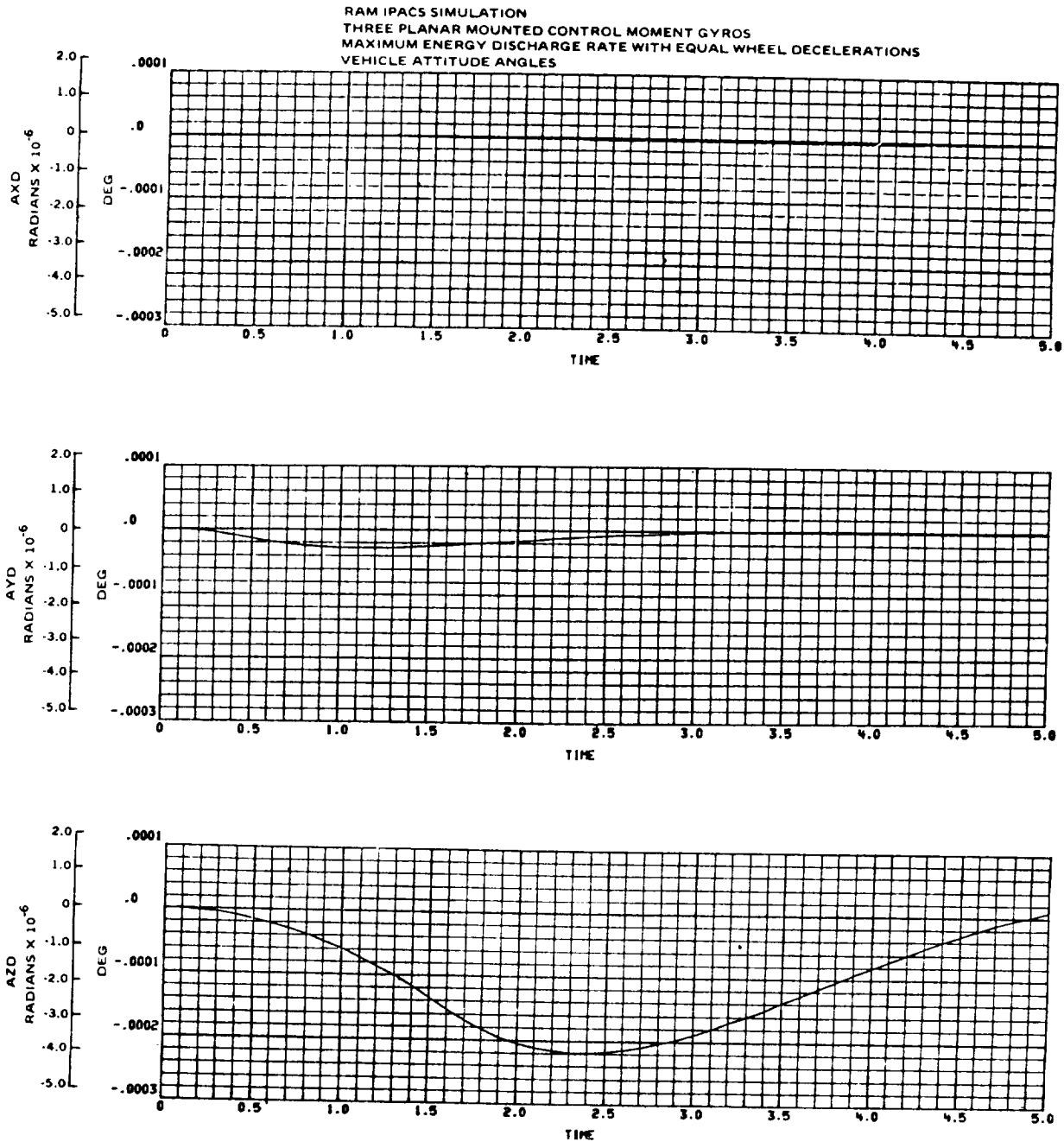

Figure 3-13. RAM-Max Energy Discharge Rate Response - Vehicle Attitude Angles

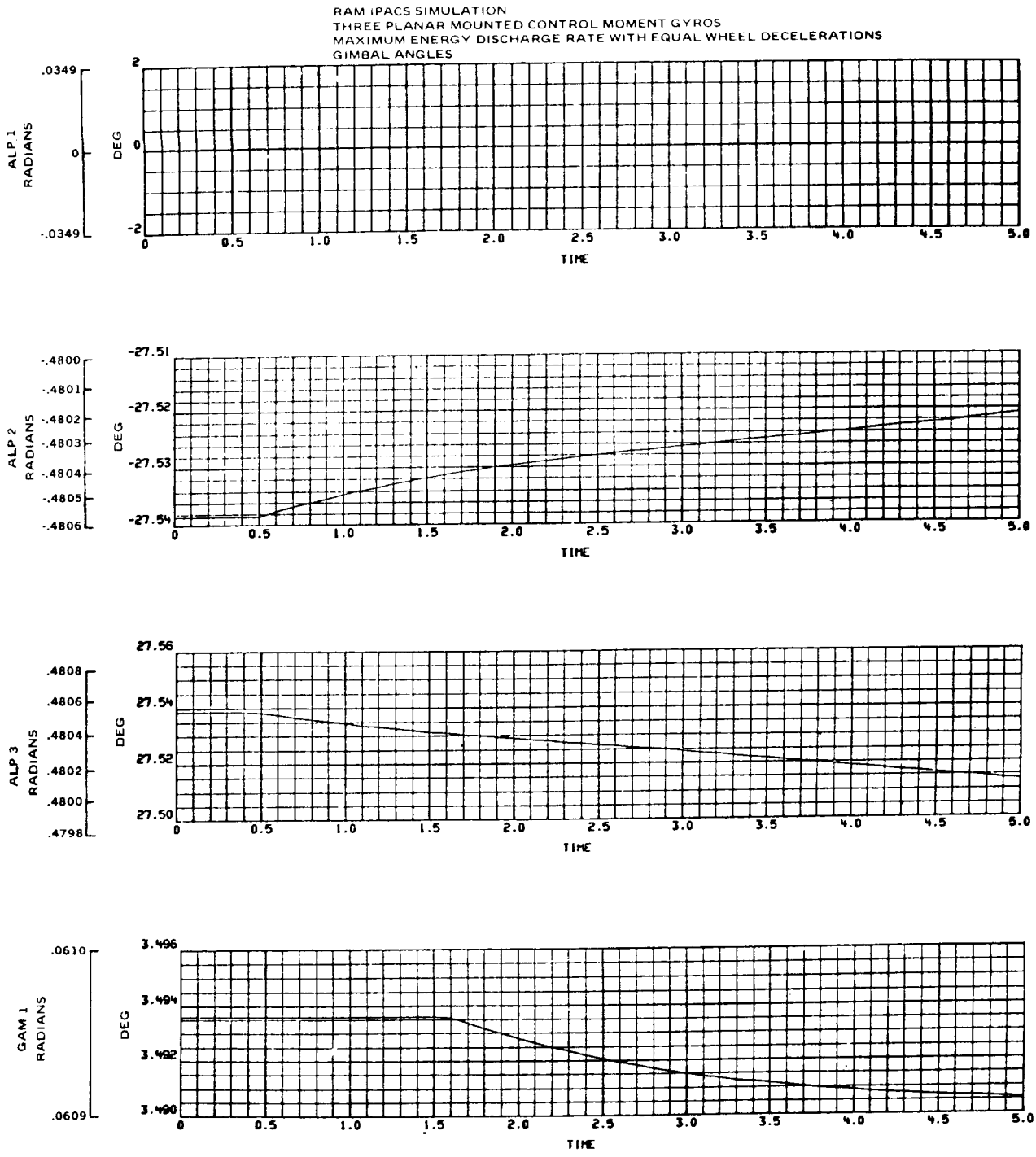

Figure 3-14. RAM-Max Energy Discharge Rate Response - Relative Gimbal Angles

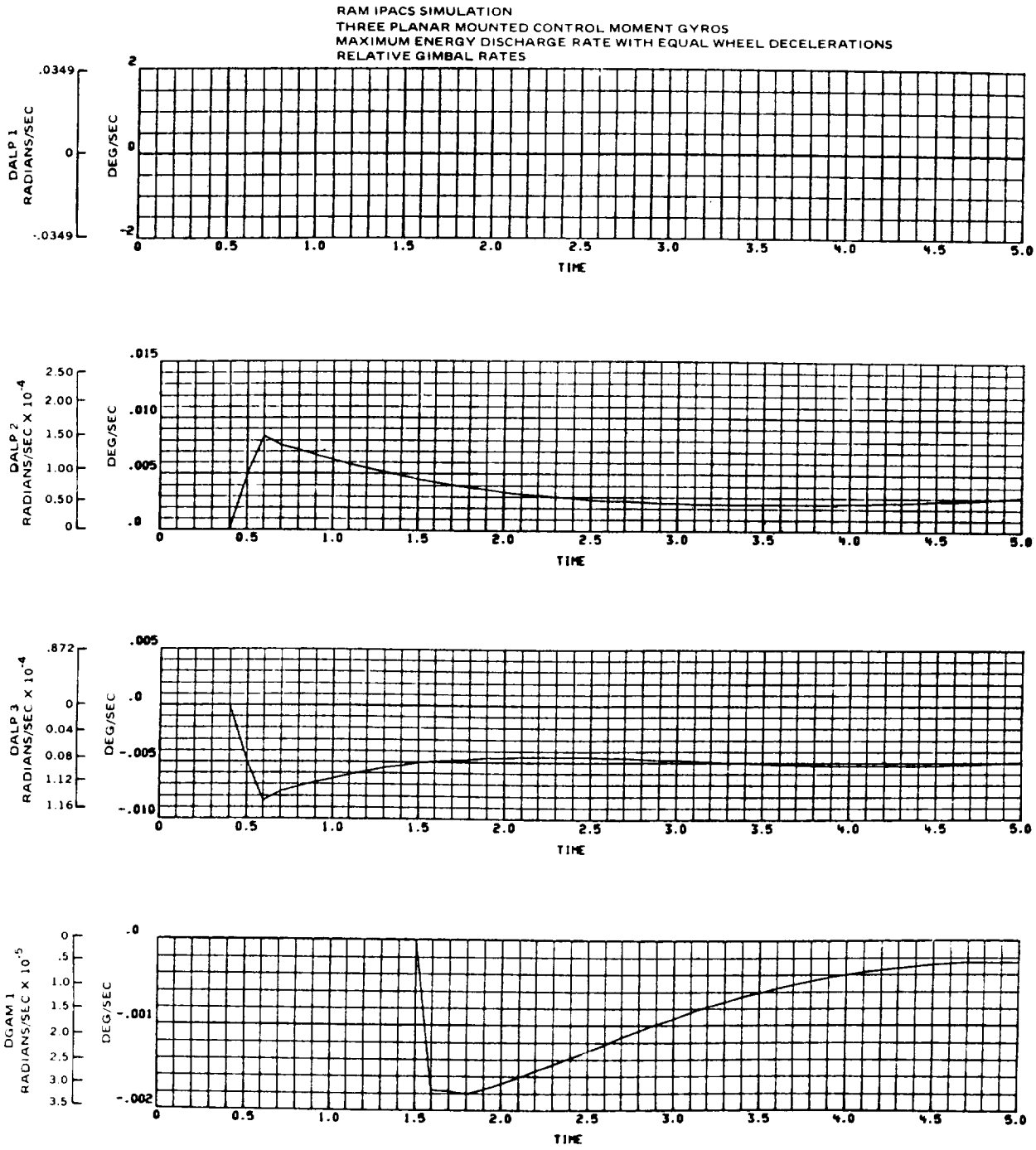

Figure 3-15. RAM-Max Energy Discharge Rate Response - Relative Gimbal Rates

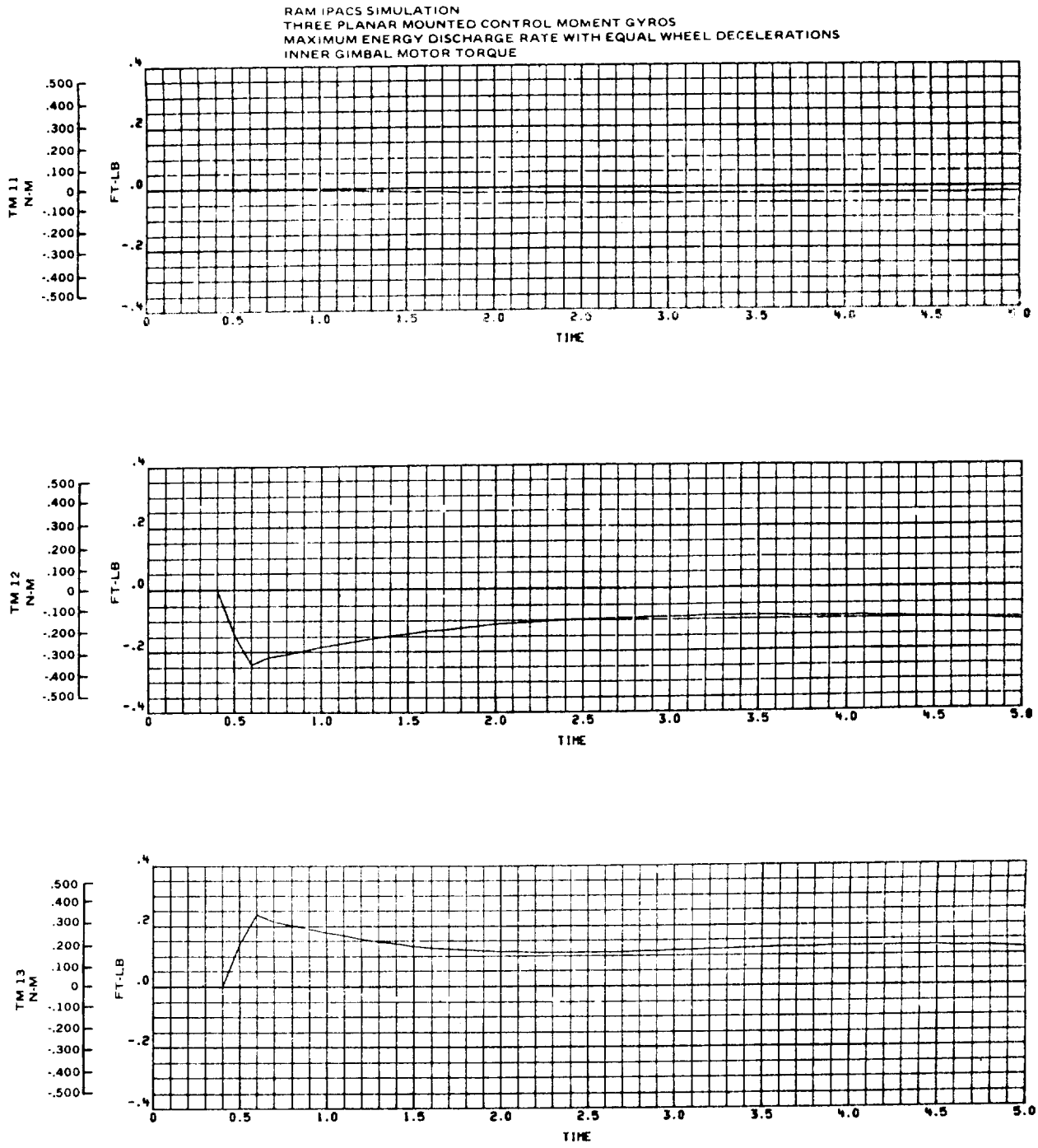

Figure 3-16. RAM-Max Energy Discharge Rate Response - Inner Gimbal Motor Torques

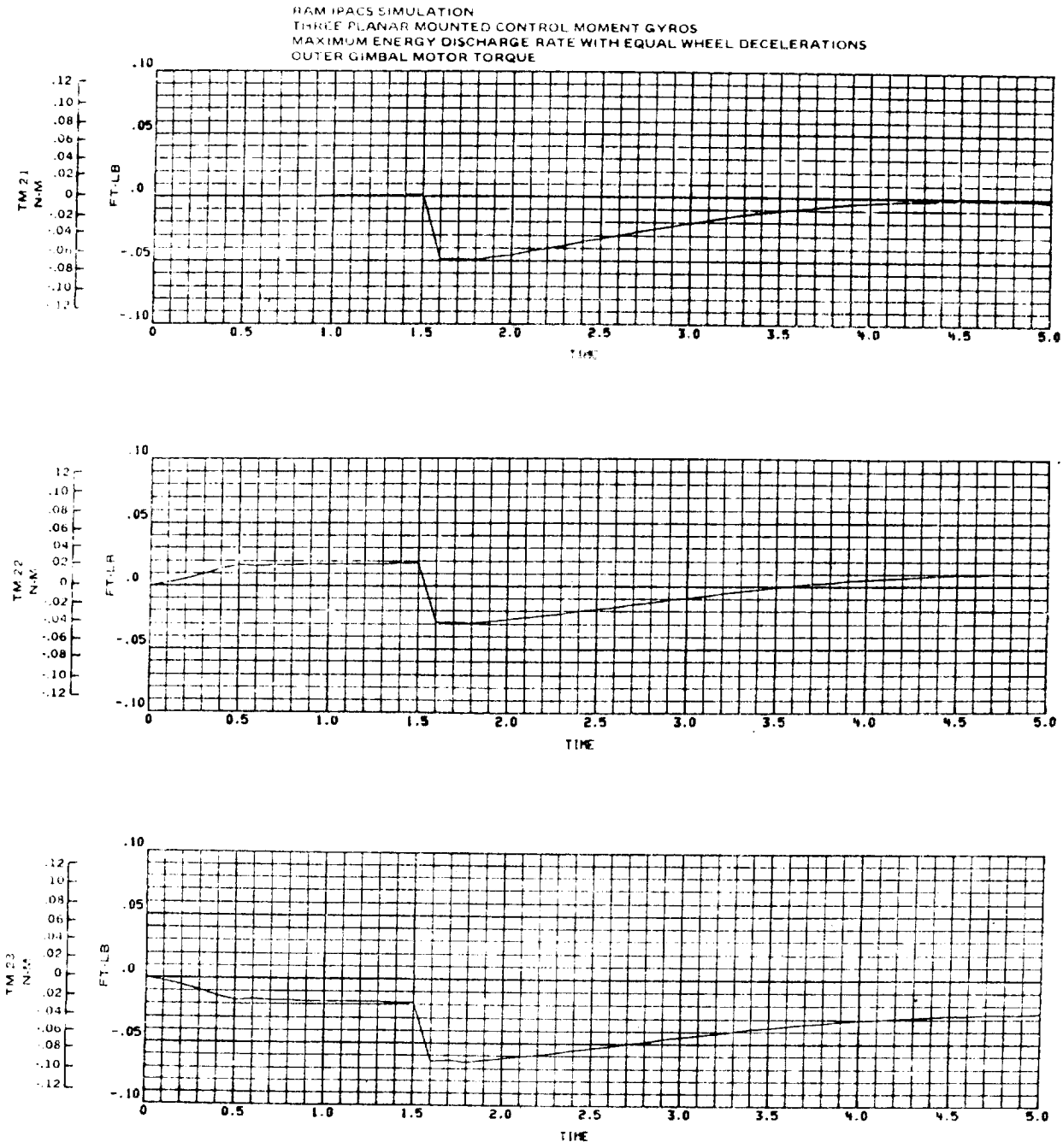

Figure 3-17. RAM-Max Energy Discharge Rate Response - Outer Gimbal Motor Torques

FORCING FUNCTIONS

- YAW ATTITUDE COMMAND = 1.745×10^{-4} RADIANS (36 ARC-SECONDS)
- ENERGY CHARGE RATE/WHEEL = 2407 WATTS (~2.16 RAD/SEC^2)
- GIMBAL FRICTION (STATIC & RUNNING) = .0237 NM (.0175 FT-LB)

INITIAL GYRO ARRAY STATE

- X, Y-PLANE MOMENTUM = 2033.7 N-M-SEC (1500 FT-LB-SEC)
- Z MOMENTUM = 406.7 N-M-SEC (300 FT-LB-SEC)
- WHEEL SPEED = 22,500 RPM

STEADY STATE CONDITIONS AT T = 10 SEC

- ATTITUDE ERRORS LESS THAN 4.847×10^{-6} RADIANS (1 ARC-SECOND)
- GIMBAL MOTOR TORQUES LESS THAN 1 N-M (.74 FT-LB)
- RATE OF CHANGE OF NET ARRAY MOMENTUM = 1.9 N-M-SEC/SEC (1.4 FT-LB-SEC/SEC)

YAW ATTITUDE ERROR HISTORY

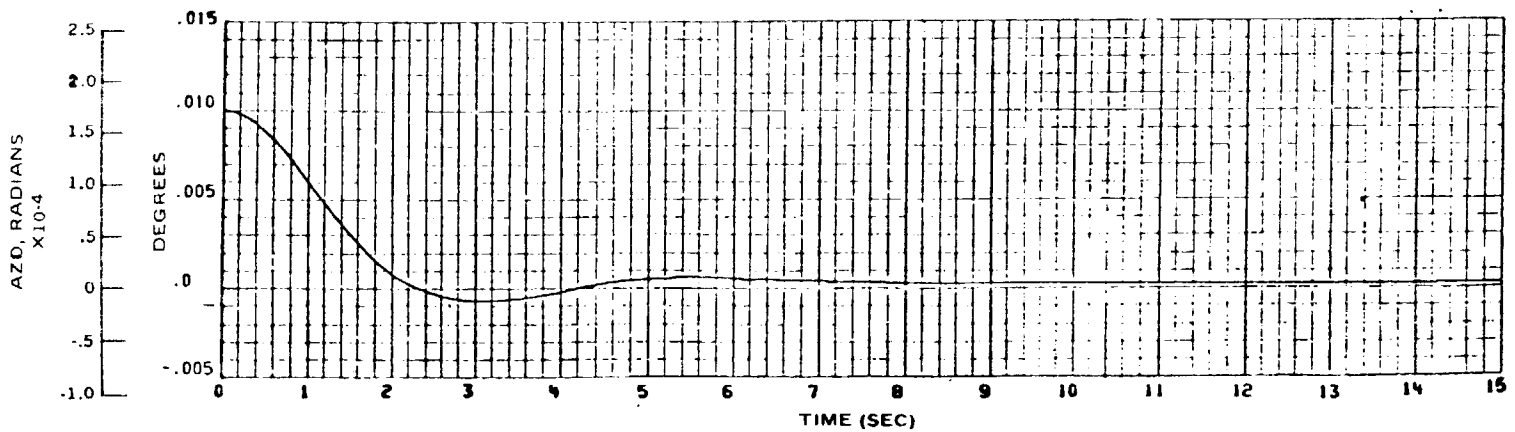

Figure 3-18. RAM IPACS - Typical Simulation Results

(.05 degrees/second); the energy charging duration corresponds to an energy storage of 2500 watt hours. The maximum inner gimbal position excursion would be less than 1/8 the outer gimbal travel. Periods of energy charge and discharge alternate, therefore, .785 radians (45 degrees) represents the maximum outer gimbal excursion from the zero nominal value. Maximum inner gimbal angles would be considerably smaller because of inner gimbal slaving. Thus, gimbal lock conditions are not likely to be caused by energy transfer torques.

Gimbal angle hangup conditions could occur, but are easy to handle, being a two dimensional problem involving outer gimbal angles only. An anti-hang-up law would act to generate outer gimbal rate commands to drive gimbals away from hangup conditions.

Capability of the RAM control system to satisfy the 4.85×10^{-6} radians (1 arc-second) attitude control accuracy requirement was tested with maximum energy charging conditions plus a yaw attitude command. The resultant three-axis attitude response of the spacecraft is presented in figure 3-18. These data indicate attitude error is reduced to within the allowable maximum within about 10 seconds following initiation of the combined energy transfer and step attitude commands. This conclusion also applies to the effects of disturbance torques which may be applied during periods of energy transfer. The digital simulation model appears to be sufficiently accurate for deterministic error studies with additional coupling terms and error sources.

Effects of initial momentum conditions The maximum charge rate conditions were used to determine the effect of initial conditions in gimbal angles on the peak gimbal motor torque during energy transfer periods.

Based upon these results, peak motor torques never exceed 50 percent of that available, thus leaving an adequate margin for countering disturbance torques. Furthermore, the peak motor torque is experienced during the few seconds following initiation of energy transfer operations. Also, the effect on controlling vehicle attitude is negligible, since attitude errors are reduced to near zero conditions within 10 seconds after onset of energy transfer torque.

Conclusions: Linear analysis shows that the RAM CMG attitude control system response can be selected analytically as a simple function of constant control system gains.

Representative gimbal friction nonlinearities do not appreciably affect system dynamic response characteristics.

System attitude errors, assuming perfect system components and friction nonlinearities, can be reduced to less than 4.85×10^{-6} radians (1 arc sec) in approximately 10 seconds.

Wheel energy can be cycled between maximum and minimum energy conditions at maximum rates without approaching gimbal lock conditions.

Maximum gimbal motor torque during energy charge/discharge conditions does not exceed 50 percent of maximum rated motor torque for any expected conditions.

TDRS Analysis and Simulation

The energy storage/attitude control system studied for TDRS type IPACS application utilizes two pairs of counter rotating momentum wheels mounted in a T-configuration. Wheel mounting as well as operating modes are defined in Figure 3-19. The indicated control concept includes vehicle position and rate determination, a pair of counter rotating pitch aligned momentum wheels operated with a constant speed differential bias (momentum bias), and a pair of counter rotating yaw aligned wheels operated without momentum bias. The usual system orientation for this type of control system defines the pitch axis as being normal to the orbital plane and the yaw axis through earth center for zero attitude error. With this configuration and sensed roll and pitch orientation, roll control results from gyroscopic coupling.

A simplified pitch control system was modeled for simulation of TDRS attitude control and energy storage functions. The pitch axis was selected because it allowed for faster response than the roll-yaw system, thus permitting economical digital simulation. Furthermore, a single axis model facilitates quicker insight into effects of simultaneous energy transfer and attitude control operations. Certain simplification of the energy transfer dynamics was justified since response of the IPACS motor/generator subsystem is virtually instantaneous when compared with dynamics of the attitude control loops. The model was formulated specifically to investigate dynamic behavior of a representative IPACS under the following conditions: (1) system response to attitude control and energy transfer commands using normal system parameters, (2) effects of torque mismatches due to unequal wheel inertias, and (3) effects of certain wheel loop failures.

Modeling and control laws.- The mathematical model used for energy-momentum (E-M) wheel simulation is presented in Figure 3-20. It includes energy storage and torque control laws, an attitude feedback loop with forward loop command shaping, and momentum wheel energy loss and malfunction logic.

Energy storage law: Energy is transferred to and from the momentum wheels via the IPACS motor/generator subsystem, which acts to command changes in the rotational speeds of the two spin opposed momentum wheels. Relationships between electrical energy transfer and momentum wheel conditions are expressed by the following energy control law:

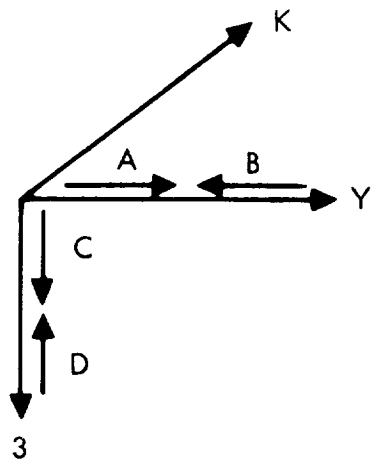

STORE E IN ALL 4 WHEELS FOR

COMMAND	ACTION
$+\Delta$ HY	$\uparrow \omega$ A
$-\Delta$ HY	$\uparrow \omega$ B
$+\Delta$ H3	$\uparrow \omega$ C
$-\Delta$ H3	$\uparrow \omega$ D

FOR HY BIAS ω A $> \omega$ B

FAILURE MODE OPERATION

A) STORE ENERGY IN GOOD PAIR
B) CONTINUE CONTROL IN AXIS OF GOOD PAIR
C) IN FAILED AXIS, RUN REMAINING WHEEL AS BI-DIRECTIONAL REACTION WHEEL

Figure 3-19. TDRS/EOS Baseline Array

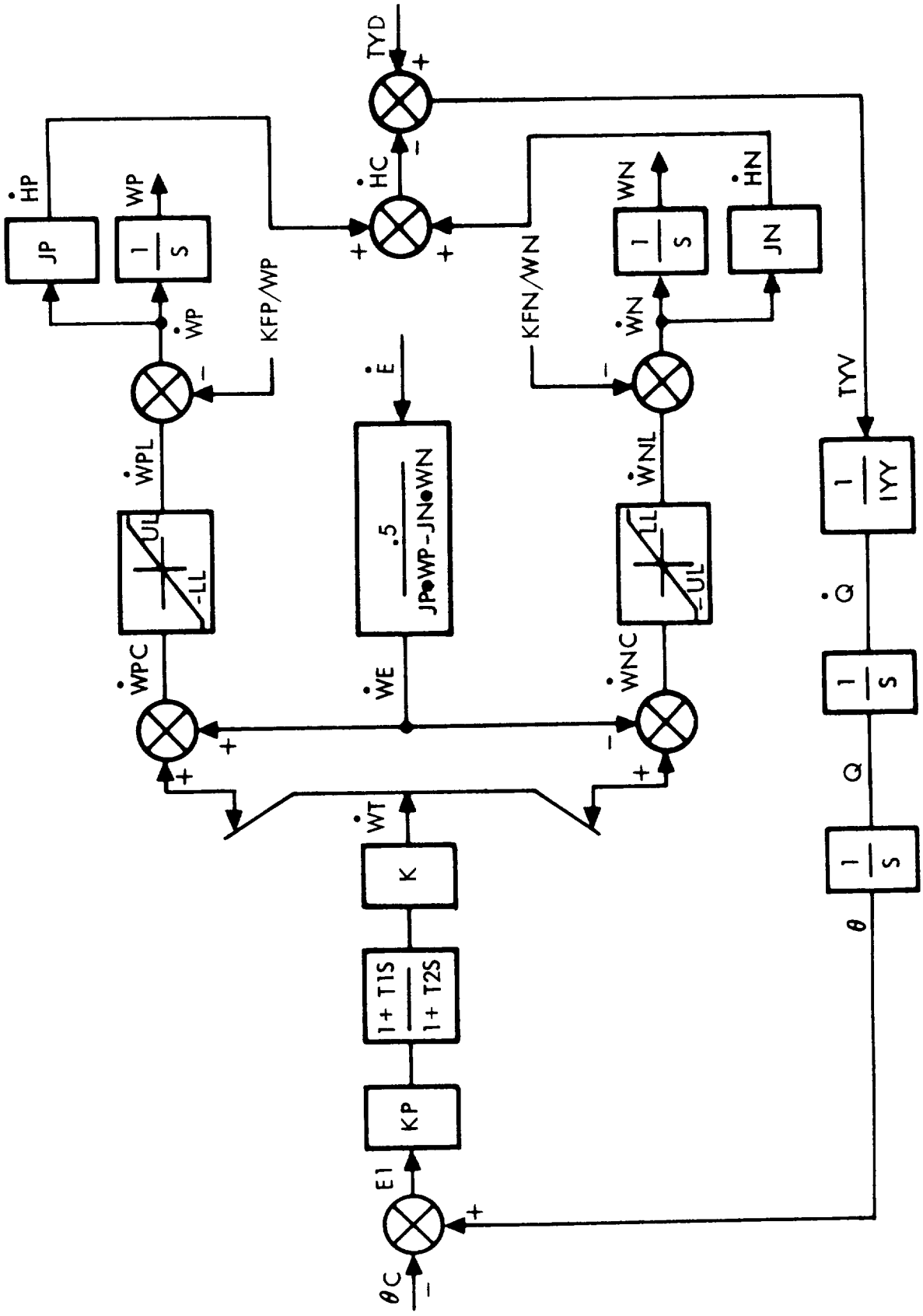

Figure 3-20. Simulation Model of E-M Wheel Pitch Control

$$\dot{WE} = \frac{.5\,\dot{E}}{JP \cdot WP - JN \cdot WN}$$

where $\dot{WE}$ is the angular acceleration commands to the two wheels required for an IPACS energy storage rate of $\dot{E}$ watts; wheel acceleration/deceleration commands to the two wheels are equal but opposite in sign. JP, WP and JN, WN are the moments of inertia and wheel speeds of the two wheels where subscripts P and N correspond to the clockwise and counterclockwise rotating wheels.

Torque control law: The equal-in-magnitude, opposite-in-sign energy transfer wheel acceleration commands for a perfect system would result in zero net torque on the vehicle. A simple method for exerting attitude control torque is to command equal-in-magnitude and equal-in-sign accelerations of the two wheels. This method permits energy transfer and attitude control wheel acceleration commands to be summed and still retain separate functional operations. Wheel acceleration commands are formed as follows:

$$\dot{WPC} = \dot{WT} + \dot{WE}$$

$$\dot{WNC} = \dot{WT} - \dot{WE}$$

where $(\dot{WPC}, \dot{WNC})$ are wheel acceleration commands formed from the attitude control commands $\dot{WT}$ and energy transfer command $\dot{WE}$. The achieved wheel acceleration may differ from the commanded value due to two causes: (1) commanded acceleration may exceed the torque capability of the motor/generator unit and (2) energy losses due to wheel bearing friction act as a braking force on wheel motion. Achieved wheel accelerations are formed from the following equations:

$$\dot{WP} = \dot{WPL} - KFP/WP$$

$$\dot{WPL} = LL \qquad \dot{WPC} < LL$$

$$= \dot{WPC} \text{ for } LL \leq \dot{WPC} \leq UL$$

$$= UL \qquad \dot{WPC} > UL$$

$$WP = \int \dot{WP}\,dt$$

$$\dot{WN} = \dot{WNL} - KFN/WN$$

$$\dot{WNL} = UL \qquad \dot{WNC} < -UL$$

$$= \dot{WNC} \text{ for } -UL \leq \dot{WNC} \leq -LL$$

$$= -LL \qquad \dot{WNC} > -LL$$

$$WN = \int \dot{WN} dt$$

where $(\dot{WP}, \dot{WN})$, $(\dot{WPL}, \dot{WNL})$, (WP, WN) are the achieved and command limited wheel accelerations and instantaneous wheel speed, respectively. (LL, UL) represent the maximum allowable wheel deceleration and acceleration of the P-wheel. These definitions similarly apply to the N-wheel.

The energy loss due to wheel bearing friction and windage losses $(\dot{EB})$ for a conceptual TDRS design is a function of the wheel speed and is approximated by the following expression

$$\dot{EB} = 1 + 2.9 \times 10^{-9} \, WP^2$$

where $\dot{EB}$ and WP have units of watts and rpm, respectively. For the TDRS IPACS, the energy loss varies between 8.25 and 2.81 watts with the wheel speed range of 50 000 rpm to 25 000 rpm. An average energy loss of 5.5 watts for $\dot{EB}$ was used in the simulation where the energy loss is given by the term KFP/WP; with KFP a constant defined as follows:

$$KFP = KFN = \frac{\dot{EB}}{JP}$$

where $\dot{EB}$ is the energy loss rate. Net torque of the two E-M wheels is given by:

$$\dot{H}_C = JP \cdot WP + JN \cdot WN$$

Torque on the vehicle is expressed as follows:

$$TYV = (-\dot{HC} + TYD)$$

where TYD is any external torques exerted on the vehicle.

Attitude control: IPACS performance characteristics and the computational accuracy of the digital simulation model are assessed from transient response data. Step commands in attitude and various energy transfer conditions are used as forcing functions. Attitude feedback, error summing, and the controller transfer function are defined by the following equations:

$$\Theta = TYV/IYYs^2$$

$$E_1 = \Theta - \Theta_c$$

$$\dot{WT} = K \cdot KP\left(\frac{1 + T1s}{1 + T2s}\right)$$

where Θ_c, and Θ are the pitch attitude command and achieved attitude. (KP, T1, and T2) are the system gain and lead compensator time constants. IYY and K are the vehicle pitch moment of inertia and a system gain modifier, with $\dot{WT}$ being the wheel acceleration command for attitude control. This system is stable for any set of parameters where T2 > T1. System natural frequency and damping ratio can be selected to suit design criteria, which, for the study are:

(1) Stable system response to near steady-state values is within two minutes.

(2) Wheel acceleration commands shall not exceed available wheel torque capability for combined forcing functions of 8.72×10^{-4} radians (.05 degree) attitude command and maximum energy charge/discharge commands.

Simulation results.- A digital simulation program of the E-M wheel pitch loop modeled in figure 3-20 was exercised for various nominal and failure effect conditions using a representative TDRS IPACS data base defined in Table 3-IV.

System parameters (KP, T1, T2) were selected to obtain an ideal system response ($\sqrt{2}/2$ damping factor) for linear system operation. However, in order to simulate representative TDRS pitch system response, the gain modifier was reduced from unity to 0.5. This provided system response corresponding to a quadratic with 0.3 damping ratio for nonlinear system operation with adverse operating conditions; 10 percent torque unbalance and/or one wheel open.

TABLE 3-IV.- TDRS IPACS PITCH CONTROL DATA BASE

Moments of inertia				
Vehicle pitch axis	IYY	392 N-m-sec^2		(289 slug-ft^2
CW momentum wheel	JP	.0329 N-m-sec^2		.0243 slug-ft^2
CCW momentum wheel	JN	.0329 N-m-sec^2		.0243 slug-ft^2)
Wheel torque limits				
Maximum acceleration	UL	.348	rad/sec^2	
Maximum decleration	LL	-.675	rad/sec^2	
Energy loads				
Wheel bearing rate	EB	5.5	watts	
System parameters				
$\sqrt{2}/2$ gain constant	KP	19.822	sec^{-1}	
Lead time constant	T_1	40	sec	
Lag time constant	T_2	6.67	sec	
Gain modifier	K	.5	-	
Wheel speeds				
Maximum		50 000	RPM	
Minimum		25 000	RPM	
Pitch bias		10%		
Attitude control accuracy				
Pointing accuracy		±.0349	radians	(±.2 degrees)

For perfect operating conditions (no system errors, system failures, or wheel friction), the attitude response to a step input is underdamped with first overshoot peak at approximately 42 seconds. The attitude error is reduced to approximately 0.2 percent within two minutes. As expected, energy transfer forcing functions act as torque-free commands to the control system as the momentum wheels are accelerated equally in opposing directions. Simulation runs with both attitude and energy transfer commands substantiate the independent effects of the attitude control and energy charging commands for vehicle rotation and momentum wheel speed changes, respectively.

Simulation runs, made for off-nominal and failure conditions, were used to assess effects of torque mismatch, energy mismatch, and wheel open failures on attitude control performance and wheel charging efficiency. Simulation conditions are identified in Table 3-V with resultant time histories presented in figures 3-21 through 3-28.

TABLE 3-V.- OFF-NOMINAL AND FAILURE MODE SIMULATION CONDITIONS

	Case Number			
	1	2	3	4
Control conditions:				
Energy command to P-wheel (W)	-30	0	-15	-15
Energy command to N-wheel (W)	-30	0	0	0
Control command to P-wheel	yes	no	yes	yes
Control command to N-wheel	←	yes	→	
Pitch attitude command [rad (deg)]	8.72×10^{-4} (.05)	8.72×10^{-4} (.05)	0 (0)	8.72×10^{-4} (.05)
Wheel parameters				
P-wheel moment of inertia [N-m sec^2 (slug-ft^2)]	←	.0329 (.0243)	→	
N-wheel moment of inertia [N-m sec^2 (slug-ft^2)]	.0296 (.0218)	.0296 (.0218)	.0329 (.0243)	.0329 (.0243)
Wheel bearing loss per wheel (W)	←	5.5	→	
P-wheel speed (rpm)	←	37 500	→	
N-wheel speed (rpm)	←	-33 750	→	

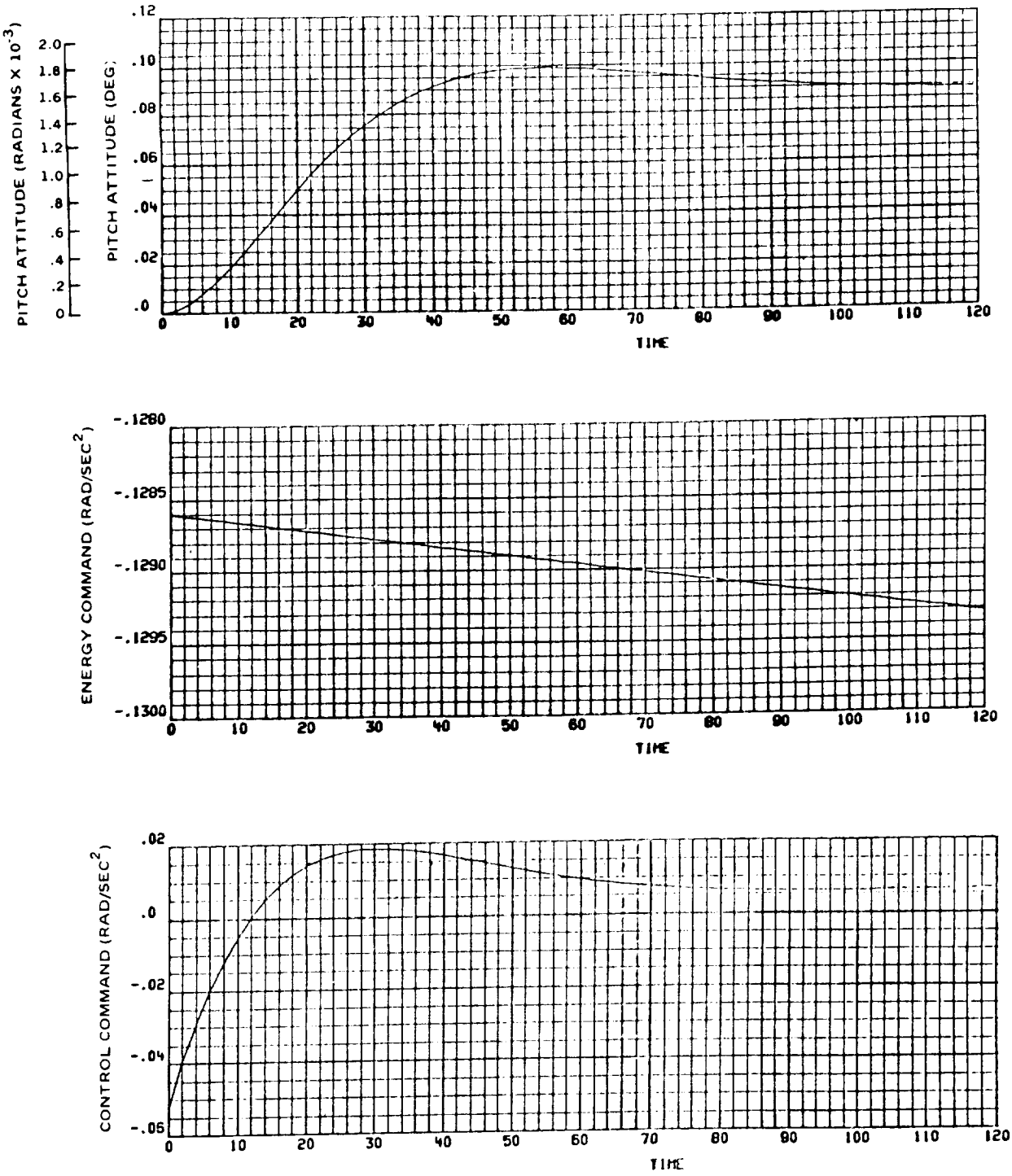

Figure 3-21. TDRS Response to Torque Mismatch With Energy Command (Case 1)

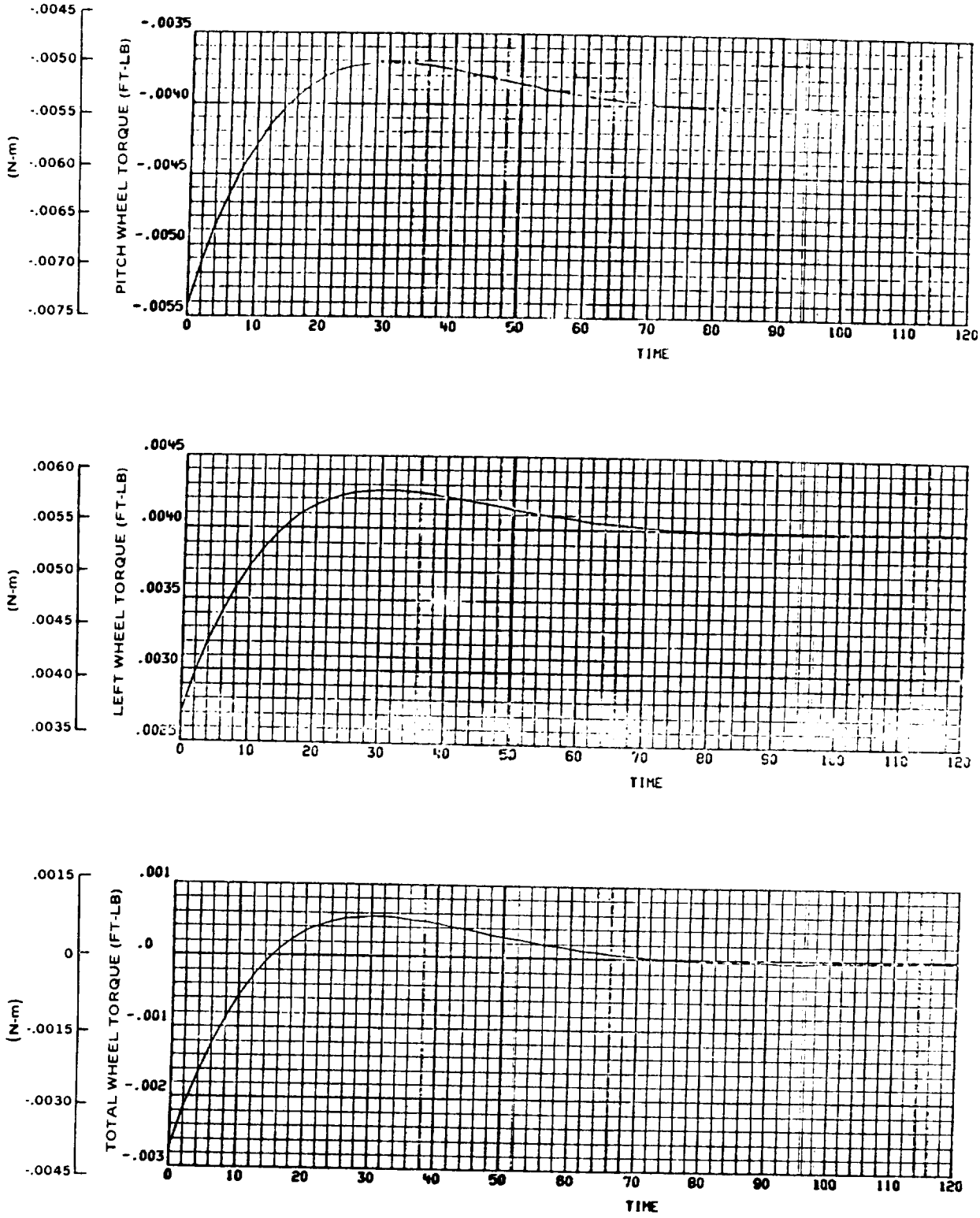

Figure 3-22. TDRS Response to Torque Mismatch With Energy Command (Case 1)

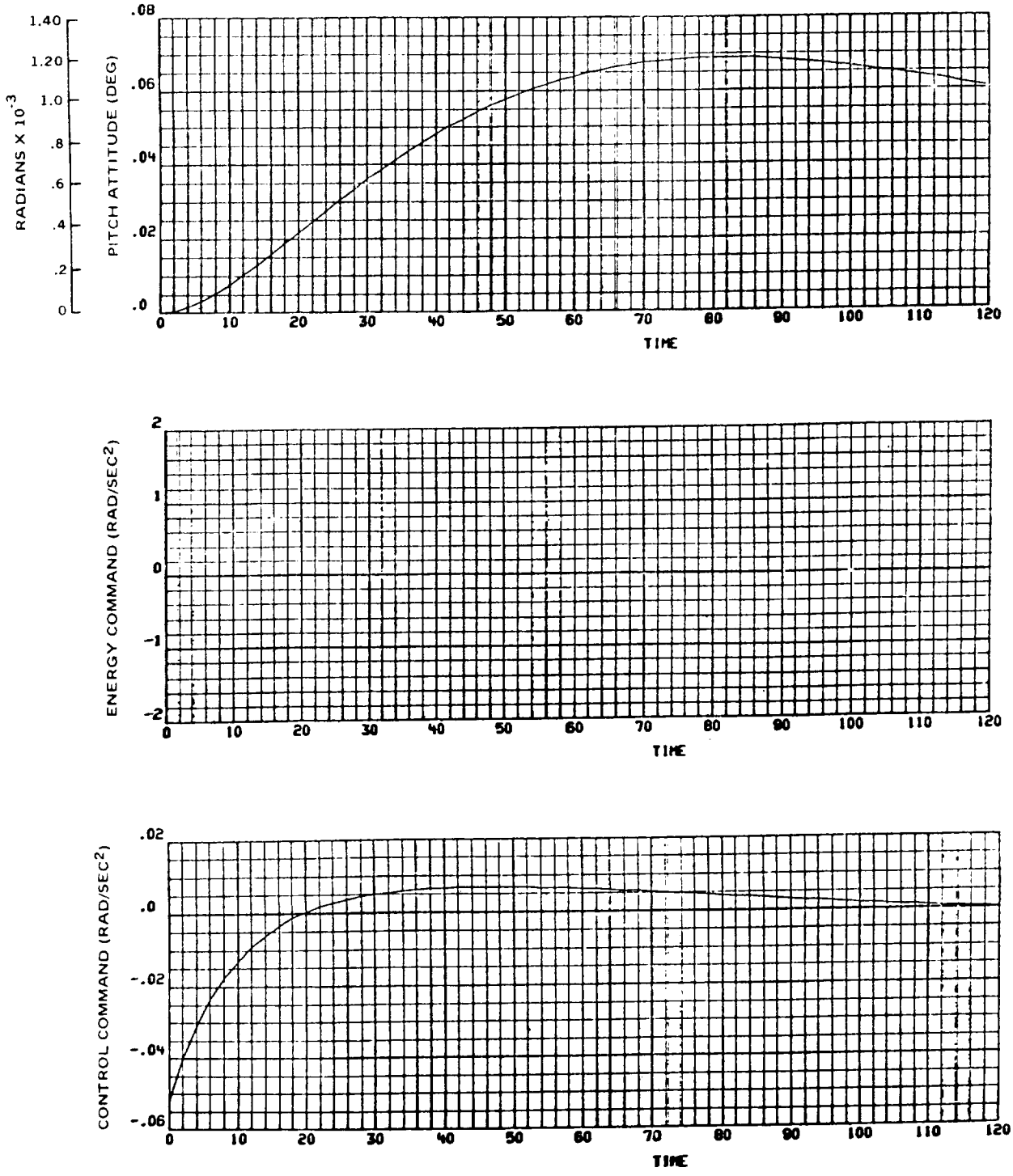

Figure 3-23. TDRS Response to Torque Mismatch With Wheel Open Failure (Case 2)

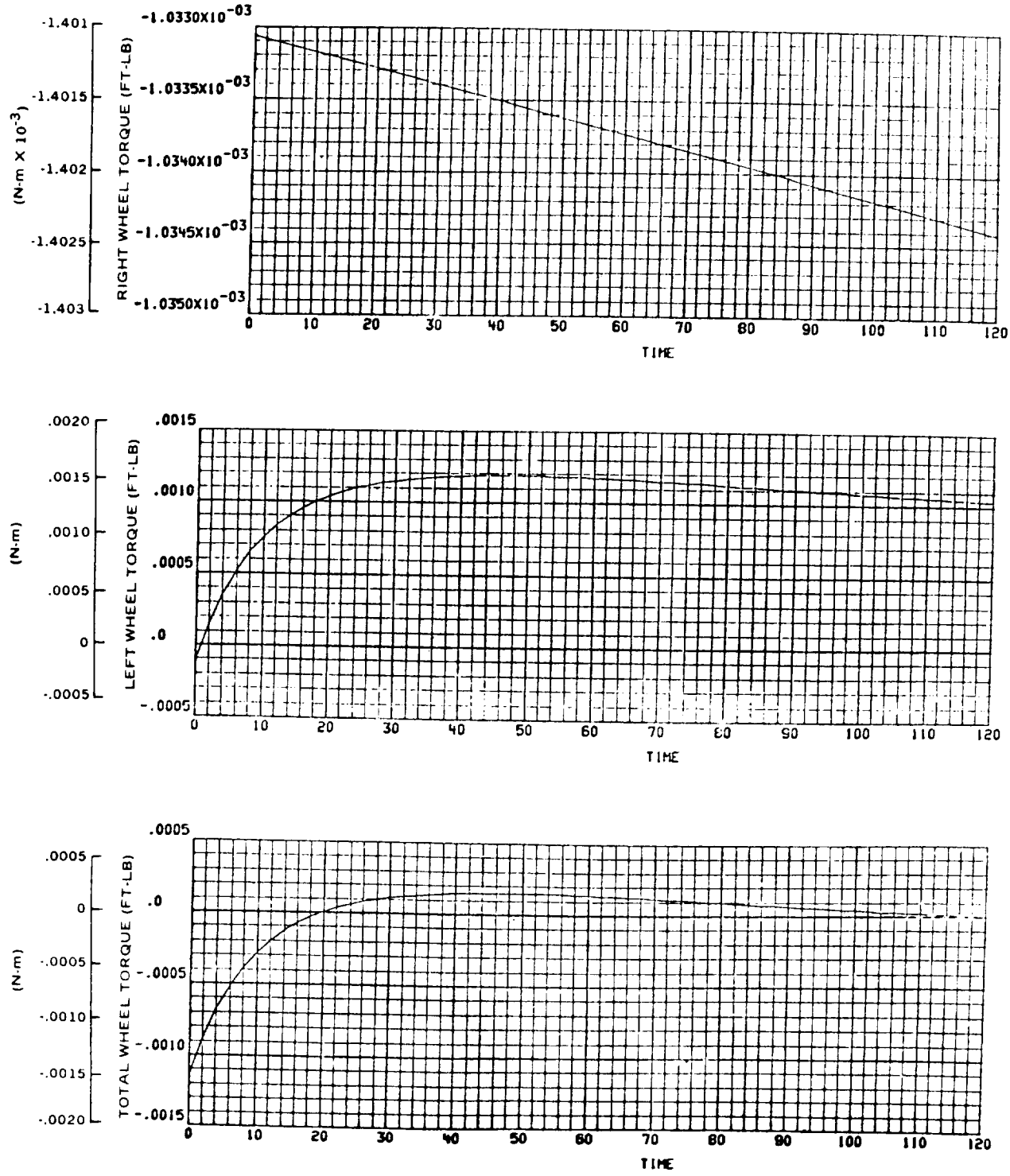

Figure 3-24. TDRS Response to Torque Mismatch With Wheel Open Failure (Case 2)

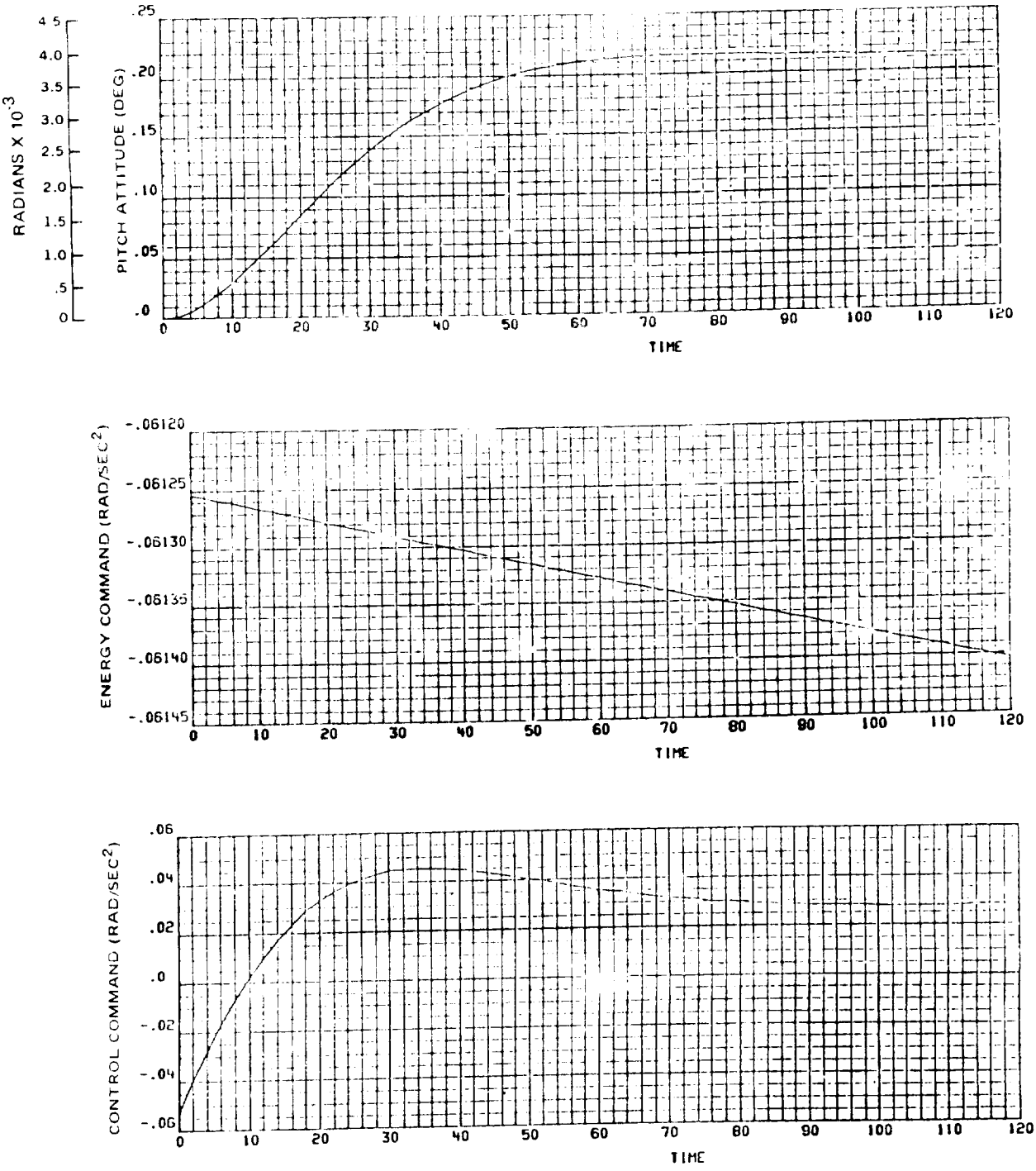

Figure 3-25. TDRS Response to Single Wheel Energy Transfer (Case 3)

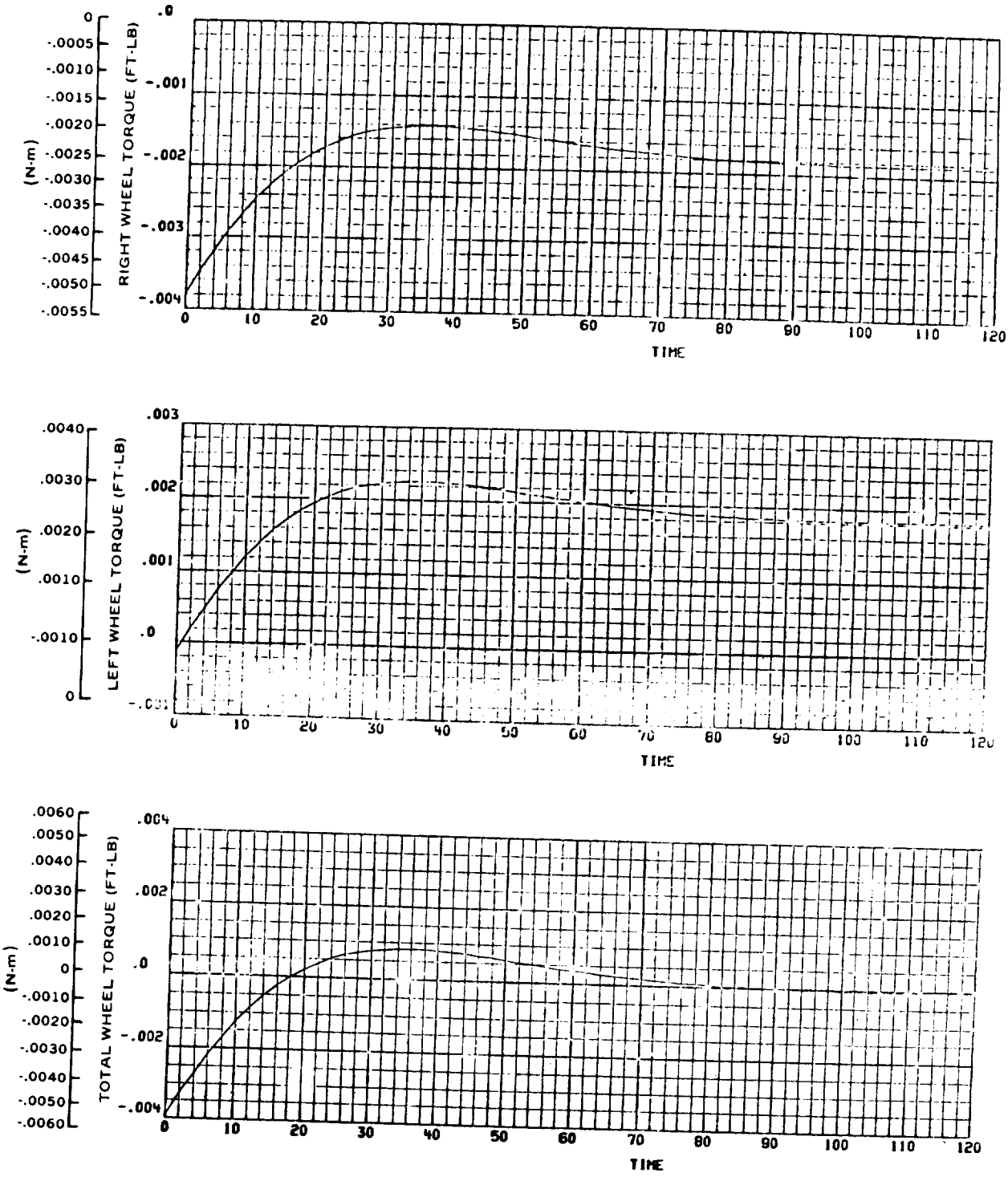

Figure 3-26. TDRS Response to Single Wheel Energy Transfer (Case 3)

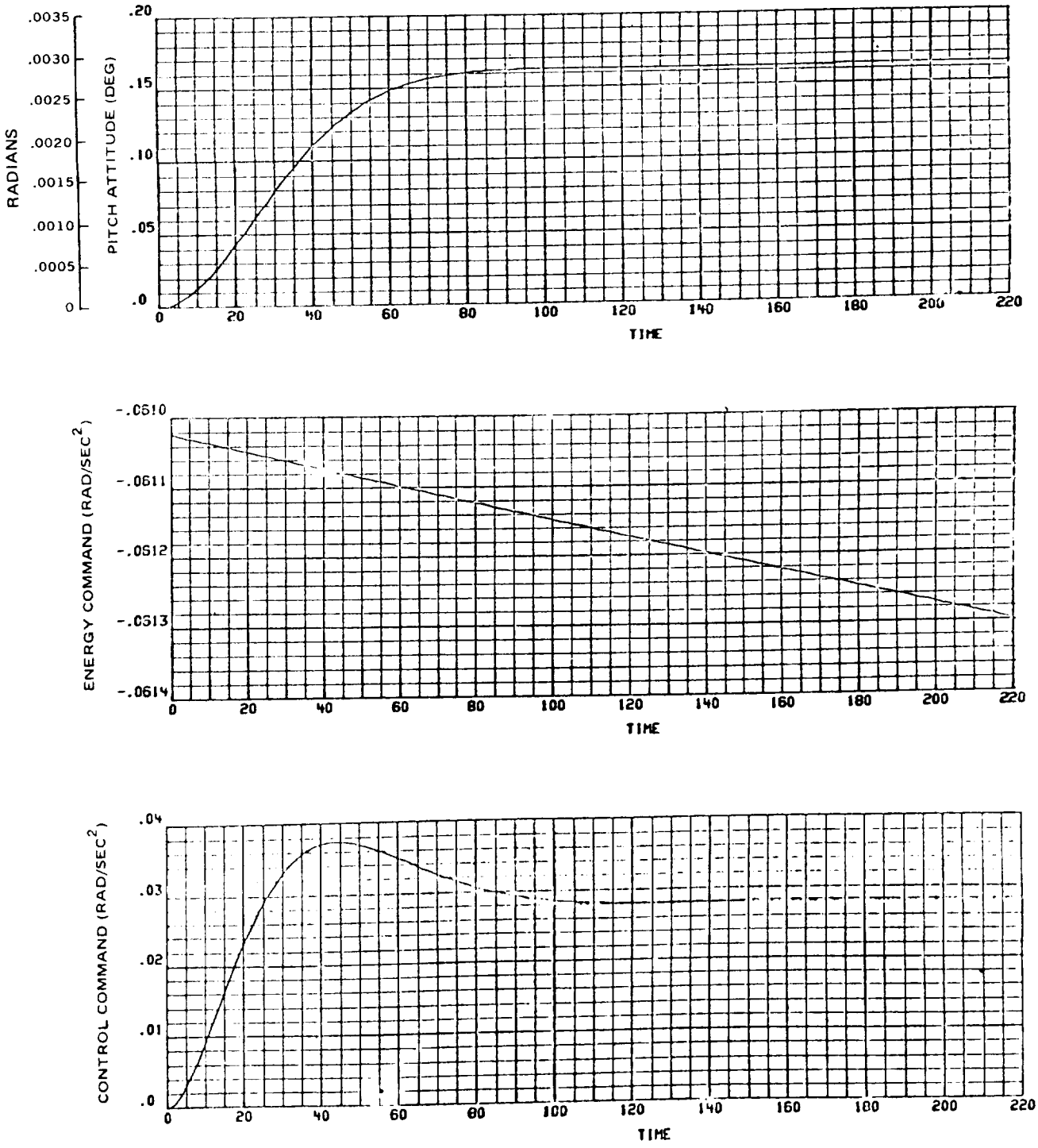

Figure 3-27. TDRS Response to Single Wheel Energy Transfer (Case 4)

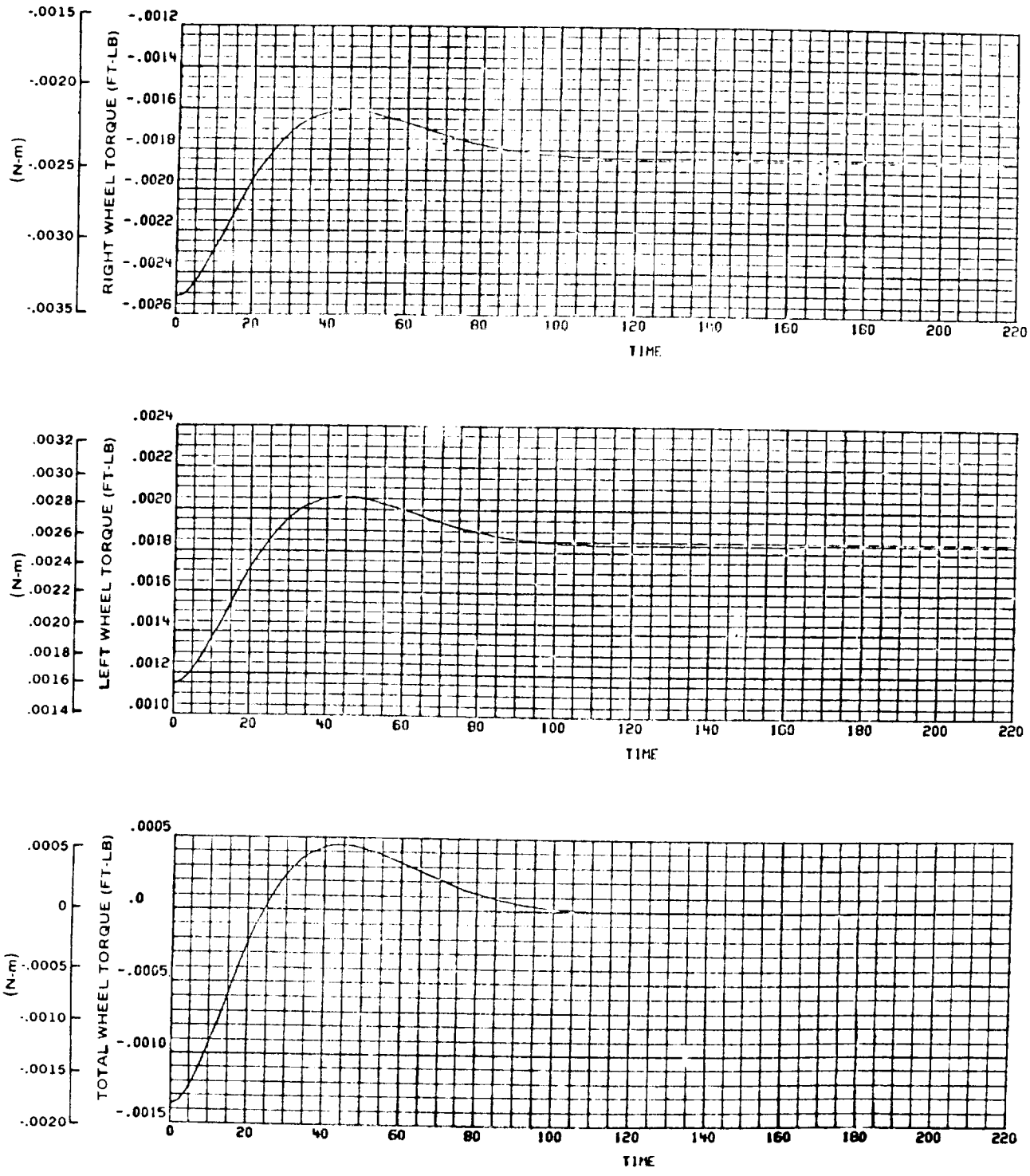

Figure 3-28. TDRS Response to Single Wheel Energy Transfer (Case 4)

Torque mismatch performance: Two simulation runs were made to determine effects of torque mismatch on system performance. The N-wheel moment of inertia was reduced by 10 percent to effect the mismatch, and both cases were given attitude commands. Case 1 attitude was also driven by an energy transfer command. Case 2 included a malfunction whereby only one wheel receives attitude control commands.

In Case 1, the attitude response overshoots the command and appears to approach a bias error greater than the command. This attitude bias or pointing error is primarily a function of the torque mismatch, energy transfer rate, and the momentum wheel speed. Steady state pointing error as a function of these parameters is presented in figure 3-29. A 10 percent torque imbalance appears to be an acceptable tolerance limit, in order not to exceed the maximum allowable pointing error for maximum charge and discharge rate conditions (250 watts at 25 000 rpm and -640 watts at 50 000 rpm for two E-M wheel pairs).

In Case 2, the effect of a wheel-open condition is to slow the system response by a factor of two. The steady state pointing error is negligible, being proportional to the sum of the two wheel decelerations due to bearing friction. Since the system will act to null the net wheel torque, both wheels will approach wheel friction induced accelerations.

Both wheels are seen to lose energy. The P-wheel is in the free wheeling mode (no command) and is slowed by bearing friction in the amount of .0425 rad/sec^2 corresponding to an average energy drain of 5.5 W. Based upon an energy storage of 285 W hr, it would take approximately 13 hours for bearing friction to slow the wheels from their maximum to minimum operating speed. If the less conservative, non-constant expression for energy loss is used, a somewhat larger estimate of 18 hours is obtained as an estimate for slowdown time.

Energy command failure effects: Two simulation runs were made to determine effects of energy commands to one wheel while both wheels receive attitude control commands.

The effect on pitch attitude error of energy charging with only one wheel of the two pitch wheels is seen by comparing pitch attitude histories of Case 3 and 4. Near steady state conditions are reached within 2 minutes of forcing function application. Difference of steady state attitudes in the two cases is seen to be equal to the difference in attitude commands. A common attitude error bias in both cases is due to energy charging from the one wheel.

An approximation to this pointing error is presented in figure 3-30 as being proportional to the ratio of the energy transfer command and the wheel speed. This approximation checks well with the simulation data of Cases 3 and 4. At steady state, the net wheel torque is zero and both wheels are

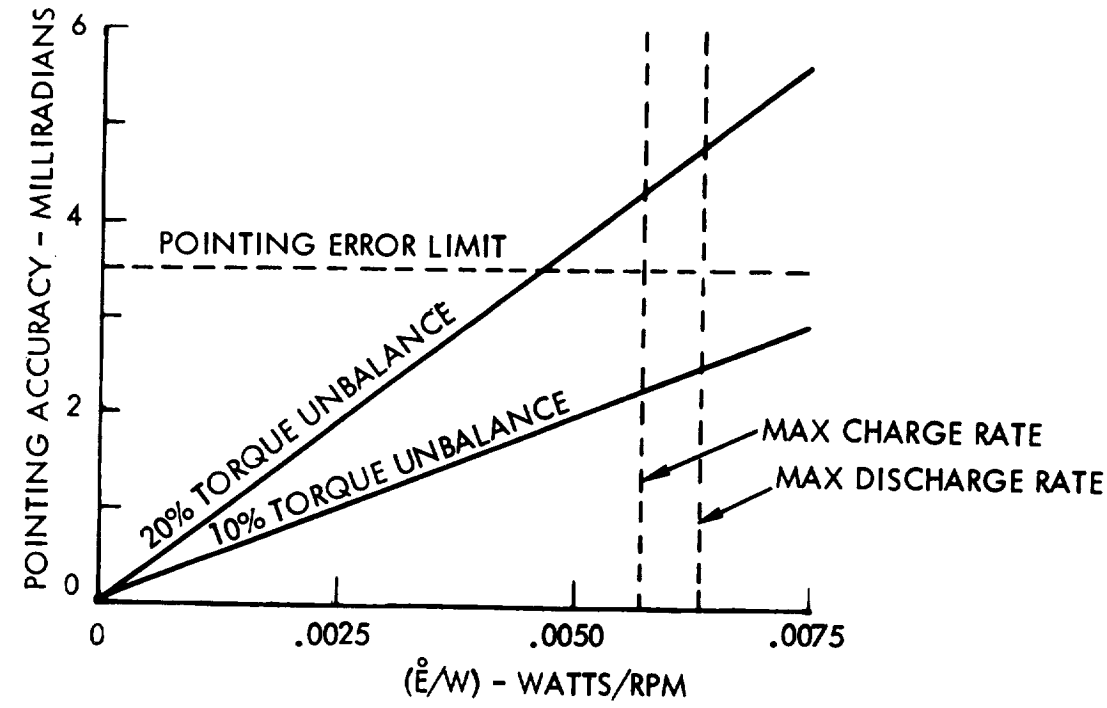

Figure 3-29. TDRS Pointing Error Due to Torque Mismatch

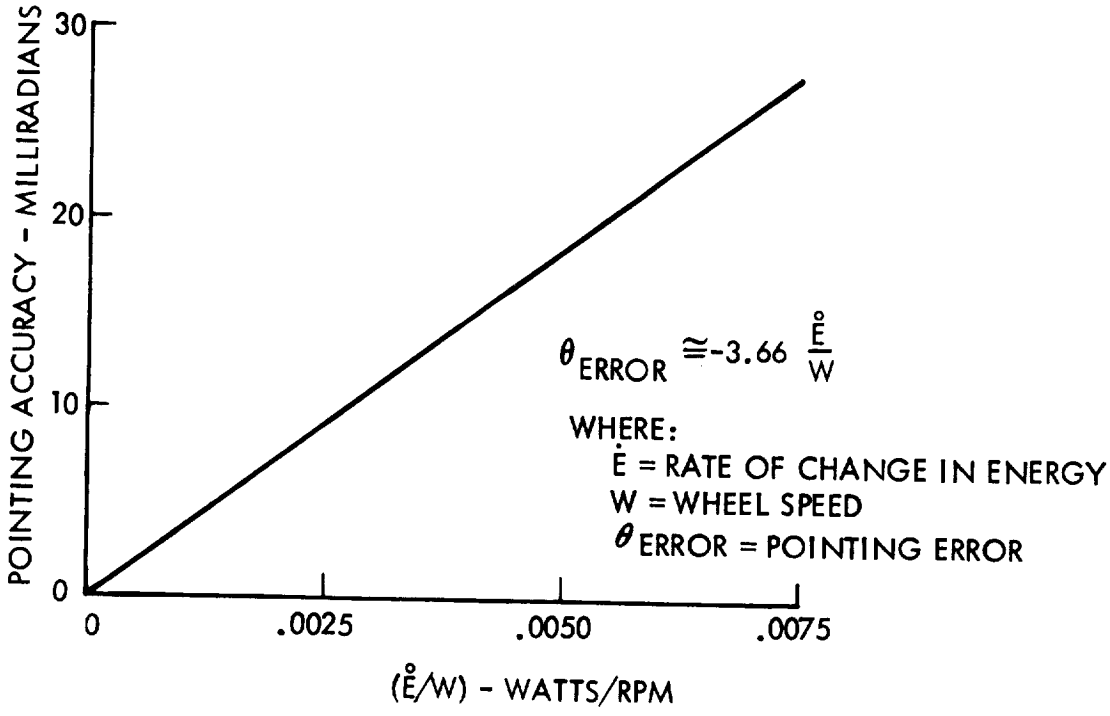

Figure 3-30. TDRS Pointing Error Due to Single Wheel Charging

losing energy at the same rate. This means that, with one wheel not receiving energy transfer commands, half of the desired energy transfer is shared between the two wheels.

In the event that this type of failure is detected, two courses of action can be considered: (1) Do not give energy commands to the pitch wheels and thereby lose the total pitch energy capability, but retain full attitude control accuracy; and (2) Give energy commands to the pitch wheels, thereby retaining half the pitch energy transfer capability with an attendant pitch attitude error during energy transfer.

The pointing error curve of figure 3-30, which gives the pointing error for any energy transfer rate, wheel speed condition, is also used to obtain the maximum allowable energy mismatch for non-failure operation, which does not result in pointing errors greater than the specified value. For the worst-case condition, maximum wheel speed of 50 000 rpm, the energy mismatch tolerance is approximately 47 W.

Conclusions: Independent wheel acceleration/deceleration commands for attitude control and energy transfer result in the desired action; torque-free energy transfer.

Wheel bearing friction has a negligible effect on attitude response characteristics, while its energy drainage effect would be to slow the wheels from maximum to minimum speed in over 13 hours.

Attitude pointing accuracy requirements permit easily satisfied tolerances to be set on torque mismatches and energy mismatches of $\pm$10 percent and $\pm$47 W.

Wheel control failures whereby only one wheel either receives torque commands or energy transfer commands result in two different effects: (1) system response slowed by half with accuracy unaffected and (2) system response unchanged but a pointing error result which is proportional to the ratio of the energy command rate and the wheel speed.

Solar Array/IPACS Equivalent Circuit Model

The IPACS motor generator subsystem (M/G) interfaces with the spacecraft solar array and the system load. For the purpose of M/G control analysis, the solar array and load are modeled as a current source and pure resistance. Furthermore, since the M/G response characteristics are nearly instantaneous compared to spacecraft control system response, the M/G can be realistically analyzed as a separate entity.

Modeling and analytical block diagram.- The mathematical model of an IPACS M/G interfaced with the spacecraft solar array and load is shown in figure 3-31. Current in each phase of the two-phase motor is controlled by current feedback, and the line or bus voltage is controlled by commanding motor current as a function of the difference between line voltage and a reference voltage. When the line voltage drops below the desired (or referenced) level, a motor current is developed such that the rotor and motor return current to the line. This action, IPACS energy discharge mode, supplements the solar array current and despins the rotor. When the line voltage goes above reference level, the reverse action occurs and energy is stored by increasing rotor speed.

The motor current feedback loop consists of time-ratio controlled power amplifiers for each motor phase, the phase inductance-resistance, and the shunt resistance used for current feedback. The time-ratio controller, represented by the variable, n, determines the percentage of line voltage that is effectively applied across each phase to overcome the back emf voltage, VF, and to produce the desired motor current.

Motor/generator regulation: Response characteristics of the IPACS M/G and the accuracy to which it can regulate line voltage and rotor speed is dependent upon the bandwidth of two control loops: (1) voltage regulator loop and (2) current feedback loop. Thus the M/G design process consists of selecting loop parameters which obtain the desired system performance.

Current regulator loop: This loop is designed to provide effective current control at the anticipated back emf frequencies (2 x rotor speed for two-pole motor) and to minimize the error between commanded and actual motor current due to the magnitude of back emf. The loop bandwidth is given by:

$$\underset{\text{(current regulator)}}{\text{Bandwidth}} \cong \frac{K1 \cdot VL \cdot KA}{KB}$$

where: VL = line voltage
KA = Table 3-VI
KB = Table 3-VI

where K1 is the adjustable parameter. The value for the inner loop feedback constant, K2, is selected such as to null the constant current error due to back emf and still retain basic current loop stability characteristics.

Voltage regulator loop: The outer voltage regulator loop is designed such that its bandwidth is much less than the current loop while still providing adequate response to solar array current variations. Loop bandwidth is given by:

$$\underset{\text{(voltage regulator)}}{\text{Bandwidth}} \cong n\, KR_L$$

where the time-ratio controller, n, can vary from 0.4 to 0.8 during quiescent operation. The integrator, K/s , acts to set the voltage regulator loop bandwidth such as to insure stability when coupled with the current loop dynamics.

Simulation results.- The IPACS M/G model of figure 3-31 was simulated digitally for a TDRS IPACS application, using M/G parameters listed in Table 3-VI. Two simulation runs were made to: (1) verify linear system design and (2) investigate effects of nonlinearities. Loop bandwidths for these data were approximately 50 000 radians/second and 25 radians/second for the current and voltage regulator loops, respectively. For TDRS IPACS, $K1 = 10\ W_{max}$, where W_{max} is the maximum rotor speed.

TABLE 3-VI.- TDRS IPACS MOTOR GENERATOR DESIGN BASE

RL = 9.3333 ohms
KA = 13.7 amps/volt
KB = 2×10^{-3} sec
KT = 4.58×10^{-3} n-m/amp (3.38×10^{-3} ft-lb/amp
KV = 4.58×10^{-3} volts/rad/sec
JW = .0329 n-m-sec^2 (.0243 ft-lb-sec^2)
ICM = ±4.0 amps
n_{Max} = ±1.0
VR = 28.00 volts
K1 = .2773
K2 = 100
K = 2.627

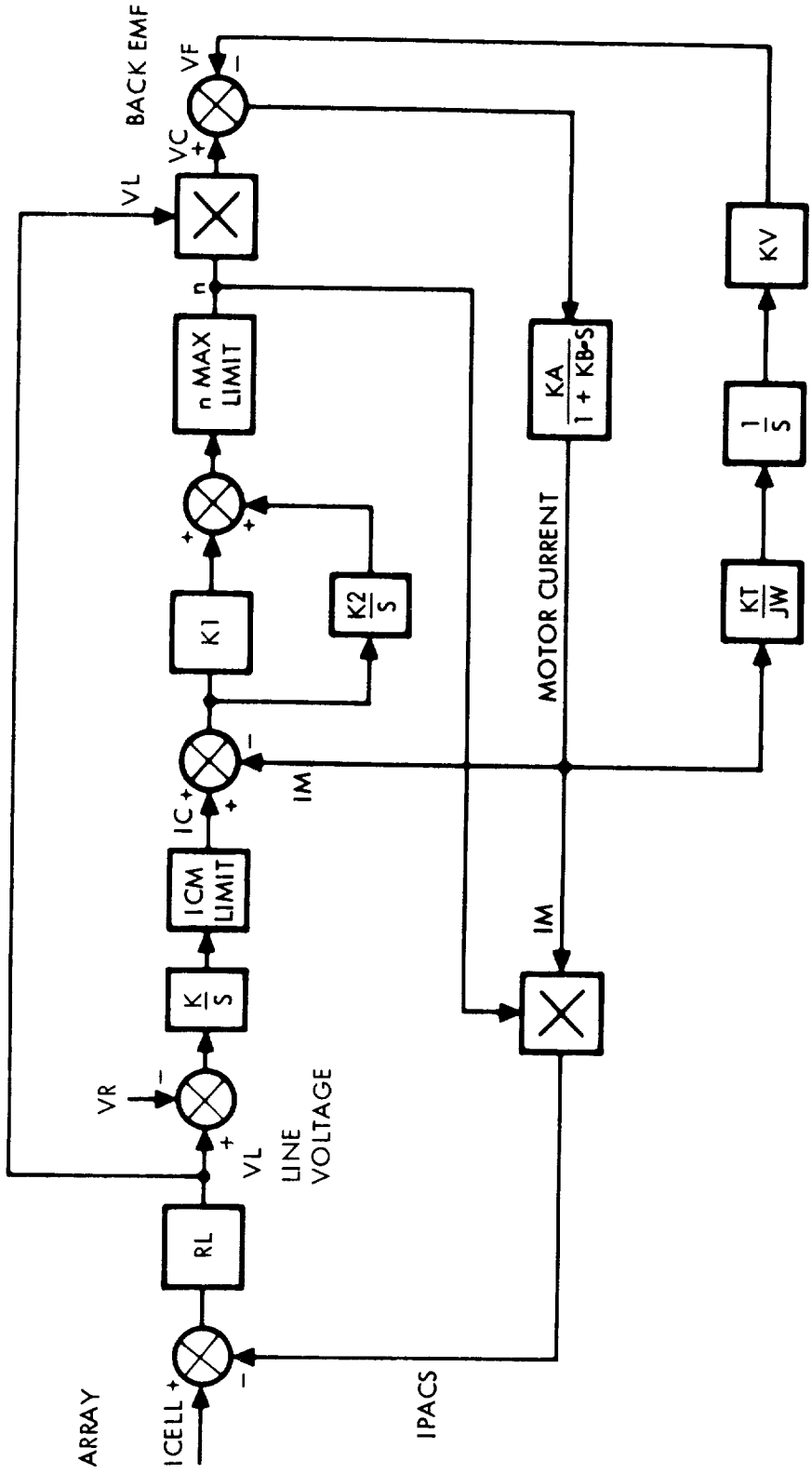

Figure 3-31. IPACS Motor/Generator Model

Small signal response: Simulation results are shown in figure 3-32 where, initially (before t = 0), the solar array current (ICELL) was set at 3 amps to produce a line voltage of 28 volts. Other initial values were: IPACS current (Ic) - 0, (IM) = 0, and (N) = .8572. At t = 0, ICELL was changed from 3.0 to 2.9 amps. As the response show, the line voltage immediately drops to 27.05 volts and the current supplied by IPACS jumps from 0 to .045 amps. Then the line voltage rises to 27.50 volts. However, due to the integrator term, K/s, the current loop has not received a command and both the IPACS current and line voltage again dip at approximately t = 10 milliseconds. From this time on, both the current and voltage rise with approximately the time constant of the voltage regulator loop; i.e., 40 milliseconds. During the run, n increased monotonically from .8572 to .8769.

The responses indicate that the bandwidth of the outer loop could be increased slightly if a faster rise to the line voltage is required. The regulation could be designed to decrease the time constant to 9 milliseconds or less and thus separate the regulation function from any attitude control function.

Large signal response: The M/G model contains two nonlinearities; the time ratio limit on n, and the commanded motor current limit on IC. A large signal run was made to determine the effect of these nonlinearities on system stability. Simulation results are shown in figure 3-33, where the system was given the same initial conditions as Case 1; however at t = 0, the current was dropped from 3.0 to 0 amps. As the time histories show, the line voltage immediately drops to zero, but recovers to 23.8 volts within 2 milliseconds as the motor current rises. Simultaneously, the IPACS current rises to 2.5 amps and the abrupt rise in the motor current saturates n to its unity limiting value. Both the line voltage and IPACS current remain constant from t = 2 milliseconds to t = 230 milliseconds. At this point, the commanded current, IC, becomes sufficiently large to desaturate n. Thereafter, current and voltage increase at the 40 millisecond time constant to their final values, 3 amps and 28 volts.

Conclusions: Simulation of a representative IPACS motor/generator shows system stability and satisfactory response characteristics for linear and nonlinear system operation.

Small current commands result in a return to steady state line voltage and IPACS current condition within 200 milliseconds.

Current commands which temporarily saturate the power bridge circuitry of the two-stage brushless dc motor/generator unit result in a step drop in line voltage until the power bridge circuitry desaturates. Then IPACS current and line voltage again return to steady state values in approximately 200 milliseconds.

The power transfer and voltage regulation functions of the IPACS motor/generator appear to be adequate for TDRS application and with an appropriate change in system constants should also satisfy RAM requirements.

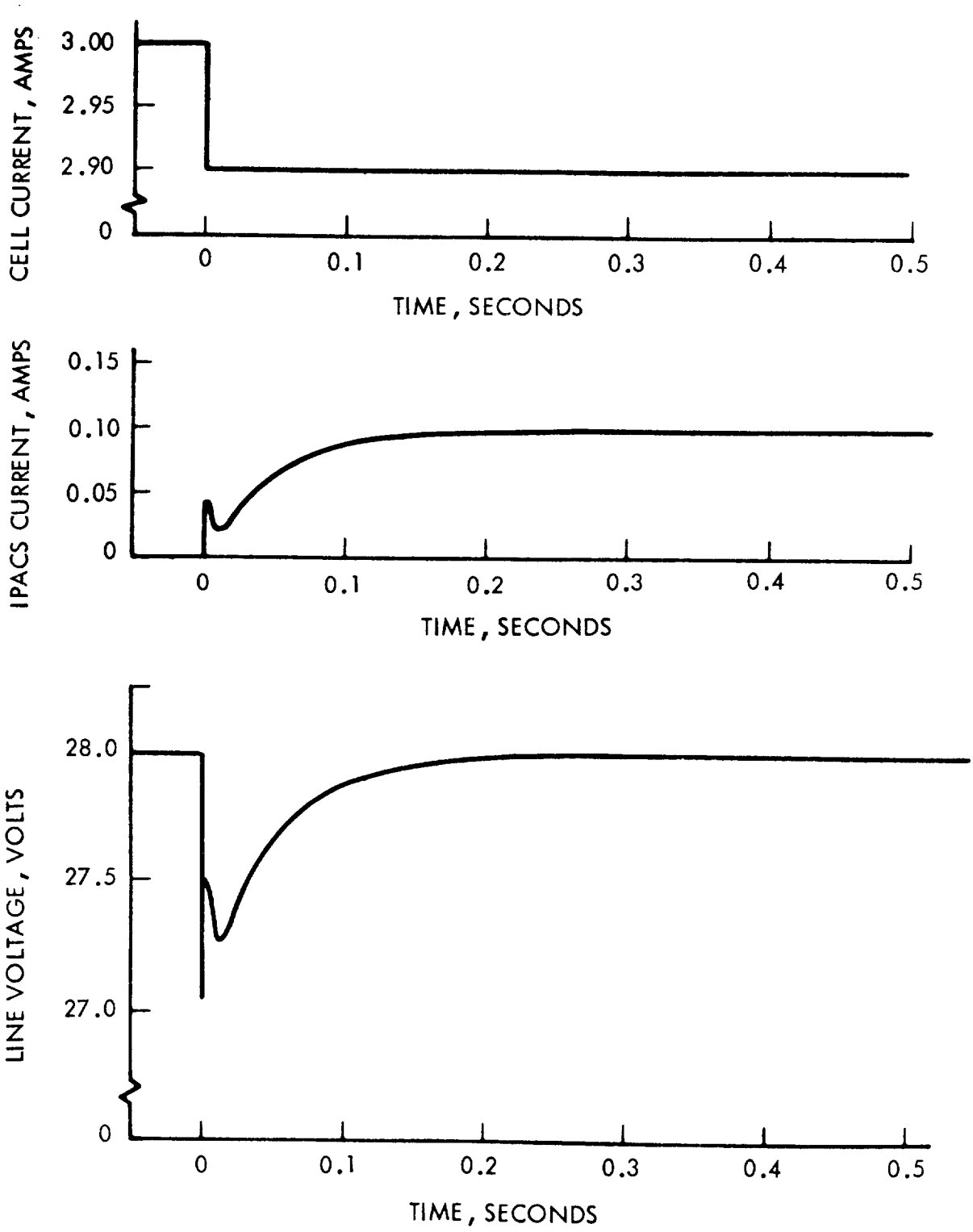

Figure 3-32. IPACS M/G Small Signal Response

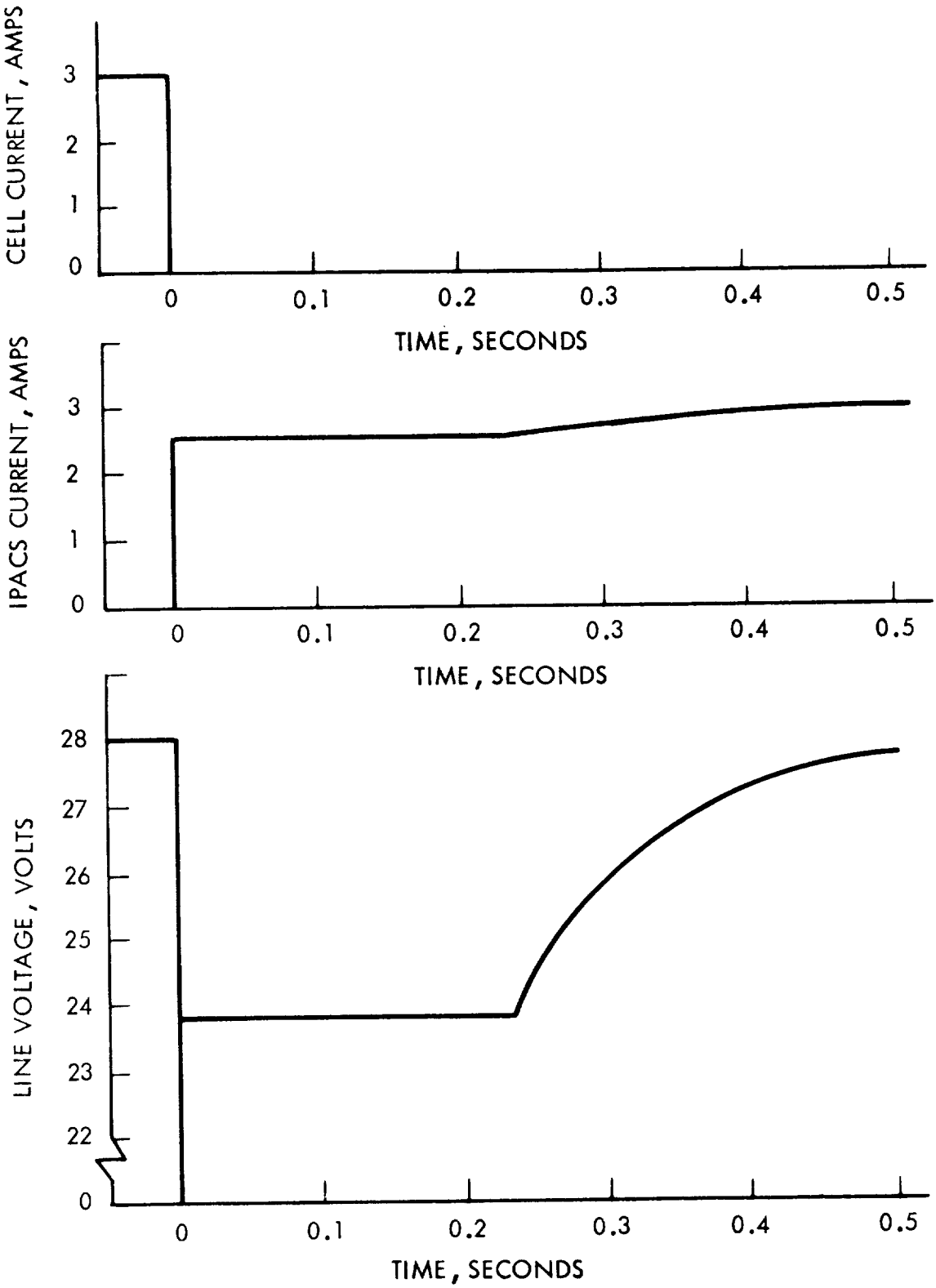

Figure 3-33. IPACS M/G Nonlinear System Response

MODULE 4 - CONCLUSIONS

Conceptual Design

The conceptual design effort verified the feasibility study parametric calculations of weight, volume, and design performance. The RAM IPACS design presents the potential of a 31 percent weight saving (498 kg or 1096 lb) over the conventional power and control system weight. The TDRS IPACS design makes possible a 10-percent weight saving (10 kg or 22 lb).

The TDRS and RAM IPACS designs are calculated to meet or exceed the functional and performance requirements specified for the mission.

Conventional ball bearings were selected for the TDRS design and the application is considered within the high-speed design practice of the present state of the art. The use of vacuum-melt M-50 tool steel and bearings selected for low race waviness and eccentricity are recommended to maximize operating life. Considering the relatively infrequent eclipse periods at synchronous orbit, the IPACS units can operate at low speeds (under 10 000 rpm) for over 75 percent of the mission duration. Wheel speeds will be increased as required for energy storage during the eclipse periods.

Further work is required to select a higher energy density rotor material for the RAM IPACS. The conceptual design is based upon a high-strength steel rotor with a nonmagnetic shaft of titanium. A study is required to evaluate the potential advantages of a titanium rotor and compare it to steel designs.

The RAM IPACS conceptual design includes conventional ball bearings. This design is considered a more severe application than TDRS. The eclipse profile associated with the low-altitude orbit will require essentially continuous operation over the design speed range (full to half-speed). Because of the relatively large rotor and corresponding bearing bore the operating DN number is at the upper limit of the current art. Bearing thermal control is expected to be passive but will require design attention. The use of M-50 tool steel also is recommended for the RAM IPACS bearings as well as the consideration of race waviness and eccentricity in selecting bearings.

Dynamic Analysis and Simulation

RAM double gimbal torque feedback control.- A generic torque feedback control law was found by simulation to provide effective control with charge-discharge wheel speed commands and external disturbances included. Linear analysis shows that the attitude control system response can be determined analytically as a simple function of constant control system gains.

Representative gimbal friction nonlinearities do not appreciably affect system dynamic response characteristics.

System attitude errors, assuming perfect system components but including friction nonlinearities, can be reduced to less than 4.85×10^{-6} rad (1 arc-sec) in approximately 10 seconds.

Wheel energy can be cycled between maximum and minimum energy conditions at maximum rates using less than half the available gimbal range.

Maximum gimbal motor torque during energy charge-discharge conditions does not exceed 50 percent of maximum rated torque for any expected conditions.

TDRS energy-momentum wheel control.- Independent wheel acceleration/deceleration commands for attitude control and energy transfer result in the desired action: torque-free energy transfer.

Wheel bearing friction has a negligible effect on the attitude response characteristics, while its energy drainage effect would be to slow the wheels from maximum to minimum speed in over 13 hours.

Attitude pointing accuracy requirements permit easily satisfied tolerances to be set on torque mismatches and energy mismatches of 10 percent and 47 W.

Solar array/IPACS equivalent circuit model.- Simulation of a representative IPACS motor-generator shows system stability and satisfactory response characteristics for linear and nonlinear system operation.

Small current commands result in a return to steady-state line voltage and IPACS current condition within 200 milliseconds. This time constant can be decreased to approach the motor constant of 4 milliseconds if required.

Current commands which temporarily saturate the power bridge circuitry of the two-stage brushless dc motor-generator unit result in a step drop in line voltage until the power bridge circuitry desaturates. Then IPACS current and line voltage again return to steady-state values at the loop time constant.

The power transfer and voltage regulation functions of the IPACS motor-generator appear to be adequate for TDRS application and with an appropriate change in system constants also will satisfy RAM requirements.

☆ U.S. GOVERNMENT PRINTING OFFICE: 1974—739-160/106